Max-Planck-Institut für Polymerforschung
Max Planck Institute for Polymer Research

Stimuli-Responsive Materials for Self-Healing in Corrosion Protection

Dissertation

zur Erlangung des akademischen Grades

„Doktor der Naturwissenschaften“

eingereicht am

Fachbereich Chemie, Pharmazie und Geowissenschaften

der Johannes Gutenberg-Universität Mainz

Li-Ping Lv

geboren in Shandong, China

Mainz, Juni 2014

JOHANNES GUTENBERG UNIVERSITÄT MAINZ

Dekan:

1. Berichterstatter:

2. Berichterstatter:

Tag der Prüfung: 22. Juli 2014

Table of Contents

1. Introduction

Self-healing (SH) materials have gained considerable attention in recent years.[1-7] Among them, extrinsic SH materials play an important role in which healing agents are embedded into the materials in advance followed by the release and healing process when cracks occur. In most of the previous studies, the self-healing process is mainly triggered upon mechanical damage. However, a redox-responsive delivery of self-healing agents is also of large interest for certain applications such as coatings for corrosion protection. Although the redox-stimulus was already investigated as a trigger in intrinsic self-healing materials,[8-11] its use for the delivery of hydrophobic self-healing agents is not yet reported. The introduction of redox-responsive units in materials allows a controlled change of interesting properties such as the permeability of the microcapsules shell,[12] the sol–gel transition of supramolecular gels,[9] or chemical or drug-delivery upon redox trigger.[13-17] Among the manifold available polymers with redox properties,[18,19] conductive polymers are particularly interesting because of their high electrical conductivity and their good thermal and environmental stabilities.[20] The change in their conductivity, structure, color, volume, or hydrophilicity in response to electro- or chemical stimuli make them suitable for applications in drug delivery,[21] actuators,[22-24] memory devices,[25] light-emitting diodes,[26] or chemicals sensors.[27]

Polyaniline (PANI),[28] as one of the most investigated conducting polymers, has three oxidation states: The fully reduced leucoemeraldine, the fully oxidized pernigraniline, and the half-oxidized emeraldine. Therefore, PANI can also exhibit redox-responsive properties upon electro- or chemical stimuli. PANI was previously reported as an intelligent system for the release of corrosion inhibitors. The polymer could be reduced upon corrosion and the doping corrosion inhibitors could be released due to the galvanic coupling between corroded iron and polyaniline.[29-31] However, the poor solubility of PANI in ordinary organic solvents still hinders its applicability.

To overcome the low solubility, PANI was processed in the form of, for example, nanocapsules by the thoroughly reported hard-template approach.[32-34] This approach however has intrinsic drawbacks. Firstly, it is difficult to keep the structural integrity of such capsules, especially for thin capsules shells. Secondly, a further step is needed to encapsulate a substance inside the capsules. Besides, emulsions were also used as soft

template to obtain hollow microspheres of polyaniline by using salicylic acid (∼1.5−3.1 μm in diameter) or β-naphthalene sulfonic acid (0.36-1.2 μm in diameter) as dopant.[35,36]

Miniemulsion polymerization is known to be a versatile technique to prepare a wide range of polymers nanoparticles with various structures.[37] Because of the stability of the miniemulsion droplets,[38] the polymerization can be performed even in unconventional conditions such as in the absence of water in nonaqueous miniemulsions[39−41] and at high temperature.[41] Moreover, the miniemulsion process was already found to be useful for the encapsulation of self-healing agents in nanocontainers.[42-47] Aniline was also found to be polymerized to yield monolithic particles in miniemulsion.[48,49]

Herein, the focus of the present thesis is to prepare polyaniline capsules in miniemulsion for the encapsulation and stimuli-responsive release of self-healing agents for corrosion protection. We first demonstrate a one-pot synthetic process for the formation of conducting polyaniline capsules via miniemulsion polymerization. The interface of the miniemulsion droplets was used as soft template to perform the oxidative polymerization of aniline, allowing the encapsulation of a self-healing agent at the same time. The release behavior of the self-healing agent was studied as a function of the oxidation state of the formed polymer shells. This is the first time that a release of hydrophobic chemicals was triggered by a redox stimulus from capsules formed with conducting polymers.

Afterwards, we show a new design for nanocontainers that allows for a selective release of one payload by pH change and another payload by chemical reduction of the nanocontainers shell. Polyaniline was chosen as material to build the shell of the nanocontainers. Unlike other pH- and redox-responsive systems reported in the literature that needs several functional components,[50-52] the PANI structure has the important advantage to be both redox- and pH-responsive with two imine nitrogens having pK_a ~ 1.1 and ~ 2.6 in the backbone.[53] The two selected payloads to be delivered were 3-nitrosalicylic acid (3-NisA) and 2-mercaptobenzothiazole (MBT). Both molecules are active substances known to be corrosion inhibitors. The first molecule has a pK_a around 3 and therefore its solubility in water can be controlled by pH change. The second molecule can bind to gold nanoparticles on the surface of PANI shell and later be released upon redox potential.

To exploit another possibility for corrosion protection, we introduce amphiphilic random copolymers that are designed to bear a corrosion inhibitor as side group, which can be released upon activation by chemical or electrochemical reduction due to its disulfide bridge to the copolymer chain. Polymer nanoparticles are obtained by self-assembly of the copolymers in water. A model dye is encapsulated in the nanoparticles and its release is triggered by reductive cleavage of the copolymer, leading hence to the co-release of the corrosion inhibitor. Unlike other disulfide-based delivery systems in which useless hydrophobic aggregates or non-functional byproducts are usually produced,[54-62] this system has the priority to co-release functional molecules that can be used for anti-corrosion.

Finally, using the electrospinning process, various self-healing agents were able to be encapsulated to the core of TiO_2 fibers. The possibility to design multifunctional fibers which can respond to multiple stimuli was also exhibited by combining the electrospinning with the miniemulsion techniques. This strategy provides possibility to develop fiber composites with multiple functionalities hence lead to more potential application.

References

[1] White, S. R.; Sottos, N. R.; Geubelle, P. H.; Moore, J. S.; Kessler, M. R.; Sriram, S. R.; Brown, E. N.; Viswanathan, S. *Nature* **2001**, *409*, 794.

[2] Chen, X.; Dam, M. A.; Ono, K.; Mal, A.; Shen, H.; Nutt, S. R.; Sheran, K.; Wudl, F. *Science* **2002**, *295*, 1698.

[3] Zheludkevich, M. L.; Shchukin, D. G.; Yasakau, K. A.; Möhwald, H.; Ferreira, M. G. S. *Chem. Mater.* **2007**, *19*, 402.

[4] Yuan, Y. C.; Yin, T.; Rong, M. Z.; Zhang, M. Q. *Express Polym. Lett.* **2008**, *2*, 238.

[5] Cordier, P.; Tournilhac, F.; Soulié-Ziakovic, C.; Leibler, L. *Nature* **2008**, *451*, 977.

[6] Cho, S. H.; White, S. R.; Braun, P. V. *Adv. Mater.* **2009**, *21*, 645.

[7] Hager, M. D.; Greil, P.; Leyens, C.; van der Zwaag, S.; Schubert, U. S. *Adv. Mater.* **2010**, *22*, 5424.

[8] Yoon, J. A.; Kamada, J.; Koynov, K.; Mohin, J.; Nicolaÿ, R.; Zhang, Y. Z.; Balazs, A. C.; Kowalewski, T.; Matyjaszewski, K. *Macromolecules* **2012**, *45*, 142.

[9] Nakahata, M.; Takashima, Y.; Yamaguchi, H.; Harada, A. *Nat. Commun.* **2011**, *2*, 511.

[10] Deng, G.; Li, F.; Yu, H.; Liu, F.; Liu, C.; Sun, W.; Jiang, H.; Chen, Y. *ACS Macro Lett.* **2012**, *1*, 275.

[11] Yan, Q.; Feng, A.; Zhang, H.; Yin, Y.; Yuan. J. *Polym. Chem.* **2013**, *4*, 1216.

[12] Ma, Y. J.; Dong, W.-F.; Hempenius, M A.; Möhwald, H.; Vancso, G. J. *Nat. Mater.* **2006**, *5*, 724.

[13] Wen, H.; Dong, C.; Dong, H.; Shen, A.; Xia, W.; Cai, X.; Song, Y.; Li, X.; Li, Y.; Shi, D. *Small* **2012**, *8*, 760.

[14] Luo, Z.; Cai, K.; Hu, Y.; Zhao, L.; Liu, P.; Duan, L.; Yan, W. *Angew. Chem. Int. Ed.* **2011**, *123*, 666.

[15] Cho, H.; Bae, J.; Garripelli, V. K.; Anderson, J. M.; Jun, H.-W.; Jo, S. *Chem. Commun.* **2012**, *48*, 6043.

[16] de Gracia Lux, C.; Joshi-Barr, S.; Nguyen, T.; Mahmoud, E.; Schopf, E.; Fomina, N.; Almutairi, A. *J. Am. Chem. Soc.* **2012**, *134*, 15758.

[17] Staff, R. H.; Gallei, M.; Mazurowski, M.; Rehahn, M.; Berger, R.; Landfester, K.; Crespy, D. *ACS Nano* **2012**, *6*, 9042.

[18] Lallana, E.; Tirelli, N. *Macromol. Chem. Phys.* **2013**, *214*, 143.

[19] Gracia, R.; Mecerreyes, D. *Polym. Chem.* **2013**, *4*, 2206.

[20] MacDiarmid, A. G. *Angew. Chem. Int. Ed.* **2001**, *40*, 2581.

[21] Abidian, M. R.; Kim, D. H.; Martin, D. C. *Adv. Mater.* **2006**, *18*, 405.

[22] Baughmann, R. H. *Synth. Met.* **1996**, *78*, 339.

[23] Baker, C. O.; Shedd, B.; Innis, P. C.; Whitten, P. G.; Spinks, G. M.; Wallace, G. G.; Kaner, R. B. *Adv. Mater.* **2008**, *20*, 155.

[24] Molberg, M.; Crespy, D.; Rupper, P.; Nuesch, F.; Manson, J. A. E.; Lowe, C.; Opris, D. M. *Adv. Funct. Mater.* **2010**, *20*, 3280.

[25] Tseng, R. J.; Haunag, J.; Ouyang, J.; Kaner, R. B.; Yang, Y. *Nano Lett.* **2005**, *5*, 1077.

[26] Gustafsson, G.; Cao, Y.; Treacy, G. M.; Klavetter, F.; Colaneri, N.; Heeger, A. J. *Nature* **1992**, *357*, 477.

[27] McQuade, D. T.; Pullen, A. E.; Swager, T. M. *Chem. Rev.* **2000**, *100*, 2537.

[28] Bhadra, S.; Khastgir, D.; Singha, N. K.; Lee, J. H. *Prog. Polym. Sci.* **2009**, *34*, 783.

[29] Cecchetto, L.; Ambat, R.; Davenport, A. J.; Delabouglise, D.; Petit, J. P.; Neel, O. *Corros. Sci.* **2007**, *49*, 818.

[30] Rohwerder, M.; Duc, L. M.; Michalik, A. *Electrochim. Acta* **2009**, *54*, 6075.

[31] Rohwerder, M.; Isik-Uppenkamp, S.; Amarnath, C. A. *Electrochim. Acta* **2011**, *56*, 1889.

[32] Niu, Z.; Zhang, Z.; Hu, Z.; Lu, Y.; Han, C. C. *Adv. Funct. Mater.* **2003**, *13*, 949.

[33] Jackowska, K.; Biegunski, A. T.; Tagowska, M. *J. Solid State Electrochem.* **2008**, *12*, 437.

[34] Li, C. Y.; Chiu, W. Y.; Don, T. M. *J. Polym. Sci., Polym. Chem.* **2007**, *45*, 3902.

[35] Zhang, L.; Wan, M. *Adv. Funct. Mater.* **2003**, *13*, 815.

[36] Wei, Z.; Wan, M. *Adv. Mater.* **2002**, *14*, 1314.

[37] Crespy, D.; Landfester, K. *Beilstein J. Org. Chem.* **2010**, *6*, 1132.

[38] Schaeffel, D.; Staff, R. H.; Butt, H. J.; Landfester, K.; Crespy, D.; Koynov, K. *Nano Lett.* **2012**, *12*, 6012.

[39] Crespy, D.; Landfester, K. *Soft Matter* **2011**, *7*, 11054.

[40] Herrmann, C.; Crespy, D.; Landfester, K. *Colloid Polym. Sci.* **2011**, *289*, 1111.

[41] Schwab, M. G.; Crespy, D.; Feng, X. L.; Landfester, K.; Müllen, K. *Macromol. Rapid Commun.* **2011**, *32*, 1798.

[42] van den Dungen, E. T. A.; Klumperman, B. J. Polym. Sci., *Polym. Chem.* **2010**, *48*, 5215.

[43] Ouyang, X. B.; Huang, X. Q.; Pan, Q. H.; Zuo, C. Q.; Huang, C.; Yang, X. L.; Zhao, Y. *B. J. Dent.* **2011**, *39*, 825.

[44] Fickert, J.; Makowski, M.; Kappl, M.; Landfester, K.; Crespy, D. *Macromolecules* **2012**, *45*, 6324.

[45] Fickert, J.; Rupper, P.; Graf, R.; Landfester, K.; Crespy, D. *J. Mater. Chem.* **2012**, *22*, 2286.

[46] Zhao, Y.; Fickert, J.; Landfester, K.; Crespy, D. *Small* **2012**, *8*, 2954.

[47] Fickert, J.; Wohnhaas, C.; Turshatov, A.; Landfester, K.; Crespy, D. *Macromolecules* **2013**, *46*, 573.

[48] Marie, E.; Rothe, R.; Antonietti, M.; Landfester, K. *Macromolecules* **2003**, *36*, 3967.

[49] Bhadra, S.; Singha, N. K.; Khastgir, D. *Synth. Met.* **2006**, *156*, 1148.

[50] Liu, R.; Zhao, X.; Wu, T.; Feng, P.Y. *J. Am. Chem. Soc.* **2008**, *130*, 14418.

[51] Klaikherd, A.; Nagami, C.; Thayumanayan, S. *J. Am. Chem. Soc*. **2009**, *131*, 4830.

[52] Bird, R.; Freemont, T.; Saunders, B. R. *Soft Matter* **2012**, *8*, 1047.

[53] Huang, W. S.; MacDiarmid, A. G.; Epstein, A. J. *J. Chem. Soc. Chem. Commun*. **1987**, 1784.

[54] Liu, J.; Pang, Y.; Huang, W.; Zhu, Z.; Zhu, X.; Zhou, Y.; Yan, D. *Biomacromolecules* **2011**, *12*, 2407.

[55] Chen, W.; Zhong, P.; Meng, F.; Cheng, R.; Deng, C.; Feijen, J.; Zhong, Z. *J. Control. Release* **2013**, *169*, 171.

[56] Wang, Y.; Wang, H.; Liu, G.; Liu, X.; Jin, Q.; Ji, J. *Micromol. Biosci.* **2013**, *13*, 1084.

[57] Yuan, W.; Zou, H.; Guo, W.; Shen, T.; Ren, J. *Polym. Chem.* **2013**, *4*, 2658.

[58] Xuan, J.; Han, D.; Xia, H.; Zhao, Y. *Langmuir* **2014**, *30*, 410.

[59] Wang, Y.-C.; Wang, F.; Sun, T.-M.; Wang, J. *Bioconjugate Chem.* **2011**, *22*, 1939.

[60] Li, J.; Huo, M.; Wang, J.; Zhou, J.; Mohammad, J. M.; Zhang, Y.; Zhu, Q.; Waddad, A. Y.; Zhang, Q. *Biomaterials* **2012**, *33*, 2310.

[61] Bahadur K. C., R.; Thapa, B.; Xu, P. *Mol. Pharm.* **2012**, *9*, 2719.

[62] Ryu, J.-H.; Roy, R.; Ventura, J.; Thayumanavan, S. *Langmuir* **2010**, *26*, 7086.

2. Theoretical Background

2.1 Self-healing

Originating from biology, self healing is described as the ability of a system to repair itself and recover its functionality using resources inherently available to it.[1] Self-healing materials are then smart system possessing the ability to heal themselves upon damages. These materials include polymers, metals, ceramics, and their composites. The damage occurring to the self-healing system can be mechanical damage, thermal damage, corrosion, or other means that can be considered as "trigger" to initiate the self healing.

The most studied approaches for building self-healing systems up to now are mainly classified in two categories: Intrinsic and extrinsic self-healing systems. The latter one is usually divided to self-healing systems based on capsular or vascular methods. The scheme shown in **Figure 2.1** demonstrates the basic concept of these three self-healing systems.

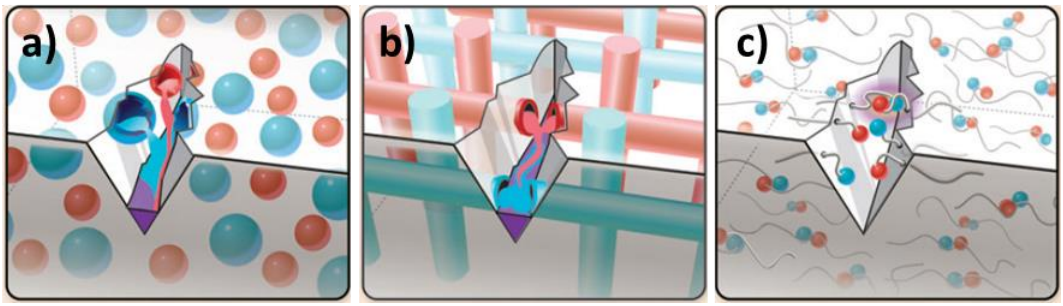

Figure 2.*1* *Illustration of different self-healing systems based on:* ***a)*** *capsular;* ***b)*** *vascular; and* ***c)*** *intrinsic method. This scheme is adapted from Blaiszik et al.*[1] *Copyright (2010) Annual Reviews.*

In extrinsic self-healing system based on capsules or vessels loaded with healing agents, the self-healing process is achieved upon the release of healing agents when capsules or vessels are broken by mechanical damage or other stimuli, whereas in the case of intrinsic systems, the self-healing process is mainly realized by using reversible bonding in the materials.

2.1.1 Intrinsic self-healing

In intrinsic self-healing systems, the matrix polymers inherently possess the ability to repair the cleaved bridges. The healing process is classified in three main types as shown in **Figure**

2.2, *i.e.* healing by reversible bonding, chain re-entanglement, or non-covalent bonding process in the polymeric matrix.

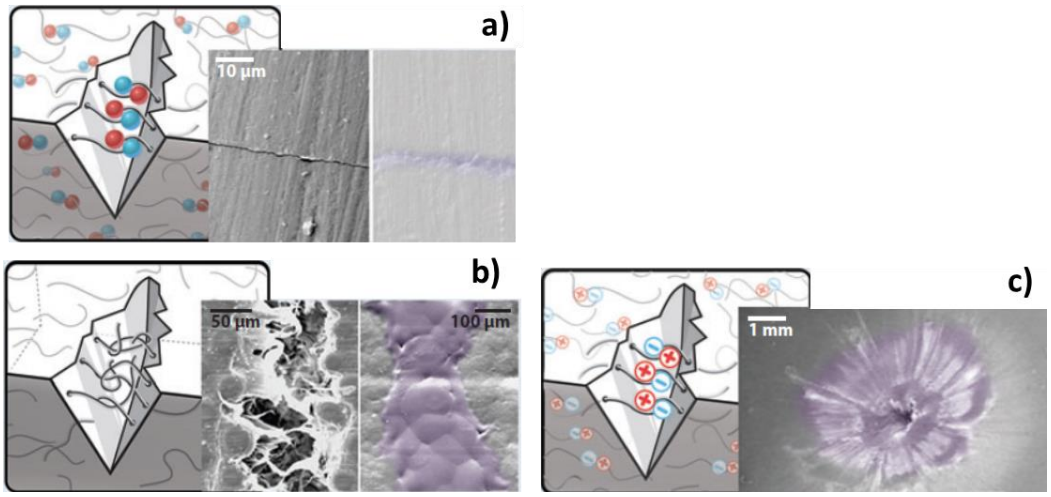

Figure 2.2 *Illustration of different intrinsic self-healing systems adapted from Blaiszik et al.[1] Copyright (2010) Annual Reviews.* ***a)*** *System based on reversible bonding, e.g. systems applying Diels-Alder-retro-Diels-Alder reactions, adapted with permission from Murphy et al.[2] Copyright (2008) American Chemical Society;* ***b)*** *System based on chain entanglement, e.g. the system of epoxy/poly(ε-caprolactone) (PCL) phase-separated blends, adapted with permission from Luo et al.[3] Copyright (2009) American Chemical Society; and* ***c)*** *System based on noncovalent bonding, e.g. an ionomer system of poly(ethylene-co-methacrylic acid) adapted from Varley et al.[4] Copyright (2008) with permission from Elsevier.*

When reversible bonding is used for self healing, the most popular system is based on Diels-Alder (DA) and retro-Diels-Alder (rDA) reactions.[5-7] For instance, by using the reversible DA cycloaddition reaction (**Figure 2.3**), Chen *et al.*[7] reported a kind of thermally re-mendable polymeric material which can repeatedly mend or "re-mend" itself. The self-healing process was realized by the cleavage of DA adducts upon heating followed with reformation of new covalent bonds upon cooling.

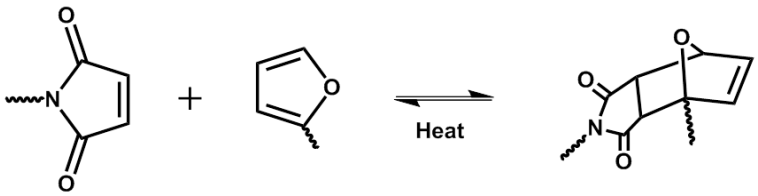

Figure 2.3 *The mechanism of intrinsic self-healing process by using Diels-Alder (DA) and retro-Diels-Alder (rDA) reaction.*

The second strategy for intrinsic self healing involves chain re-entanglement between the two broken sections of a polymer matrix when they are brought together. Healing of the cracked polymers is actuated by thermal diffusion of polymer chains across the interface between the two fractured edges. One example is a class of thermally mendable polymeric materials composed of epoxy/poly(ε-caprolactone) (PCL) phase-separated blends.[3] In the system, the molten PCL phase induced by heating could fill the crack plane by its volumetric thermal expansion process.

The third approach for intrinsic self healing is related to non-covalent bonding process. In this case, the healable materials usually embody latent functional groups which can react with each other and form new covalent bonds to bridge the damaged area. The formation of new bonds is triggered by external stimuli such as UV irradiation.[8]

In addition to the above mentioned strategies, systems involving for example metal-ligand interactions,[9] hydrogen-bonding interactions,[10] aromatic π-π stacking interactions,[11] or molecular diffusion[12] for intrinsic self-healing were also investigated.

2.1.2 Extrinsic self-healing: capsular type

Different from an intrinsic self-healing system in which the healing process is achieved by using functions inherently belong to the material itself, an extrinsic self-healing system usually refer to the systems containing external healing functionalities, *i.e.* the introduction of healing agents.

The first main extrinsic self-healing systems are based on capsular method. These systems involve capsular reservoirs loaded with healing agents which could release out upon rupture of the capsules. Depending on different sequestered method of the self-healing agent, four main strategies are proposed. (**Figure 2.4**)

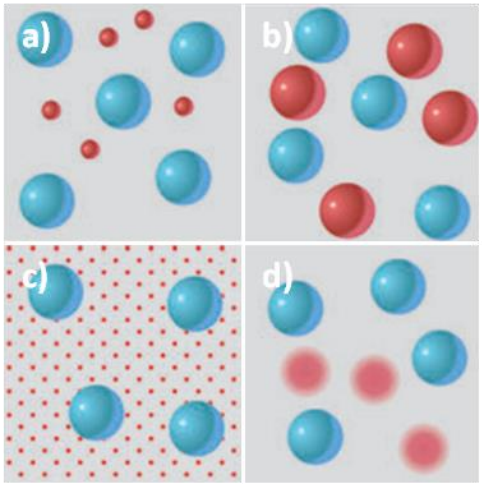

Figure 2.4 *Self-healing materials based on capsules. The scheme is adapted from Blaiszik et al.*[1] *Copyright (2010) Annual Reviews.* ***a)*** *Capsule-catalyst system in which the catalyst is dispersed in a matrix and the healing agents are loaded in the capsules.* ***b)*** *Multi-capsule system in which different components of healing agents are loaded in separated capsules.* ***c)*** *Latent functionality system in which functional groups in a matrix could react with healing agents released from capsules upon damage.* ***d)*** *Phase separated system in which one healing agent is phase separated in the matrix while the other healing agents are loaded in the capsules.*

One representative example of the self-healing system involving capsules and catalyst was proposed by Whites *et al.*[13] By dispersing Grubbs' first-generation catalyst and microcapsules loaded with monomer dicyclopentadiene (DCPD) in an epoxy matrix, they were able to design a polymer composite with autonomic healing property (**Figure 2.5**). Cracks ruptured the microcapsules and induced the release of DCPD into the crack gap by capillary force. When the released monomers contacted the catalysts dispersed in the matrix, ring-opening metathesis polymerization (ROMP) took place. After polymerization, the crack gap was filled with the formed polymers and therefore the damage was healed (**Figure 2.5c**).

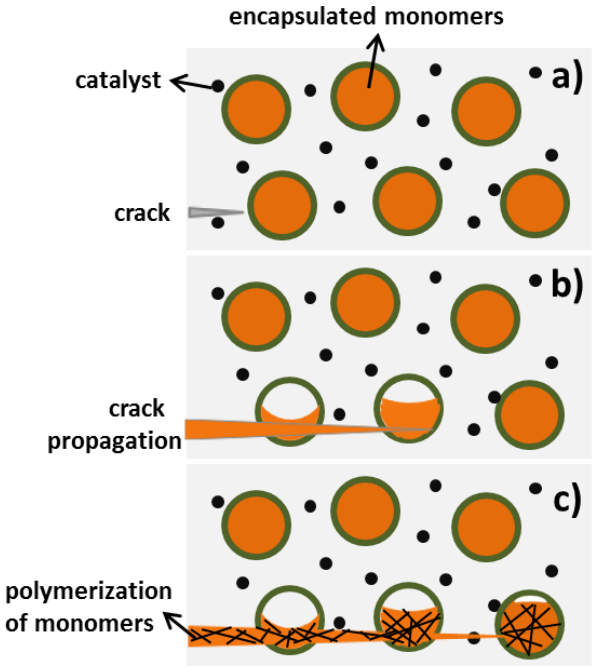

Figure 2.5 *Concept of self-healing system based on capsules adapted from White et al.*[13] *Copyright (2001) Nature Publishing Group.* ***a)*** *The catalysts and microcapsules encapsulated with monomers are dispersed in the matrix.* ***b)*** *Crack occurs and breaks the microcapsules.* ***c)*** *Polymerization of the released monomers takes place after monomers contact with catalyst in the crack gap. The formed polymers fill the crack plane and heal the defect.*

In the multi-capsule system, healing agents that can react with each other are separately encapsulated (**Figure 2.4b**). For example, Yuan *et al.*[14] reported self-healing polymeric composites in which two types of microcapsules containing epoxy or a mercaptan hardener were embedded. The release of the two reactive components was then triggered by the breakage of the capsules. Thanks to the high flow ability and molecular miscibility of the two healants, self healing was achieved after the two released components contacted to react.

The latent functionality system refers to a system in which the matrix is capable of interacting with healing agents which are loaded in the capsules and release out afterwards. (**Figure 2.4c**) The difference of this system from the above mentioned ones is that the matrix itself contains reactive functional groups which can be used for self-healing reaction. A system involving solvent-based self healing is one example.[15,16] In an epoxy matrix containing residual amines, capsules loaded with a mixture of epoxy monomer and solvent (chlorobenzene) were embedded. After the fracture of the capsules, the release of solvent facilitated the reaction between the residual amines and the epoxy in the matrix.

Furthermore, the release of epoxy monomers to the crack plane provided more chance for the curing process.

The last capsule-based system for self healing involves both healing agents that phase-separated in the matrix and that are encapsulated into capsules (**Figure 2.4d**). One example of this system was found in the research of Cho *et al*.[17] A siloxane-based healing agent mixture, *i.e.* hydroxyl end-functionalized polydimethylsiloxane (HOPDMS) and polydiethoxysiloxane (PDES), phase-separated as droplets in the matrix. The tin-based catalyst for polycondensation between HOPDMS and PDES was encapsulated in polyurethane microcapsules and embedded in the matrix. The polycondensation between HOPDMS and PDES was only initiated by the catalyst which was released upon damage of the microcapsules.

2.1.3 Extrinsic self-healing: vascular type

Except for capsules, vascular containers could also be used for delivering healing agents (**Figure 2.6**). One of the differences between capsular- and vascular-based healing systems is that the encapsulation of healing agents in capsules is performed before the incorporation of capsules in the matrix. However, in the case of a vascular-based system, the vascular network is usually integrated to the matrix followed by the sequestration of healing agents. In addition, the vascular-based system provides large reservoirs for healing agents and is therefore more capable of handling multiple damages.[1]

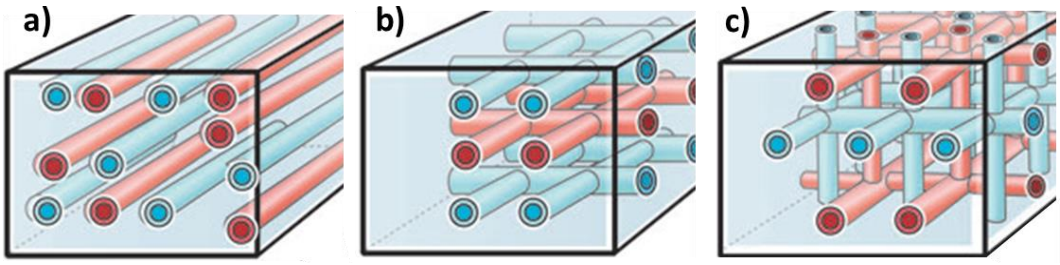

Figure 2.6 *Vascular self-healing systems according to the vascular connectivity.* ***a)***, ***b)***, *and* ***c)*** *respectively represent one-dimensional (1D), two-dimensional (2D) and three-dimensional (3D) network in which healing agents are encapsulated into the channels/fibers. This scheme is adapted from Blaiszik et al.*[1] *Copyright (2010) Annual Reviews.*

The most direct and simple way to fabricate vascular-based healing system is to introduce fiber network with 1D into the composite matrix.[18-20] For example, Bleay *et al*.[21] reported a

smart repair system in which glass fibers filled with a two-part epoxy resin were dispersed in the polymer matrix. The repairing process was found when the repair medium was released from the fractured fibers to the damaged area of the composites.

Although it is more difficult to manufacture 2D or 3D networks than 1D ones, the former two provide several advantages over the latter one. For example, by employing the interconnected nature of 3D networks, it is possible to supply monomers to the reservoirs and repeatedly heal the samples for several consecutive cycles.[22] The number of healing cycles could be further increased by using isolated interpenetrating networks to load different components for self-healing reactions.[23,24]

2.2 Corrosion mechanism

2.2.1 Corrosion process

Corrosion is described as the process when materials (usually metals) are gradually destructed by a chemical reaction in a surrounding environment.[25,26] A typical corrosion process of metal is depicted in **Figure 2.7**.

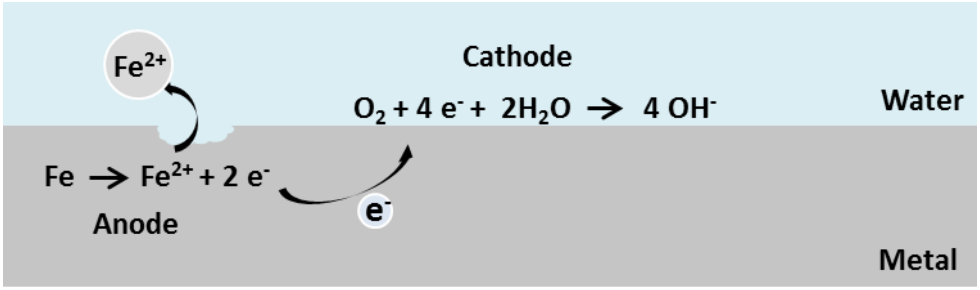

Figure 2.7 *Schematic illustration of the corrosion process in metallic system. Iron is used as an example.*

As described in **Figure 2.7**, oxidative and reductive reactions occur in a corrosion system, which is regarded as a short-circuited electrochemical cell. At the anodic site, corrosion starts with the oxidation of metal where metal ions and electrons are produced. The generated electrons then flow through the metal to the cathodic site and reduce oxygen in the presence of water. Although reduction of oxygen is mostly common, there are other reactions possible to take place at the cathodic site, for example the reduction of protons or other metal cations:[25]

$$2\,H^+ + 2\,e^- \rightarrow H_2$$

$$M^{2+} + 2\,e^- \rightarrow M$$

where M represents a more noble metal than iron.

2.2.2 Protection from corrosion

As shown above, the corrosion cell consists of four parts: the anode where metal is oxidized and corroded, the cathode where electron-acceptors are reduced, the electrolyte which is usually water or moisture, and the electrical connection between anode and cathode which is usually a conductive wire or the metal bulk itself. The corrosion process will be stopped if any of these four components is eliminated.[27] Based on this principle, three main strategies for corrosion protection are proposed: coatings, cathodic protection, and anodic protection.[28]

Applying a protective coating on the surface is the most direct way to protect the metallic system.[29] The coatings on one hand could act as resistant material for the metal because it can reduce the exposure to the oxygen and water from the environment.[30] On the other hand, they can also be used to incorporate active compounds such as corrosion inhibitors which can suppress electrochemical reactions by forming an insulating or impermeable layer on the exposed metal.[31] Besides, by plating a more active metal layer on the substrate metal, *e.g.* a zinc layer on an iron substrate, the substrate metal can be also well protected due to the sacrificial zinc layer.[32] This process is known as galvanization.

The mechanism of cathodic protection is to make the metal surface to be protected as cathode of the electrochemical cell.[25] As was shown previously, only the anode of the short-circuited electrochemical cell is corroded. Changing the metal substrates from an anode to a cathode or decreasing the difference of electrochemical potential between anode and cathode will then put them in a safer position. The strategy is to supply electrons to the metal substrates by using, for example, an external current power source.[33] Alternatively, a more active metal could also be used as the sacrificial anode.[33]

Anodic protection is usually used to protect metals which are easily passivated.[34] The corrosion of the metal surface is then controlled by making it the anode of an electrochemical cell and moving the corrosion potential to the passive region.[31] After

forming a passivated layer the surface of the metal to be protected become inert. Supplying a small anodic current to maintain the passive status can then resist corrosion process.[35]

2.3 Intrinsically conducting polymers (ICPs)

Intrinsically conducting polymers are a class of polymers that can conduct electricity.[36] They keep the mechanical properties of conventional polymers and meanwhile possess the properties like electrical, electronic, optical properties of metal.[37] However, it was only in 1977 when iodine-doped polyacetylene was shown to exhibit a dramatic increase of electrical conductivity and a metal-insulator transition, the intrinsically conducting polymers were recognized and started to attract people's attention.[38] Alan MacDiarmid, Alan Heeger and Hideki Shirakawa who contributed to the discovery and development of conductive polymers were then jointly awarded the 2000 Nobel Prize in Chemistry.[37, 39]

Except for polyacetylene (PA), other common conducting polymers including polyaniline (PANI), polypyrrole (PPy), polythiophene (PT), and their derivatives are also widely investigated due to their good thermal and environment stability compared to PA.[37, 40, 41] (**Figure 2.8**)

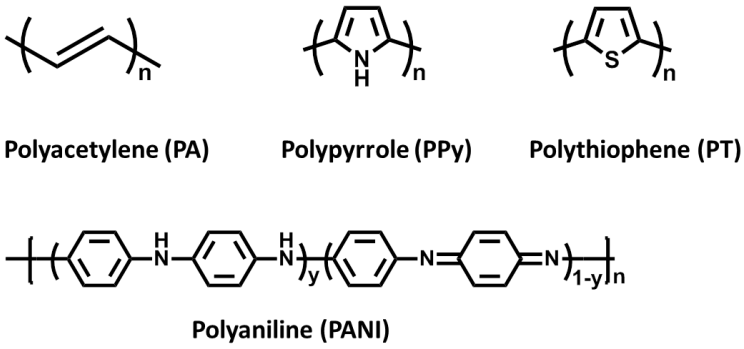

Figure 2.8 *Chemical structures of common conducting polymers.*

Among all the conducting polymers, polyaniline is one of the most studied because it has different oxidation and protonated states.[42] Since the topics presented in this thesis are mostly related to PANI, discussion about synthesis, properties and applications relevant to PANI is mainly described in the present chapter.

2.3.1 Synthesis of polyaniline (PANI)

Methods to synthesize polyaniline include electrochemical and chemical polymerization. The synthesis process by using electrochemical technique is usually performed by using a three-electrode setup (working, counter, and reference electrodes) submersed in a solution where the monomer and electrolyte are dissolved.[40] Oxidative polymerization of monomers then takes place at the working electrode when current passes through the solution. The insoluble polymer chains will deposit on the surface of electrode and form a film of polyaniline.[40, 43]

In addition to the electrochemical synthesis of PANI, chemical polymerization of aniline monomers initiated by oxidants such as ammonium persulfate is also widely used. (**Figure 2.9**) Although still debatable, one common mechanism for the oxidative polymerization of aniline is referred to as a "non-classical chain polymerization" according to the reports of Wei *et al*.[44,45] This process involves oxidative coupling in which the oxidation of aniline monomers first form a cation radical followed by the coupling process to form di-cations. Repetition of this process leads to the final polymers as shown in **Figure 2.10**.[44-46]

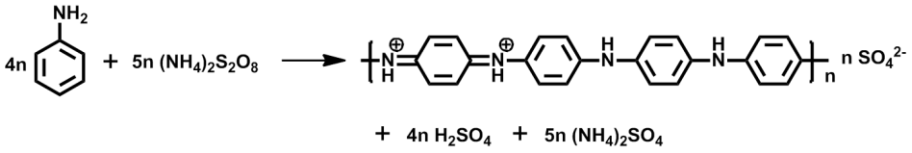

Figure 2.9 *Chemical polymerization of aniline initiated by ammonium persulfate.*

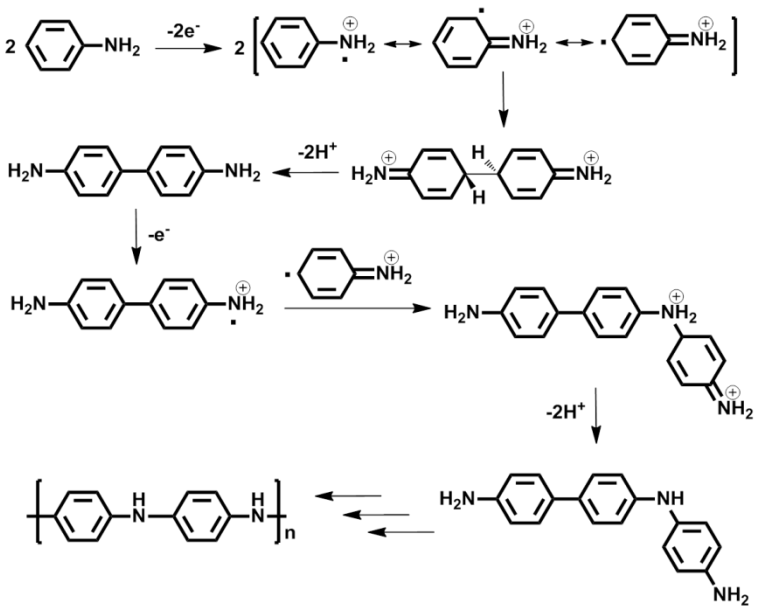

Figure 2.10 *Oxidative polymerization mechanism of aniline adapted with permission from Heth et al.*[47] *Copyright (2010) American Chemical Society.*

Due to the difference of polymerization techniques, PANI films are mainly produced by electrodeposition method, whereas a variety of PANI structures in the form of, for example particles,[48-50] capsules,[51,52] tubes,[53-55] and fibers[56-58] could be formed by using chemical polymerization.[59] Polyanilines are usually formed directly to these desired structures due to their poor solubility.[60] There are also various preparation methods to synthesize distinct PANI structures.[61] One is the thoroughly reported hard-template approach which involves the support and then removal of a template.[51,62,63] The other approach is called soft-template synthesis which is often referred to as template-free or self-assembly method.[64-66] Compared to hard-template method which usually needs multiple steps to obtain the final structure, the soft-template synthesis is much simpler and inexpensive. For example, using emulsions as soft template, hollow microspheres of PANI with salicylic acid (~1.5-3.1 μm in diameter) or β-naphthalene sulfonic acid (0.36-1.2 μm in diameter) as dopant were obtained.[67,68]

2.3.2 Properties of PANI

PANI with different oxidation states can be obtained depending on y (**Figure 2.8)**. Characterized by using the ratio of amine to imine nitrogens, the average oxidation state of PANI can be varied continuously from the fully reduced leucoemeraldine (y=1) to half-oxidized emeraldine (y=0.5) and then to the fully oxidized pernigraniline (y=0).[37,69] The half-oxidized emeraldine is then the polyaniline with equal number of amine and imine nitrogens. It was regarded that apart from the oxidative polymerization of aniline itself, the subsequent transitions of PANI between different oxidation states are also a redox process (**Figure 2.11**).[70] Based on varied parameters used for the reaction, such as oxidation potential, pH of medium, and concentration of reactants, PANI with different oxidation states can be obtained.[70,71]

PANI with different oxidation states could be either in their base form or in the protonated salt form.[37,72,73] The protonation process is attributed to the amine and imine nitrogens exist in the backbone of PANI.[74] Depending on the oxidation state and the pH of the acid medium used, the imine nitrogen atoms with pK_a ~ 1.1 and ~ 2.6 in the polyaniline chain could in

principle be completely or partially protonated.[37,74,75] The transition of PANI among different oxidation and protonation states by chemical or electrochemical reactions could be achieved as displayed in **Figure 2.11**.

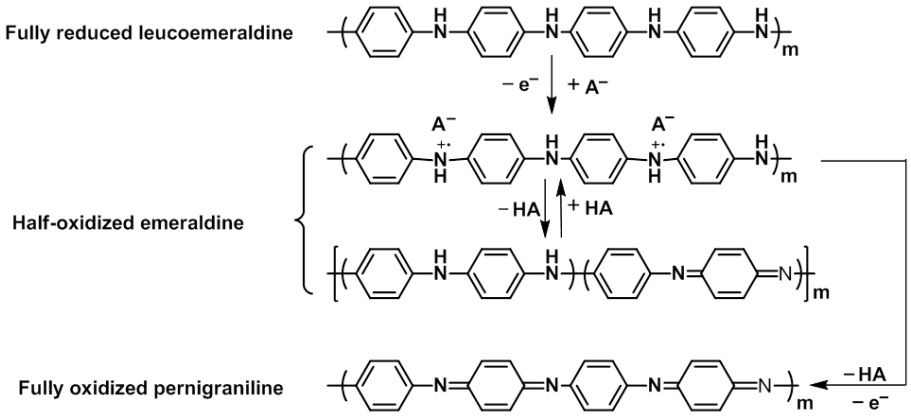

Figure 2.11 *Transition of polyaniline between different oxidation or protonation states by chemical or electrochemical reaction. This scheme is originated from Gospodinova et al.*[70] *Copyright (1998) with permission from Elsevier.*

The properties of materials are determined by their structures. Due to the possibility to have different structures, PANI exhibits distinct properties in many aspects: For instance, physical, physicochemical, or electrochemical properties are reflected by its oxidation potential,[76] optical absorption,[77] pK_a,[74] conductivity,[69] and crystallinity.[78] The conductivity of PANI, for example, depends on two aspects: the oxidation and the protonated states of PANI.[74] When doped with acid, emeraldine base will convert to highly electrically conducting emeraldine salt in which the PANI chain is half-oxidized and imine nitrogens in the chain are protonated.[72,74] The increased conductivity is attributed to the significant π delocalization in the PANI backbone.[74] In comparison, the fully reduced leucoemeraldine and fully oxidized pernigraniline forms of PANI cannot exhibit much conductivity even doped with protonic acid.

In addition to the structure-related properties mentioned above, other properties such as permeability,[79,80] hydrophilicity,[79] chain elasticity,[81] hydrogen-bonding interaction,[82] and density[83] were also found to be switchable according to different states of PANI. Schmidt *et al.*[79] reported that electrochemically formed PANI membranes in the oxidized state exhibited higher permeability to water than the reduced state. Two possible reasons were used to explain the observation: increase in hydrophilicity and structural changes during

oxidation.[79,80] Firstly, the counter-ions entered into PANI film during oxidation could act as a carrier for water molecules. Secondly, upon oxidation, more imino groups were found in the PANI backbones leading to a planar and perhaps rigid structure. Thus, more water swelled the polymer membranes.[79] With regard to the flexibility of PANI chain, Yu *et al.*[81] also reported that the oxidized PANI is more rigid than the reduced PANI. This observation was explained by the conformational difference arising from the changed structure. In reduced PANI, more bezenoid diamine exists in the backbone and therefore most of the nitrogen atoms are connected to the aromatic rings by rotatable single bonds. However, in oxidized PANI where imino groups are present in the backbone, the nitrogens mostly connect to the aromatic rings by double bonds. The increased rigidity of PANI chain was then explained by these non-rotatable double bonds.[81]

Other characteristics related to structure change of PANI include the density and molecular hydrogen bonding interaction. For example, Kim *et al*.[82,83] showed that the emeraldine base form packs more compactly than the leucoemeraldine base due to the amine-imine hydrogen bonding interaction that exists in emeraldine (**Figure 2.12**). Based on this characteristic, amphiphilic molecules containing tetraaniline and poly(ethylene glycol) blocks were designed. It was found that the vesicular system formed from these amphiphilic molecules exhibited a switchable micellar-to-vesicular transition upon electrochemical oxidation and reduction.

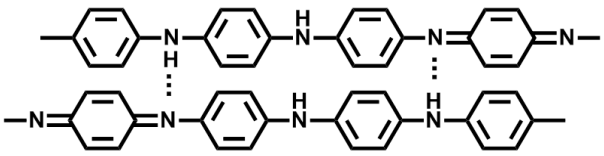

Figure 2.12 *Intermolecular hydrogen bonding interaction between amine-imine in emeraldine form of PANI.*

2.3.3 Application of PANI: corrosion protection

Due to the properties corresponding to different states, PANI has found its use in application of, for example, biomedical engineering,[40] gas or chemical sensors,[56,84] actuators,[85] digital memory device,[86] capacitors and energy storage devices,[87,88] ion-exchange materials,[89] corrosion protection,[31] and solar cell.[90] In the present section, the description of PANI used for corrosion protection is mainly presented.

According to the previous reports, conducting polymers such as PANI could be used for corrosion control in metallic system.[31,43] The mechanism for corrosion protection was assumed to include several aspects such as barrier protection, inhibition, anodic protection, and other mechanisms. As already mentioned in the previous **section 2.2.2**, there are different approaches to protect metal from corrosion. The most direct way is to apply a coating on the surface of the metal to isolate it from the outside corrosive environment.[29] Therefore, a PANI coating would also work as a barrier to protect the metal. Besides, as was mentioned already, the permeability of PANI membrane, for example, for water molecules or gas, is possible to be switched upon the different protonation or oxidation states.[79,91,92] Then the barrier function of PANI coatings for corrosion protection could be in principle adjusted by varying the states of PANI.

According to many studies, however, PANI coatings used for corrosion protection act not only as barrier.[93,94] For example, it was found that PANI could also act as an corrosion inhibitor in that the protonated diimine in PANI might form a ligand with the metal surface which improves the adhesive interaction.[95]

Another mechanism that PANI is used for anti-corrosion is the anodic protection. As was described previously, the main idea for anodic protection is to move the corrosion potential of the metal to the passive region.[31] In the case when conducting polymers in the oxidized state were used for anodic protection, the possible reactions are shown in **Figure 2.13**. It was reported that the corrosion potential of metal coated with PANI is higher than the bare metal. The ennobling process then makes the metal more passive to corrode.[31,96,97]

a) Reaction between oxidized intrisically conducting polymer (ICP) and metal (M):

$$\frac{1}{n}M + \frac{1}{m}ICP^{m+} + \frac{y}{n}H_2O \longrightarrow \frac{1}{n}M(OH)_y^{(n-y)+} + \frac{1}{m}ICP^0 + \frac{y}{n}H^+$$

b) Re-oxidized reaction of ICP:

$$\frac{m}{4}O_2 + \frac{m}{2}H_2O + ICP^0 \longrightarrow ICP^{m+} + m\,OH^-$$

Figure 2.13 a) *Possible reaction between oxidized ICP^{m+} and metal proposed for anodic protection;* ***b)*** *The reduced ICP^0 is possible to be re-oxidized in the presence of oxygen and water. These two reactions are adapted from Spinks et al.[31] Copyright (2001) with permission from Springer.*

The use of the mechanism related to the shift of the electrochemical interface was another possibility to protect metals with PANI.[31] For example, Schauer *et al*.[98] suggested that the PANI coating played a role in separating the cathodic site from the anodic site of the corrosion process by shifting the electroactive interface from the metal/PANI to the PANI/solution interface. This process assisted the decrease in concentration of hydroxyl ions at the interface of metal/PANI and thus reduced the chance of detachment between metal and the coating.[98]

Last but not the least, PANI coatings for anti-corrosion could also be achieved by doping with anionic corrosion inhibitors. Corrosion protection was realized by the reduction of PANI upon corrosion due to the galvanic coupling between corroded metal and PANI. The doping corrosion inhibitors were then released out upon reduction of PANI.[43,99-102] One drawback of this anions-doped PANI system, however, is that instead of the release of anionic inhibitors, fast incorporation of cations to the PANI backbones is also possible and results in the loss of functions of the coating system.[101,103]

2.4 Formation of capsules

Capsules are usually referred to as containers with shells of polymeric or inorganic material and cores loaded with liquid material. Due to their core-shell structure, capsules can be used, for example, as drug delivery systems,[104] for corrosion protection,[105] and self-healing materials.[106] One of the advantages of capsules involves the protection of encapsulated components in the core during their application. Besides, by functionalizing the shell, it is also possible to make the capsules stimuli-responsive.[107]

According to reported literatures, many approaches can be used to synthesize capsules. Methods such as layer-by-layer technique,[108] solvent evaporation-induced phase separation,[109] polymerization-induced phase separation,[110] and interfacial polymerization[111] can be used for the preparation of capsules. Of all these methods, the most studied ones are based on colloidal system.

2.4.1 Colloids and their stability

A colloid is a heterophase mixture containing at least two immiscible components, with one of which (dispersed phase) distributes in the other (continuous phase).[112] Stability of colloids,

which depends on the balance of attractive and repulsive forces between individual particles, is crucial for their application. Without external interference, colloids tend to aggregate due to the attractive interaction between particles arising from van der Waals forces. To keep colloids stable, repulsive forces between colloidal particles are needed. Two main types of stabilization of colloidal dispersions are considered: Electrostatic stabilization and steric stabilization, which respectively refer to coulombic repulsion between two similarly charged surfaces and entropy hindrance of polymer chains (**Figure 2.14**).

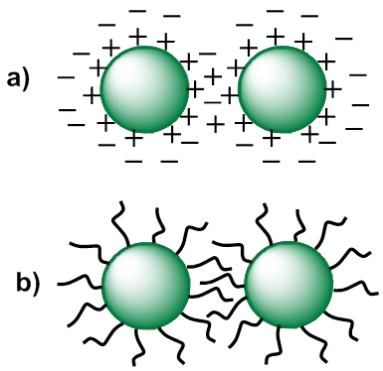

Figure 2.14 *Two main types of stabilization of colloidal particles based on:* ***a)*** *electrostatic potential and* ***b)*** *steric potential.*

Electrostatic stabilization can be achieved by using charged surfactants or stabilizers. The colloid stability is determined by the combination of van der Waals attraction and electrostatic repulsion, which is known as DLVO (Derjaguin and Landau, Verwey and Overbeek) theory:[113, 114]

$$V_T = V_A + V_R$$

with V_T the potential energy of the total interaction, V_A the attractive attraction and V_R the repulsive interaction.

V_A is derived from the van der Waals' attraction between particles and given by:

$$V_A \approx \frac{-AR}{12D}$$

with A the Hamaker constant, R the radius of the particle, and D the shortest interparticle distance.

V_R represents the electrostatic repulsion which could be given by:

$$V_R \approx \psi_0 \cdot \exp(-kD) \text{ with } k = \sqrt{\frac{2c_0\ e^2}{\varepsilon\ \varepsilon_0\ k_B T}}$$

where ψ_0 is the Stern potential, *D* is the interparticle distance, *k* is a constant combining ion concentration c_0, the Boltzmann constant k_B and dielectric constants of the bulk electrolyte solution (ε) and of vacuum (ε_0). *k* is usually presented as the reciprocal of the Debye length (λ_D) which is described as the distance to which the electrostatic potential is decayed to 1/e of the surface potential.

Then the total potential energy of interaction between two like-charged particles with interparticle distance of *D* could be described as follows:

$$V_T = V_A + V_R + V_B = \frac{-AR}{12D} + \psi_0 \cdot \exp(-kD) + \frac{1}{D^{12}}$$

The strong repulsion potential (Born repulsion V_B) between particles with interparticle distance smaller than the radius of the particles is also included. The potential energy of van der Waals attraction, electrostatic repulsion, Born repulsion and the total interaction against interparticle distance are all illustrated in **Figure 2.15a**.[115] It can be seen that when two charged particles get close to each other, the electrostatic repulsion will prevent them from approaching. There exists an energy barrier (V_m) for the particles to overcome, below which the particles have no sufficient energy to contact with each other, so the colloidal dispersion is stable. However, once the energy barrier is overcompensated, the strong van der Waals attractive force will draw the particles together and irreversible coagulation (primary minimum) occurs. In some cases, a secondary minimum exists at longer distances where the aggregation of the particles is usually reversible (flocculation).

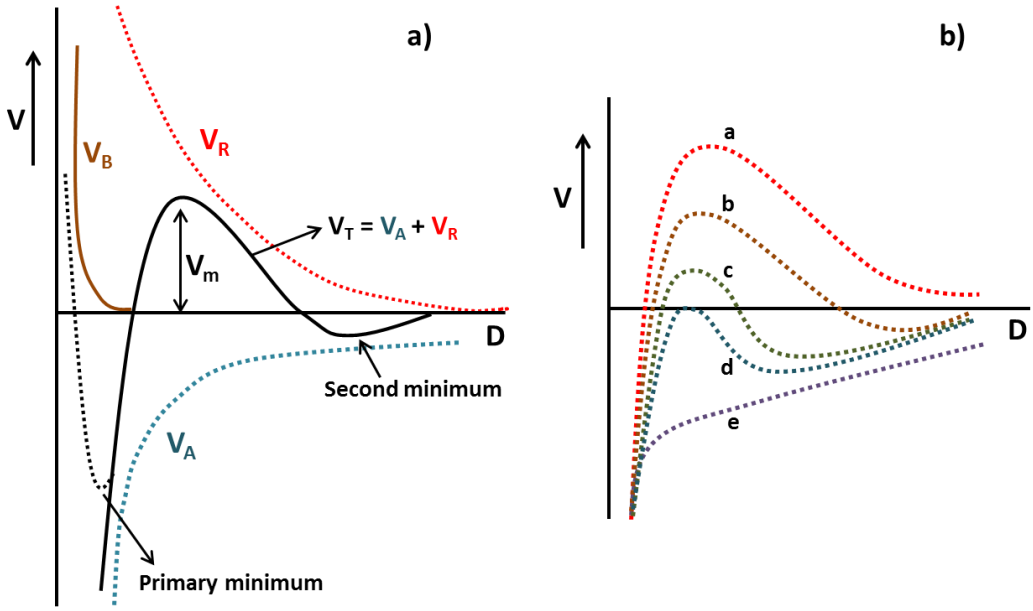

Figure 2.15 *Illustration of **a)** interaction potential between two particles with different distances according to DLVO theory; **b)** Influence of electrolyte concentration (increased from a to e) on the energy barrier. Adapted with permission from Napper.*[115] *Copyright (1970) American Chemical Society.*

The hight of energy barrier (V_m) as indicated in **Figure 2.15a** determines the stability of the colloids and could be easily influenced by the concentration of ions in the dispersion. **Figure 2.15b** shows that as electrolyte concentration in the dispersion increases, the energy barrier of the system decreases and even disappears. This observation is due to the increased screen effect of the electrolyte on the charges of the particles. The colloids then become unstable with lower energy barrier.

As was mentioned, steric stabilization is another mechanism for colloidal stability. Unlike the electrostatic stabilization which involves electrostatic repulsion usually by ionic surfactants adsorbed on the surface of particles, the steric stabilization mainly refers to the steric hindrance caused by non-ionic polymers that adsorbed or chemically attached to the surface of particles.[116]

As shown in **Figure 2.16a**, the colloidal particles are covered with polymer chains which form a protective layer with thickness δ. When the interparticle distance D is closer than 2 δ, the attached polymers chains will encounter and overlap followed with the increase of chain density and decrease of chain movement in the region between the two particles. The steric potential (V_S) then rises to resist the van der Waals attraction potential (V_A) (**Figure 2.16 b**).

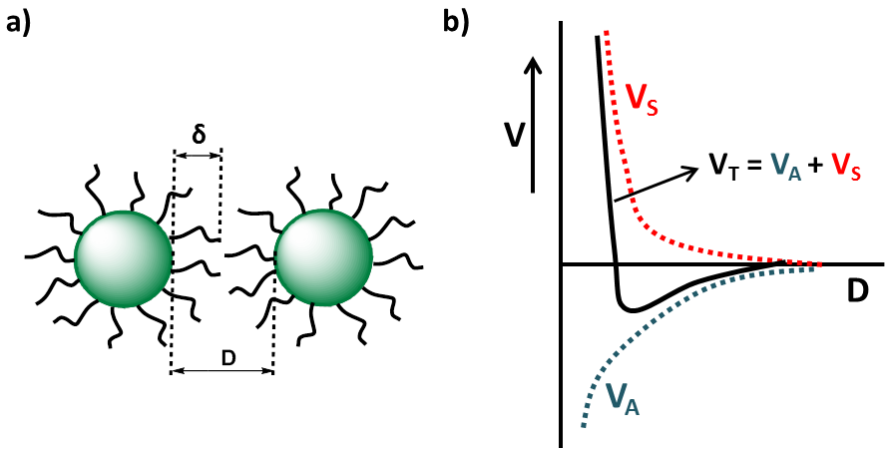

Figure 2.16 Schematic illustration of steric stabilization of colloidal particles by non-ionic polymer.[117]

Similarly to the influence of electrolyte on the electrostatic repulsion for stabilization, factors like quality of solvent, temperature, and amount of polymer adsorbed on the particles also play a role on the steric stabilization process.[118,119] For example, when a "good" solvent (Flory-Huggins parameter $\chi<0.5$) for the polymers is used, the repulsive forces between the polymer segments will make the polymer coils swell and supply a strong steric potential for the stabilization. However, when the solvent is not good enough for the polymer, *i.e.* with a polymer/solvent interaction parameter $\chi >0.5$, the polymer coils will then shrink and cannot act efficiently for the stabilization process.[119]

2.4.2 Miniemulsion

Emulsions refer to dispersed systems with liquid droplets (dispersed phase) in another non-miscible liquid (continuous phase).[120] According to the nature of the two phases, the emulsion systems can be classified in two types: oil-in-water (o/w) or direct emulsion, and water-in-oil (w/o) or inverse emulsion. The direct emulsion (o/w) is most commonly used. Depending on the difference in their components, emulsion systems named macroemulsion, microemulsion, and miniemulsion could be found. Macroemulsions, regarded as conventional emulsions, are kinetically stabilized mixtures of immiscible liquids. The size of droplets formed from one liquid of macroemulsion is usually larger than 100 nm. Due to its thermodynamically unstable property, macroemulsions require energy input such as stirring or shaking to form.[121] Different from macroemulsion, microemulsions are thermodynamically stable liquid mixtures containing oil, water, and surfactant. The size of

dispersed droplets is from 10 to 100 nm. Their formation could be achieved by simple mixing and do not require high shear force. However, a large amount of surfactants (>10 wt% compared to the dispersed phase) is usually used.[121]

Originated from reports of Ugelstad *et al.*,[122,123] miniemulsions are kinetically stable system obtained by supplying a high shear force to a mixture of two immiscible liquid phases together with a certain amount of surfactants (well below that used in microemulsion).[124] Droplets with sizes of around 50-500 nm are generated by high shear force. However, these droplets must be stabilized against the Ostwald ripening and coalescence (**Figure 2.17**).[125]

Ostwald ripening refers to a process where the molecules of the small droplets tend to diffuse to the larger ones. The driving force for the Ostwald ripening process is the *Laplace* pressure (P_L) which is determined by the radius of the droplet (R) and the interfacial tension (σ_{LL}) between two liquids:

$$P_L = \frac{2 \cdot \sigma_{LL}}{R}$$

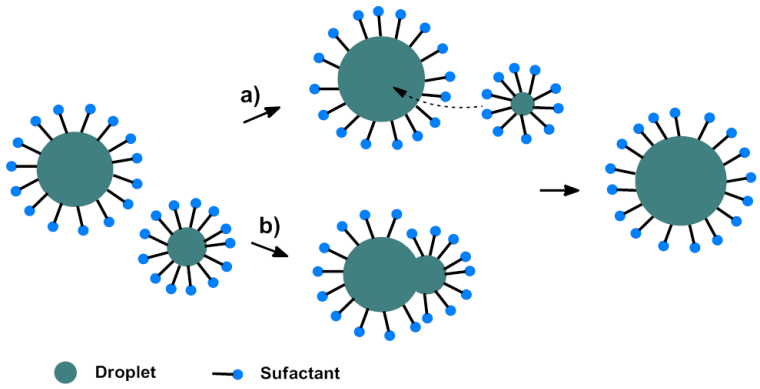

Figure 2.17 *Schematic illustration of **a)**: Ostwald ripening and **b)**: coalescence process in a miniemulsion system.*

One approach to suppress Ostwald ripening is to add an osmotic agent, *i.e.* hydrophobes with an extremely low water solubility such as hexadecane to the dispersed phase in direct miniemulsions. The generated osmotic pressure is then supposed to counteract the *Laplace* pressure (**Figure 2.18**).[124] The coalescence between droplets is usually suppressed by the addition of surfactants.

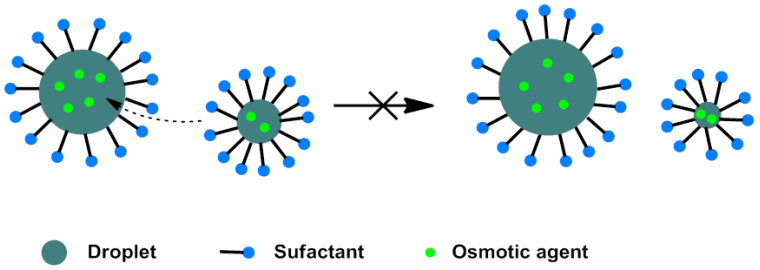

Figure 2.18 *Schematic illustration of the function of osmotic agent against Oswald ripening.*

2.4.3 Formation of capsules

It was reported by Torza and Mason[126] that when two immiscible liquid droplets (liquid-1 and liquid-3) suspended in a third immiscible liquid (liquid-2), the final equilibrium configuration could be predicted by the interfacial tensions between each phase (σ_{ij}, σ_{jk}, σ_{ik}). The spreading coefficient of each phase (S_i, S_j, S_k) was defined as:

$$S_i = \sigma_{jk} - (\sigma_{ij} + \sigma_{ik})$$

They proposed that if the interfacial tension $\sigma_{12} > \sigma_{23}$ was assumed, *i.e.* $S_1 = \sigma_{23} - (\sigma_{12} + \sigma_{13}) < 0$, there are only three possible configurations that can be found (**Figure 2.19**): complete engulfing (core-shell) when $S_2 < 0$ and $S_3 > 0$; partial engulfing when $S_2 < 0$ and $S_3 < 0$; and non-engulfing (individual droplets) when $S_2 > 0$ and $S_3 < 0$.

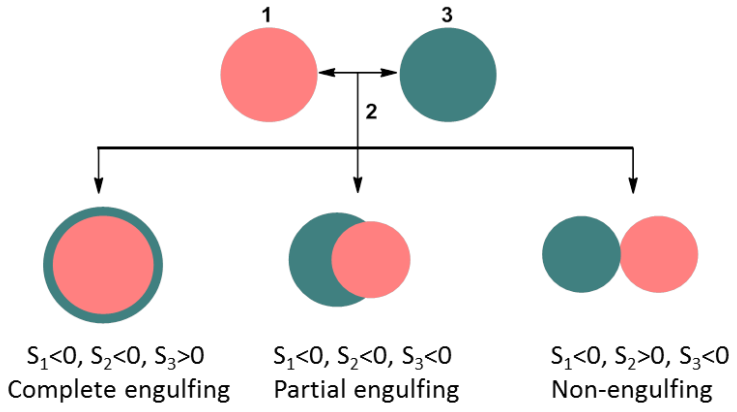

Figure 2.19 *Possible equilibrium configurations obtained according to different spreading coefficient of three phases: liquid-1 and 3 are immiscible droplets dispersed in immiscible medium liquid-2. This scheme is originated from Torza and Mason.*[126] *Copyright (1970), with permission from Elsevier.*

The approach proposed above, however, relies mainly on immiscible compounds with low molecular weights that can readily diffuse as suggested by Sundberg *et al.*[127] In the case

when polymers with higher molecular weight are present in the system, the equilibrium morphologies are not always obtained. This observation is attributed to the diffusive restrictions of the polymer phase with respect to the mobility of the polymer chain.[127,128] In these systems, the variation of free energy is considered as the driving force for the final configuration. For example, as proposed by Chen *et al.*,[128] in a system with polymer-1, polymer-2 and water, the total free energy change (ΔG) for all the possible configurations can be described by the following equation:

$$\Delta G = \sum \sigma_{ij} A_{ij} - \sigma_0 A_0$$

with σ_{ij} and A_{ij} the interfacial tension and interfacial area between i and j. σ_0 and A_0 refer to the initial interfacial tension and area. The configuration with a minimal free energy change will be the thermodynamically favored one.

The final morphology of a system with multiphases can be influenced by several parameters, *e.g.* the interfacial tension between the phases which is dependent on not only the nature of the phases but also the influence of the surfactant used,[127] the chain mobility of the polymer phases,[129] the speed of solvent evaporation or the temperature during the preparation process,[130,131] reaction kinetics,[132] and so on.

Based on the above mentioned principles, three approaches, *i.e.* polymerization-induced phase separation, interfacial polymerization, and solvent evaporation-induced phase separation, used to generate capsular structures are described in this section.

2.4.3.1 Polymerization-induced phase separation

The approach of polymerization-induced phase separation refers to the fact that capsules are formed due to the phase separation between solvent and the formed polymers during the polymerization. As shown in **Figure 2.20**, two phases, *i.e.* the continuous phase and the dispersed phase are first prepared for the miniemulsion. The dispersed phase composed of hydrophobic oil, monomer, and hydrophobic initiator will form droplets after ultrasonication and are stabilized by a surfactant in the continuous phase. The monomer and initiator are miscible with the hydrophobic oil in the dispersed droplets before polymerization. When polymerization starts, the formed polymers become immiscible with the hydrophobic oil. Based on the above mentioned thermodynamic consideration with respect to the interfacial

tension of polymer/oil, polymer/water and oil/water, phase separation occurs in the droplets. In an appropriate case, the polymer chains precipitate at the interface of droplets, resulting in capsules with a polymer shell and a liquid core.

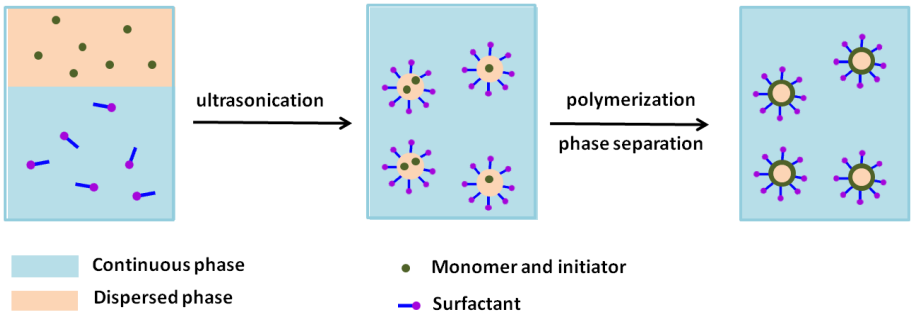

Figure 2.20 *Schematic illustration of capsules formed via polymerization-induced phase separation in miniemulsion.*

One common example are poly(methyl methacrylate) (PMMA) nanocapsules formed directly by polymerization of MMA with hexadecane (HD) as hydrophobic oil in dispersed phase of miniemulsion.[110] The different interfacial tensions between PMMA/HD, PMMA/water and water/HD drives to the final core-shell structure. On the contrary, when monomer with a higher hydrophobicity, for example styrene (St) or butyl methacrylate (BA) was used, no capsules were generated due to the higher interfacial tension of polymer/water.[110]

2.4.3.2 Interfacial polymerization

Capsules could also be formed through interfacial polymerization of two different monomers, or monomer and its initiator from two phases. Different types of polymerization can take place at the interface, *e.g.* radical polymerization,[111] polyaddition reaction,[133,134] oxidative polymerization,[135] anionic polymerization,[136] and polycondensation reaction.[137-139] **Figure 2.21** demonstrates the general concept of interfacial polymerization in direct miniemulsion to form capsules. Hydrophilic component A and hydrophobic component B are respectively dispersed in the water phase and the oil phase. At the droplet interface, reactive components provided in each phases contact and polymerize to generate a polymer which is insoluble in both phases. The formed polymer chains then precipitate to the interface to build a shell surrounding a liquid core.[140]

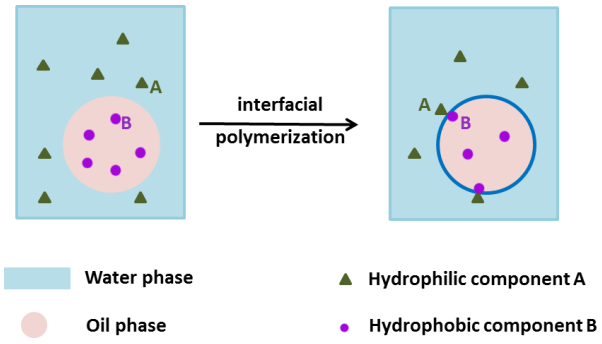

Figure 2.21 *Schematic illustration of capsules formed via interfacial polymerization in direct miniemulsion.*

2.4.3.3 Phase separation induced by solvent evaporation

Different from the above mentioned two approaches which involve polymerization during the capsule preparation process, the formation of capsules by the solvent-evaporation method mainly relies on phase separation between preformed polymers and a solvent.[106,141-143] **Figure 2.22** shows the preparation process of capsules using the solvent evaporation method in direct miniemulsion. The dispersed phase consists of the preformed polymer with its good solvent (usually with a low boiling point) and a non-solvent. After mixing with the continuous phase containing surfactant and water, the whole system is treated with ultrasonication to generated small miniemulsion droplets. As the good solvent of the preformed polymer with a low boiling point evaporates, phase separation occurs between the polymer and its non-solvent in the dispersed droplets. Similarly to the formation of capsules by polymerization-induced phase separation, when the preformed polymer exhibits appropriate interfacial tension with the oil phase and water phase, the polymer chains would move to the interface of the droplets and solidify to build the shell surrounding its non-solvent.

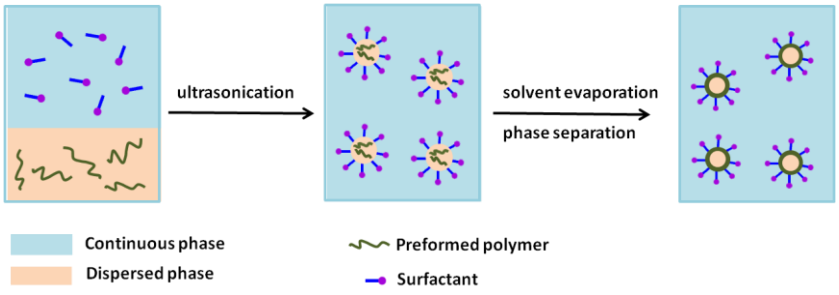

Figure 2.22 *Schematic illustration of capsules formed via solvent evaporation in direct miniemulsion.*

By combing the solvent-evaporation method with miniemulsion technique, various types of polymers were found to form capsules.[106] This method provides also the possibility to encapsulate functional compounds such as self-healing agent,[106] drug,[141] antiseptic agent,[142] fluorescence dye[143] in the liquid core by direct dissolving them in the dispersed phase.

2.5 Formation of fibers

Due to their large surface area to volume ratio, the flexibility in surface functionalities and good mechanical performance, one-dimensional (1D) nanostructures have gained much interest for various applications,[144-146] for example drug delivery,[147] tissue engineering,[148] catalysis,[149] chemical or biological sensors.[56,150] Of all methods to prepare 1D nanostructures, electrospinning is regarded as the easiest and most efficient one.[151-154] Using the electrostatic repulsion between surface charges, the viscoelastic jet is stretched to form fibers during the electrospinning process. The characteristics of generated fibers such as their morphology and diameters, uniformity, or pore size can be controlled by adjusting processing parameters.[155] Moreover, the addition of more components to the initial solution also provides the possibility to generate fiber materials with multifunctional properties.[156] Fiber composites composed of polymer/polymer, polymer/inorganic, or inorganic/inorganic materials can be formed by the electrospinning technique.[157]

Emulsion electrospinning and coaxial electrospinning are two electrospinning techniques that provide the possibility to form fibers with diverse structures and properties.[158] Emulsion electrospinning, for example, combines electrospinning with the emulsion technique.[159,160] Usually, a stable w/o emulsion is used instead of a polymer solution for the electrospinning. The w/o emulsion consists of an organic phase in which a polymer is dissolved and another immiscible phase composed of an aqueous solution. When electrospun, the aqueous phase in the emulsion is stretched and form a continuous core inside of the fibers, resulting in fibers with core-sheath structures.[161]

2.5.1 Electrospinning

A typical electrospinning set-up usually consists of a high-voltage power supply, a syringe connected to a metallic nozzle, a syringe pump, and a conductive collector (**Figure 2.23**). Before the electrospinning process, a liquid that is often a polymer solution but can also be, for example a polymer melt, a colloidal dispersion, or a sol-gel precursor is prepared.[146,153]

The as-prepared liquid for electrospinning is then loaded into the syringe and pushed steadily to the tip of the nozzle by a syringe pump. At the tip of the nozzle, a suspended droplet is formed due to the surface tension of the electrospinning liquid. When a high positive voltage is applied to the metallic nozzle, an electric field is generated between the conductive nozzle and the collector. The droplet is then charged and stretched by the electric field to form a Taylor cone. Once the applied voltage is high enough, *i.e.* the electrostatic force overcomes the surface tension of the droplet, a liquid jet produced from the Taylor cone and fly towards the collector. Solvent evaporates during this process and solid fibers are then deposited on the collector.

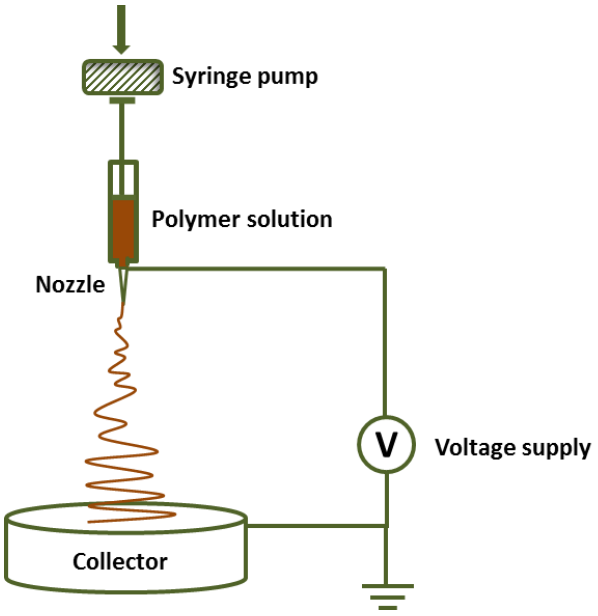

Figure 2.23 *Schematic illustration of a typical electrospinning set-up.*

Using the electrospinning process, a large amount of polymers have been found to form fibers from polymer solutions or polymer melts.[144,162] Investigations on how the properties of electrospinning liquid or the processing parameters influence the morphologies and diameters of formed fibers has also been widely reported.[163-168] When a polymer solution, for example, is used for electrospinning, the properties such as concentration, viscosity and conductivity of the solution may influence the size of formed fibers.[169] For example, it was found that the average diameter of Nylon 6 fibers was larger when the concentration of the polymer solution was increased.[170]

In addition to the characteristic of the electrospinning liquid, processing parameters used for electrospinning, for example applied voltage, distance from nozzle to collector, flow rate,

environmental humidity *etc*. would also play a role on the final morphology of fibers.[171] Decrease in diameter of fibers was found when applied voltage or distance from nozzle to collector was increased, or the flow rate of the electrospinning liquid was decreased.[170,172]

Last but not the least, the evaporation speed of solvents used was also considered to have an influence on the surface morphology of fibers, *e.g.* a porous structure was generated when a solvent with high volatility was used.[173]

2.5.2 Coaxial electrospinning

Coaxial electrospinning is developed from conventional electrospinning but with two different materials separately injected from two coaxial capillaries in the metallic nozzle (**Figure 2.24**). Similarly to the normal electrospinning process, when a sufficient voltage is applied to both outer and inner part of the nozzle, the compound droplet at the tip will be deformed to form a jet. The shell fluid is usually electrospinnable by itself and forms the sheath to stabilize the core material. If appropriate electrospinning materials and processing parameters are chosen, core-shell nanofibers can be fabricated.[174]

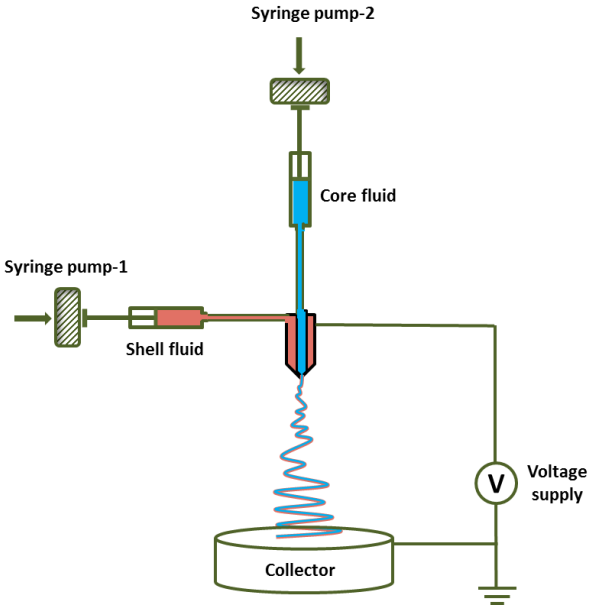

Figure 2.24 *Schematic illustration of a coaxial electrospinning set-up.*

Except that different materials could be introduced to the fibers, coaxial electrospinning has also other advantages. Hollow structures, for example, can be formed after removal of the core material of fibers. The possibility to encapsulate non-electrospinnable functional materials in the fibers can also be achieved by coaxial electrospinning. For example, using

PVP and titanium isopropoxide (Ti(O*i*Pr)$_4$) as shell fluid and mineral oil as core fluid, Xia *et al.*[175] successfully produced fibers with PVP/TiO_2 as shell and mineral oil as core by coaxial electrospinning process. PVP/TiO_2 hollow fibers were then easily obtained after the core material was extracted by octane. By dissolving compounds such as ferrofluid or organic dyes in the core liquid, TiO_2 hollow fibers incorporated with magnetic nanoparticles or fluorescent dye could also be prepared.[176]

However, due to its complexity, coaxial electrospinning also exhibits disadvantages compared to conventional electrospinning. For example, the materials used, size of core-shell capillaries, feeding ratio and immiscibility of the two components, viscosity, and conductivity of core-shell liquids must be carefully chosen to get a stable compound Taylor cone. The Taylor cone should be then properly stretched to form a continuous and uniform core-shell structure.[177,178]

2.6 References

[1] Blaiszik, B. J.; Kramer, S. L. B.; Olugebefola, S. C.; Moore, J. S.; Sottos, N. R.; White, S. R. *Annu. Rev. Mater. Res.* **2010**, *40*, 179.

[2] Murphy, E. B.; Bolanos, E.; Schaffner-Hamann, C.; Wudl, F.; Nutt, S. R.; Auad, M. L. *Macromolecules* **2008**, *41*, 5203.

[3] Luo, X. F.; Ou, R. Q.; Eberly, D. E.; Singhal, A.; Viratyaporn, W.; Mather, P. T. *ACS Appl. Mater. Interfaces* **2009**, *1*, 612.

[4] Varley, R. J.; van der Zwaag, S. *Acta Mater.* **2008**, *56*, 5737.

[5] Goodall, G. W.; Hayes, W. *Chem. Soc. Rev.,* **2006**, *35*, 280.

[6] Stevens, M.; Jenkins, A. *J. Polym. Sci., Chem. Ed.,* **1979**, *17*, 3675.

[7] Chen, X.; Dam, M. A.; Ono, K.; Mal, A.; Shen, H.; Nutt, S. R.; Sheran, K.; Wudl, F. *Science* **2002**, *295*, 1698.

[8] Ghosh, B.; Urban, M. W. *Science* **2009**, *323*, 1458.

[9] Sivakova, S.; Bohnsack, D. A.; Mackay, M. E.; Suwanmala, P.; Rowan, S. J. *J. Am. Chem. Soc.* **2005**, *127*, 18202.

[10] Cordier, P.; Tournilhac, F.; Soulie´-Ziakovic, C.; Leibler, L. *Nature 2008*, *451*, 977.

[11] Burattini, S.; Colquhoun, H. M.; Greenland B. W.; Hayes, W. *Faraday Discuss.* **2009**, *143*, 251.

[12] Wool, R.; O'Connor, K. *J. Appl. Phys.* **1981**, *52*, 5953.

[13] White, S. R.; Sottos, N. R.; Geubelle, P. H.; Moore, J. S.; Kessler, M. R. *Nature* **2001**, *409*, 794.

[14] Yuan,Y. C.; Rong, M. Z.; Zhang, M. Q.; Chen, J.; Yang, G. C.; Li, X. M. *Macromolecules* **2008**, *41*, 5197.

[15] Caruso, M. M.; Delafuente, D. A.; Ho, V.; Sottos, N. R.; Moore, J. S.; White S. R. *Macromolecules* **2007**, *40*, 8830.

[16] Caruso, M. M.; Blaiszik, B. J.; White, S. R.; Sottos, N. R.; Moore, J. S. *Adv. Funct. Mater.* **2008**, *18*, 1898.

[17] Cho, S. H.; Andersson, H. M.; White, S. R.; Sottos, N. R.; Braun, P. V. *Adv. Mater*. **2006**, *18*, 997.

[18] Dry, C. M. *Compos. Struct.* **1996**, *35*, 263.

[19] Bond, T. R. *Smart Mater. Struct.* **2006**, *15*, 704.

[20] Pang, J. W. C.; Bond, I. P. *Compos. Sci. Technol*. **2005**, *65*, 1791.

[21] Bleay, S. M.; Loader, C. B.; Hawyes, V. J.; Humberstone, L.; Curtis, P.T. *Composites A* **2001**, *32*, 1767.

[22] Toohey, K. S.; Sottos, N. R.; Lewis, J. A.; Moore, J. S.; White, S. R. *Nat. Mater.* **2007**, *6*, 581.

[23] Toohey, K. S.; Hansen, C. J.; Lewis, J. A.; White, S. R.; Sottos, N. R. *Adv. Funct. Mater*. **2009**, *19*, 1399.

[24] Hansen, C. J.; Wu, W.; Toohey, K. S.; Sottos, N. R.; White, S. R.; Lewis, J. A. *Adv. Mater.* **2009**, *21*, 4143.

[25] Revie, R. W.; Uhlig, H. H. *Corrosion and Corrosion Control* **2008**, *4th ed.,* John Wiley & Sons, Inc.

[26] Brondel, D.; Edwards, R.; Hayman, A.; Clamart, F.; Hill, D.; Mehta, S.; Semerad, T.; *Oilfield Review* **1994**, *6*, 4.

[27] Jones, D. A. *Principles and Prevention of Corrosion*, **1996**, *2nd ed*., Prentice-Hall, New Jersey.

[28] Kumar, V. *Corrosion Rev*. **1998**, *16*, 317.

[29] Burn, R. M.; Bradley, W. W. *Protective coatings for metals* **1967**, *3rd ed.* Reinhold Publ. Corp., New York.

[30] Gray, J. E.; Luan, B. *J. Alloy. Compd*. **2002**, *336*, 88.

[31] Spinks, G. M.; Dominis, A. J.; Wallace, G. G.; Tallman, D. E. *J Solid State Electrochem* **2002**, *6*, 85.

[32] Marcus, P. *Mechanisms in Theory and Practice* **2012**, *3rd ed*. CRC Press, Taylor & Francis Group, LLC.

[33] Bushman, J. B. *Corrosion and Cathodic Protection Theory*, Bushman & Associates, Inc. Medina, Ohio USA.

[34] Tomashov, N. D.; Chernova, G. P. *Passivity and Protection of Metals against Corrosion* **1967**, *1st ed*. Plenum Press, New York.

[35] Tomashov, N. D.; Altovsky, R. M.; Chernova, G. P. *J. Electrochem. Soc*. **1961**, *108*, 113.

[36] Inzelt, G. *"Chapter 1: Introduction". In Scholz, F. Conducting Polymers: A New Era in Electrochemistry*. *Monographs in Electrochemistry*. **2008**, Springer. pp. 1-6.

[37] MacDiarmid, A. G. *Angew. Chem. Int. Ed.* **2001**, *40*, 2581.

[38] Shirakawa, H.; Louis, E. J.; MacDiarmid, A. G.; Chiang, C. K.; Heeger, A. J. *J. Chem. Soc. Chem. Comm.* **1977**, 16, 578.

[39] Shirakawa, H. *Angew. Chem. Int. Ed.* **2001**, *40*, 2574.

[40] Guimarda, N. K.; Gomezb,N.; Schmidt,C. E. *Prog. Polym. Sci.* **2007**, *32*, 876.

[41] Feast, W. J. *Synthesis of conducting polymers*. In: Skotheim, T. A. editor. *Handbook of conducting polymers*, **1986**, *vol. I*, New York: Marcel Dekker, 1-43.

[42] Bhadra, S.; Khastgir, D.; Singha, N. K.; Lee, J. H. *Prog. Polym. Sci.* **2009**, *34*, 783.

[43] Tallman, D. E.; Spinks, G.; Dominis, A.; Wallace, G. G. *J Solid State Electrochem* **2002**, *6*, 73.

[44] Wei, Y.; Jang, G.-W.; Chan, Ch.-Ch.; Hsuen, K. F.; Hariharan, R.; Patel, S. A.; Whitecar, C. K. *J. Phys. Chem.* **1990**, *94*, 7716.

[45] Wei, Y.; Hsueh, K. F.; Jang, G.-W. *Polymer*, **1994**, *35***,** 3572.

[46] Wei, Y.; Hariharan, R.; Patel, S. A. *Macromolecules* **1990**, *23*, 758.

[47] Heth, C. L.; Tallman, D. E.; Rasmussen, S. C. *J. Phys. Chem. B* **2010***, 114,* 5275.

[48] Xia, H.; Wang, Q. *J. Nanopart. Res.* **2001**, *3*, 401.

[49] Kim, B.-J.; Oh, S.-G.; Han, M.-G.; Im, S.-S. *Langmuir* **2000**, *16*, 5841.

[50] Kim, B. - J.; Oh, S.-G.; Han, M.-G.; Im, S.-S. *Synth. Met.* **2001**, *122*, 297.

[51] Niu, Z.; Yang, Z.; Hu, Z.; Lu, Y.; Han, C. C. *Adv. Funct. Mater.* **2003**, *13*, 949.

[52] Zhang, L.; Liu, P. *Soft Mater.* **2010**, *8*, 29.

[53] Lee, M.; Kim, J. E.; Fang, F. F.; Choi, H. J.; Feller, J.-F. *Macromol. Chem. Phys.* **2011**, *212*, 2300.

[54] Li, G.; Pang, S.; Liu, J.; Wang, Z.; Zhang, Z. *J. Nanopart. Res.* **2006**, *8*, 1039.

[55] Xia, H; Tao, X. *J. Mater. Chem.* **2011**, *21*, 2463.

[56] Huang, J.; Virji, S.; Weiller, B. H.; Kaner, R. B. *J. Am. Chem. Soc.* **2003**, *125*, 314.

[57] Li, D.; Huang, J.; Kaner, R. B. *Accounts Chem. Res.* **2009**, *42*, 135.

[58] Zhang, X.; Goux, W. J.; Manohar, S. K. *J. Am. Chem. Soc.* **2004**, *126*, 4502.

[59] Stejskal, J.; Sapurina, I.; Trchová, M. *Prog. Polym. Sci.* **2010**, *35*, 1420.

[60] Lin, H,-K.; Chen, S.-A. *Macromolecules* **2000**, *33*, 8117.

[61] Xia, L.; Wei, Z.; Wan, M. *J. Colloid Interf. Sci.* **2010**, *341*, 1.

[62] Jackowska, K.; Bieguński, A. T.; Tagowska, M. *J. Solid State Electrochem.* **2008**, *12*, 437.

[63] Li, C.-Y.; Chiu, W.-Y.; Don, T.-M. *J. Polym. Sci., Polym. Chem.* **2007**, *45*, 3902.

[64] Carswell, A. D. W.; O'Rear, E. A.; Grady, B. P. *J. Am. Chem. Soc*. **2003**, *125*, 14793.

[65] Wei, Z.; Zhang, Z.; Wan, M. *Langmuir* **2002**, *18*, 917.

[66] Wan, M. *Adv. Mater.* **2008**, *20*, 2926.

[67] Zhang, L.; Wan, M. *Adv. Funct. Mater.* **2003**, *13*, 815.

[68] Wei, Z.; Wan, M. *Adv. Mater.* **2002**, *14*, 1314.

[69] Focke, W. W.; Wnek, G. E.; Wei, Y. *J. Phys. Chem.* **1987**, *91*, 5813.

[70] Gospodinova, N.; Terlemezyan, L. *Prog. Polym. Sci.* **1998**, *23*, 1443.

[71] de Albuquerque, J. E.; Mattoso, L. H. C.; Faria, R. M.; Masters, J. G.; MacDiarmid, A . G. *Synth. Met.* **2004**, *146*, 1.

[72] Epstein, A. J.; Ginder, J. M.; Zuo, F.; Woo, H.-S.; Tanner, D. B.; Richter, A. F.; Angelopoulos, M.; Huang, W.-S.; MacDiarmid, A. G. *Synth. Met.* **1987**, *21*, 63.

[73] MacDiarmid, A. G.; Chiang, J. C.; Richter, A. F.; Epstein, A. J. *Synt. Met.* **1987**, 18, 285.

[74] Chiang, J.-C.; MacDiarmid, A. G. *Synth. Met.* **1986**, *13*, 193.

[75] W.S. Huang, A.G. MacDiarmid, A.J. Epstein *J. Chem. Soc. Chem. Commun.* **1987**, 1784.

[76] Genies, E. M.; Tsintavis, C. *J. Electroanal. Chem.* **1985**, *195*, 109.

[77] Moon, D. K.; Ezuka, M.; Maruyama, T.; Osakada, K.; Yamamoto, T. *Makromol. Chem.* **1993**, *194*, 3149.

[78] Pouget, J. P.; Jozefowicz, M. E.; Epstein, A. J.; Tang, X.; MacDiarmid, A. G. *Macromocules* **1991**, *24*, 779.

[79] Schmidt, V. M.; Tegtmeyer, D.; Heitbaum, J. *J. Electroanal. Chem.* **1995**, *385*, 149.

[80] Inzelt, G.; Pineri, M.; Schultze, J. W.; Vorotyntsev, M. A. *Electrochim. Acta* **2000**, *45*, 2403.

[81] Yu, Y.; Zhang, Y.; Jiang, Z.; Zhang, X.; Zhang, H.; Wang, X. *Langmuir* **2009**, *25*, 10002.

[82] Kim, H.; Jeong, S.-M.; Park, J.-W. *J. Am. Chem. Soc.* **2011**, *133*, 5206.

[83] Kim, H.; Park, J.-W. *J. Mater. Chem.* **2010**, *20*, 1186.

[84] Irimia-Vladu, M.; Fergus, J. W. *Synth. Met.* **2006**, *156*, 1401.

[85] Smela, E.; Lu, W.; Mattes, B. R. *Synth. Met.* **2005**,*151*, 25.

[86] Tseng, R. J.; Huang, J.; Ouyang, J.; Kaner, R. B.; Yang, Y. *Nano Lett.* **2005**, *5*, 1077.

[87] Gupta, V.; Miura, N. *Electrochim. Acta* **2006**, *52*, 1721.

[88] Sung, J. H.; Kim, S. J.; Lee, K. H. *J. Power Sources* **2004**, *126*, 258.

[89] Doblhofer, K.; Armstrong, R. D. *Electrochim. Acta* **1988**, *33*, 453.

[90] Liu, Z.; Zhou, J.; Xue, H.; Shen, L.; Zang, H. Chen, W. *Synth. Met.* **2006**, *156*, 721.

[91] Kuwabata, S.; Martin, C. R. *J. Membr. Sci.* **1994**, *91*, 1.

[92] Yang, J.; Sun, Q.; Hou, X.; Wan, M. *Chin. J. Polym. Sci.* **1993**, *11*, 121.

[93] Pud, A. A.; Shapoval, G. S.; Kamarchik, P.; Ogurtsov, N. V.; Gromovaya, V. F.; Myronyuk, I. E.; Kontsur, Y. V. *Synth. Met.* **1999**, *107*, 111..

[94] Lu, W. K.; Elsenbaumer, R. L.; Wessling, B. *Synth. Met.* **1995**, *71*, 2163.

[95] Klavetter F. L.; Alper, K.; Goddard, Y. A. Abstracts, *217th ACS national meeting*, **1999**, Anaheim, Calif., MSE-031.

[96] Wessling, B. *Adv. Mater.* **1994**, *6*, 226.

[97] Talo, A.; Passiniemi, P.; Forsen, O.; Ylasaari, S. *Synth. Met.* **1997**, *85*, 1333.

[98] Schauer, T.; Joos, A.; Dulog, L.; Eisenbach, C. D. *Prog. Org. Coat.* **1998**, *33*, 20.

[99] Barisci, J. N.; Lewis, T. W.; Spinks, G. M.; Too, C. O.; Wallace, G. G. *J. Intell. Mater. Syst. Struct.* **1998**, *9*, 723.

[100] Kendig, M.; Hon, M.; Warren, L. *Prog. Org. Coat.* **2003**, *47*, 183.

[101] Rohwerder, M.; Michalik, A. *Electrochim. Acta* **2007**, *53*, 1300.

[102] Rohwerder, M.; Isik-Uppenkamp, S.; Amarnath, C. A. *Electrochim. Acta* **2009**, *56*, 1889.

[103] Paliwoda-Porebska, G.; Rohwerder, M.; Stratmann, M.; Rammelt, U.; Duc, L.; Plieth, W. *J. Solid State Electrochem.* **2006**, *10*, 730.

[104] De Cock, L. J.; De Koker, S.; De Geest, B. G.; Grooten, J.; Vervaet, C.; Remon, J. P.; Sukhorukov, G. B.; Antipina, M. N. *Angew. Chem. Int. Ed.* **2010**, *49*, 6954.

[105] Vimalanandan, A.; Lv, L.- P.; Tran, T. H.; Landfester, K.; Crespy, D.; Rohwerder, M. *Adv. Mater.* **2013**, *25*, 6980.

[106] Zhao, Y.; Fickert, J.; Landfester, K.; Crespy, D. *small* **2012**, *8*, 2954.

[107] Delcea, M.; Möhwald, H.; Skirtach, A. G. *Adv. Drug Del. Rev.* **2011**, *63*, 730.

[108] Sukhishvili, S. A. *Curr. Opin. Colloid Interface Sci.* **2005**, *10*, 37.

[109] O'Donnell, P. B.; McGinity, J. W. *Adv. Drug Del. Rev.* **1997**, *28*, 25.

[110] Tiarks, F.; Landfester, K.; Antonietti, M. *Langmuir* **2001**, *17*, 908.

[111] Scott, C.; Wu, D.; Ho, C.-C.; Co, C. C. *J. Am. Chem. Soc.* **2005**, *127*, 4160.

[112] "colloid." *Encyclopaedia Britannica. Encyclopaedia Britannica Online Academic Edition.* Engyclopædia Britannica Inc. **2014**. Web. 27 Apr. 2014.

[113] Derjaguin, B. V.; Landau, L. *Acta Physicohim. (URSS)* **1941**, *14*, 633.

[114] Verwey, E. J. W.; Overbeek, J. Th. G. *Theory of Stability of Lyophobic Colloids*, Elsevier, Amsterdam, **1948**.

[115] Napper, D. H. *Ind. Eng. Chem. Prod. Res. Develop.* **1970**, *9*, 467.

[116] Napper, D. H. *J. Colloid Interf. Sci.* **1977**, *58*, 390.

[117] Cooper, S. *http://community.dur.ac.uk/sharon.cooper/lectures/colloids/interfacesweb 1.html #_Toc449417600 .*

[118] Napper, D. H.; Netschey, A. *J. Colloid Interf. Sci*. **1971**, *37*, 528.

[119] Abbott, S.; Holmes, N. *Nanocoatings: Principles and Practice: From Research to Production.* **2013**, DEStech Publications, Inc, page 82-83.

[120] Landfester, K. *Annu. Rev. Mater. Res.* **2006**, *36*, 231.

[121] Shah, D. O. *Macro- and microemulsions: theory and applications*. **1985**, Washington, D.C., American Chemical Society. Page 1-13.

[122] Ugelstad, J.; Lervik, H.; Gardinovacki, B.; Sund, E. *Pure and Appl. Chem.* **1971**, *26*, 121.

[123] Ugelstad, J.; El-Aasser, M. S.; Vanderhoff, J. W. *J. Polym. Sci.: Polym. Lett. Ed.* **1973**, *11*, 503.

[124] Landfester, K. *Macromol. Symp.* **2000**, *150*, 171.

[125] Landfester, K.; Bechthold, N.; Forster, S.; Antonietti, M. *Macromolecular Rapid Communications* **1999**, *20*, 81.

[126] Torza, S.; Mason, S. G. *J. Colloid Interf. Sci.* **1970**, *33*, 67.

[127] Sundberg, D. C.; Casassa, A. P.; Pantazopoulos, J.; Muscato, M. R. *J. Appl. Polym. Sci.* **1990**, *41*, 1425.

[128] Chen, Y.-C.; Dimonie, V.; El-Aasser, M. S. *Macromolecules* **1991**, *24*, 3779.

[129] Okubo, M.; Katsuta, Y.; Matsumoto, T. *J. .Polym. Sci. Part C-Polym. Lett.* **1982**, *20*, 45.

[130] Hong, Y.; Gao, C. Y.; Shi, Y.; Shen, J. *Polym. Adv. Technol.* **2005**, *16*, 622.

[131] Lee, S.; Rudin, A. *J. Polym. Sci. A: Polym. Chem.* **1992**, *30*, 2211.

[132] Williams, R. J. J.; Rozenberg, B. A.; Pascault, J.-P. *Adv. Polym. Sci.* **1997**, *128*, 95.

[133] Herrmann, C; Crespy, D.; Landfester, K. *Colloid Polym. Sci.* **2011**, *289*, 1111.

[134] Johnsen, H.; Schmid, R. B. *J. Microencapsul.* **2007**, *24*, 731.

[135] Zhang, L.; Liu, P.; Ju, L.; Wang, L.; Zhao, S. *Macromol. Res.* **2010**, *18*, 648.

[136] Limouzin, C.; Caviggia, A.; Ganachaud, F.; Hémery, P. *Macromolecules* **2003**, *36*, 667.

[137] Crespy, D.; Stark, M.; Hoffmann-Richter, C.; Ziener, U.; Landfester, K. *Macromoleucles* **2007**, *40*, 3122.

[138] Torini, L.; Argillier, F.; Zydowicz, N. *Macromolecules* **2005**, *38*, 3225.

[139] Fickert, J.; Rupper, P.; Graf, R.; Landfester, K.; Crespy, D. *J. Mater. Chem.* **2012**, *22*, 2286.

[140] Landfester, K. *Angew. Chem. Int. Ed.* **2009**, *48*, 4488.

[141] de Faria, T. J.; de Campos, A. M.; Senna, E. L. *Macromol. Symp.* **2005**, *229*, 228.

[142] Paiphansiri, U.; Tangboriboonrat, P.; Landfester, K. *Macromol. Biosci.* **2006**, *6*, 33.

[143] Staff, R. H.; Gallei, M.; Mazurowski, M.; Rehahn, M.; Berger, R.; Landfester, K.; Crespy, D. *ACS Nano* **2012**, *6*, 9042.

[144] Katti, D. S.; Robinson, K. W.; Ko, F. K.; Laurencin, C. T. *J. Biomed. Mate. Res. B* **2004**, *70*, 286.

[145] Boundriot, U.; Dersch, R.; Greiner, A.; Wendorff, J. H. *Artif Organs* **2006**, *30*, 779.

[146] Patel, A. C.; Li, S.; Wang, C.; Zhang, W.; Wei, Y. *Chem. Mater.* **2007**, *19*, 1231.

[147] Sawicka, K.; Gouma, P.; Simon, S. *Sensor. Actuat. B-Chem.* **2005**, *108*, 585.

[148] Huang, Z.-M.; Zhang, Y.-Z.; Kotaki, M.; Ramakrishna, S. *Compos. Sci. Technol.* **2003**, *63*, 2223.

[149] Yoo, H. S.; Kim, T. G.; Park, T. G. *Adv*. *Drug Del. Rev.* **2009**, *61*, 1033.

[150]Lu, X.; Wang, C.; Wei, Y. *small* **2009**, *5*, 2349.

[151] Xia, Y.; Li, D. *Adv. Mater.* **2004**, *16*, 1151.

[152]Teo, W. E.; Ramakrishna, S. *Nanotechnology* **2006**, *17*, R89-R106.

[153] Greiner, A.; Wendorff, J. H. *Angew. Chem. Int. Ed*. **2007**, *46*, 5670.

[154] Reneker, D. H.; Yarin, A. L. *Polymer* **2008**, *49*, 2387.

[155] Tan, S.-H.; Inai, R.; Kotaki, M.; Ramakrishna, S. *Polymer* **2005**, *46*, 6128.

[156] Wang, C.; Wang, M. *Front. Mater. Sci.* **2014**, *8*, 3.

[157] Wang, H.-S.; Fu, G.-D.; Li, X.-S. *Recent Patens on Nanotechnol.* **2009**, *3*, 21.

[158] Yarin, A. L. *Polym. Adv. Technol.* **2011**, *22*, 310.

[159] Crespy, D.; Friedemann, K.; Popa, A.-M. *Macromol. Rapid Commun*. **2012**, *33*, 1978.

[160] Xu, X.; Yang, L.;Xu, X.; Wang, X.; Chen, X.; Liang, Q.; Zeng, J.; Jing, X. *J. Control. Release* **2005**, *108*, 33.

[161] Xu, X.; Zhuang, X.; Chen, X.; Wang, X.; Yang, L.; Jing, X. *Macromol. Rapid Commun*. **2006**, *27*, 1637.

[162] Subbiah, T.; Bhat, G. S.; Tock, R. W.; Parameswaran, S.; Ramkumar, S. S. *J. Appl. Polym. Sci.* **2005**, *96*, 557.

[163] Bhardwaj, N.; Kundu, S. C. *Biotechnol. Adv.* **2010**, *28*, 325.

[164] Deitzel, J. M.; Kleinmeyer, J.; Harris, D.; Tan, N. C. B. *Polymer* **2001**, *42*, 261.

[165] Zong, X.; Kim, K.; Fang, D.; Ran, S.; Hsiao, B. S.; Chu, B. *Polymer* **2002**, *43*, 4403.

[166] Thompson, C. J.; Chase, G. G.; Yarin, A. L.; Reneker, D. H. *Polymer* **2007**, *48*, 6913.

[167] Casper, C. L.; Stephens, J. S.; Tassi, N. G.; Chase, D. B.; Rabolt, J. F. *Macromolecules* **2004**, *37*, 573.

[168] Wang, X. M.; Huang, Y. A.; Bu, N. B.; Duan, Y. Q.; Yin, Z. P. *Chin Sci Bull (Chin Ver)* **2012**, *57*, 860.

[169] Jun, Z.; Hou, H.; Schaper, A.; Wendorff, J. H.; Greiner, A. *e-Polymer* **2003**, *no. 009*.

[170] Chowdhury, M.; Stylios, G. *Intern. J. Basic & Appl. Sci.* **2010**, *10*, 70.

[171] Nezarati, R. M.; Eifert, M. B.; Cosgriff-Hernandez, E. *Tissue Eng. Part C Methods* **2013**, *19*, 810.

[172] Homayon, H.; Ravandi, S. A. H.; Valizadeh, M. *Carbohydr. Polym*.**2009***, 77*, 656.

[173] Megelski, S.; Stephens, J. S.; Chase, D. B.; Rabolt, J. F. *Macromolecules* **2002**, *35*, 8456.

[174] Sun, Z. C.; Zussman, E.; Yarin, A. L.; Wendorff, J. H.; Greiner, A. *Adv. Mater.* **2003**, *15*, 1929.

[175] Li, D.; Xia. Y. *Nano Lett.* **2004**, *4*, 933.

[176] Li, D.; McCann, J. T.; Xia, Y. *small* **2005**, *1*, 83.

[177] Elahi, M. F.; Wang, L.; Guan, G.; Khan, F. *J. Bioengineer & Biomedical Sci.* **2013**, *3*, 121.

[178] Khajavi, R.; Abbasipour, M. *Scientia Iranica F* **2012**, *19*, 2029.

3. Methods

3.1 Dynamic light scattering (DLS)

Dynamic light scattering is a technique that can be used to determine the size distribution profile of particles in dispersion. The principle of DLS is based on the influence of Brownian motion of particles on the fluctuations of intensity of the scattered light.[1,2] When a laser beam passes through the dispersion, the light will be scattered to all directions by the particles. The signal of scattered light at a fixed angle can be detected. Due to the distinction in Brownian motion of particles with different size, *i.e.* small particles move faster than larger ones, the fluctuation of intensity of scattering light also varies over time. Faster movement of small particles leads to larger fluctuation of signal and the contrary is found for large particles. The variations of these fluctuations can be recorded using a photomultiplier detector (PMT). By calculating the translation diffusion coefficient D of the particles using the autocorrelation function, the hydrodynamic radius (R_h) of the particles can be obtained according to the Stokes-Einstein equation:[3,4]

$$R_h = \frac{k_B T}{6\pi\eta D}$$

with k_B the Boltzmann constant, T the temperature and η the shear viscosity of the solvent.

3.2 Ultraviolet–visible spectroscopy (UV-vis)

It is known that different molecules absorb radiation of different wavelengths. When a sample is exposed to light energy that matches the energy difference between a possible electronic transition within the molecule, a fraction of the light energy would be absorbed and the electrons could be promoted to the higher energy state orbital.

Molecules that contain π-electrons or non-bonding electrons (n-electrons) can absorb energy in the form of ultraviolet or visible light to excite the electrons to the higher anti-bonding molecular orbitals.[5,6] Ultaviolet-visible spectroscopy is then the technique to record the degree of energy absorbed by molecules upon different wavelengths in the ultraviolet-visible spectral region. By plotting absorbance (A) versus wavelength (λ) a UV-vis spectrum is obtained.

It is possible to quantitatively determine the concentration of an absorbing species in solution by UV-vis spectroscopy using the Beer-Lambert law which states that the absorbance of a solution is directly proportional to its concentration and the path length[5,6]:

$$\mathrm{A} = \lg \frac{I_0}{I} = \varepsilon \cdot c \cdot L$$

with A the absorbance, I_0 the intensity of the light at a given wavelength, I the transmitted intensity, ε a constant known as molar absorptivity, c the concentration of the absorbing species and L the path length through the sample.

3.3 Scanning electron microscopy (SEM)

The working mechanism of a scanning electron microscope is based on the interaction between incident electron probe and a specimen. When this probe is focused and scanned upon the surface of a solid specimen, secondary, backscattered and Auger electrons, X-rays, *etc.* are generated. For the scanning electron microscopy (SEM) measurements in the present thesis, the emission of secondary electrons from the region of specimen where the electron beam hits was recorded. The emission information of secondary electrons relies mainly on the surface topography of the specimen. Therefore it is possible to obtain the morphology of specimen by collecting the information of secondary electrons and transferring it to an image.

Especially, low voltage SEM imaging is a direct and efficient way to observe the surface morphology: By means of this technique polymer capsules, particles and fibers investigated in the present thesis were imaged without the need of classical sputter or carbon coating.

3.4 Transmission electron microscopy (TEM)

Transmission electron microscopy (TEM) is a technique in which an accelerated electron beam transmits through a thin specimen and interacts with it. The transmitted electrons are detected. Due to the different interaction between incident electron beam and the specimen, electrons after transmission will then bring different information. For example, the difference in contrast of the sample indicates the variation of density of electrons that transmit through, *i.e.* darker areas of the image represent fewer electrons were transmitted through (denser areas in the sample).[7]

It is then possible to use TEM to observe, for example the morphology of capsules due to the different density of the shell and core. In the present thesis, SEM and TEM techniques are used together to determine both the surface morphology and also the internal structure of the synthesized capsules.

3.5 References

[1] Brown, W. ed. *Dynamic Light Scattering: the Method and Some Applications.* **1993**, Clarendon Press, Oxford.

[2] Berne, B. J.; Pecora, R. *Dynamic Light Scattering* **2000**, Courier Dover Publications, ISBN 0-486-41155-9.

[3] *Nicomp 380 User Manual*, **2003**, Santa Barbara.

[4] Elias, H. G. Makromoleküle, Band 1, *Grundlagen*; 5. Auflage ed.; Hüthig & Wepf Verlag, **1990**.

[5] Skoog, D. A.; West, D. M.; Holler, F. J. *Analytical Chemistry: An Introduction* (Saunders Golden Sunburst Series) 7th Ed., **1999**.

[6] Skoog, D. A.; West, D. M.; Holler, F. J.; Crouch, S. R. *Fundamentals of Analytical Chemistry* 8th Ed., **2003**.

[7] Flegler, S. L.; Heckman, J. W.; Klomparens, K. L. *Elektronenmikroskopie*; Spektrum Akademischer Verlag: Heidelberg, **1995**.

4. Results and Discussion

4.1 Self-healing system based on conducting polymers

4.1.1 Motivation

As mentioned in **chapter 2.1**, self-healing (SH) materials have gained considerable attention in recent years.[1-7] Among them, extrinsic SH materials play an important role in which healing agents are embedded into the materials in advance followed by the release and healing process when cracks occur. However, the self-healing process reported in the previous studies is mainly triggered upon mechanical damages.[1,6] Therefore, to design materials which exhibit self healing behavior upon other damages, such as corrosion defect, is also interesting.

Since conducting polymers like polyaniline (PANI) or polypyrrole (PPy) already found uses in application of corrosion protection,[8-13] the construction of self-healing system based on conducting polymers is promising. In this chapter, procedures to form conducting self-healing systems are presented. In the first section, polyaniline capsules loaded with hydrophobic self-healing agents are synthesized and their redox responsive release behavior is investigated. In the second section, colloid systems based on polypyrrole and polypyrrole derivatives are presented. Finally, attempts to form solvent-soluble conducting polymers and multicompartment particles are described.

This chapter is based on the paper "*J. Am. Chem. Soc.* **2013,** *135*, 14198-14205" with copyright (2013) from American Chemical Society and the paper "*Polymer* **2014**, *55*, 715-720" with copyright (2014) from Elsevier.

4.1.2 Redox responsive release of self-healing agents from PANI capsules

In the present section, we demonstrate a one-pot synthetic process for the formation of conducting polyaniline capsules via miniemulsion polymerization. The interface of the miniemulsion droplets was used as soft template to perform the oxidative polymerization of aniline, allowing the encapsulation of a self-healing agent at the same time. The release behavior of the self-healing agent was studied as a function of the oxidation state of the formed PANI shells (**Figure 4.1**).

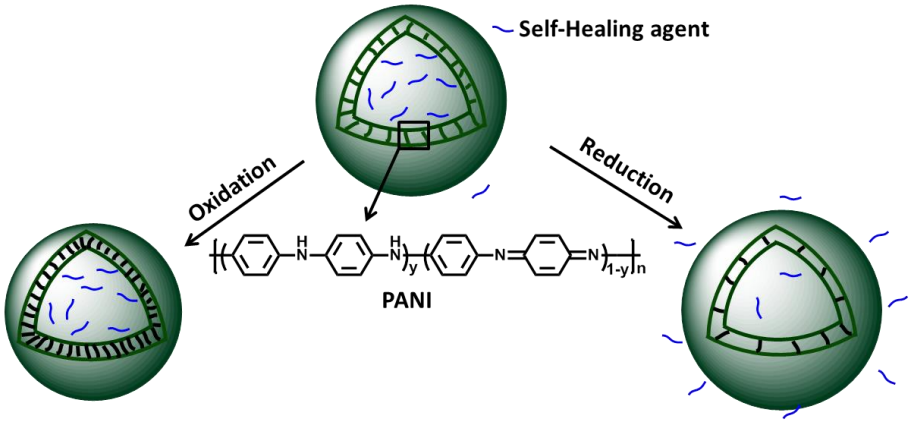

Figure 4.1 *Oxidation states of polyaniline depending on y.*

4.1.2.1 Synthesis of capsules loaded with self-healing agents

Oxidative polymerization of aniline (ANI) was conducted in direct miniemulsion to form PANI capsules. In the initial stage, there were two separated phases: the continuous phase composed of the aqueous solution of surfactant, and the dispersed phase containing the monomer and the nonpolar solvents. After mixing and ultrasonication, the miniemulsion dispersion was formed in which droplets containing some monomer and the nonpolar solvents were stabilized by the surfactant (**Figure 4.2**). The droplet interface between the aqueous phase and the oil phase was used as template for the precipitation of the growing polymer chains. The partition coefficient f_{ANI} was estimated to be equal to 11 as determined by ^{1}H NMR, that means, ~92% of the ANI was present in the dispersed phase. Thus, as the aqueous solution of oxidant, *i.e.* ammounium persulfate (APS), was added to the miniemulsion, APS molecules reacted with the ANI in the continuous phase and the growing chain nucleated the miniemulsion droplets (**Figure 4.3**). The polymer chains precipitated after a critical degree of polymerization on the interface of the droplets, because of the poor solubility of the polymer in water and in the (anti)solvent present in the dispersed phase, mainly from the inside of the droplets.

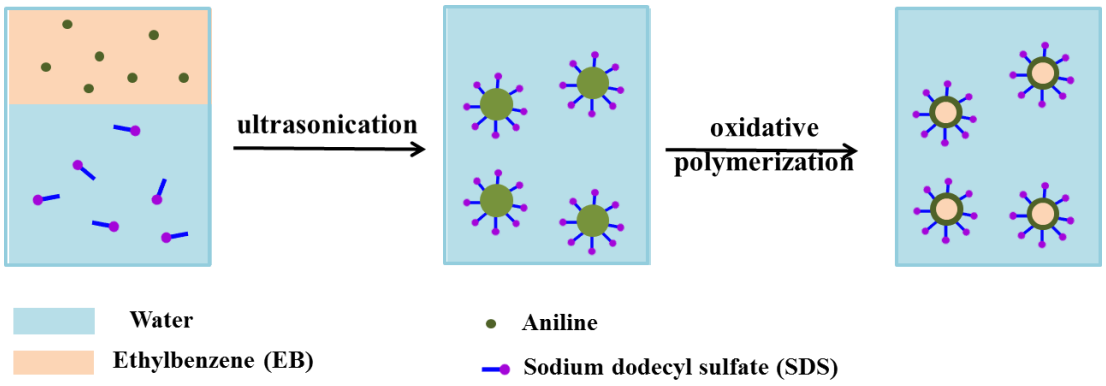

Figure 4.2 *Oxidative polymerization of aniline in miniemulsion to form conductive polymer capsules in the presence of ethylbenzene (EB).*

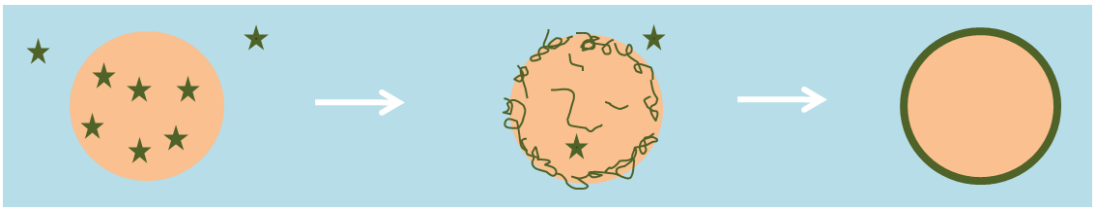

Figure 4.3 *Schematic representation of the polymerization reaction of the aniline monomers (green stars).*

The kinetics of the reaction was followed by calorimetry and revealed two interesting informations (**Figure 4.4**). First of all, the reaction took less than 30 min to be completed with most of the heat generated in the first 3 min. Second, the profile displayed two peaks whereas only one peak was observed in a polymerization of ANI in DMSO prepared for comparison **(Figure 4.4 a, b**). One probable explanation for this difference is the partition of the monomer in the two liquid phases. It is important to note that the samples were not completely thermally equilibrated because of stability issue of the miniemulsions relative to the reaction speed and therefore the classical setup was modified accordingly. After the polymerization, PANI capsules filled with EB are detected. It has been reported previously that the addition of a second stabilizer after the emulsification,[14] for example, polyvinylalcohol (PVA) or polyvinylpyrrolidone (PVP), was necessary to stabilize the polymer particles because of the high ionic strength of the dispersions. The increase of viscosity due to the addition of the stabilizer in the continuous phase allows for lowering the rate of coalescence since the droplets diffuse more slowly. The polymerization of aniline without

additional stabilizer (PVA or PVP) for the synthesis of capsules did not result in stable dispersions.

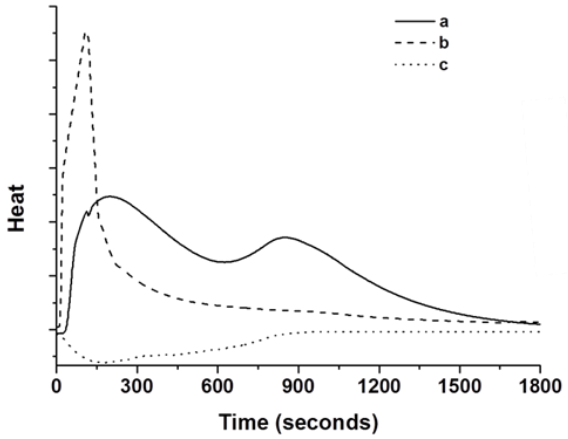

Figure 4.4 *Calorimetric thermograms of the polymerization of **a**: aniline in miniemulsion; **b**: aniline in DMSO; **c**: control measurement with aniline in miniemulsion and water added instead of APS aqueous solution.*

The morphology of PANI (**Figure 4.5**) particles was observed by electron microscopy. It was found that different morphologies were formed while increasing the ratio of ANI: EB. PANI with lower monomer concentration (PANI-1) appeared as hollow spheres with thin shells as determined by TEM (**Figure 4.5b**). Particles prepared with a higher amount of monomer (PANI-2) exhibited a multihollow morphology and kept their structural integrity even under the high vacuum of SEM (**Figure 4.5c**). The formation of particle structures with multiple domains inside is kinetically controlled and can be achieved owing to the high concentration of monomer in the droplet and because the polymerization reaction is very fast. The small amount of solvent and remaining nonreacted monomer is dispersed in the PANI particles after the polymerization and form multihollow structure after evaporation. The average diameters of these PANI capsules are 720 and 690 nm (**Table 1**). The relatively large size and distribution of size is a clear indication that the miniemulsions were destabilized during the polymerization reaction due to the high ionic strength in the dispersion. We also found that below the feed ratio of monomer in the dispersed phase, the type of surfactant and additional stabilizer (PVA or PVP) exhibited effects on the colloidal morphology. For example, when PVP K30 was employed instead of PVA (carbonyl groups from PVP and hydroxyl groups from PVA have different hydrogen-bonding interaction with PANI chains and water; there was certain amount of hydrophobic polyvinyl acetate left in PVA sample), aggregates of

nanoparticles were formed (**Figure 4.6a**) which indicated that PVP K30 is not an efficient stabilizer in our system. Changing the ionic surfactant SDS to the nonionic Lutensol AT50 and using PVP K30 as additional stabilizer led to the formation of microrods (**Figure 4.6b**). In order to slow down the reaction and the coalescence, ANI was polymerized in heterophase slightly above 0 °C. Compared to the synthesis performed at room temperature, the color change of the miniemulsion took longer time as polymerization proceeded, which indicated a slower reaction. However, the colloidal morphology of PANI was found to be the same as shown in **Figure 4.6 c, d**.

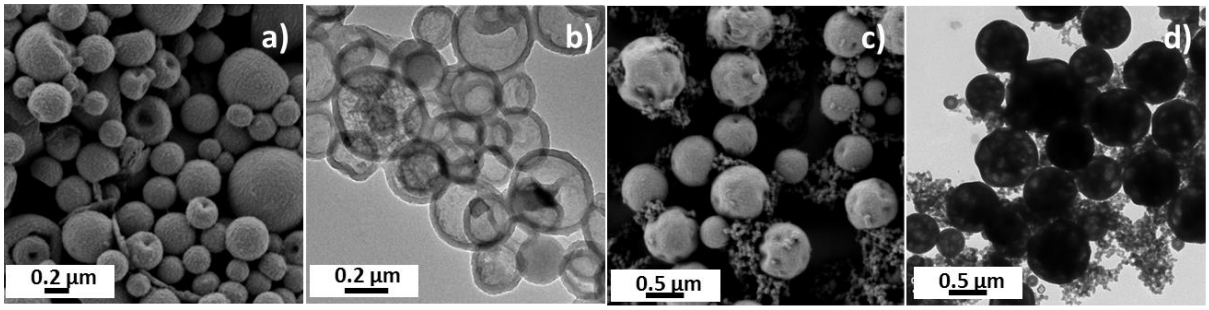

Figure 4.5 *SEM and TEM micrographs of the PANI with (**a, b**) lower fraction of monomer (PANI-1), (**c, d**) higher fraction of monomer (PANI-2).*

Table 1. *Summary of characteristics of PANI dispersions.*

Polymer	M[a]/EB [v/v]	conversion[b] [%]	M_w [c] [g·mol^{-1}]	d[d] [nm]	morphology [d]
PANI-1	29/71	72	20.050	720 ± 530	hollow sphere
PANI-2	95/5	79	10.950	690 ± 320	multi-hollow sphere
PANI/PDMS-DE	34/66	*n.a.*	*n.a.*	120 ± 50	hollow sphere
PANI/PDMS-DC	29/71	*n.a.*	*n.a.*	300 ± 140	hollow sphere

[a] M= aniline; [b] calculated from ^{1}H-NMR spectroscopy; [c] obtained from GPC; [d] determined from 100 particles by electron microscopy.

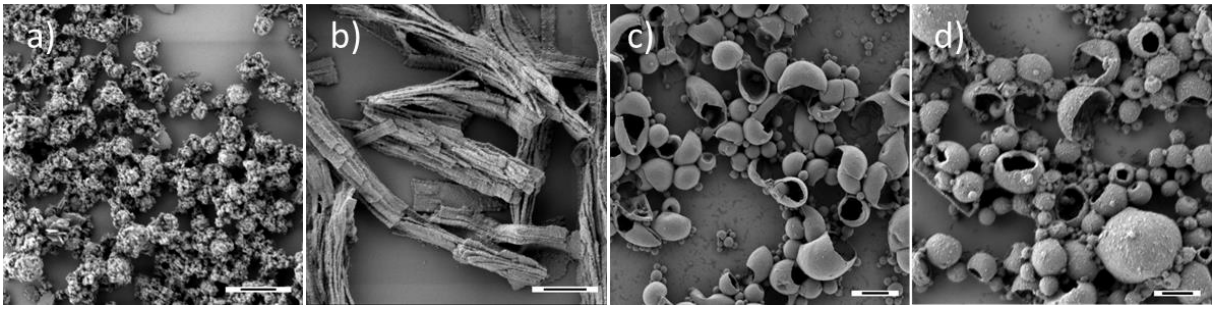

Figure 4.6 *SEM micrographs of PANI prepared: with different stabilizers* ***a)*** *SDS and PVP K30;* ***b)*** *Lutensol AT50 and PVP K30; or under different temperature* ***c)*** *RT;* ***d)*** *0 °C. The scale bars represent 1 µm.*

The reactive efficiency of aniline in miniemulsion polymerization was determined by the conversion of monomer as shown in **Table 1**. The calculation of conversion was obtained by comparing the signal of aniline in ^{1}H NMR spectra before and after the polymerization reaction (**Figure 4.7**). For these measurements, the nonpolar solvent, EB, was used as internal standard. As shown in **Table 1**, PANI-1 and -2 had 72 and 79% of converted monomer, respectively.

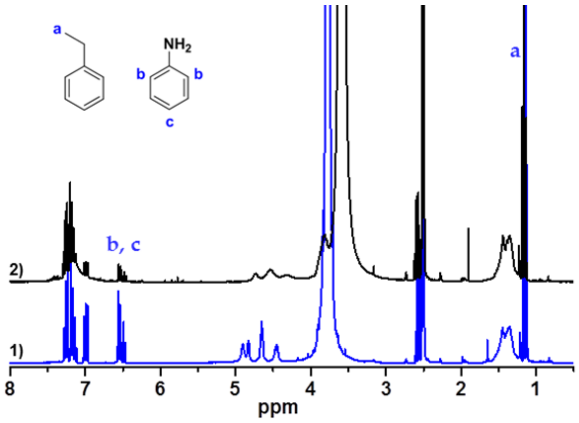

Figure 4.7 *^{1}H NMR spectra of PANI-1 dispersions before (**1**) and after (**2**) polymerization.*

In order to encapsulate self-healing agents into PANI capsules, polydimethylsiloxane diepoxide- or dicarboxylic acid-terminated (PDMS-DE or PDMS-DC) which are selected as healing agents[15] for a self-healing reaction based on polycondensations, were dissolved in the dispersed phase of the miniemulsion dispersion. The morphologies of both capsules PANI/PDMS-DE and PANI/PDMS-DC were shown in **Figure 4.8**. Both exhibited capsular structure and the diameter was ~ 120 ± 50 nm and ~ 300 ± 140 nm (**Table 1**) respectively after being estimated by counting at least 100 capsules from microscope images. Besides, the shell thickness was estimated ~ 17 ± 6 nm and ~ 56 ± 7 nm, respectively. The encapsulation of self-healing agents was confirmed by ^{1}H NMR as shown in **Figure 4.9.** The characteristic peaks assigned to PDMS-DE or PDMS-DC were found from the purified capsule samples. After comparing the signal of self-healing agents before and after purification in ^{1}H NMR spectra, ~94% and 89% of encapsulation efficiency were calculated for PANI/PDMS-DE and PANI/PDMS-DC capsules, respectively.

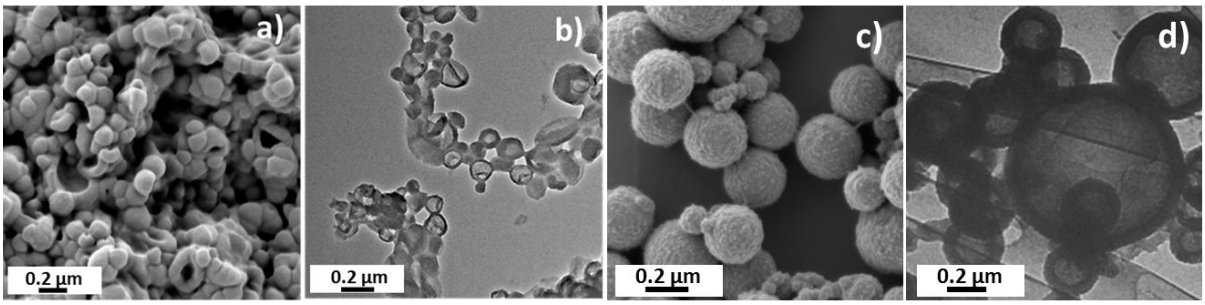

Figure 4.8 *SEM and TEM micrographs of (**a, b**) PANI/PDMS-DE or (**c, d**) PANI/PDMS-DC capsules after purification.*

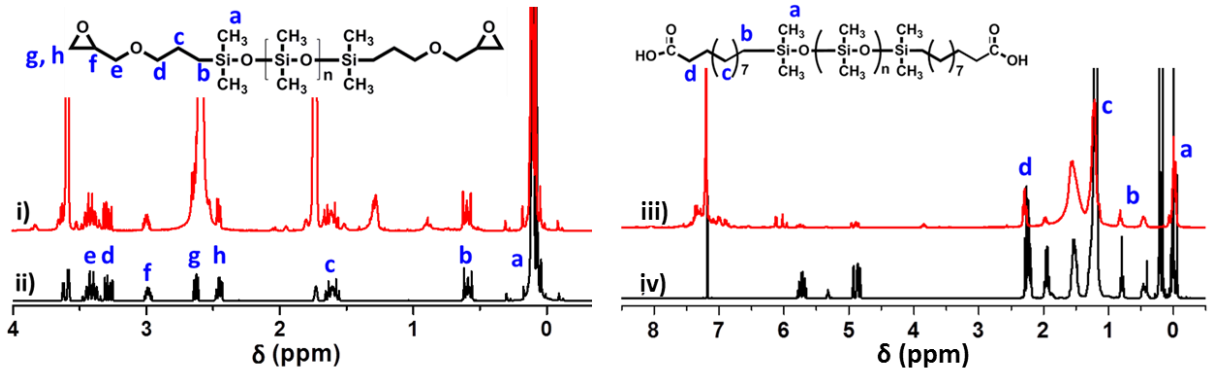

Figure 4.9 *^{1}H NMR spectra of **i)** or **iii)**: PANI/PDMS-DE or PANI/PDMS-DC capsules after purification, drying, grinding and dissolution of the PDMS-DE or PDMS-DC in $CDCl_3$; **ii)** pure PDMS-DE and **iv)** pure PDMS-DC dissolved in $CDCl_3$.*

4.1.2.2 Redox responsive release of self-healing agents

Before the study of release of self-healing agents, electro- and chemical redox-responsive properties of PANI capsules were investigated. The reversibility of the electrochemical oxidation/reduction process of PANI/PDMS-DE capsules was determined by cyclic voltammetry measurements. Stable PANI capsule dispersion in water was dropped on an ITO slide followed by drying of the sample overnight. It was found that even after 80 reduction/oxidation cycles in 1 M aqueous hydrochloric acid, a remarkable signal intensity still could be obtained in cyclic voltammograms (**Figure 4.10**) which indicates good electro-chemical redox quality and make these capsules promising for the anti-corrosion application.

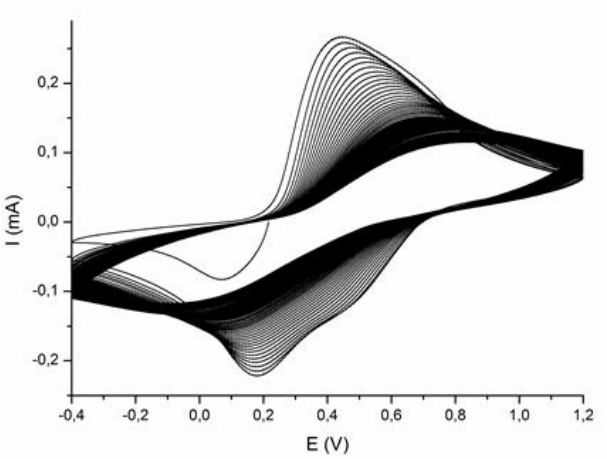

Figure 4.10 *Cyclic voltammograms of PANI. Measurements were carried out over 60–80 reduction/oxidation cycles with applied scan rates of 50 mV* s^{-1}.

The chemical redox-responsive properties of PANI capsules were also studied by optical spectroscopy and electron microscopy. A previous study showed that the oxidation degree of PANI can be estimated by comparing the intensity of the quinonoid and the benzenoid peak appearing in IR spectra. The degree of oxidation x was calculated from the intensity of the quinonoid peak I_Q relative to the benzenoid peak I_B,[16,17] using the equation:

$$x = \frac{I_Q}{I_Q + I_B}$$

Thus, the oxidation degree of the fully reduced polyaniline is estimated to 0 and the fully oxidized polyaniline to 50%. The chemical structures of PANI before and after oxidizing or reducing were characterized by FT-IR spectroscopy as shown in **Figure 4.11a**. Absorption peaks at around 1138, 1295, 1497, and 1578 cm^{-1} were attributed to the C=N stretching, C–N stretching, and stretching vibrations of the benzenoid and quinonoid rings, respectively. According to the above equation, the oxidation degree of PANI-1 and PANI-2 was calculated to be 45%. As for PANI-1, the oxidation degree (44%) did not vary much after oxidation by H_2O_2 after 12 h. After the reduction of PANI-1 by N_2H_4, the oxidation degree was estimated to be 38%, which means that the oxidation degree was decreased by ~16% compared to the non-reduced PANI (45%). The quinonoid peak sharply decreased compared to the benzenoid peak upon reduction (**Figure 4.11a**, red line). These observations were confirmed by UV–vis spectroscopy (**Figure 4.11b**). The peaks around 600 nm were assigned to the excitonic transition between the highest occupied molecular orbital (HOMO) of the benzenoid ring

(nonbonding nitrogen lone pair) and the lowest unoccupied molecular orbital (LUMO) of the quinonoid ring.[18,19] The absorption peak around 600 nm exhibits a blue-shift when PANI is oxidized and disappears upon reduction.[20] In our case, the PANI after oxidation did not exhibited much change, *i.e.* the maximum absorption changed from 571 to 567 nm after oxidation (**Figure 4.11b**), but the reduced PANI showed a pronounced intensity decrease (~ 42%) due to the lower oxidation degree after reduction. The change of color could be visually evidenced (**Figure 4.12**), especially after reduction of the PANI.

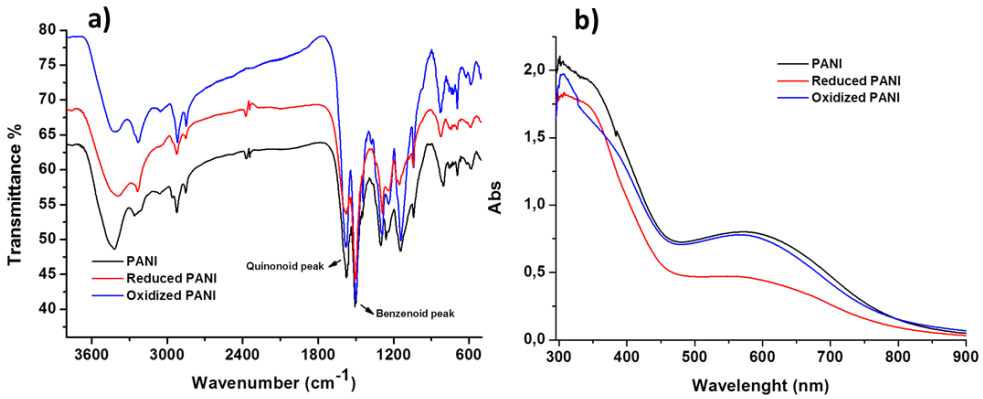

Figure 4.11 ***a)*** *FT-IR and* ***b)*** *UV-vis spectra of purified PANI-1 before and after reduction or oxidation by N_2H_4 or H_2O_2 aqueous solutions for 12 h. The molar ratio of ANI unit to N_2H_4 or H_2O_2 was 1:43.*

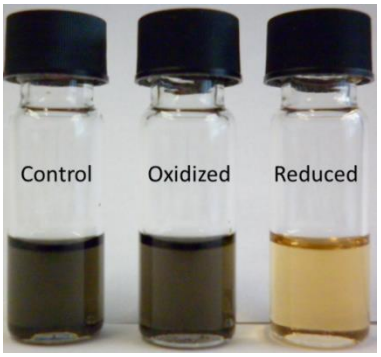

Figure 4.12 *Photographs of 0.1 mg·mL^{-1} of PANI in NMP after addition of water (control), H_2O_2 (oxidized) and N_2H_4 (reduced) after 12 h.*

The morphology of the capsules after reduction and oxidation was also observed by electron microscopy. After oxidation, the morphology of the PANI capsules (**Figure 4.13a, b**) was similar to the initial PANI-1 capsules (**Figure 4.5a, b**). However, the reduced PANI sample exhibited many collapsed capsules (**Figure 4.13c, d**). This is also an indirect indication that

the reduction of the PANI was successful because it is known that reduced PANI possesses a decreased rigidity.[21]

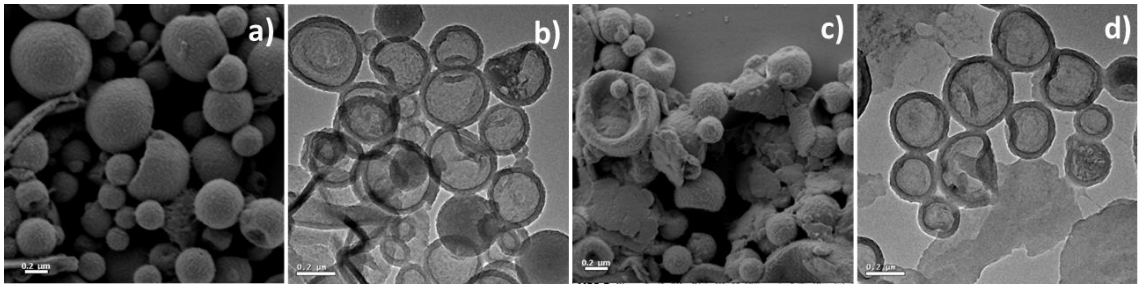

Figure 4.13 *SEM and TEM micrographs of purified PANI-1 after oxidation (**a**-**b**) or reduction (**c**-**d**) by H_2O_2 or N_2H_4 aqueous solution for 12 h. The molar ratio of ANI units to N_2H_4 or H_2O_2 was set as 1:43. The scale bars represent 0.2 µm.*

The redox-responsive properties of the PANI/PDMS-DE capsules were also investigated by using FT-IR and UV-vis spectroscopy for characterization (**Figure 4.14**). The oxidation degrees calculated from the FT-IR spectra changed from 45% to 44% and decreased to 40% after reduction. The UV−vis absorption maxima exhibited a very minor blue-shift (612 to 610 nm) after oxidation and a large decrease of intensity (~62%) after reduction. The same trends to PANI capsules without encapsulation of self-healing agents were observed for the morphologies of the PANI/PDMS-DE capsules after oxidation or reduction, that is, the morphology after oxidation remained similar to the untreated capsules whereas the structures of the reduced capsules were collapsed and film formation due to the release of PDMS-DE could be detected (**Figure 4.15**).

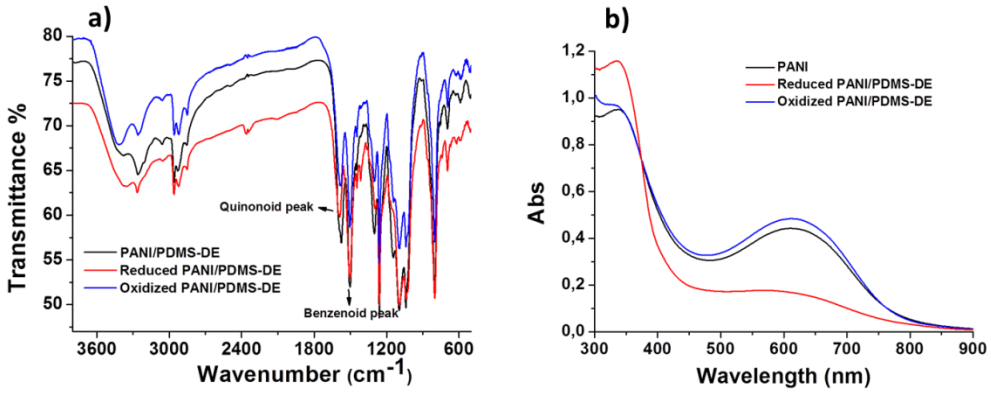

Figure 4.14 *(**a**) FT-IR and (**b**) UV−vis spectra of purified PANI/PDMS-DE before and after reduced or oxidized by N_2H_4 or H_2O_2 aqueous solution for 12 h. The molar ratio of ANI unit to N_2H_4 or H_2O_2 was set as 1:43.*

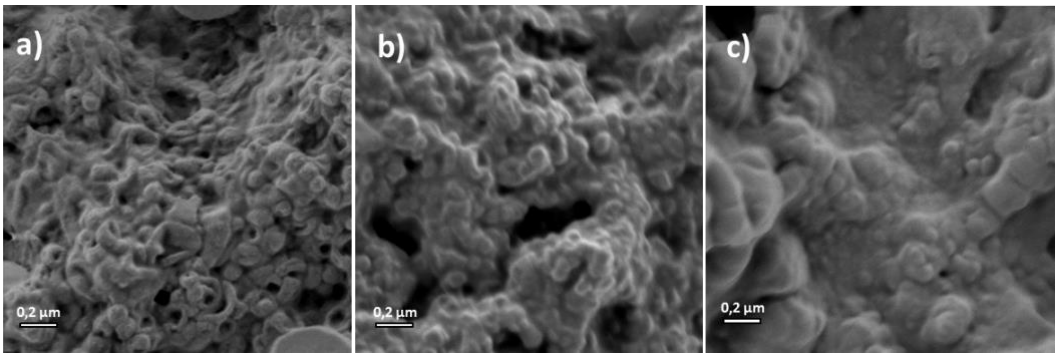

Figure 4.15 *SEM micrographs of purified PANI/PDMS-DE dispersed in THF before (**a**) and after oxidation (**b**) or reduction (**c**) by H_2O_2 or N_2H_4 aqueous solutions for 12 h. The molar ratio of ANI unit to N_2H_4 or H_2O_2 was set as 1:43.*

Finally, the redox-responsive release of PDMS-DE or PDMS-DC from PANI capsules was monitored by ^{1}H NMR spectroscopy by comparing the chemical shift of released PDMS-DE or PDMS-DC at 0 ppm to the one of pyrene at 8.5 ppm taken as internal standard. The release curves shown in **Figure 4.16a** demonstrated three different behaviors of PANI/PDMS-DE capsules depending on the nature of the added solution (reductant, oxidant, or water). The reduced sample exhibited a fast release of PDMS-DE in the first 30 min, which is corroborated by the quick color change after addition of the reductant. The control sample (addition of water) showed also a release of PDMS-DE because of the diffusion of PDMS-DE in THF. The addition of the oxidant caused a slower release behavior, even compared to the control sample. After addition of an excess of the reductant to the previously oxidized capsules, the release stimulated by reduction was again observed. A similar behavior was observed for the PANI/PDMS-DC capsules (**Figure 4.16b**). A notable difference was the amount of nonselective release at t = 0 that was lower (∼28%) than for the PANI/PDMS-DE capsules explained by the thicker shell of PANI/PDMS-DC capsules. When the capsules are purified prior to the release experiment to remove the non-encapsulated PDMS, the non-selective release at t = 0 dropped to ∼13%. The release properties of the capsules can be therefore optimized by increasing the shell thickness and by removing the non-encapsulated self-healing agents prior to their uses.

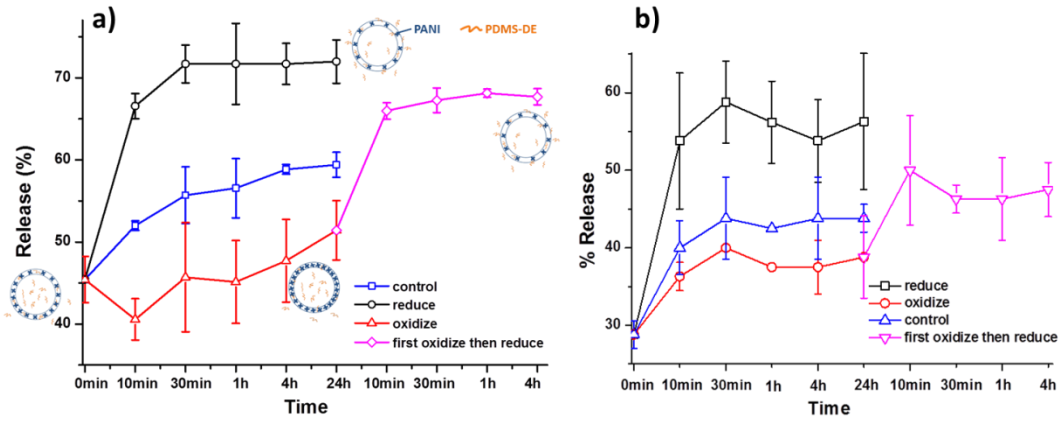

Figure 4.16 *Release of **a**) PDMS-DE or **b**) PDMS-DC from PANI capsules under different conditions. In the control experiment, the same volume of solvent and reactants are used but without oxidizing or reducing agents.*

Upon oxidation of the PANI, some benzenoid rings will be partly oxidized to quinonoid rings, leading to amine-imine intermolecular hydrogen bonding.[22] The polymer chains are then more compact and hinder the release process. In the case of the reduced sample, several factors play a role. First, the hydrogen bonding becomes weaker and polymer chains therefore are looser in the capsule membrane. Second, the presence of more rotatable single bonds in reduced PANI decreases the rigidity of the PANI chains and increases their mobility. Third, it is known that PANI exhibits different permeability and wettability depending on the redox and doping state.[23] For example, more water permeability was found for doped PANI films than undoped (reduced) films due to the increase of hydrophilicity in the oxidized state.[23] The release of PDMS-DE of PDMS-DC from PANI capsules under reduction is therefore promoted by the presence of more flexible PANI chains and the decreased hydrophilicity of the membrane facilitating the permeability of the hydrophobic PDMS.

4.1.2.3 Incorporation of capsules into composite coatings

To make self-healing capsules possible for the application of corrosion protection, one of the most important factors is their stability when incorporated into the coatings on metal. Therefore, the stability of one of the self-healing capsules, PANI/PDMS-DC, was determined when embedded either in a hydrophilic PVA film or in a hydrophobic acrylate coating since they were already investigated as passivation layers for anticorrosion.[24-28]

The PVA film with embedded capsules was re-dissolved in water to extract the capsules that were isolated and analyzed by gravimetry and atomic force microscopy (AFM). The morphology of the capsules before and after embedding exhibited only minor differences (**Figure 4.17**). Indeed, less than 5% of the observed capsules were found to have a collapsed structure after their extraction from the PVA. The determination of the amount of PDMS-DC in the extracted capsules by ^{1}H NMR spectroscopy measurements revealed that only a minor amount (~1%) of PDMS-DC was leaking from the inner core of the capsules.

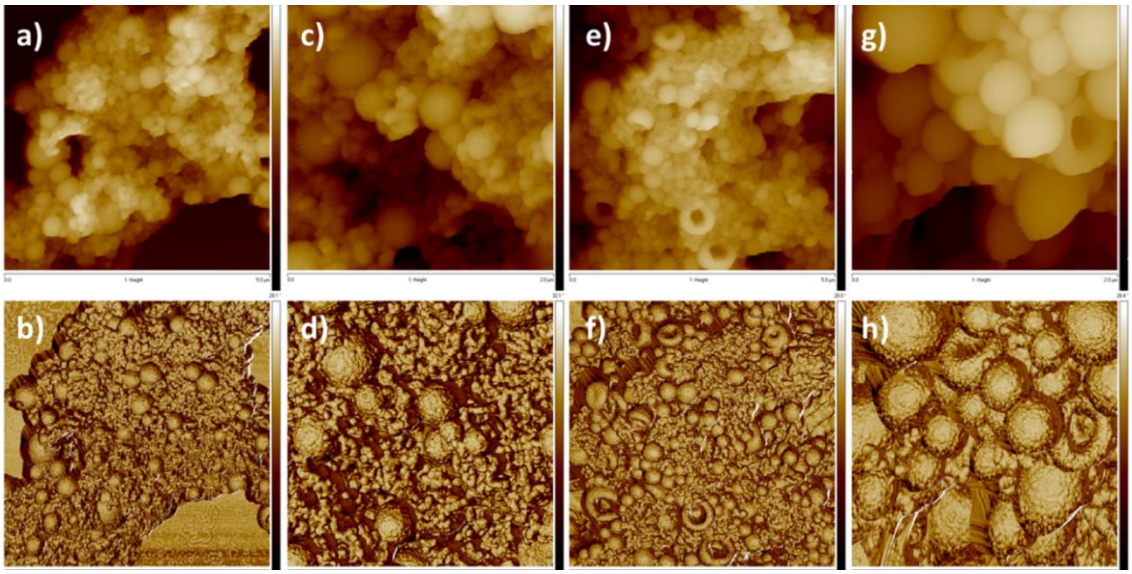

Figure 4.17 *AFM height (**a**, **c**, **e**, **g**) and phase (**b**, **d**, **f**, **h**) images of the PANI/PDMS-DC capsules before (**a**, **b**) and after (**e**, **f**) embedding in PVA film. The scales represent 5 µm×5 µm. (**c**, **d**) and (**g**, **h**) are the magnification images (2 µm×2 µm) of samples **a**) and **e**), respectively.*

It was not possible to extract selectively the capsules from the hydrophobic acrylate coatings. However, SEM images of the cross-section of acrylate coatings (**Figure 4.18**) showed that the capsule structure remained intact after being embedded in the acrylate coatings. The comparison between EDX spectra taken on the acrylate matrix and on a capsule embedded in the acrylate coating reveals the presence of silicon in the latter location (**Figure 4.19**).

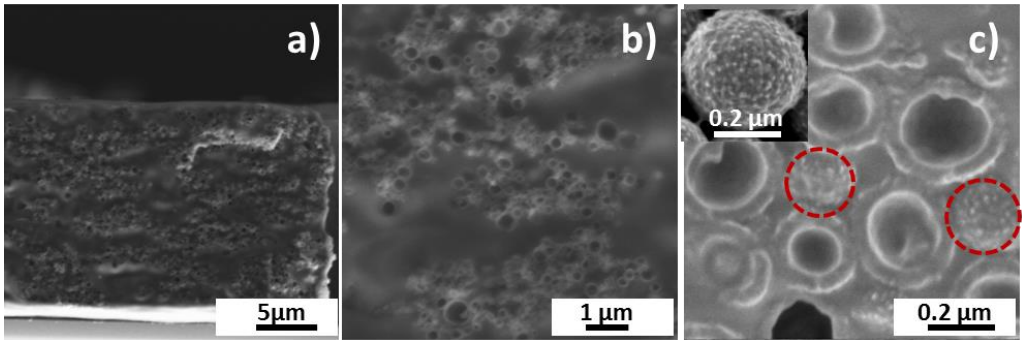

Figure 4.18 *SEM cross-section micrographs of hydrophobic acrylate coatings with embedded PANI/PDMS-DC capsules. The inset image in* ***c****) displays the surface of a PANI/PDMS-DC capsule prior to embedding in the acrylate coating, showing its similarity with the capsules remaining in the sectioned coating (red circles).*

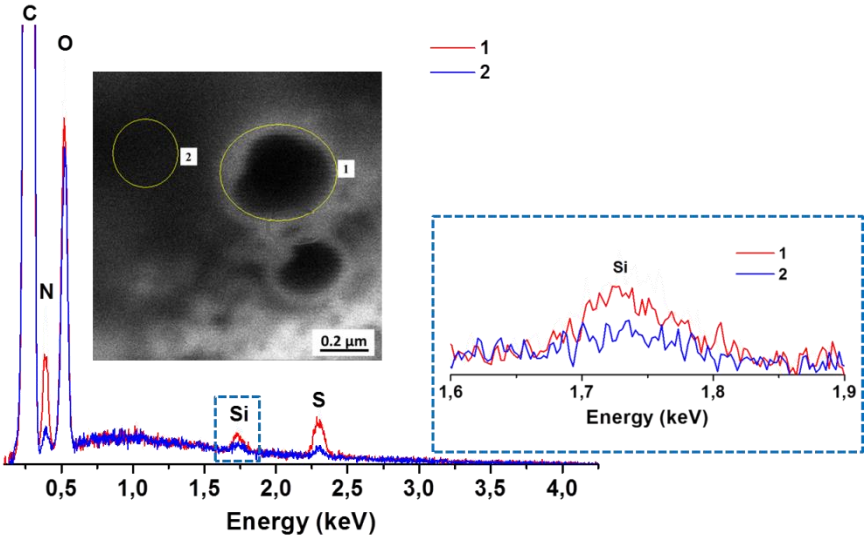

Figure 4.19 *SEM-EDX spectra of PANI/PDMS-DC capsules embedded in the hydrophobic acrylate coating. The spectrum 1 is taken on a capsule (area 1) whereas the spectrum 2 is taken near the capsule (area 2), i.e. on the matrix. The Si signal from PDMS is detected in the area 1, indicating that the PDMS is encapsulated in the PANI containers that are embedded in the acrylate coating.*

Because the PDMS-DC is the only possible source of silicon in the system, the results indicates that PDMS-DC remained encapsulated in the PANI containers that are embedded in the acrylate coatings. The capsules/acrylate coating could be also prepared on a zinc foil (**Figure 4.20**). Silicon from PDMS-DC could not be detected from EDX measurements performed on the matrix of the capsules/acrylate coating whereas a clear signal for silicon

was detectable at the location of the capsules (**Figure 4.21**). The PDMS-DC self-healing agent could therefore be kept inside the capsules after being embedded in the hydrophobic acrylate coating.

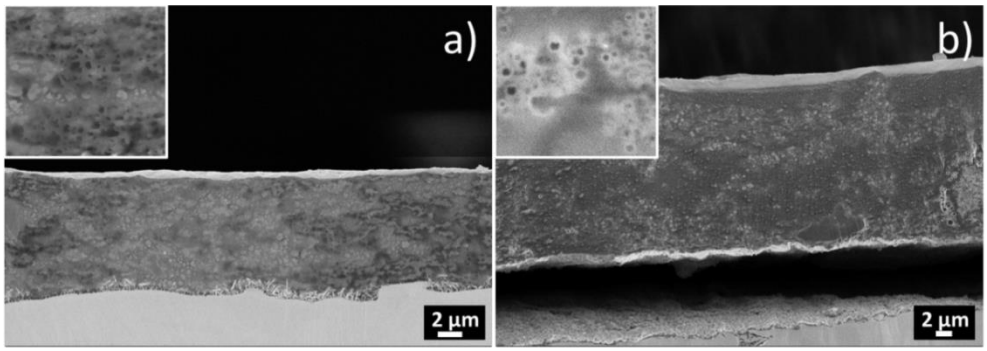

Figure 4.20 *SEM micrographs of cross-sections of the acrylate coating on zinc with incorporated **a**: PANI/PDMS-DE; **b**: PANI/PDMS-DC.*

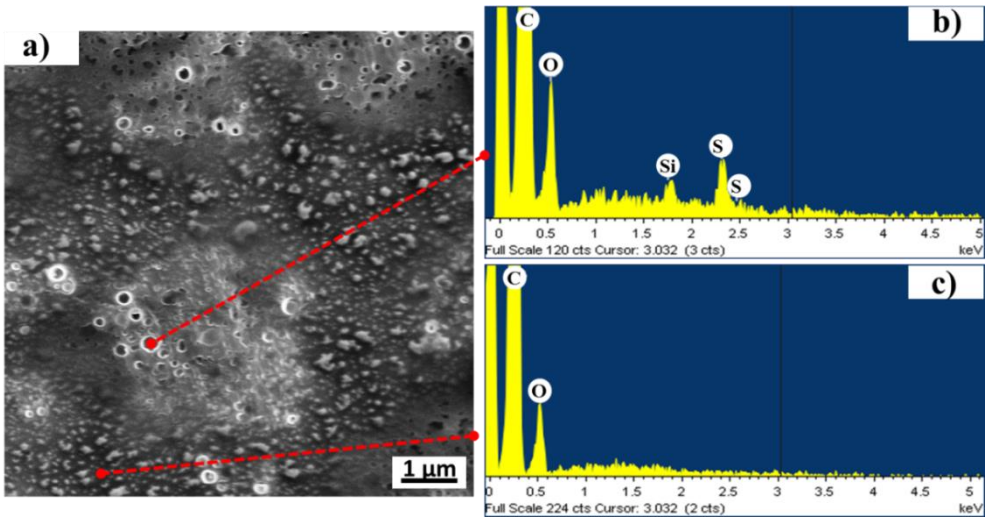

Figure 4.21 ***a**: SEM cross-section image of the PANI/PDMS-DC capsules/acrylate coating on a zinc foil. **b**: EDX spectrum of one capsule (indicated with a red dot) in the coating. **c**: EDX spectrum of the matrix (indicated with another red dot)*

In summary, PANI capsules loaded with different SH agents were synthesized and the responsive release of SH agents was achieved by varying the oxidation state of the capsule shell. Further investigation on the stability of PANI capsules showed that these capsules maintained their structures and contents when embedded in the polymeric coatings which made them promising for the application of anti-corrosion.

4.1.3 Colloidal system based on PPy and its derivatives

Except polyaniline, polypyrrole is another conducting polymer which is widely investigated.[29] Similar to PANI, it has also different oxidation states upon chemical or electrochemical redox reactions. (**Figure 4.22**) However, as already mentioned previously, the problem of solubility is a major drawback for the applicability of polypyrrole. Therefore to synthesize nanostructures based on polypyrrole and its derivatives is of importance for practical applications. In this section, formation of polypyrrole nanostructures via miniemulsion polymerization is presented. In addition, nanoparticles based on polypyrrole derivative are also prepared and their electrochemical properties were investigated.

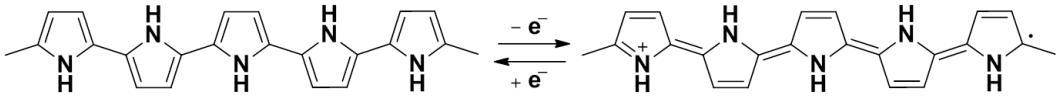

Figure 4.22 *Chemical structure of polypyrrole in different oxidation states.*

4.1.3.1 Formation of PPy nanostructures via miniemulsion polymerization

Various PPy nanostructures were synthesized via miniemulsion polymerization as shown in **Table 2**. By changing the preparation conditions such as the feed ratio of monomer in the dispersed phase, the weight ratio between the dispersed phase and the continuous phase, the concentration of stabilizer, reaction temperature as well as the type of surfactant, different morphologies of polypyrrole was formed.

The first parameter changed was the feed ratio of pyrrole in the dispersed phase. As shown in **Table 2** (PPy-1 and PPy-3) and **Figure 4.23** (**a**, **c**), when the volume ratio of pyrrole in dispersed phase was 96% or decreased to 30%, polypyrrole nanoparticles were generated in both case with distinct particle size, which was due to the different amounts of monomer in the dispersed phase. Besides, the formation of PPy particles was also determined under different reaction temperatures. It was found that the particle size become smaller when the reaction temperature decreased from room temperature to 0 °C as shown in **Figure 4.23** (**a**-**b**) or (**c**-**d**). This phenomenon could be attributed to the decrease of coalescence rate as the temperature decreased.

Table 2. *Summary of characteristics of PPy dispersions.*

Entry	Py/EB/HD [a] [v/v]	Disp/Cont [b] [wt/wt]	*Conc.*$_{PVA}$ (wt %)	Reaction T (°C)	Conversion [c] [%]	Morphology
PPy-1	96/4/0	1/4	6	r.t.	*n.a.*	**Figure 4.23**
PPy-2				0	*n.a.*	
PPy-3	30/70/0			r.t.	*n.a.*	
PPy-4				0	100	
PPy-5	96/4/0	1/19		r.t.	*n.a.*	**Figure 4.24**
PPy-6				0	90	
PPy-7	30/70/0			r.t.	95	
PPy-8				0	92	
PPy-9	30/35/35			r.t.	87	**Figure 4.26**
PPy-10				0	90	
PPy-11	30/28/42			r.t.	92	
PPy-12				0	95	
PPy-13			3	r.t.	96	**Figure 4.27**
PPy-14*				0	66	
PPy-15*	20/32/48				71	

[a] Py= pyrrole, EB=ethylbenzene, HD=hexadecane; [b] Disp/Cont=dispersed phase/continuous phase; [c] calculated from ^{1}H NMR spectroscopy; [*] The conversion of monomer of these samples was determined by using EB as internal standard. In other samples, pyrene was used as internal standard.

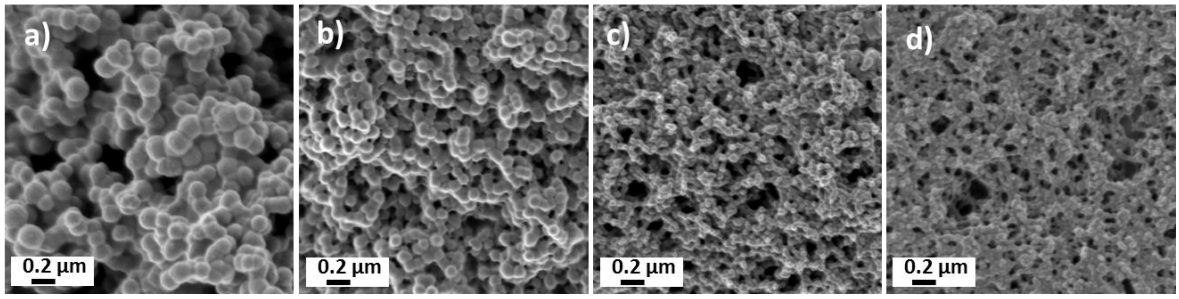

Figure 4.23 *SEM micrographs of polypyrrole structures: **a**) PPy-1; **b**) PPy-2; **c**) PPy-3; **d**) PPy-4.*

To further decrease the coalescence rate, the weight ratio between the continuous phase and the dispersed phase in miniemulsion was increased as shown in **Table 2.** In the case of samples with a higher feed ratio of the monomer, there were nanochains composed of nanoparticles generated in sample PPy-5 and 6 (**Figure 4.24 a, b**) compared to sample PPy-1 and 2. (**Figure 4.23 a, b**). This could be explained that, nanoparticles in sample PPy-1 or 2 aggregated because of strong coalescence among the particles (actually, the sample

agglomerated after polymerization), however in the latter case, coalescence in the miniemulsion dispersion was partially reduced by dilution of the continuous phase, and that is probably why nanochains were formed (**Figure 4.24a, Figure 4.25 a**).

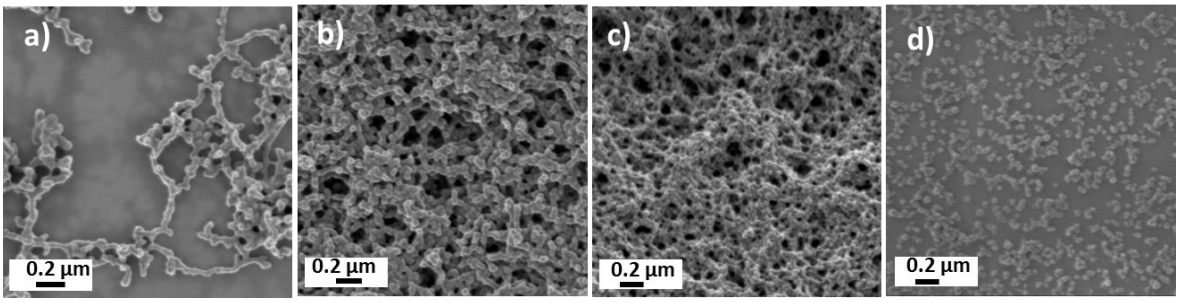

Figure 4.24 *SEM micrographs of polypyrrole structures:* ***a****) PPy-5;* ***b****) PPy-6;* ***c****) PPy-7;* ***d****) PPy-8.*

In other samples when less monomer was used, *i.e.* 30% of pyrrole in the dispersed phase, no significant difference was found, *i.e.* sample PPy-7 (**Figure 4.24 c**) compared to sample PPy-3 (**Figure 4.23 c**), after increasing the feed ratio of continuous phase. But in all cases, the particle size of PPy decreased regardless of the feed ratio of the monomer and the reaction temperature. Moreover, TEM micrographs indicated the solid structure of both samples as shown in **Figure 4.25**.

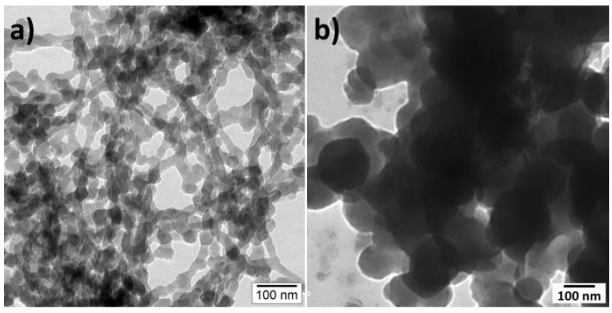

Figure 4.25 *TEM micrographs of polypyrrole structures:* ***a****) PPy-5;* ***b****) PPy-7.*

PPy nanocapsules are also considered to be interesting and useful in many cases due to their core-shell structures which provide possibility to load functional components.[30] Therefore the preparation of PPy nanocapsules is also discussed in the present chapter.

As discussed previously, after varying several preparation parameters mentioned above, only PPy nanoparticles were generated. Capsular structures were then observed when a mixture of ethylbenzene (EB) and hexadecane (HD) (1:1, v: v) was used in the dispersed phase, as shown in **Figure 4.26 (a, b)** although high polydispersity of the particle size was

found. A further increase of the feed ratio of HD compared to EB in the dispersed phase (3:2, v: v) led to more uniform capsules as shown in **Figure 4.26 (c, d)** and **Figure 4.27 (a, b, c)**. A TEM micrograph in **Figure 4.28** further indicated the core-shell structure with a hollow core in sample PPy-14 and 15.

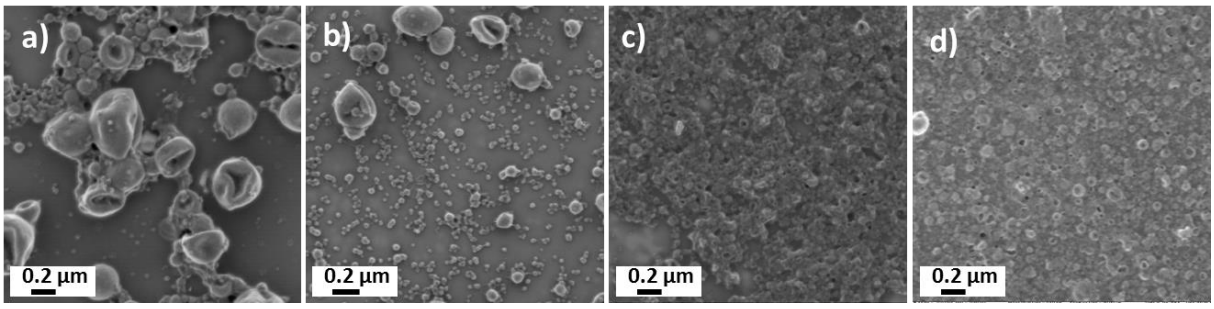

Figure 4.26 *SEM micrographs of polypyrrole structures: **a**) PPy-9; **b**) PPy-10; **c**) PPy-11; **d**) PPy-12.*

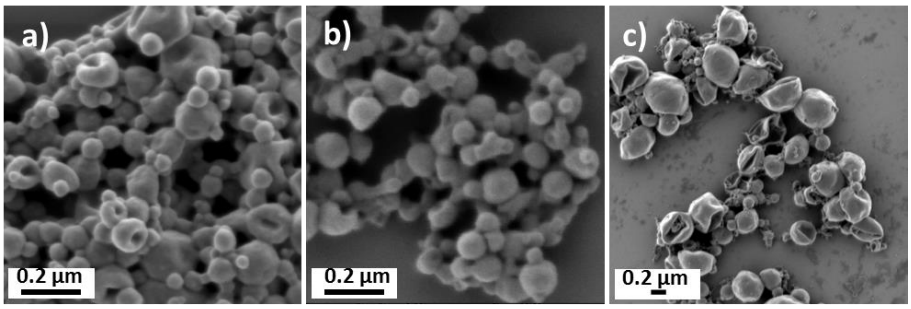

Figure 4.27 *SEM micrographs of polypyrrole structures: **a**) PPy-13; **b**) PPy-14; **c**) PPy-15.*

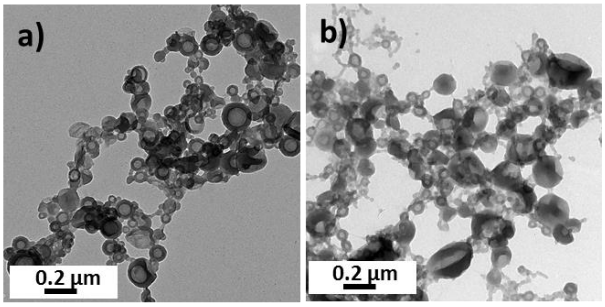

Figure 4.28 *TEM micrographs of polypyrrole structures: **a**) PPy-14; **b**) PPy-15.*

Compared to the formation of PANI capsules in which only EB was used as solvent in the dispersed phase of miniemulsion (**chapter 4.1.2**), PPy nanocapsules were only formed when a mixed solvent, *i.e.* EB and HD, was used. This observation can be explained by considering the solvent quality of EB and HD for the monomers, and the fact that the oxidation of pyrrole is faster than for aniline.[31] The reasons were given as follows: the case of Py polymerization in miniemulsion is rather unconventional compared to ANI because the

partition coefficient f_{Py} was estimated to be 0.8, that means, a significant amount of the monomer (~55%) was in the continuous phase. Thus, the growing chains of polypyrrole probably precipitated both from the inside and the outside of the miniemulsion droplets. A scheme displaying the formation of the PPy is depicted in **Figure 4.29**.

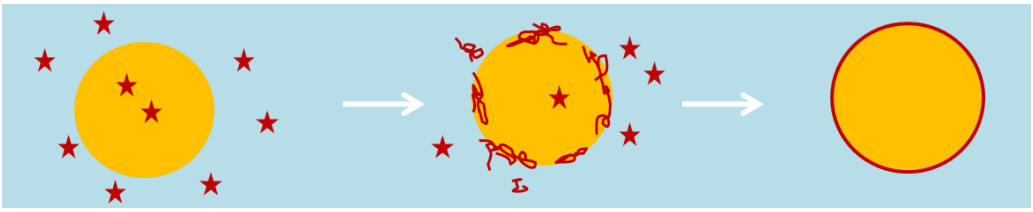

Figure 4.29 *Schematic representation of the polymerization reaction of pyrrole monomer. The red stars represent pyrrole monomers.*

So the faster oxidation of pyrrole induces that the PPy chains precipitated too fast to be able to diffuse to the interface of the droplets when only EB was used in the dispersed phase. That is the reason why only nanoparticles were formed in this case. However, when HD, which is much less soluble in water than EB and therefore more efficient to hinder Ostwald ripening of the miniemulsions, was added into the dispersed phase, the composition of the solvent was shifted toward a lower quality for pyrrole monomers. And it consequently changed the partition of the monomer in the dispersed phase and continuous phases as shown above. Thus, in the case of Py and for droplets containing a high amount of HD, the PPy chains can precipitate from the continuous phase to the droplets interfaces inducing the formation of PPy capsules.

At last, the conversion of pyrrole monomer in miniemulsion polymerization was determined as shown in **Table 2**. The calculation of conversion was obtained by comparing the signal of pyrrole in ^{1}H NMR spectra before and after the polymerization reaction (**Figure 4.30**). As shown in **Table 2**, it was found that PPy samples prepared with higher feed ratio of monomer, concentration of stabilizer, or reaction temperature exhibited higher conversion of monomer.

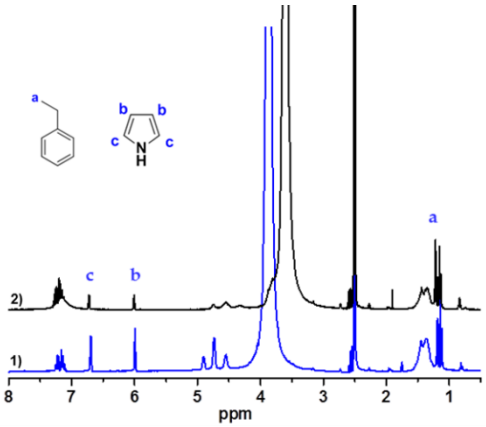

Figure 4.30 *^{1}H NMR spectra of PPy-14 dispersions before (**1**) and after (**2**) polymerization.*

4.1.3.2 Porous nanoparticles based on polypyrrole derivatives for supercapacitors

In this chapter, a Py derivative (see the chemical structure in **Figure 4.31**) is used to form nanoparticles via the miniemulsion technique. The electrochemical performance of these nanoparticles before and after pyrolysis was investigated.

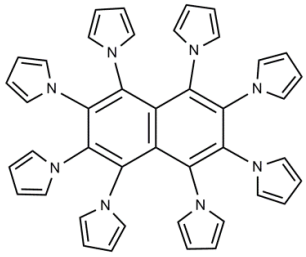

Figure 4.31 *Chemical structure of octapyrrolylnaphthalene (OPN).*

Polyoctapyrrolylnaphthalene (POPN) nanoparticles were prepared via miniemulsion polymerization process as shown in **Figure 4.32**. The dispersed phase containing the octapyrrolylnaphthalene (OPN) monomer and chloroform were first mixed with a continuous phase composed of surfactant and water. After the miniemulsification process, monomer/chloroform droplets were formed and oxidative polymerization of the monomers started after addition of initiator. The morphology of the formed POPN nanoparticles was observed by electron microscope. A multi-hollow structure was found to form according to TEM micrographs (**Figure 4.33b**). This observation was probably due to the evaporation of chloroform during the polymerization process. Furthermore, the thermal property and chemical structure of these polymeric nanoparticles were determined as shown in **Figure 4.34**. TGA spectrum exhibited only 60% of weight loss even when the handling temperature

increased to 1000 °C, indicating good thermal stability of POPN. Peaks around 1100 cm^{-1}, 1300 cm^{-1}, 1400 cm^{-1} and 1600 cm^{-1} in FT-IR spectrum were respectively attributed to the breathing vibrations of pyrrole rings, the C-N stretching vibration in the ring and C-C stretching vibrations in the pyrrole ring.

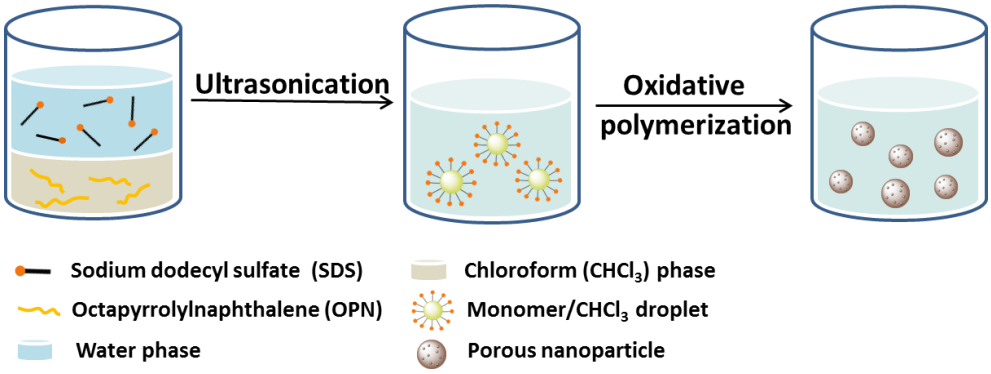

Figure 4.32 *Illustration of the synthesis of porous POPN nanoparticles via miniemulsion polymerization.*

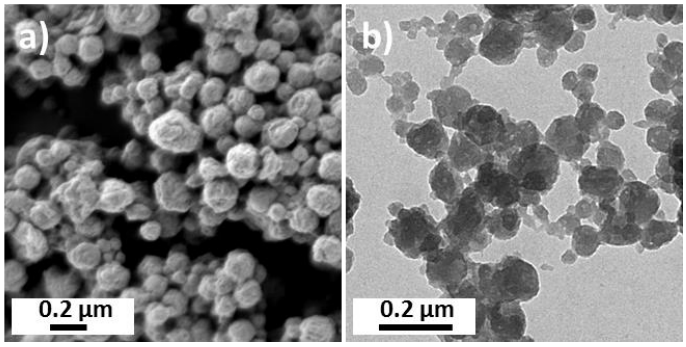

Figure 4.33 *SEM (**a**) and TEM (**b**) micrographs of POPN nanoparticles.*

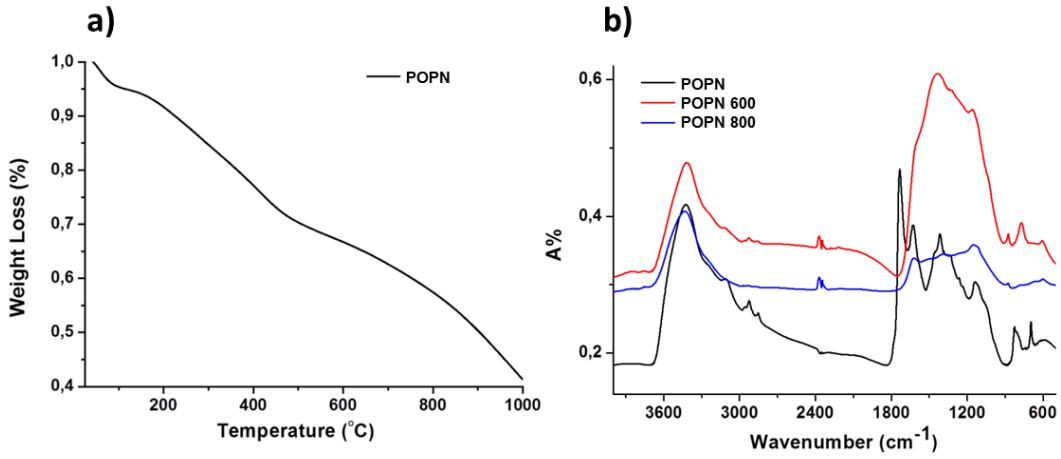

Figure 4.34 *TGA curve (**a**) and FT-IR spectra (**b**) of POPN nanoparticles after purification.*

The FT-IR spectra of POPN nanoparticles after pyrolysis at 600 °C (POPN 600) and 800 °C (POPN 800) were also investigated as shown in **Figure 4.34 b**. The vibration of C-N and C-C stretching in the ring was destroyed to some extent because of the thermal treatment during the pyrolysis process. This phenomenon become more obvious as temperature increased from 600 °C to 800 °C. The change in morphology of the nanoparticles after pyrolysis was also showed in **Figure 4.35**. The nanoparticles probably were aggregating and sintering during the pyrolysis process as many bigger particles were found compared to the original sample according to the SEM micrographs. Furthermore, the surfaces of the particles appeared rougher and more porous after thermal treatment compared to the original sample.

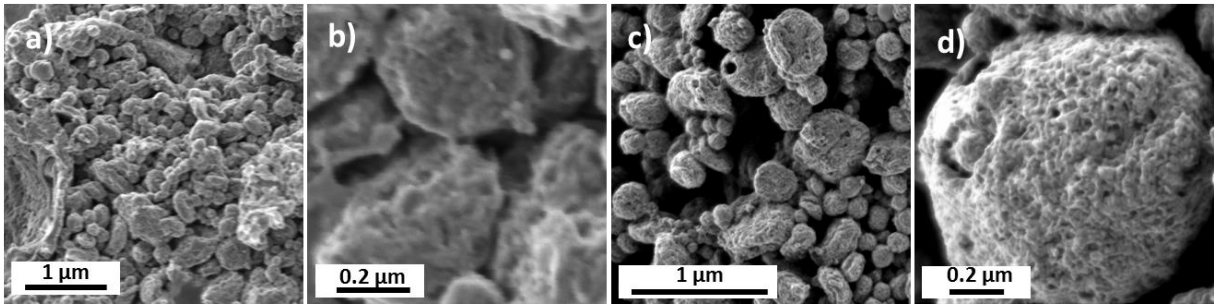

Figure 4.35 *SEM micrographs of POPN nanoparticles after pyrolysis at 600 °C (**a**, **b**) or 800 °C (**c**, **d**). **b**) and **d**) are respectively from the image of **a**) and **c**) with higher magnification.*

The electrochemical performance of POPN porous particles was further investigated. As shown in **Figure 4.36**, all the cyclic voltammetry (CV) profiles showed typical electrical double layer behavior at all the sweeping rates. However, the specific capacitance of each sample was quite different as shown in **Figure 4.37**. In POPN sample without pyrolysis, the specific capacitance obtained at 2 mV s^{-1} was only ~40 F g^{-1} while in the other POPN sample after pyrolysis under 600 °C, the value increased to 100 F g^{-1}. The specific capacitance of POPN sample after pyrolysis under 800 °C was almost 4 times as high as the untreated one, *i.e.* 156 F g^{-1} at the scan rate of 2 mV s^{-1}. Moreover, even when the scan rate increased to 100 mV s^{-1}, the capacitance value of POPN 800 was still ~80 F g^{-1} which indicated much better electrochemical performance than sample POPN and POPN 600. The possible explanation for the different electrochemical performance among these samples could be the change in chemical components as well as the morphology as shown previously. Firstly, after thermal treatment, the components of POPN nanoparticles become more carbon-

based which could contribute to the better electrochemical properties. Secondly, the more porous structure may provide particles with higher surface area which would contribute to high energy densities for supercapacitors.[32] These nanoparticles based on polypyrrole derivatives are promising electrode materials for high-performance electrochemical supercapacitors.

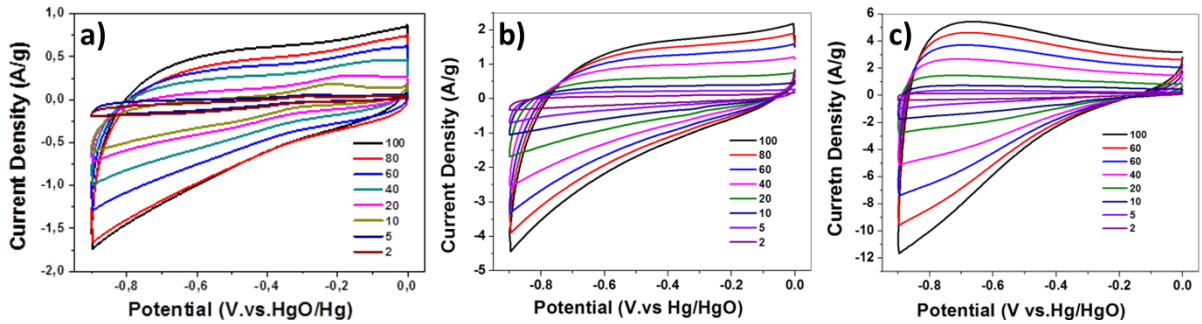

Figure 4.36 *Cyclic voltammetry of electrodes prepared with POPN before (**a**) and after pyrolysis at 600 °C (**b**) or 800 °C (**c**) and measured at different scan rates (mV s^{-1}) in 1M of H_2SO_4 electrolyte.*

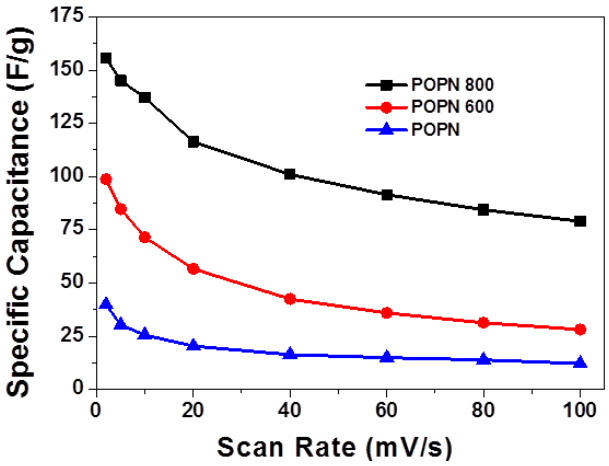

Figure 4.37 *Specific capacitance as a function of scan rates for POPN before and after pyrolysis at 600 °C or 800 °C.*

4.1.4 Other attempts

In the previous chapter, nanocapsules or nanoparticles based on polyaniline or polypyrrole and their derivatives were prepared and their properties were studied for various potential applications. In this section, some other attempts are also presented. In the first section, attempts to synthesize solvent-soluble conducting copolymers are presented. In the second section, tricompartment particles with organic/inorganic components were synthesized.

4.1.4.1 Synthesis of solvent-soluble conducting copolymers

It is known that due to the stiffness of the main chains, conducting polymers composed of conjugated double bonds usually have poor solubility in most of the solvents. To avoid the problem of poor solubility, synthesis of conducting polymers directly in their applied form was usually adopted. Although difficult to be dissolved, conducting polymers that are soluble are interesting because they can be processed from solution. Moreover, it is also possible to combine their physical, mechanical as well as electrical properties.[33] Examples of soluble conducting polymers include polythiophene derivatives,[34-37] polyaniline derivatives,[38] and polyacetylene block copolymers.[39] Besides, by doping with functionalized protonic acid solutes, the polyaniline complex was also found to be soluble in common organic solvents.[40, 41] In this chapter, efforts to synthesize soluble conducting polymers are presented. The idea was to copolymerize thiophene or pyrrole monomers with the thiophene units from the side chain of a soluble polymer (**Figure 4.38**). The synthetic routes followed the previously reported method.[42,43]

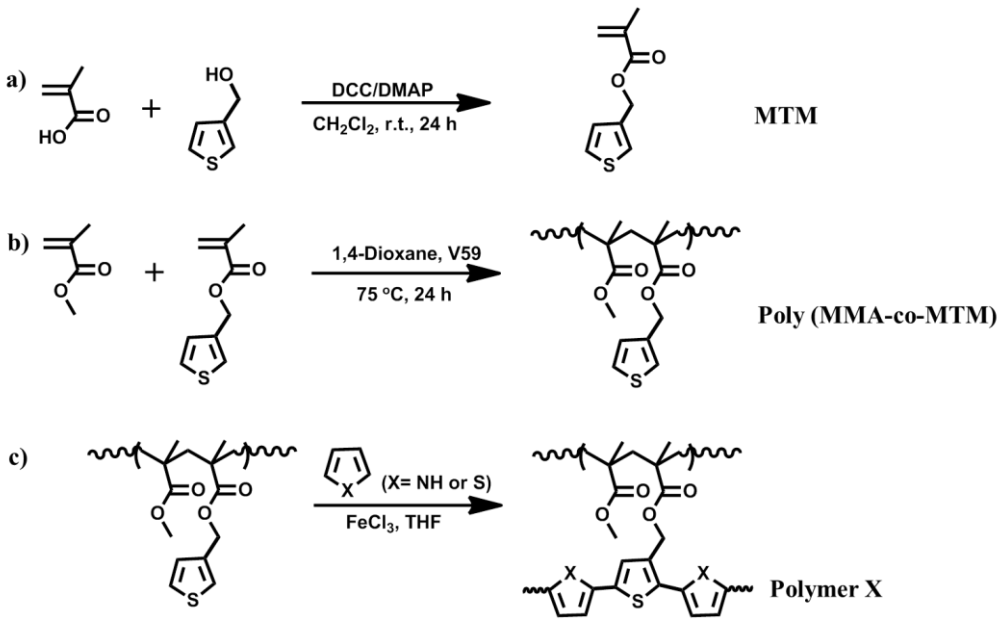

Figure 4.38 Synthesis *of conducting graft-copolymers. Polymer X=Poly(MMA-co-MTM-g-PPy) or Poly(MMA-co-MTM-g-PTP).*

The first step was to synthesize the monomer 3-methylthienyl methacrylate (MTM) containing thiophene unit as shown in **Figure 4.38 a**. The radical copolymerization of MTM and MMA was initiated by V59 in 1,4-dioxane at 75 °C. After precipitating the product in

methanol, the synthesized copolymer was collected and dried under vacuum. ^{1}H NMR spectra in **Figure 4.39 and 4.40** indicated the successful synthesis of MTM and poly(MMA-*co*-MTM), respectively. By comparing the respective signal from MMA (δ 3.5 ppm) and MTM (δ 4.9 ppm), the molar ratio of MMA to MTM in the copolymer was calculated to be 23:1. The molecular weight (M_w) of the copolymer was estimated to be 43500 g mol^{-1} by GPC measurement.

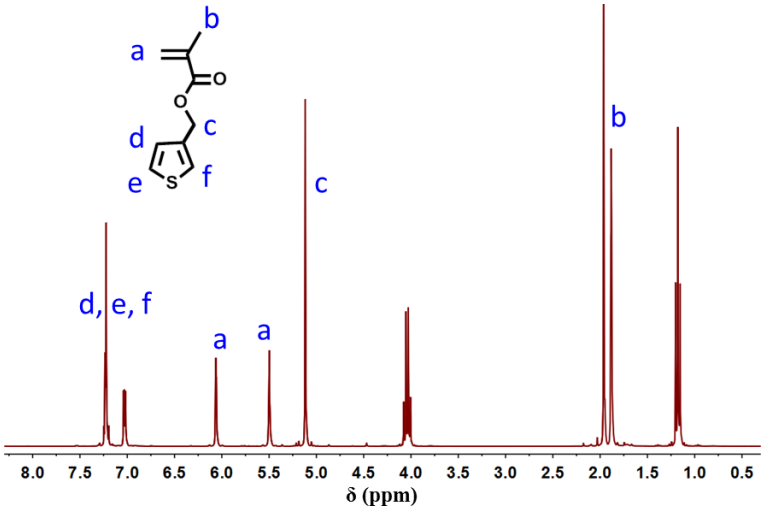

Figure 4.39 *^{1}H NMR spectrum of the 3-methylthienyl methacrylate monomer in $CDCl_3$.*

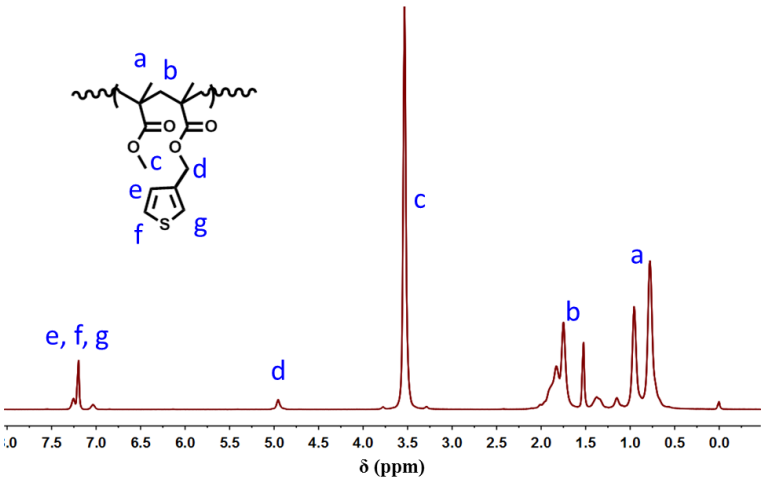

Figure 4.40 *^{1}H NMR spectrum of the synthesized copolymer poly(MMA-co-MTM) in $CDCl_3$.*

After the synthesis of poly(MMA-*co*-MTM) copolymers, monomers such as pyrrole or thiophene were added and oxidative polymerization was expected to occur in the presence of the oxidant $FeCl_3$. The resulted products were analyzed by using ^{1}H NMR as shown in **Figure 4.41**. However, there was nearly no copolymerization of the pyrrole or thiophene monomer with the thiophene units from poly(MMA-*co*-MTM) copolymers. It was expected

that the molar ratio of protons from pyrrole ring or thiophene ring (position f, g as indicated in **Figure 4.41**) compared to that of the copolymer backbones (postion a, b as indicated in **Figure 4.41**) would increase if pyrrole or thiophene monomers were polymerized to the thiophene units of the copolymers. However, the signal of pyrrole or thiophene rings did not exhibit obvious increase after copolymerization as shown in **Figure 4.40** and **4.41.** There are probably two reasons for the observation. Firstly, because of the steric hinderance effect, free pyrrole or thiophene monomers preferred to react with themselves instead of the thiophene segments in the copolymers. Secondly, once oxidative polymerization of pyrrole or thiophene occurred, the pH value of the solution decreased due to the generation of protonic acid. As a result, the ester bonds from the poly(MMA-*co*-MTM) were possibly hydrolyzed when pH value of the solution decreased below ~ 6.[44] Based on the reasons metioned above, the procedure to copolymerize thiophene or pyrrole monomers with the thiophene units from the side chain of a soluble polymer was not feasible with the present preparation conditions.

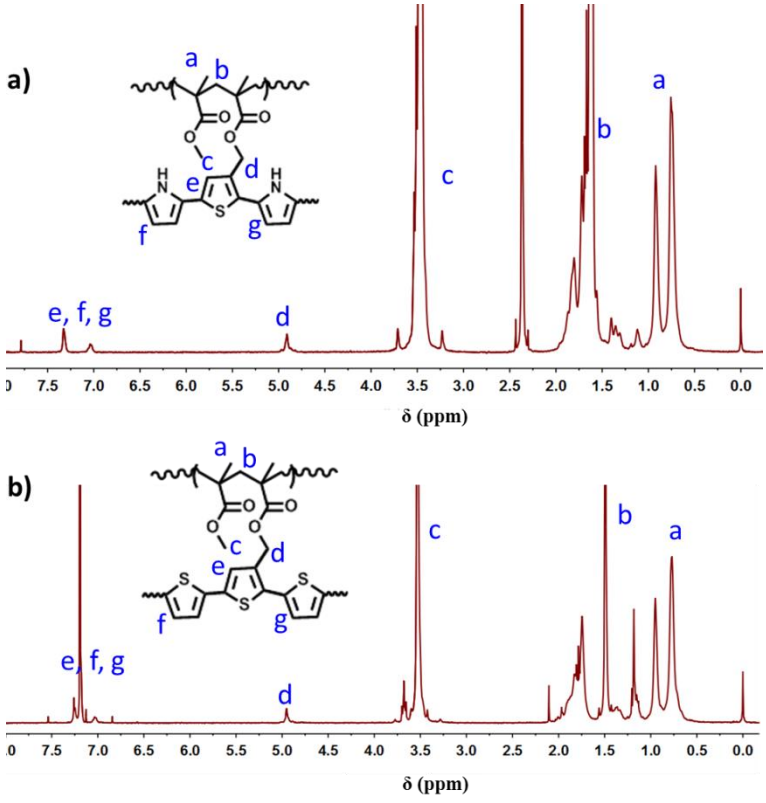

Figure 4.41 *^{1}H NMR spectra of the copolymers: **a**) poly(MMA-co-MTM-g-PPy) in d-DMSO and **b**) poly(MMA-co-MTM-g-PTP) in $CDCl_3$.*

4.1.4.2 Decoration of colloid with TiO_2 nanoparticles

Colloidal systems based on conducting polymers were presented in the previous chapters. However, most of them consist of only organic components or form structures no more than binary. Multicompartment structures are of great interest for applications because they may exhibit more than one functionality due to the multiple components. The probably simplest multicompartment colloidal morphology is the Janus particle that displays two compartments.[45-47] Multicompartment colloidal structures can be also produced by assembling spherical homogeneous particles[48-50] or patchy particles,[51] yielding so-called colloidal molecules.[52,53] On the other hand, the assembly of multicompartment building blocks gives rise to hierarchical structures with generally more compartments per macrostructure than the ones present in the initial units.[54-57]

Tricompartment particles have one more compartment than Janus particles. In the classification of Gillespie[58] used to describe the so-called colloidal molecules, tricompartment particles with two different chemical species can exist as bent (AX_2E_n, n =1,2) or linear structures (AX_2 or AX_2E_n, n = 3,4). The latter is however difficult to obtain in practice. Approaches include the use of an external magnetic field to orient the particles and are therefore limited to magnetic particles,[59] or the employment of several steps in seeded-emulsion polymerization techniques.[60,61] Lithographic methods were also employed to create multiphase triblock rod-like particles.[62]

Herein, we demonstrate a facile and scalable one-pot method to obtain tricompartment submicron particles with three different chemical compositions in a linear triblock fashion. The strategy relies on the internal phase separation between the polymers and the TiO_2 nanoparticles during the preparation of the multicompartment particles. The experimental approach combines the emulsion-solvent evaporation with the miniemulsion polymerization techniques. The first technique was found to yield to the formation of nanocapsules[15,63,64] with only a very low extent of coalescence when the evaporation is carried out from miniemulsion droplets.[65,66] It was also used to prepare aggregates of iron oxide nanoparticles to form larger particles[67] and hybrid Janus magnetic particles.[68-70] The phase separation in droplets/ particles prepared by the emulsion-solvent evaporation technique between two homopolymers,[71] or of blends of homopolymers or diblock copolymers in the presence of gold nanoparticles was investigated.[72] The morphology could be controlled by

the type and concentration of stabilizer[71] and by the hydrophobicity of the polymers.[72] The miniemulsion polymerization on the other hand offers the possibility to synthesize a large variety in composition and morphology of polymer nanoparticles.[73]

In the first step, Janus particles were formed with one inorganic and one organic face (**Figure 4.42**). For this, a polymer with low affinity towards the TiO_2 nanoparticles (polyvinylformal: PVF) was selected. Then these two components were dissolved or dispersed together in a low boiling point solvent (chloroform). The hydrophobic liquid could be emulsified in the form of tiny droplets stabilized using a surfactant and dispersed in water. After evaporation of chloroform, the Janus nanoparticles with a hydrodynamic diameter of 142 ± 11 nm (**Table 3,** entry 2) could be formed as shown by transmission electron microscopy (TEM) in **Figure 4.43b**. The amount of TiO_2 in the Janus nanoparticles could be increased from 20 to 48 wt.% (compared to PVF), although for this amount the structures of the nanoparticles were less controlled (entry 6, **Table 3**). Indeed, the TiO_2 patches were not always distributed in one single domain on the PVF particles surfaces as it was the case when less TiO_2 was employed (entry 2).

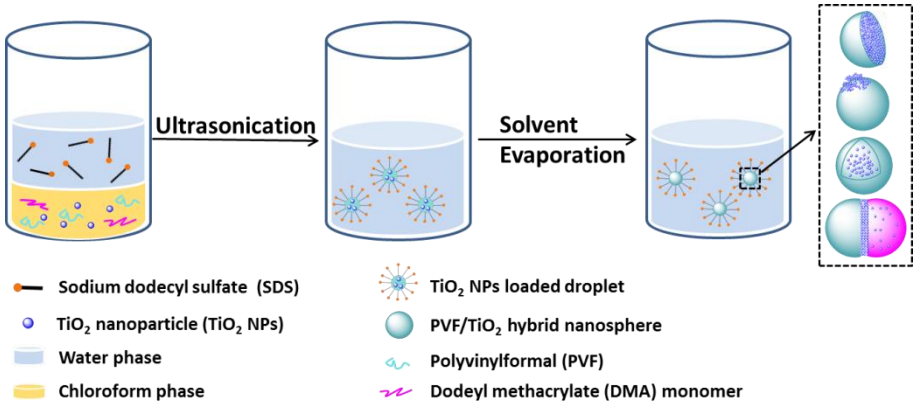

Figure 4.42 *Illustrations for the preparation of PVF/TiO_2 and PVF/PDMA/TiO_2 hybrid nanoparticles with the different possible morphologies.*

In order to add another compartment to the nanoparticles, hexadecane (HD) was added to the dispersed phase because it is a non-solvent for PVF. In this case, Janus morphologies with one liquid phase (HD), one PVF phase, and additionally TiO_2 nanoparticles in the middle were formed (entry 1A of **Table 3**). The sizes of the particles were larger (~220 nm compared to ~140 nm without HD) due to the additional volume of HD in the particles. The TiO_2 nanoparticles adsorbed on the PVF/HD interfaces to lower their interfacial tension instead of

Table 3 *Characteristics of the PVF/TiO_2 hybrid particles and their observed morphologies.*

Entry	HD [mg]	TiO_2/xylene [mg]	SDS [mg]	Evap. ***t*** [h]	Morphology	D_h ** [nm]
1A	250			12	HD/PVF Janus with TiO_2 plate	222 ± 73
1B			20	6	HD/TiO_2-PVF core-shell	245 ± 94
2	0			12	PVF/TiO_2 Janus hybrid	142 ± 11
3A		50	15	12	HD/polymer Janus with TiO_2 plate	305 ± 124
3B	250				HD/TiO_2-PVF core-shell	265 ± 102
4A *			20	6	HD/TiO_2-PVF core-shell	233 ± 79
4B *		100			HD/TiO_2-PVF core-shell	265 ± 110
5	250	120	15	12	HD/PVF Janus with TiO_2 plate	293 ± 103
6	0	120	15	12	PVF/TiO_2 Janus hybrid	188 ± 55

* *prepared at 45 °C;* ** *determined by DLS.*

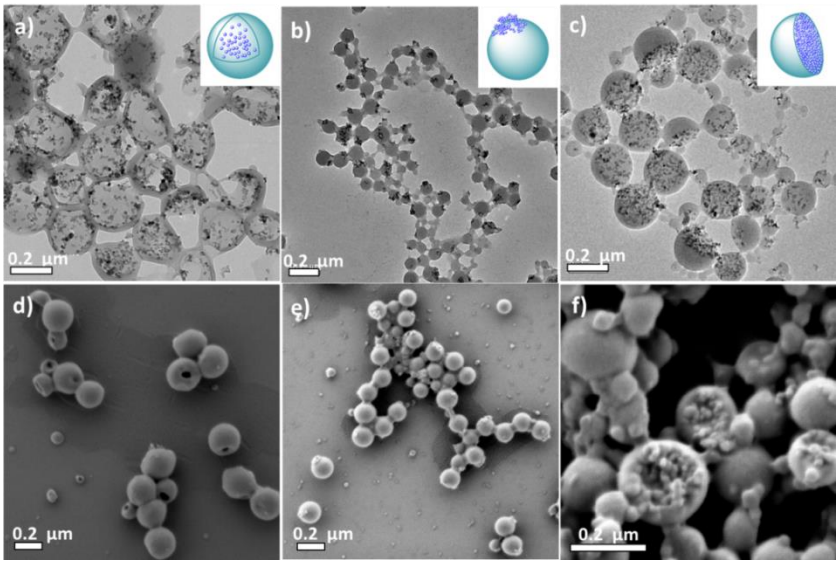

Figure 4.43 *SEM and TEM micrographs of PVF/TiO_2 particles with different morphologies:* ***a****,* ***d****) entry 4B;* ***b****,* ***e****) entry 2;* ***c****,* ***f****) entry 1A.*

being expelled outside the nanoparticles. Depending on the concentration of TiO_2 in the dispersed phase, the PVF/HD interface was partially (entry 1A, **Figure 4.43c, f**) or completely (entry 5, **Figure 4.44a, d**) covered with TiO_2. Interestingly, the structure of the particles changed from core-shell with TiO_2 nanoparticles in the core (**Figure 4.43a, d**) to Janus particle with an inorganic plate between the 2 organic phases when the time of evaporation increased from 6 h to 12 h. This observation was independent of the surfactant concentration and TiO_2 amount in the intervals that were employed (**Table 3**, Entry 3B, 4A-B).

After at least 10 h, the chloroform evaporated completely whereas there was still ~30% of chloroform left after 6 h as measured by ^{1}H NMR spectroscopy.[74] Based on these values, it is expected that the remaining chloroform decrease the interfacial tension in the case of an evaporation time of 6 h. This in turn affects the final particle morphology[75] according to the possible equilibrium configurations determined by the interfacial tensions between the different phases.[76] Because $\sigma_{PVF/(HD+CHCl3)} << \sigma_{PVF/water} < \sigma_{(HD+CHCl3)/water}$, completely engulfed morphologies (with spreading coefficient S1 < 0, S2 < 0, S3 > 0) can be formed[76] and therefore core-shell structures were formed after 6 h. The morphology was trapped by fast removal of the chloroform under the high vacuum of the electron microscope. When chloroform was removed for 12 h, high interfacial tension between hexadecane and PVF induced the partially engulfed morphology: $\sigma_{PVF/water} < \sigma_{HD/water}$, $\sigma_{PVF/water} < \sigma_{HD/PVF}$ (spreading coefficient S1, S2, S3 < 0). The TiO_2 nanoparticles were dispersed in hexadecane and therefore stayed on the hexadecane side of the acorn structures-leading TiO_2 plates after removal of the hexadecane. As expected for colloids prepared from miniemulsion, the colloids were larger (D_h= 305 nm, entry 3A of **Table 3**) when the concentration of surfactant was decreased.

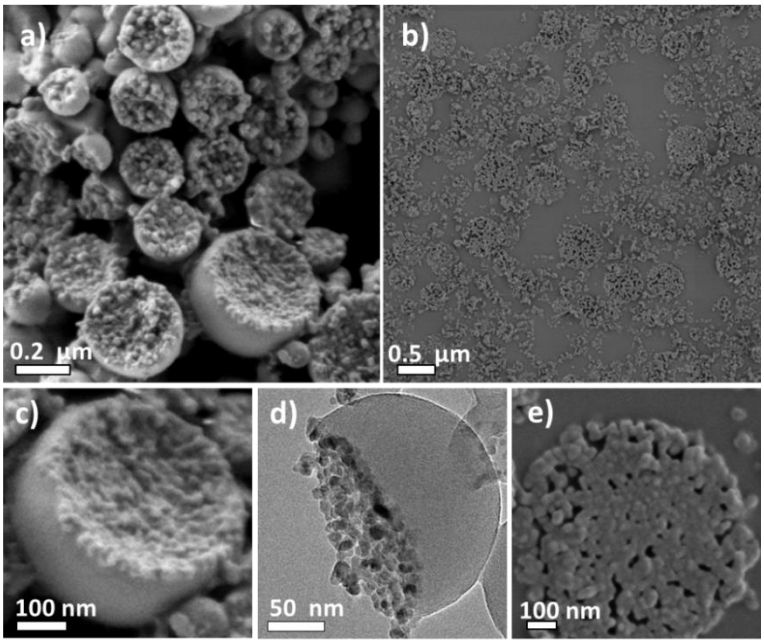

Figure 4.44 *SEM micrographs of PVF/TiO_2 hybrid hemisphere, entry 5:* ***a****) before and* ***b****) after calcination at 800 °C for 16 h.* ***c****) and* ***d****), high-magnification SEM and TEM image of one hemisphere.* ***e****), high-magnification SEM image of one hybrid hemisphere after calcination.*

Furthermore, we could use the polymer/hexadecane interface as a template for fabricating TiO_2 nanodisks. For this, the Janus particles with high load of TiO_2 at their interface were calcinated and observed by scanning electron microscopy (SEM) (**Figure 4.44b, e**). This method represents a novel extension to traditional colloid engineering for which usually the surfaces of particles or capsules are the templates and therefore yield spherical capsular structures only.

To introduce a second polymeric compartment in the hybrid structure, a monomer was chosen to replace HD (**Table 4**). Dodecyl methacrylate (DMA) was selected because it is very hydrophobic, liquid at room temperature, and can be easily polymerized by free-radical polymerization. Because poly(DMA) (PDMA) has a very low T_g around -48 °C,[77] it was cross-linked with 5 or 10 wt.% divinylbenzene (DVB) compared to the total amount of monomers to lock the structure and avoid film formation upon deposition of the nanoparticles on surfaces. We verified that Janus particles with a DMA face and a PVF face could be formed similarly to the PVF/HD Janus particles by observing the particles before polymerization. As shown in **Table 5**, hemispheres with relatively flat surface covered by TiO_2 were fabricated before polymerization with high (H1) and low (H3) amount of TiO_2, respectively (**Table 4**). Depending on the concentration of the cross-linker (5 or 10 wt.% DVB), different morphologies were observed after 1 h polymerization. Janus particles could be already observed for high amount of DVB (H1) whereas film formation from the DMA/PDMA domains was observed with a lower amount of DVB (**Table 5**, H2) still with TiO_2 present at the Janus interface. After the polymerization, polymer/ polymer Janus particles with hydrodynamic diameters >200 nm and decorated with TiO_2 at the Janus interface were observed (**Table 5**). The morphologies are particularly remarkable because one face is an elastomer whereas the other face is an amorphous polymer with a high T_g ($T_{g[PVF]}$ ~ 108 °C).[78] Even when lower amount of TiO_2 was used in the particles, the obtained morphologies were similar although the TiO_2 domains were less clearly identifiable (**Table 5**, H3 and H4).

Table 4 *Characteristics of the tricompartment nanoparticles with two different polymers and TiO_2.*

Entry	Hydrophobic monomers [mg]		Hydrophilic monomers *	TiO_2/xylene [mg]	Surfactant	D_h ** [nm]
	DMA	DVB				
H1	252	28		120	SDS	239 ± 72
H2	266	14	no	120		250 ± 51
H3	252	28		50		236 ± 56
H4	266	14				251 ± 52
H5	252	28	PEGMA (M_n ~ 360 g mol^{-1})	120		270 ± 97
H6			PEGMA (M_n ~ 950 g mol^{-1})			257 ± 54
H7			AEMA			aggregates
H8			VBS			307 ± 130
H9			AEMA		CTAB	378 ± 208
H10			DVP		SDS	292 ± 128
H11			no		CTAB	408 ± 68

* *PEGMA: poly(ethyleneglycol methacrylate) monomethyl ether, AEMA: 2-aminoethyl methacrylate hydrochloride, VBS: sodium 4-vinylbenzenesulfonate, DVP: dimethyl vinylphosphonate;* ** *determined by DLS before the dialysis of the latexes.*

Finally, the distribution of TiO_2 in the multicompartment particles could be further tuned by varying the charge of the surfactant and comonomer. It is well-known that monomers of opposite polarities can be efficiently copolymerized by miniemulsion polymerization to yield nanoparticles with a functional surface.[73] For this, various hydrophilic comonomers with different charges (negative, positive, and electroneutral) were selected and copolymerized with DMA. The formation of the tricompartment structures was facilitated by employing the negatively charged surfactant and negatively charged or neutral comonomer (**Table 4 and 5**: H5-6, H8, and H10). On the contrary, the employment of positively charged comonomer and/or surfactant yielded Janus particles with the polymerized face decorated with TiO_2 (**Figure 4.45b**). In all cases, the morphologies evolved from hemispheres decorated with a TiO_2 plate before polymerization (t = 0, **Table 5a**) to the final morphologies that was fixed even before completion of the polymerization (**Table 5 b, c**). The combination of a negatively charged surfactant and a positively charged comonomer (H7, **Table 4**) led to precipitation due to lack of electrostatic repulsion between the particles. The difference between the two main morphologies (**Figure 4.45**) is explained by the negative charge of TiO_2 at pH ~7.[79-82] Indeed, the negative charges of the polymerized face confined the TiO_2 mainly in the middle

of the tricompartment particles whereas the TiO_2 nanoparticles are adsorbing on the positively charged polymerized face.

Table 5 *Temporal evolution of the particles morphology during the polymerization. The scale bars represent 200 nm.*

Entry	*t* = 0 (a)	*t* = 1 h (b)	*t* = 6 h (c)
H1	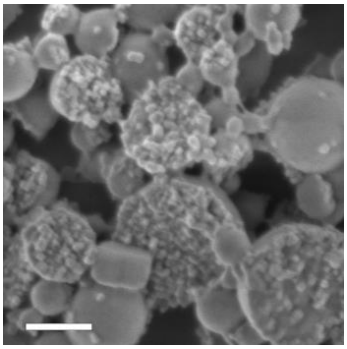	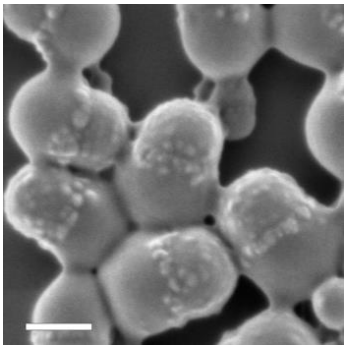	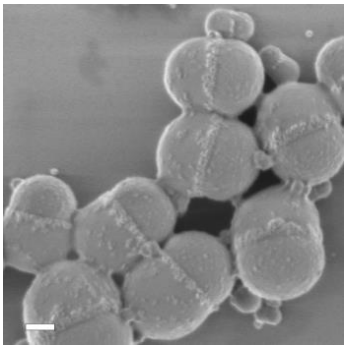
H2	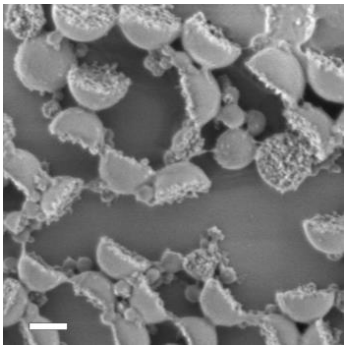	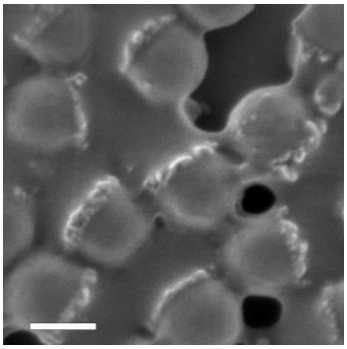	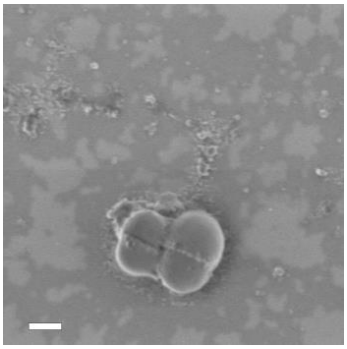
H3	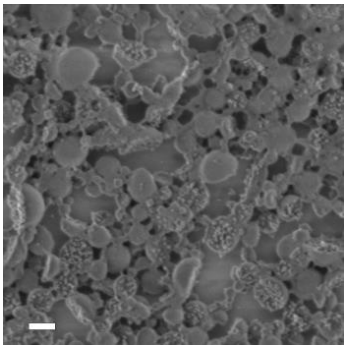	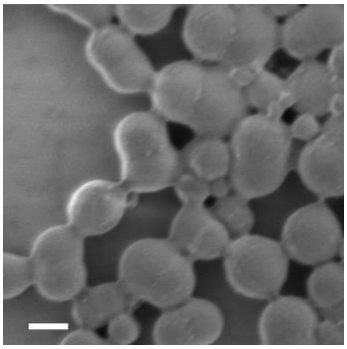	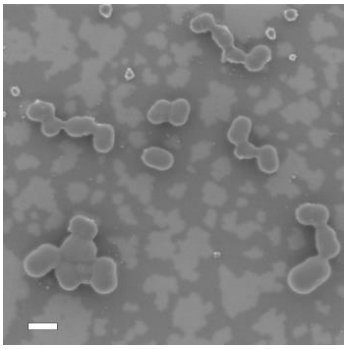

H4	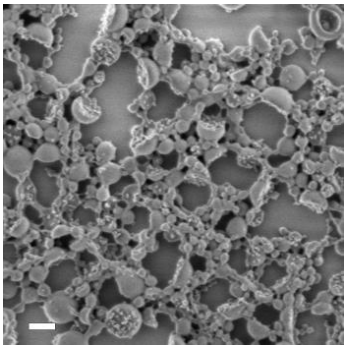	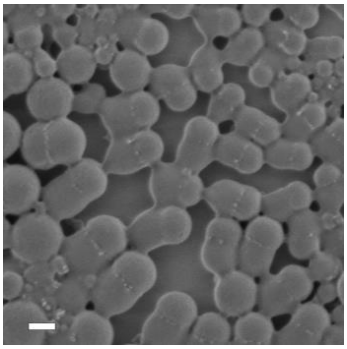	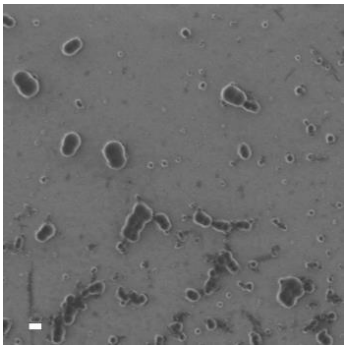
H5	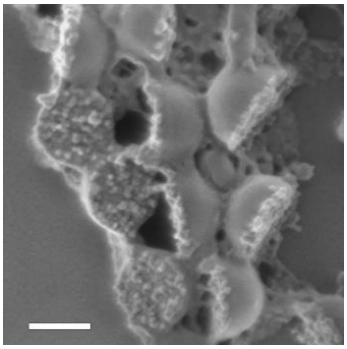	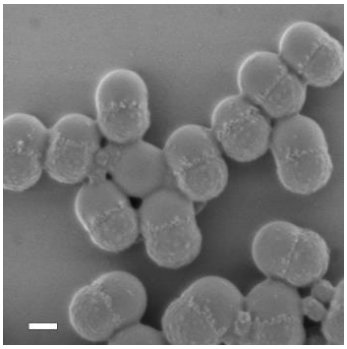	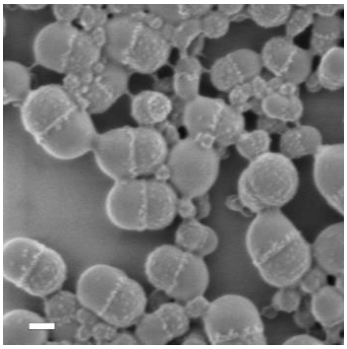
H6	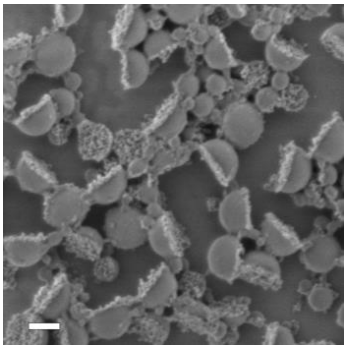	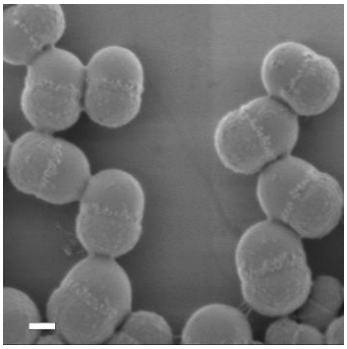	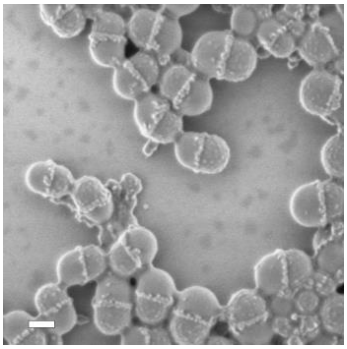
H7	***unstable dispersions***		
H8	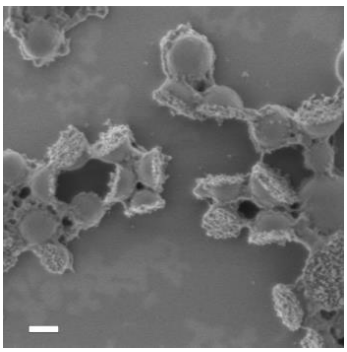	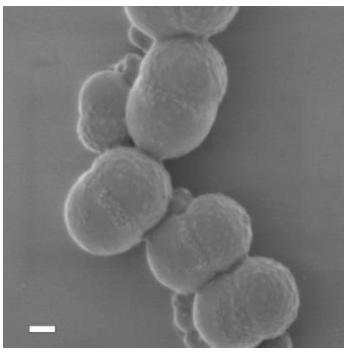	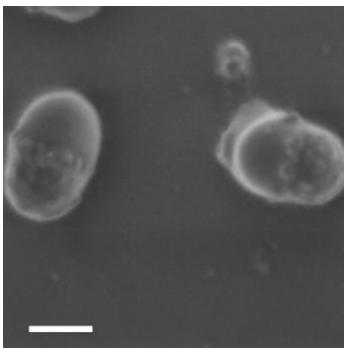

H9	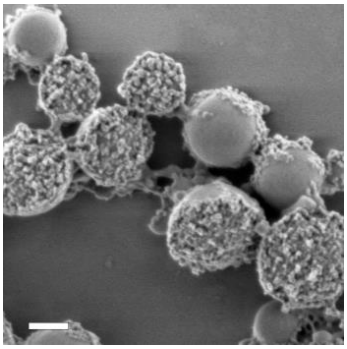	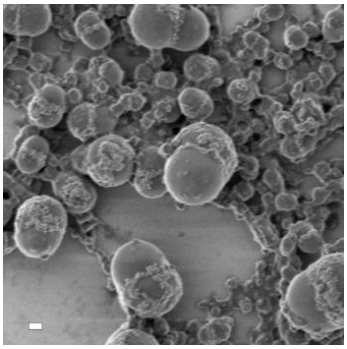	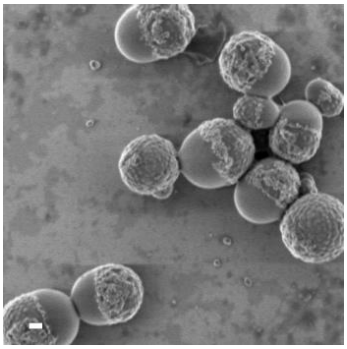
H10	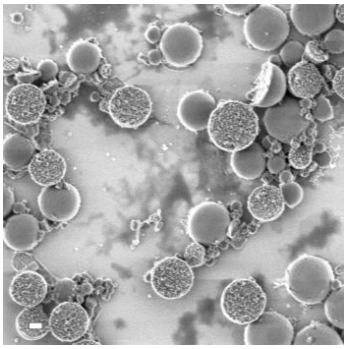	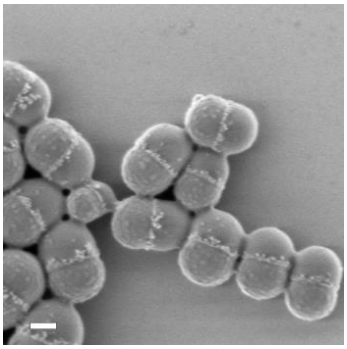	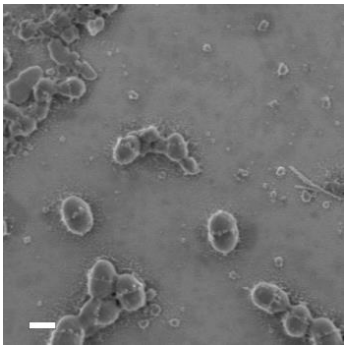
H11	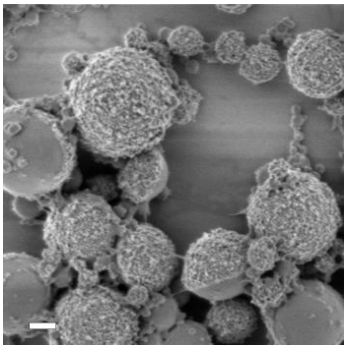	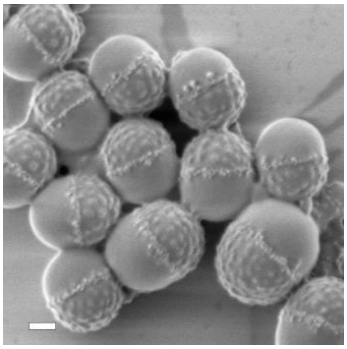	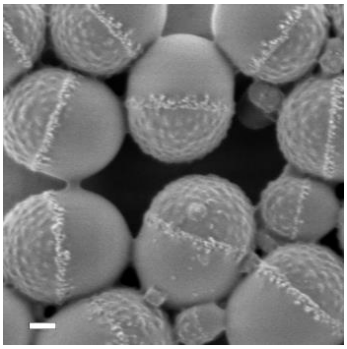

The polydispersity in size of all the systems were also investigated by varying the concentration of surfactant and TiO_2 nanoparticles, the temperature and time of the evaporation process, and the nature of the hydrophilic comonomers. It was found that the polydispersity decreased when the weight ratio of surfactant compared to the dispersed phase increased. As shown in **Table 3**, the samples with entry 1A and 2 displayed lower polydispersity than entry 3A and 6, respectively. This phenomenon could be explained by the higher stability of the formed droplets when more surfactant was employed. When the amount of SDS in **Table 3** was lower than 5 mg, no stable miniemulsion could be formed after ultrasonication (data not shown). Finally, a change of other parameters such as the amount of TiO_2, and the temperature and time of solvent evaporation did not influence

significantly the polydispersity in size of the particles. Overall, the polydispersity in size of the nanoparticles is relatively large, which represent the main limitation of the system.

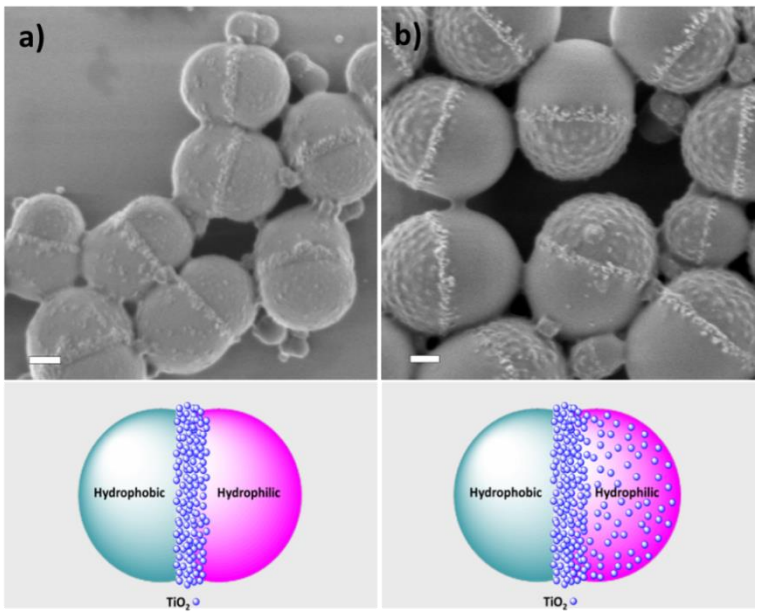

Figure 4.45 *SEM micrographs (top) and schematization of the two major structures produced in the hybrid polymer/polymer/TiO_2 nanoparticles* ***a****: tricompartment nanoparticles,* ***b****: Janus polymer nanoparticles with 1 face decorated with TiO_2. The scale bars represent 200 nm.*

In summary, hybrid submicron particles with a large portfolio of morphologies were fabricated by successive phase separation between polymers and inorganic nanoparticles confined in miniemulsion droplets. For instance, Janus particles with one face selectively decorated with TiO_2 or nanoparticles designed in a linear triblock fashion with three different chemical compositions for the blocks could be prepared. The method could be extended for the synthesis of tricompartment particles with other chemistry. Because of the different chemical composition of the compartment, directional interactions could be also used for their self-assembly in suprastructures.

4.1.5 Conclusion

In this chapter, preparation and characterization of conducting nanostructures for self-healing were described. In the first part, redox-responsive nanocapsules consisting of conductive polyaniline shells were synthesized by using the interface of miniemulsion droplets as a template for oxidative polymerizations. The redox properties of the capsules were investigated by optical spectroscopies, electron microscopy, and cyclic voltammetry.

Self-healing chemicals such as diglycidyl ether or dicarboxylic acid terminated polydimethylsiloxane (PDMS-DE or PDMS-DC) were encapsulated into the nanocapsules during the miniemulsion process and their redox-responsive release was monitored by ^{1}H NMR spectroscopy. The polyaniline capsules exhibited delayed release under oxidation and rapid release under reduction, which make them promising candidates for anticorrosion applications.

In the second part, various nanostructures such as nanoparticles, nanochains and nanocapsules were synthesized by miniemulsion polymerization. Due to the high water-solubility and fast reaction speed of pyrrole monomers, the formation of polypyrrole nanocapsules required the addition of a superhydrophobic solvent, HD, into the dispersed phase. Besides, porous nanoparticles based on the polypyrrole derivative polyoctapyrrolylnaphthalene (POPN), were synthesized and exhibited good electrochemical performance, which make it promising for applications in supercapacitors.

In the last part, two other attempts toward the synthesis of solvent-soluble conducting polymers and tricompartment particles containing conducting inorganic nanoparticles were presented. The latter case also showed the possibility to fabricate core-shell, Janus, and tricompartment structures in which the three different components are arranged in a linear triblock fashion.

4.2 Dual delivery of corrosion inhibitors from dual responsive capsules

4.2.1 Motivation

The previous chapter described redox responsive release of self-healing (SH) agents from PANI capsules. In this system, the release of SH agent was achieved by applying one external trigger to the containers. In nanoscience, the design of a delivery system carrying more than one cargo that can be selectively released by activation with different external stimuli is challenging.

In the first section of this chapter, we propose a new design for nanocontainers that allows for a selective release of one payload by pH change and another payload by chemical reduction of the nanocontainers shell. We selected polyaniline (PANI) as material to build the shell of the nanocontainers. Unlike other pH- and redox-responsive systems reported in the literature that needs several functional components,[83-86] the PANI structure has the important advantage to be both redox- and pH-responsive with two imine nitrogens having pK_a ~ 1.1 and ~ 2.6.[87] With regards to the payloads encapsulated into PANI capsules, polymethylsiloxane-based agents with reactive groups at both ends were used as SH agents in the previous systems. The self healing reaction was then expected based on polycondensations of these two chemicals. However, in the present system, the two selected SH payloads to be delivered were 3-NisA (3-nitrosalicylic acid) and MBT (2-mercaptobenzothiazole). Both payload molecules are active substances known to be corrosion inhibitors. The first molecule has a pK_a around 3 and therefore its solubility in water can be controlled by pH change while the second molecule can bind to gold and then later be reduced electrochemically. The strategy for the stimuli-selective of the two payloads is summarized in the **Figure 4.46**.

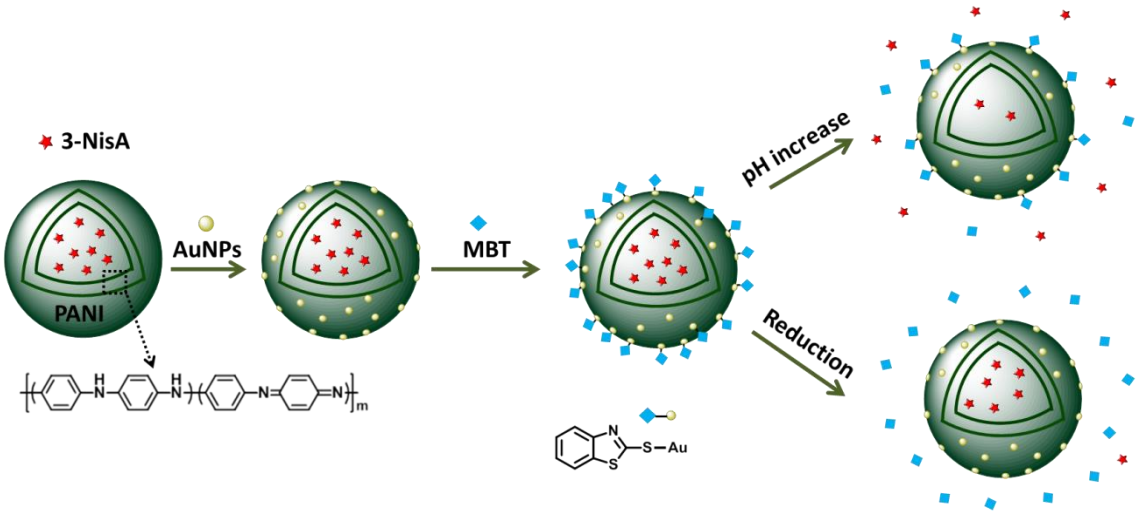

Figure 4.46 *Scheme representing the formation of the dual-delivery nanocontainers and the subsequent selective release of the payloads (corrosion inhibitors) upon pH change or reduction.*

In the second part of this chapter, the encapsulation of various corrosion inhibitors into PANI capsules as well as their redox-responsive property for corrosion protection will also be presented.

This chapter is based on paper "*Adv. Mater.* **2013**, *25*, 6980-6984" with copyright (2013) from WILEY-VCH Verlag GmbH & Co. KGaA and paper "*Chem. Mater.* **2014**, 26, 3351-3353" with copyright (2014) from American Chemical Society.

4.2.2 Synthesis of dual-responsive polyaniline capsules

4.2.2.1 Synthesis of PANI/3-NisA capsules

The PANI nanocontainers loaded with 3-NisA were synthesized by miniemulsion polymerization following a previously reported procedure.[88] By dissolving the 3-NisA in the dispersed phase before emulsification, 3-NisA is efficiently encapsulated in the nanocontainers.[89] The geometry of the nanocontainers is well-defined and the hollow structure can be identified by transmission electron microscopy (TEM) as shown in **Figure 4.47**. At this point, the nanocontainers can be addressed either by pH or redox potential change because of the PANI shell and have the ability to deliver one active molecule (3-NisA).

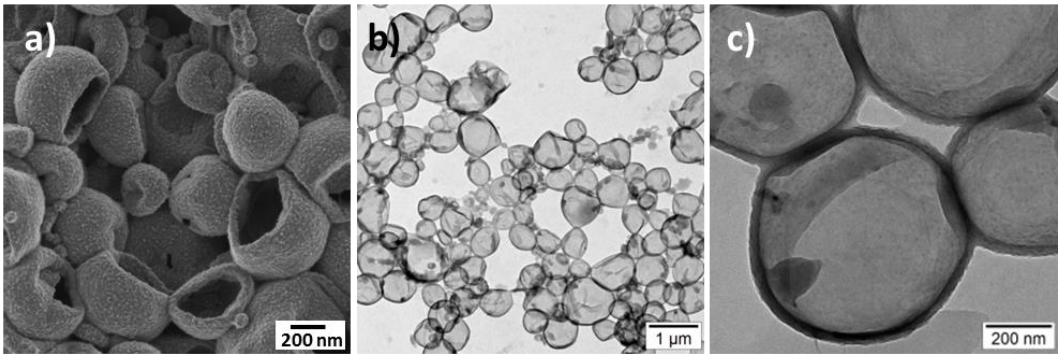

Figure 4.47 ***a****) SEM and* ***b****) TEM micrographs of PANI/3-NisA capsules;* ***c)*** *TEM micrograph of PANI/3-NisA capsules with high magnification.*

4.2.2.2 Synthesis of MBT-Au @PANI/3-NisA capsules

The PANI/3-NisA nanocontainers were then successfully decorated with gold nanoparticles (AuNPs, ~ 20 nm in diameter) by electrostatic adsorption, which was evidenced by SEM and TEM (**Figure 4.48**). The presence of gold nanoparticles on the PANI shell is interesting for two aspects. On the one hand, it allows for a stable electronic contact between the capsules and a potential zinc plate to be protected against corrosion, hence circumventing the possibility of a Fermi-level misalignement that could occur if the gold (or another metal) nanoparticles was not present.[89] On the other hand, the presence of the gold nanoparticles on the shell provides a possibility for a second loading of a payload on the nanocontainers. Indeed, thiol-functionalized molecules can be adsorbed and the gold-thiol (Au-S) bond could be cleaved on gold´s surface.[90,91] The cleavage of Au-S is described with the following reductive reaction[92]:

$$\text{R-S-Au} + e^- \longrightarrow \text{R-S}^- + \text{Au}$$

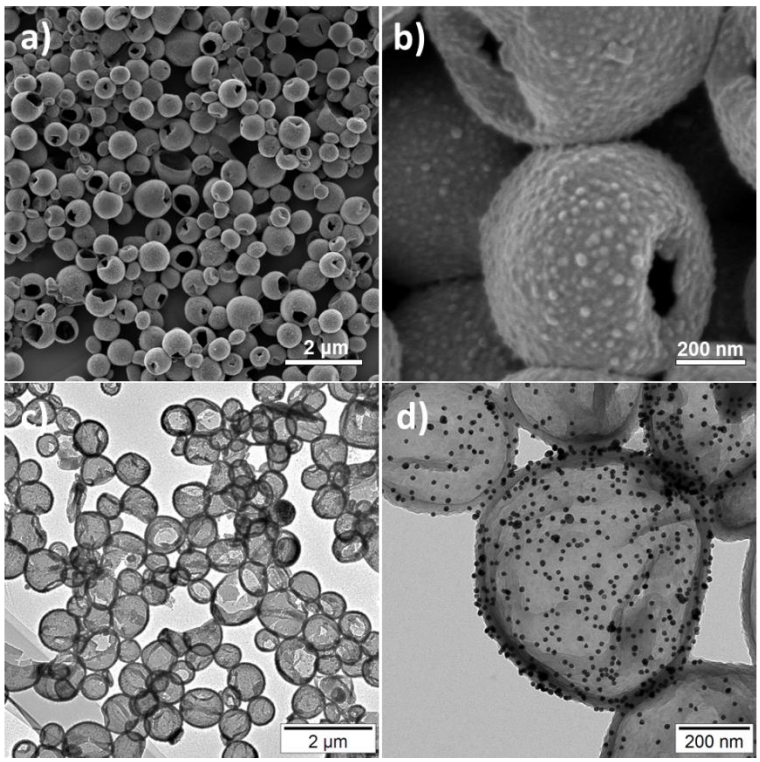

Figure 4.48 ***a****) SEM and* ***c****) TEM micrographs of AuNPs@PANI/3-NisA capsules;* ***b****) and* ***d****) are micrographs with high magnification.*

Therefore, after obtaining the AuNPs@PANI/3-NisA capsules, another corrosion inhibitor 2-mercaptobenzothiazole (MBT) was loaded on the gold nanoparticles adsorbed on PANI capsules. As expected, no significant change in the size or the morphology of the nanocontainers could be detected (**Figure 4.49**). The success and the reversibility of the adsorption of MBT on gold nanoparticles could be verified with UV-spectroscopy by monitoring the change in the surface plasma resonance absorption of the AuNPs. As shown in **Figure 4.50**, λ_{max} of AuNPs exhibited a red shift from 520 nm to 528 nm when MBT was added due to the bonding between the thiol group and AuNPs. When the reducing agent TCEP·HCl was added, the absorption peak of AuNPs was more shifted and became broad. The color of the solution turned from wine red to colorless. The intensity of the absorption peak around 311 nm was attributed to the MBT increased after addition of TCEP·HCl. This observation can be explained by the detachment of MBT molecules from AuNPs after being reduced.

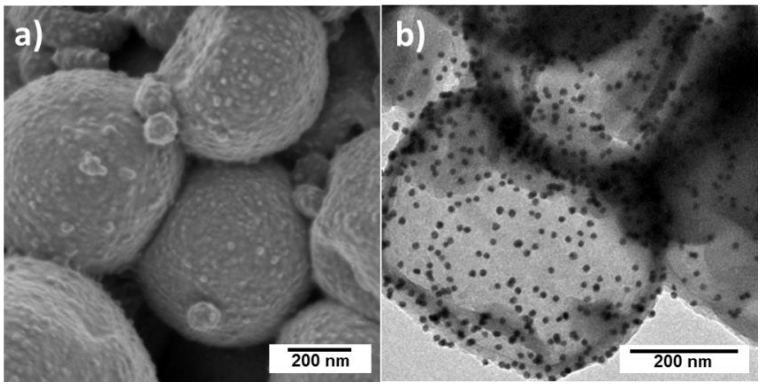

Figure 4.49 ***a****) SEM and* ***b****) TEM micrographs of MBT-Au@PANI/3-NisA capsules after purification.*

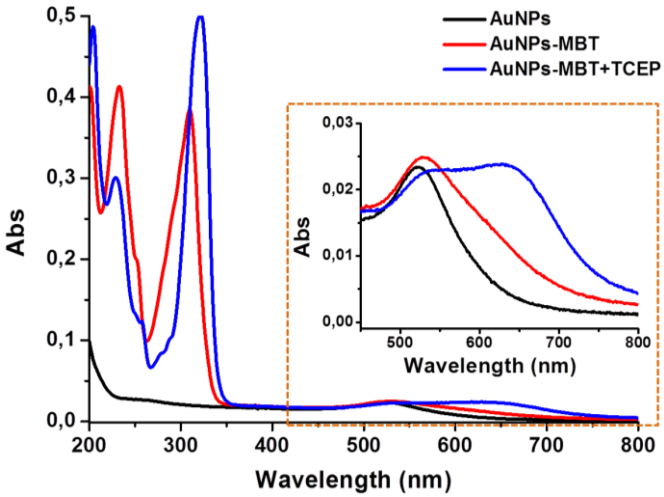

Figure 4.50 *UV-Vis spectra of the AuNPs dispersion before (black line) and after treatment with MBT (red line), and then TCEP·HCl (blue line). The inset is a magnified area of the spectra in the 450-800 nm range.*

Finally, MBT-Au@PANI/3-NisA nanocontainers loaded with ~ 5 wt% of 3-NisA and ~ 6.9 wt% MBT compared to the PANI shell were fabricated.

4.2.3 pH responsive release of 3-NisA from MBT-Au@PANI/3-NisA capsules

The two stimuli, pH change or reduction, were employed and expected to activate the release of the two payloads from the MBT-Au@PANI/3-NisA nanocontainers.

The release behavior of the first payload (3-NisA) was determined by dialyzing the purified nanocontainers dispersion against aqueous solutions of different pH. The absorptions of the 3-NisA payload and the PANI can be well distinguished (**Figure 4.51**) and the release could therefore be detected by UV-Vis spectroscopy (**Figure 4.52**).

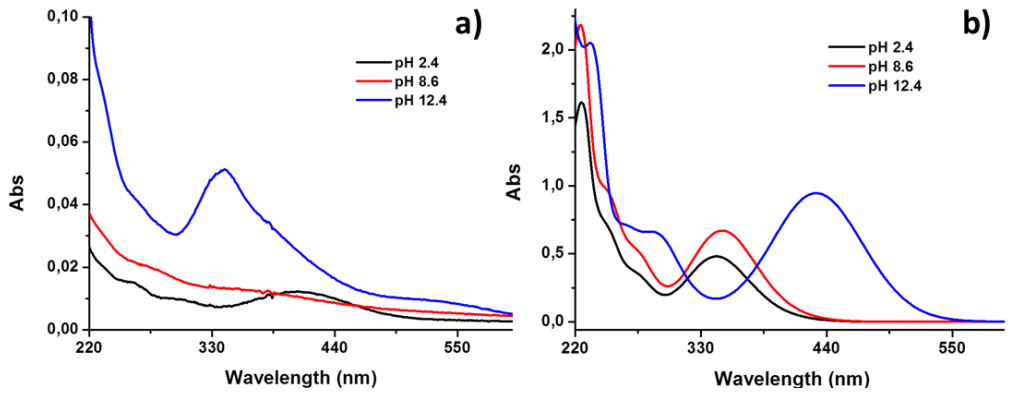

Figure 4.51 *UV spectra at different pH conditions of* ***a:*** *the medium outside the dialysis bag containing the aqueous dispersion of purified PANI capsules; and* ***b:*** *3-NisA dissolved in water.*

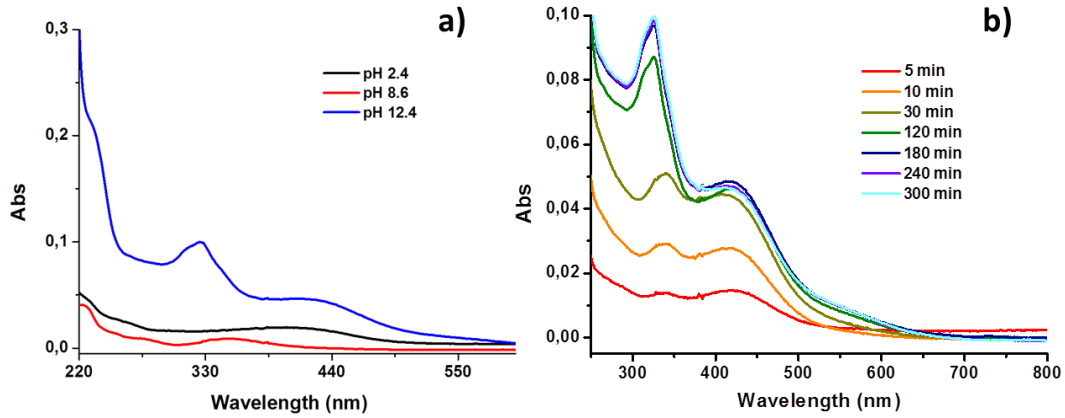

Figure 4.52 ***a****) UV spectra at different pH conditions of the medium outside the dialysis bag containing the aqueous dispersion of purified PANI/3-NisA capsules;* ***b****) UV spectra of 3-NisA released to the medium outside the dialysis bag at pH 12.4 after different period of time.*

The release of 3-NisA from PANI/3-NisA (**Figure 4.53a**) and MBT-Au@PANI/3-NisA nanocontainers (**Figure 4.53b**) was found to be pH-selective. Indeed, no significant release of 3-NisA was observed at pH = 2.4, whereas a slow and a fast release were observed at pH values of 8.6 and 12.4, respectively. The large differences of the release´s profiles are attributed to the PANI capsules shell, the pH-dependent water solubility of 3-NisA, and the interactions between PANI and 3-NisA under different pH conditions. At pH = 2.4, the PANI and the 3-NisA are protonated (**Figure 4.54**) and 3-NisA is only poorly soluble in water. However, when the pH value is increased well above the pK_a of PANI and 3-NisA, the PANI is deprotonated to the emeraldine base state and the 3-NisA becomes highly water soluble.

Besides, it was found that the PANI/3-NisA capsules showed a complete and faster release compared to the MBT-Au@PANI/3-NisA capsules (**Figure 4.53**). This is due to two reasons. Firstly, it is known that molecules with carboxylic group can adsorb on gold[93] and therefore the interaction between the carboxylic group of 3-NisA and AuNPs may hinder the diffusion of 3-NisA molecules to the outside medium of dialysis bag. Secondly, there might be π-π stacking interactions between the benzene rings of 3-NisA and MBT which could also slow the release of 3-NisA.

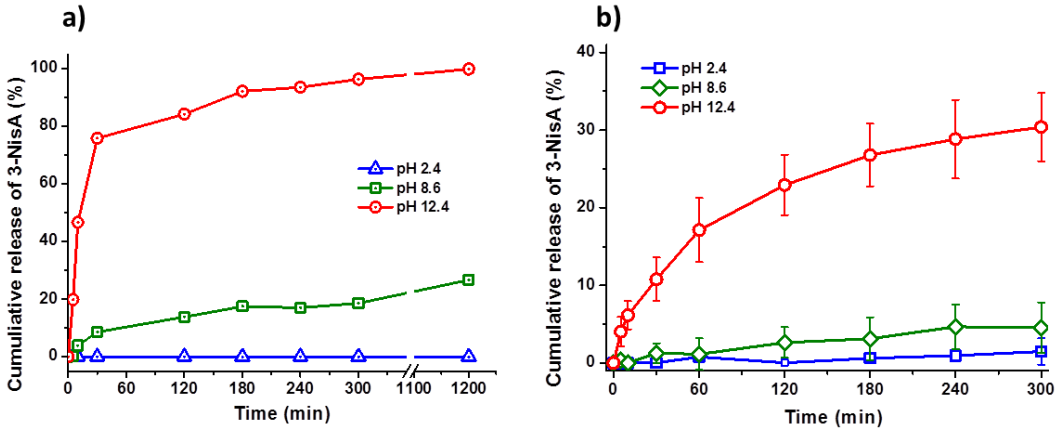

Figure 4.53 *Temporal evolution of the release of 3-NisA from **a**) PANI/3-NisA nanocontainers or **b**) MBT-Au@PANI/3-NisA nanocontainers at different pH values.*

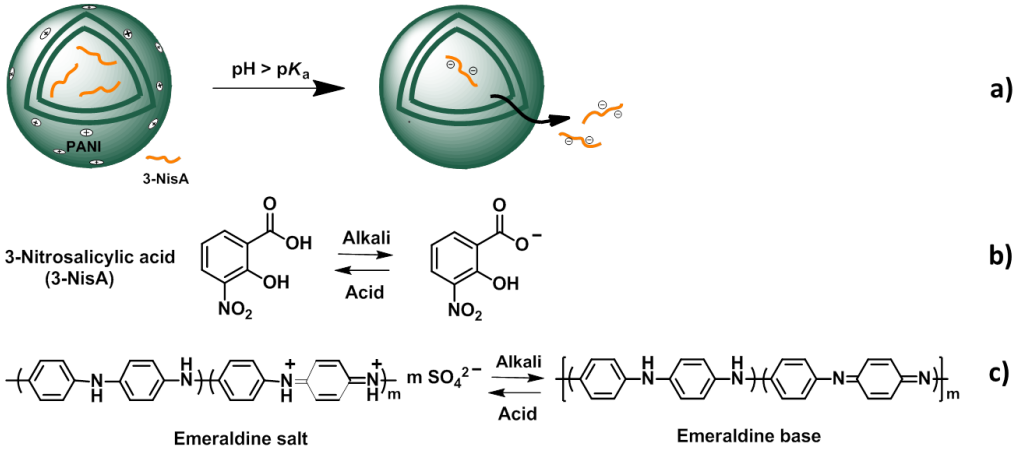

Figure 4.54 ***a**) Illustration of the release mechanism of 3-NisA from PANI capsules; **b**) change of the chemical structure of 3-NisA at different pH condition; **c**) scheme of the protonation and deprotonation of PANI.*

The nanocontainers were found to release a small amount of MBT (~ 24%) at high pH due to the cleavage of Au-S bonds[94] (**Figure 4.55**). No significant release was detected at lower pH values (2.4 and 8.6) (**Figure 4.55**).

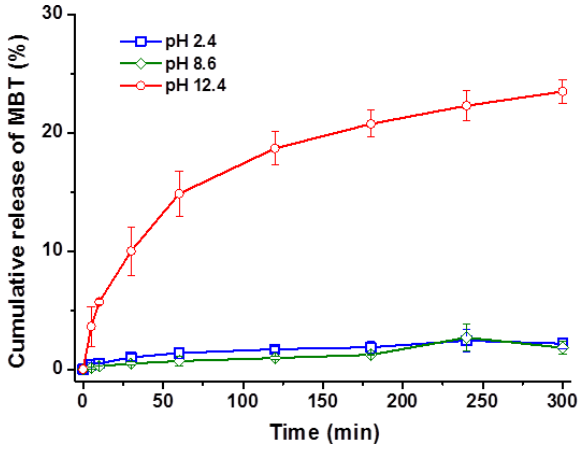

Figure 4.55 *Temporal evolution of the release of MBT from MBT-Au@PANI/3-NisA nanocontainers at different pH values.*

4.2.4 Redox responsive release of MBT from MBT-Au@PANI/3-NisA capsules

The release of the two payloads were then investigated after activation of the nanocontainers by the second possible stimulus, *i.e.* reduction with different concentration of the reducing agent TCEP·HCl. **Figure 4.56** showed the UV-Vis spectra of released MBT at different reductive conditions. The release curves were then plotted in **Figure 4.57**. It was found that without activation of the nanocontainers (simple dilution with water as control sample), almost no release of MBT was detected. The addition of the reducing agent triggered the delivery of MBT with a fast release in the first 2 h (**Figure 4.57**). The rate and amplitude of release was controlled by the concentration of the reducing agent, *i.e.* more reductive condition induced more release of MBT. Remarkably, no detectable release of 3-NisA could take place under these conditions, meaning that the release of MBT was purely selective.

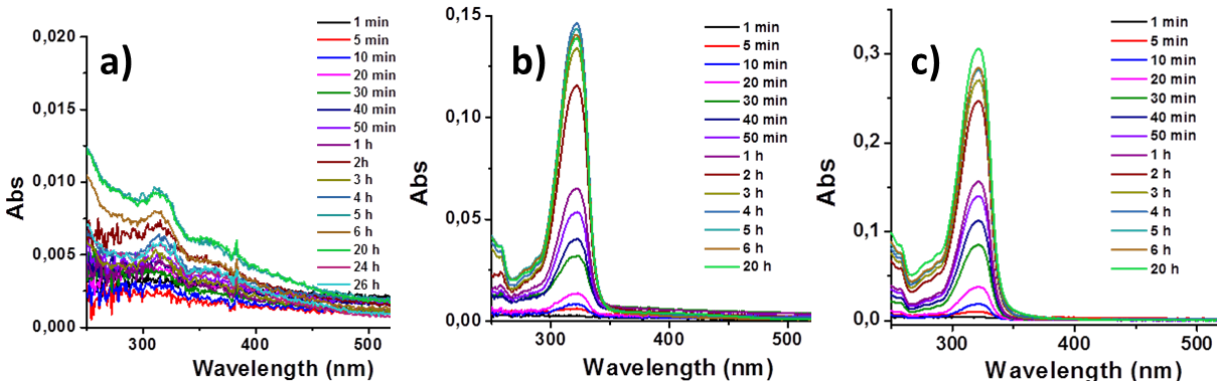

Figure 4.56 *UV spectra of MBT released to the medium outside the dialysis bag with the molar ratio of TCEP to MBT of:* ***a****) 0:1;* ***b****) 1:1 and* ***c****) 10:1 after different period of time.*

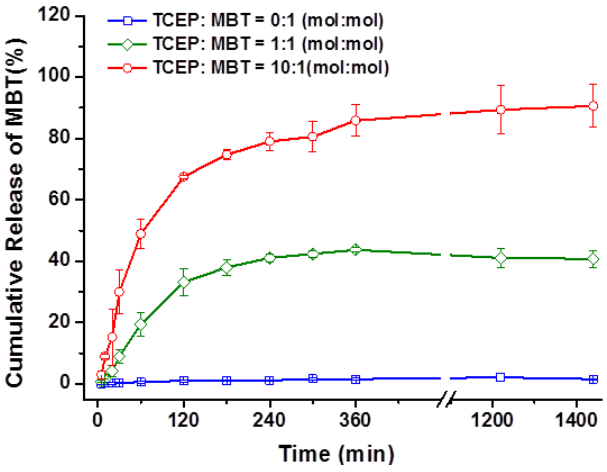

Figure 4.57 *Temporal evolution of the release of MBT from MBT-Au@PANI/3-NisA capsules under reductive conditions.*

4.2.5 Release of 3-NisA and MBT under combined stimuli

To study the release of 3-NisA and MBT under combined stimuli (pH change and reduction), certain amounts of TCEP·HCl were dissolved in an aqueous solution of pH ~12.4 to obtain a solution with different concentrations of TCEP·HCl that were named pH-R1 and pH-R2, respectively. The pH value of the two solutions after addition of TCEP·HCl did not change much. pH-R1 decreased to 12.3 and pH-R2 to 12.2. Then the release behavior of 3-NisA and MBT was investigated under the condition of pH-R1 or pH-R2.

As was shown from the release profiles in **Figure 4.58**, the release behavior of 3-NisA and MBT exhibited a similar trend throughout the experimental time compared to the case when

the release was conducted under only pH ~ 12 or under reductive condition for 3-NisA or MBT (**Figure 4.53b, Figure 4.57**).

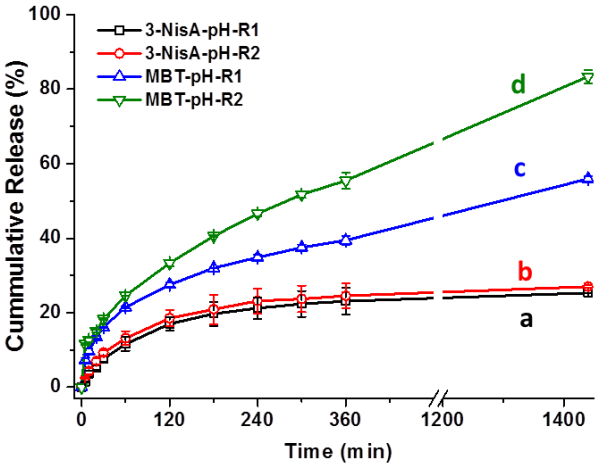

Figure 4.58 *Release profiles of payloads from MBT-Au@PANI/3-NisA capsules under combined stimuli:* ***a****) 3-NisA and* ***c****) MBT in medium of pH ~ 12 and with the molar ratio of TCEP·HCl to MBT of 1:1 (pH-R1);* ***b****) 3-NisA and* ***d****) MBT in medium of pH ~ 12 and with the molar ratio of TCEP·HCl to MBT of 10:1 (pH-R2).*

However, there were differences in the release behavior of especially MBT between the case of single stimulus and combined stimuli. During the first 120 min, the capsules were found to exhibit a much faster release of MBT, *i.e.* ~ 67%, upon only reducing agent (R2: with molar ratio of TCEP·HCl to MBT of 10:1), than that, *i.e.* ~ 33%, upon combined stimuli (pH-R2). This observation was probably attributed to the influence of alkali solution on the reducing agent TCEP·HCl. Although it was reported that TCEP was highly stable in both acid and basic solution,[95] the deprotonated process of TCEP·HCl in alkali solution might still decrease the interaction between TCEP and sulfur-gold bonds.

Nevertheless, the difference of the release behavior between single reductive condition and combined pH-reductive condition was found to decrease as experimental time increased. As shown in **Figure 4.57** and **Figure 4.58**, similar release amounts of MBT, *i.e.* ~ 90% and ~ 83% respectively for the single stimulus and combined stimuli, were observed after 24 h.

The morphology of PANI/Au capsules was observed by SEM after pH change or reductive treatment with TCEP·HCl. After treatments with aqueous solutions of pH 2.4 or 8.6, the morphology of MBT-Au@PANI/3-NisA capsules did not exhibit obvious change (**Figure 4.59 a, b**). However, collapsed PANI capsules were observed after the treatment with the solution

of pH 12.4 (**Figure 4.59 c**). On the contrary, after the treatment with the reducting agent TCEP·HCl, the morphology of MBT-Au@PANI/3-NisA capsules (**Figure 4.59 d, e, f**) did not show much change, indicating the stability of these nanocontainers under reduced condition.

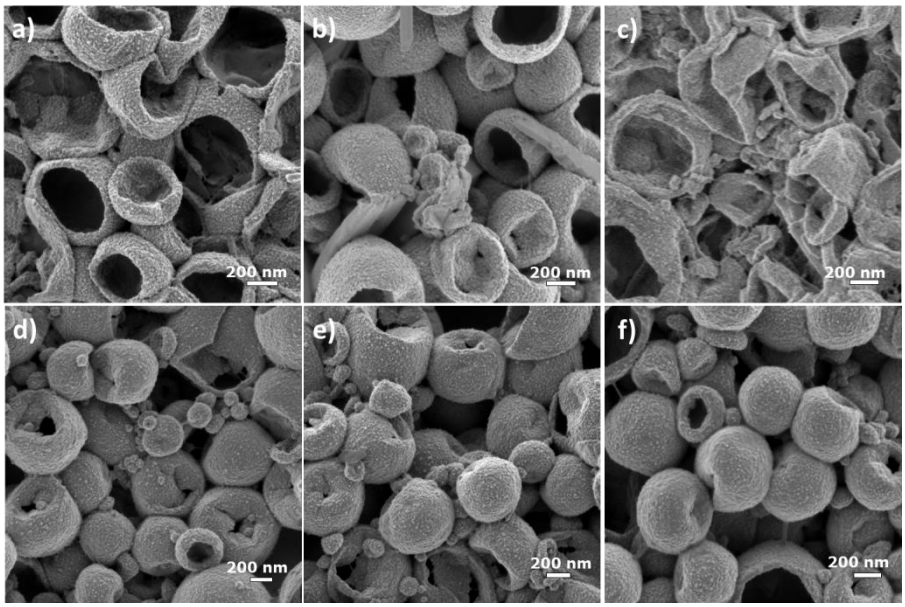

Figure 4.59 *SEM micrographs of MBT-Au@PANI/3-NisA capsules after treatment with aqueous solution of **a**: pH 2.4, **b**: pH 8.6, and **c**: pH 12.4; or an aqueous solution of TCEP·HCl with molar ratio compared to MBT of **d**: 0:1, **e**: 1:1, and **f**: 10:1.*

4.2.6 Electrochemically redox-responsive capsules for corrosion protection

The ideal corrosion protection for metal system is the one when the release of self-healing agents or corrosion inhibitors only takes place when corrosion is initiated. Triggers for the corrosion of a metal system are usually the change of pH, ionic strength, and the electrochemical potential. The first two have been already investigated in depth.[96-98] However the most reliable and case-selective one is the change in electrochemical potential as it always and only decreases when corrosion happens. On the contrary, the change in pH or ionic strength is sometimes susceptible to the local environment.

Examples of utilizing the electrochemical potential as trigger to release anionic inhibitors from conducting polymers (CPs) were reported.[99-102] In those cases, the active anions were stored as counter-charge to the oxidized conducting polymer backbone. The release was then triggered upon onset of corrosion and the subsequent reduction of the CPs due to the injection of electrons. However, there still exist issues to be considered. First of all, the

release efficiency of the anionic inhibitors is based on their mobility. Secondly, to maintain the overall charge neutrality, the CP backbones would also incorporate cations instead of releasing out stored anions and this could even accelerate the corrosion process.[9,103-105] Thirdly, in some cases when CPs are applied for anticorrosion in non-noble metals such as zinc, they tend to react with the metal, which results in the formation of an insulating layer. Once the insulating layer is formed, the contact between the CPs and metal is blocked, *i.e.* electronically decoupled (Fermi-level misalignment), and then the functions of CPs for corrosion protection will be lost.

In the previous section, conducting nanocapsules loaded with corrosion inhibitor in the core (PANI/3-NisA) were proposed and the capsule shell was decorated with gold nanoparticles. The as-prepared AuNPs@PANI/3-NisA capsules are promising for corrosion protection because the corrosion inhibitor is protected by the capsule shell and the AuNPs adsorbed on the shell could bridge the contact between CPs and metal. In the present section, PANI capsules loaded with different corrosion inhibitors are prepared. Then the electrochemically redox-responsive self-healing behavior of AuNPs@PANI/3-NisA capsules for corrosion protection is presented.

4.2.6.1 Synthesis of polyaniline capsules loaded with different corrosion inhibitors

As demonstrated previously, two different corrosion inhibitors, 3-NisA and MBT, were incorporated into the PANI capsules. Several other corrosion inhibitors could also be encapsulated by dissolving them in the dispersed phase of the miniemulsion before generation of capsules. Since different corrosion inhibitors were found to exhibit distinct property and efficiency in different cases,[106,107] the synthesis of PANI capsules loaded with different corrosion inhibitors will then provide more possibility for the potential application. The corrosion inhibitors used in the present section are listed in **Figure 4.60**.

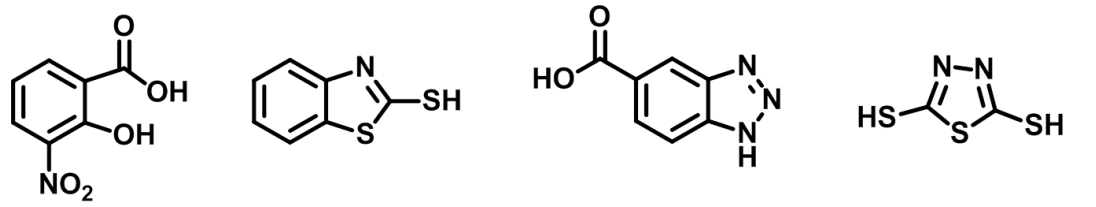

3-nitrosalicylic acid (3-NisA) | **2-mercaptobenzothiazole (MBT)** | **benzotriazolecarboxylic acid (BTA-COOH)** | **2,5-dimercapto-1,3,4-thiadiazole (DT)**

Figure 4.60 *Chemical structures of corrosion inhibitors loaded in the capsules.*

The morphologies of PANI capsules loaded with corrosion inhibitor were observed by SEM measurements as shown in **Figure 4.61**. All samples exhibited similar capsular structure. To further confirm the encapsulation, PANI/MBT and PANI/BTA-COOH capsules were first purified to remove the non-encapsulated MBT or BTA-COOH and then placed inside a dialysis bag. The outside medium was an aqueous solution with pH 12.4. After 1d of dialysis, the outside medium was taken and investigated by using UV-Vis spectroscopy. The UV spectrum of each sample was collected as shown in **Figure 4.62.** The absorption peak of each corrosion inhibitor indicates the encapsulation of MBT or BTA-COOH into PANI capsules.

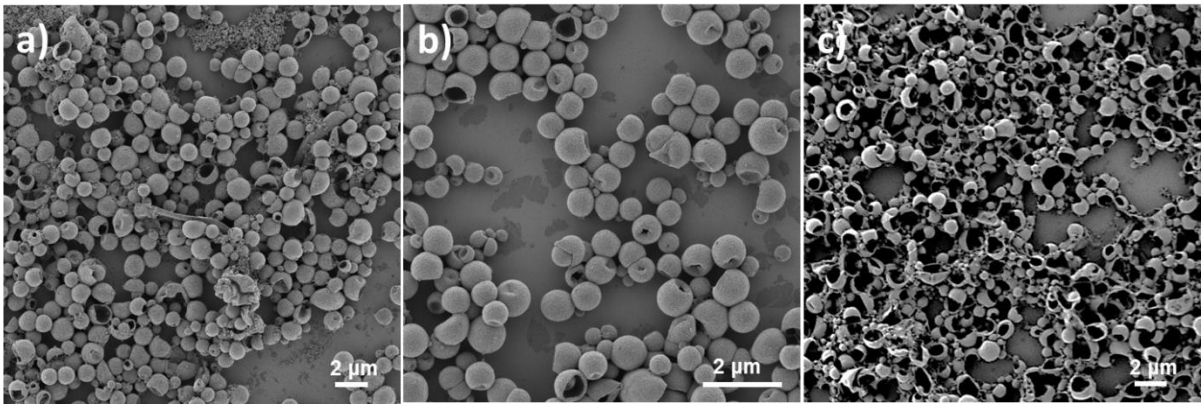

Figure 4.61 *SEM micrographs of **a**) PANI/MBT; **b**) PANI/BTA-COOH; and **c**) PANI/DT capsules after purification.*

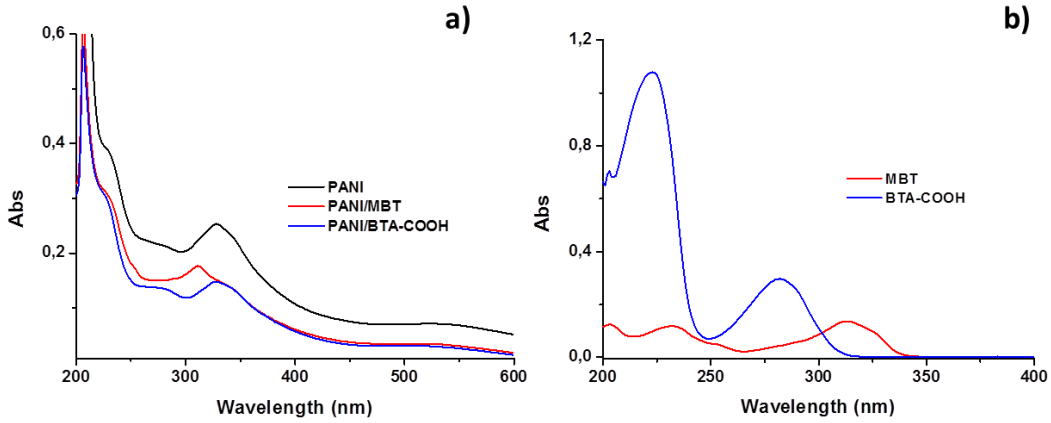

Figure 4.62 *UV spectra of **a**) the medium outside the dialysis bag containing the aqueous dispersion of purified PANI, PANI/MBT or PANI/BTA-COOH capsules. The pH value of the medium was 12.4; and **b**) MBT or BTA-COOH dissolved in water at pH 12.4.*

4.2.6.2 Preparation of coating incorporated with AuNPs@PANI/3-NisA capsules

We further investigated the anticorrosion properties of the PANI capsules loaded with corrosion inhibitors. To prepare a model coating with capsules, the dispersion of AuNPs@PANI/3-NisA capsules was first drop-casted on zinc specimens and dried. Then PVB/ethanol solution was spin-coated on the capsule film followed by drying process. The PVB/PANI composite coating was then formed as shown in **Figure 4.63**. Three parts were clearly observed from the SEM micrograph: PVP topcoat, PANI capsules interlayer and the zinc substrate.

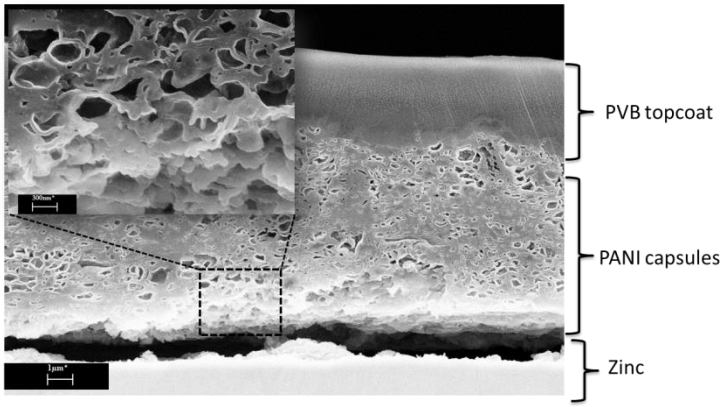

Figure 4.63 *SEM micrograph of the cross section of the model coating prepared by ion-milling shows the PVB topcoat and the capsules interlayer on zinc. The scale bar represents 1 µm.*

4.2.6.3 Electrochemically redox responsive self-healing behavior

Figure 4.64 showed the cyclic voltammograms (CV) of PANI capsules decorated with AuNPs and the electrochemical redox-responsive release of 3-NisA from the capsules. CV measurements indicated a cyclic redox response and reversibility of the chemical-structure changes of the shell material of PANI capsules in corrosive environments. The release curve showed that when no potential was applied to the PANI capsules (areas with white background, oxidized state), the release of 3-NisA was prevented by the PANI shells. However, when a negative potential was applied to the PANI capsules (yellow-shaded area, reduced state), the permeability of the PANI shell was expected to increase which resulted in a release of corrosion inhibitor. This release could be further stopped by re-oxidizing the capsule shell. The possible release mechanism was displayed in **Figure 4.64 C** and correlated to a volume change of the PANI by incorporation of cations. Upon reduction, cations from

electrolyte injected into PANI shell and resulted in a higher permeability for 3-NisA to diffuse out. In contrary, oxidation leads to decreased permeability and retarded release.

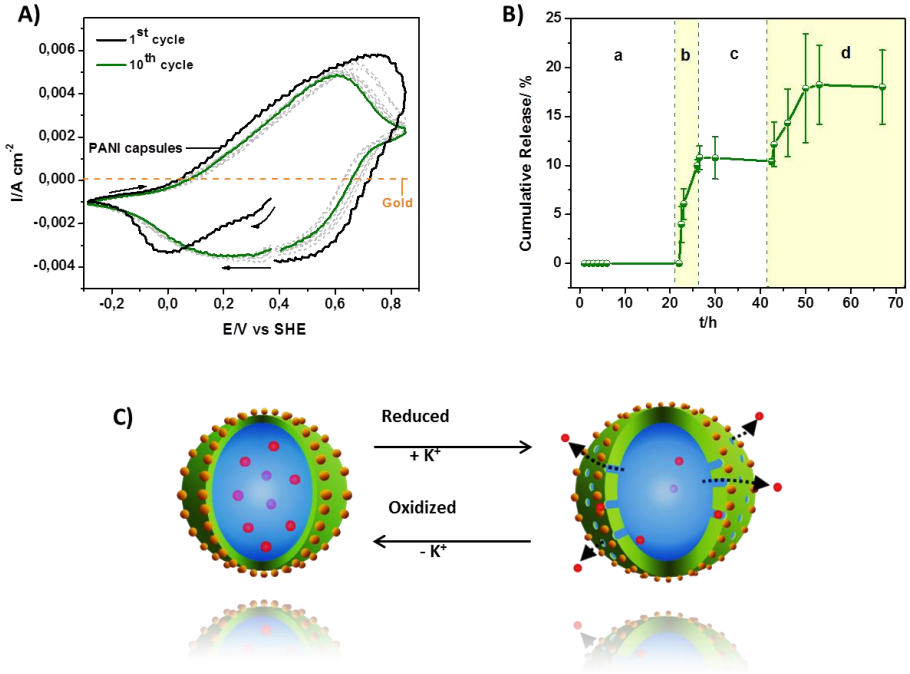

Figure 4.64 ***A****) CV of PANI capsules in 0.5 M KCl on gold.* ***B****) Cumulative release of 3-NisA from PANI capsules under reduced and oxidized conditions. The yellow-shaded area (b, d) corresponds to the time where the capsules were reduced (−500 mV) and the areas with the white background to the oxidized state (a) or re-oxidized state of the capsules (c). The potentials simulate the onset of corrosion of a metal (reduced, higher permeability and release) and the passivation of a metal (oxidized, lower permeability, and decreased release).* ***C****) Schematic illustration of the release mechanism.*

The self-healing performance of the PVB/PANI coating system was investigated by monitoring the corrosion potential. As shown in **Figure 4.65**, in the control measurements where only PVB topcoat or PANI capsules without 3-NisA were used, active corrosion of zinc [−700 to −800 mV vs. standard hydrogen electrode (SHE)] was clearly identified. Only for the coating containing the capsules with 3-NisA a distinct shift of the potential to higher potential was observed which indicated the passivation of the defect, *i.e.* a self-healing process.

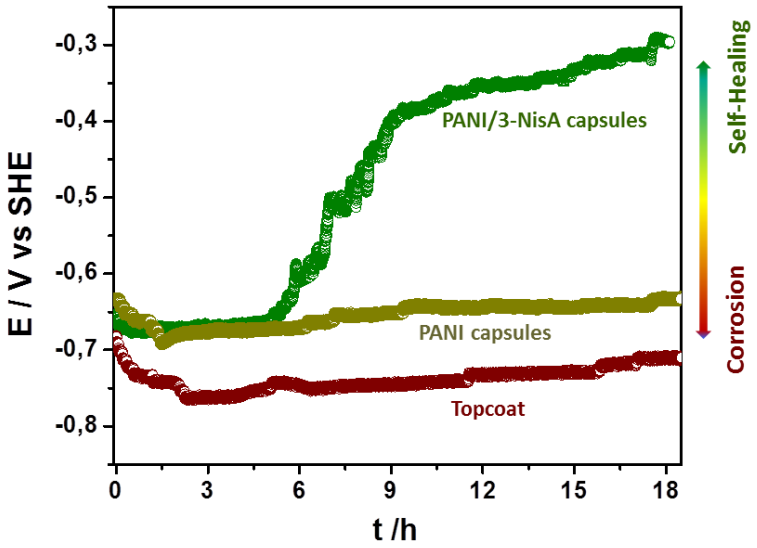

Figure 4.65 *Corrosion potential monitored by SKP in the defect of different model coating systems covered with 1 M KCl.*

4.2.7 Conclusion

In this chapter, the synthesis and characterization of PANI capsules loaded with different corrosion inhibitors were presented. Firstly, PANI nanocontainers that allow for a selective release of one corrosion inhibitor by pH change and another corrosion inhibitor by chemical reduction of the nanocontainers shell were fabricated. To achieve this goal, 3-NisA was first encapsulated into the core of PANI capsules and then another corrosion inhibitor MBT was incorporated by formation of gold-thiol (Au-S) bond between MBT and gold nanoparticles which were adsorbed on the capsule shell. This dual delivery system was found to exhibit a pH-responsive release of 3-NisA and a reduction-responsive release of MBT.

Secondly, PANI capsules loaded with varied corrosion inhibitors were formed and characterized. PANI/3-NisA capsules were further investigated for their self-healing performance in a model coating system. The results indicated that these PANI/3-NisA capsules exhibited a self-healing behavior for the corrosion process of zinc in a model system.

4.3 Dual self-healing materials based on amphiphilic copolymers

4.3.1 Motivation

In previous chapters, we presented self-healing (SH) systems based on PANI capsules for anticorrosion application. SH agents or corrosion inhibitors (CIs) were first incorporated into PANI capsules and then released by applying pH- or redox-stimuli to the capsules.

Amphiphilic copolymer assemblies are another type of nanocarriers for the delivery of active agents. Hydrophobic payloads such as drugs or dyes can be sequestered into their core and protected by the outer shell.[108-112] The payload can also be released by triggering the assemblies with an external trigger such as pH, temperature, redox potential, and ionic strength.[113-119]

Herein, we introduce amphiphilic random copolymers which are designed to bear a corrosion inhibitor as side group, which can be released upon activation by chemical or electrochemical reduction. Polymer nanoparticles are obtained by self-assembly of the copolymers in water. A model dye is encapsulated in the nanoparticles and its release is triggered by reductive cleavage of the copolymer, leading hence to the co-release of the corrosion inhibitor.

The schematic illustration of the self-assembly and the subsequent possible reductive cleavage of the assemblies are shown in **Figure 4.66**. Unlike other disulfide-based delivery systems in which useless hydrophobic aggregates or non-functional byproducts are usually produced, this system had the priority to co-release a corrosion inhibitor.

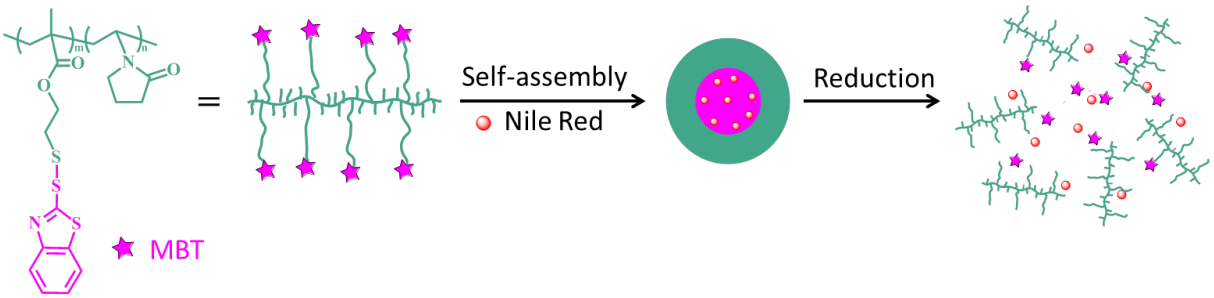

Figure 4.66 *Schematic illustration of the self-assembly and the subsequent possible reductive cleavage of the assemblies.*

4.3.2 Self-assembly of the amphiphilic copolymers poly(VP-*co*-MBTMA) in water

MBTMA was selected as comonomer for the synthesis of the amphiphilic copolymers because its disulfide bond can be cleaved by reduction. The cleavage involves the release of the functional molecule MBT, which is an efficient corrosion inhibitor.[120,121] MBTMA was prepared according to a previously reported procedure[122,123] (see **Figure 4.67a**) and the chemical structure was proven by ^{1}H NMR spectrum as shown in **Figure 4.67b**. The monomer 1-vinyl-2-pyrrolidone was selected as second comonomer because its polymer is water soluble, non-ionic, and relatively chemically inert. MBTMA and VP were then copolymerized by free-radical polymerization at different ratios as shown in **Figure 4.68a** and **Table 6**. The molar ratio of the comonomers inside the copolymer was evaluated by ^{1}H NMR spectroscopy by integrating the signals corresponding to the benzenoid proton from MBT and the ethyl protons from VP.

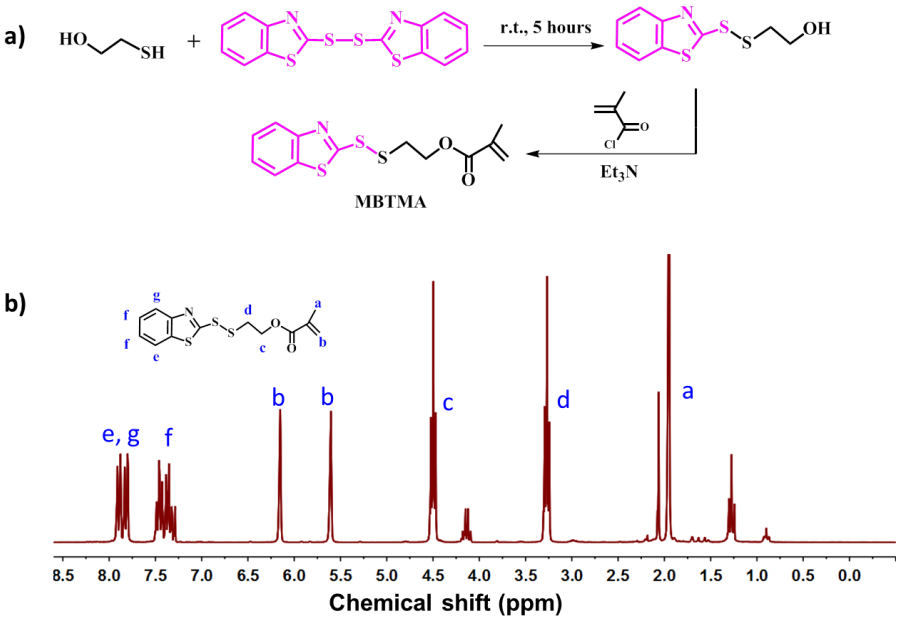

Figure 4.67 ***a)*** *Synthesis of polymerizable monomer MBTMA following the previously reported method;* [122,123] ***b)*** *^{1}H NMR spectrum of MBTMA in $CDCl_3$.*

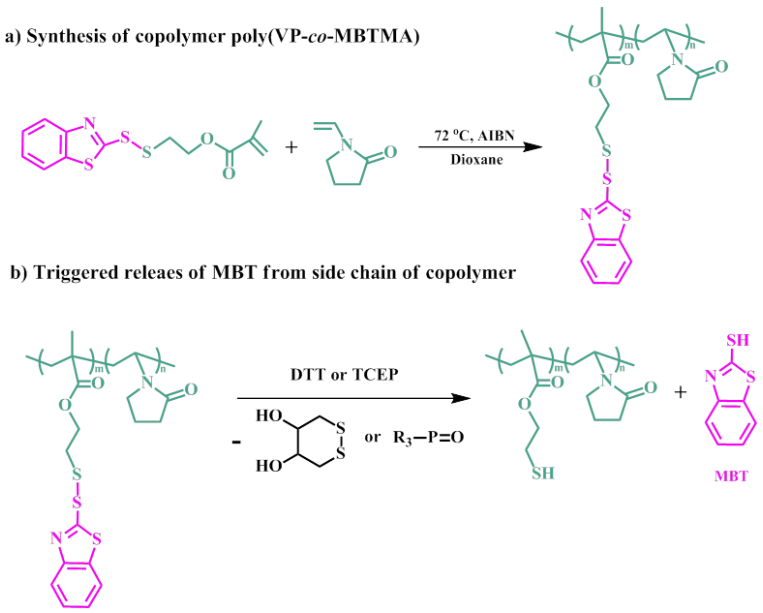

Figure 4.68 ***a****) Synthesis of the copolymer poly(VP-co-MBTMA);* ***b****) Triggered release of MBT from the copolymers by reductive reaction. R= CH_2CH_2COOH.*

Table 6 *Summary of characteristics of poly(VP-co-MBTMA) copolymers.*

Entry	Molar ratio of VP:MBTMA		Yield	M_w [b]	D_h [c]	CAC [d]
	Monomer	Copolymer [a]	[%]	[g mol^{-1}]	[nm]	[g L^{-1}]
P1	52:1	70:1	73	24770	230 ± 40	0.22
P2	29:1	36:1	71	47000	250 ± 40	0.044
P3	14:1	16:1	65	6770	260 ± 50	0.009
P4	9:1	4:1	28	2600	430 ± 70	*n.a.*

[a] Calculated with ^{1}H NMR spectroscopy; [b] Estimated by GPC; [c] Measured by DLS; [d] Estimated from fluorescence spectroscopy using pyrene as probe.

The self-assembly process of the amphiphilic copolymers is illustrated in **Figure 4.66**. The copolymers were found to aggregate in the form of nanoparticles in water. The hydrophobic MBTMA segments built the core whereas the hydrophilic VP segments formed the corona. Remarkably, the assemblies could be formed even at low amount of MBTMA (P1, VP:MBTMA = 70:1, **Table 6**) due to the hydrophobic interactions and the π-π stacking interactions between the aromatic groups of MBT.[124] Indeed, on the contrary to the ^{1}H NMR spectra of the copolymers dissolved in $CDCl_3$ (**Figure 4.69a**), only the protons of the VP and of the main chain of MBTMA could be detected in the spectra of the assemblies measured in D_2O (**Figure 4.69b**). The morphology of the assemblies of the copolymer P1-P4 was investigated by electron microscopy and assemblies were identified as nanoparticles (**Figure**

4.70). In the case of P4, the copolymer cannot form nanoparticles directly by sonication in water because of the large amount of MBTMA in the copolymer, making it more hydrophobic. To prepare the nanoparticles, the copolymer P4 was first dissolved in certain amount of THF and then dialyzed against water. As shown in **Table 6**, the hydrodynamic diameter of the nanoparticles increased as the molar ratio of hydrophobic units in the copolymers increased.

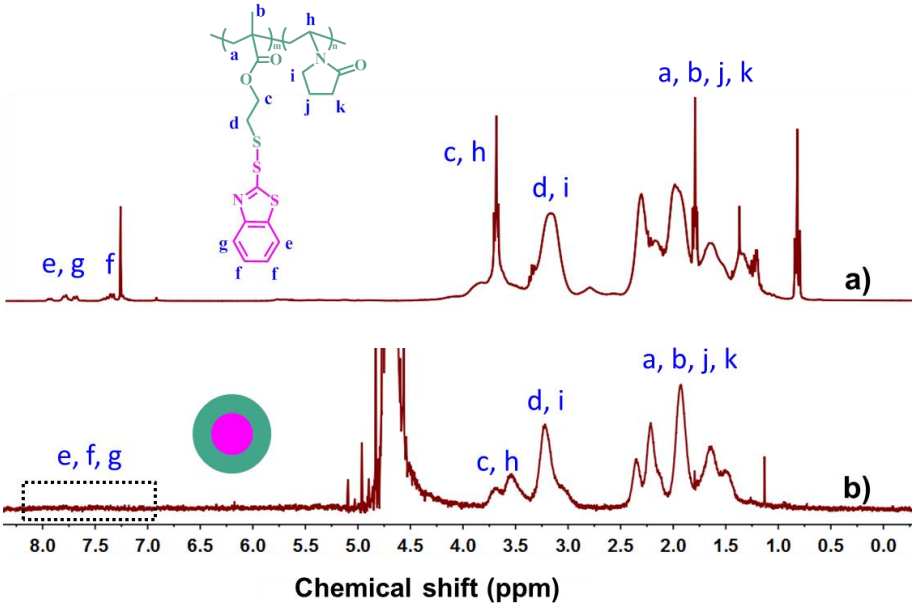

Figure 4.69 *^{1}H NMR spectra of: **a**) The copolymer poly(VP-co-MBTMA) P2 dissolved in $CDCl_3$; **b**) The assembly from P2 in D_2O. The dashed frame indicates the area where MBT shows the characteristic peaks in dissolved condition.*

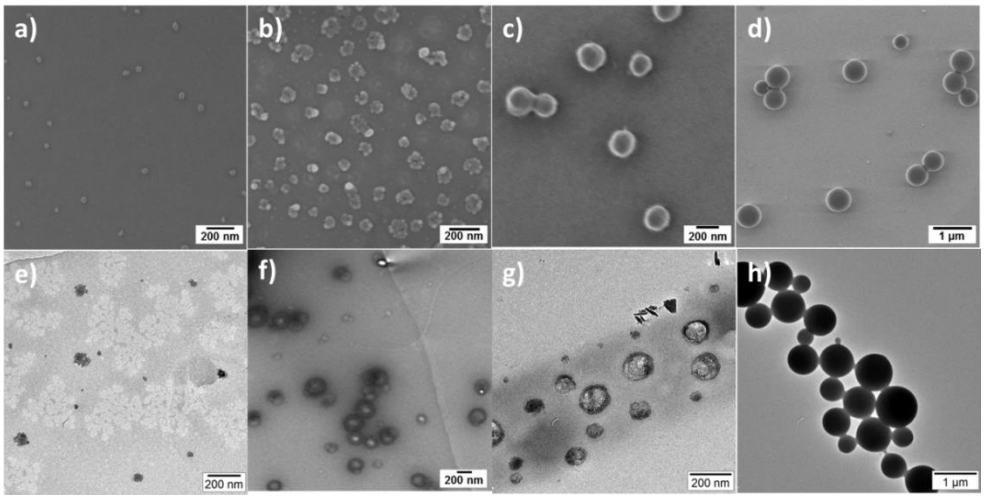

Figure 4.70 *SEM (**a**-**d**) and TEM (**e**-**h**) micrographs of the polymer assemblies from: P1 (**a**, **e**), P2 (**b**, **f**), P3 (**c**, **g**) and P4 (**d**, **h**).*

The critical aggregation concentration (CAC) of the assemblies was evaluated by fluorescence spectroscopy with pyrene as fluorescent probe because its fluorescence depends strongly on the environment. The emission spectra of pyrene (**Figure 4.71**) in the copolymer nanoparticles with different concentration showed different fluorescence behavior. By comparing the fluorescent intensity of the first (I_1) and third vibronic peak (I_3) of pyrene, I_1/ I_3 versus concentration of polymeric assemblies was plotted as shown in **Figure 4.72**. The CAC of each polymeric assemblies was then obtained as shown in **Table 6**. After comparing the CAC values for the assemblies from P1, P2 and P3, it was found that assemblies were easier to form when the copolymers in the present work owned higher hydrophobic/hydrophilic molar ratios, *i.e.* hydrophobic segments in the copolymer facilitate the formation of assemblies.

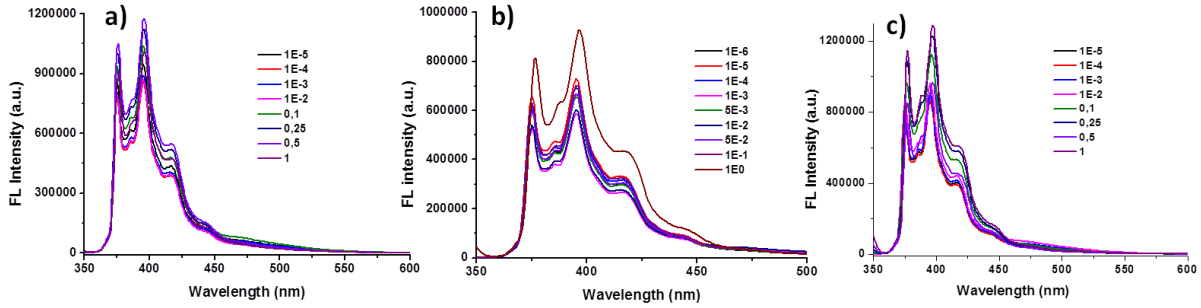

Figure 4.71 *Fluorescence emission spectra of pyrene in the copolymer nanoparticles with the copolymer : **a**) P1; **b**) P2; and **c**) P3 at different concentrations.*

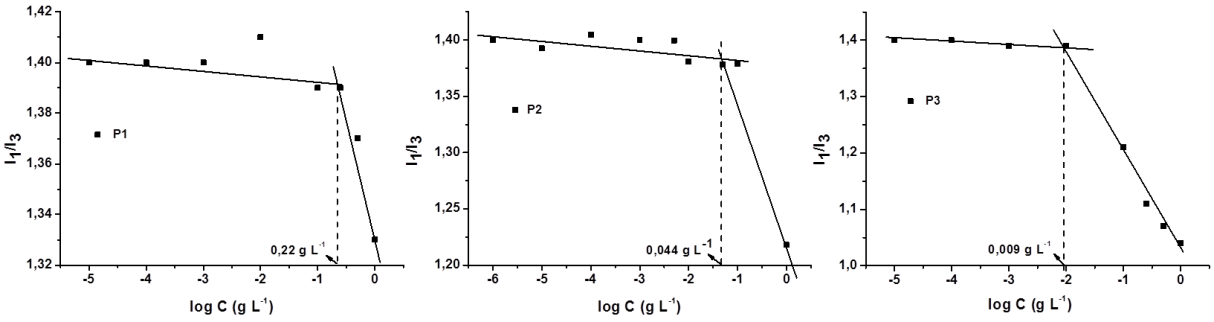

Figure 4.72 *Critical aggregation concentration (CAC) of polymer assemblies of the copolymers P1-P3.*

4.3.3 Release of the corrosion inhibitor MBT from the nanoparticles

The release of MBT from the copolymers and from the nanoparticles is expected to occur upon cleavage of the disulfide bond present as side chain in the copolymer (**Figure 4.68b**).

We investigated by UV spectroscopy the release of MBT upon chemical reduction with DTT by dissolving the copolymers in THF (1 mg mL^{-1}). As shown in **Figure 4.73**, the maximum absorption peak of MBT around 330 nm was found to increase after the reduction of copolymers P1-P4; hence indicating the release of MBT.

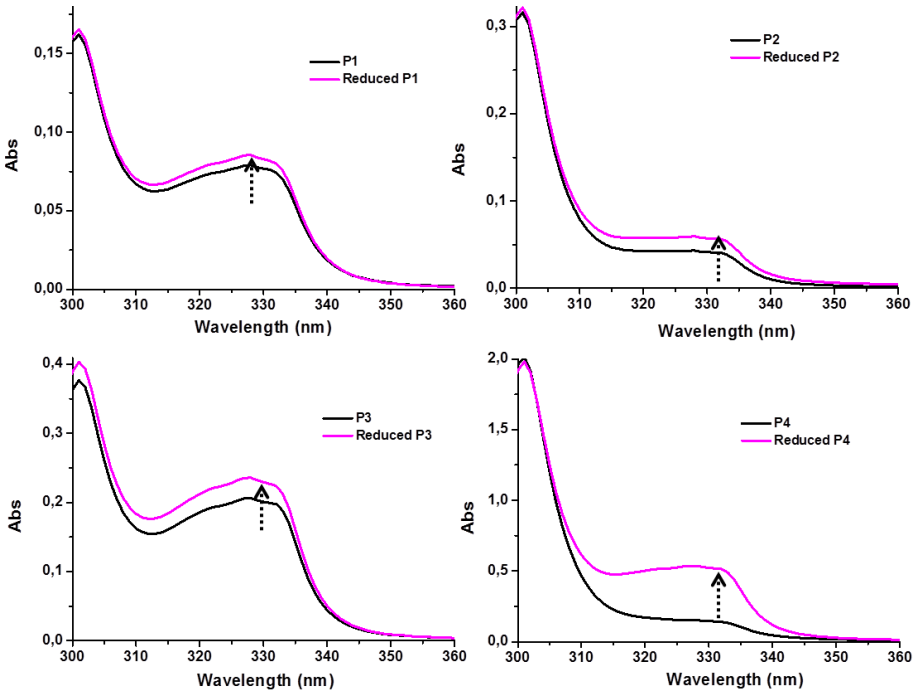

Figure 4.73 *UV-Vis spectra of poly(VP-co-MBTMA) copolymers before (black line) and after (violet line) reduction with DTT in THF. The molar ratio of DTT to MBTMA units in the copolymer was 50/1.*

To investigate the release of MBT from the nanoparticles, dispersions with a concentration of 1 mg mL^{-1} were dialyzed against an aqueous medium containing the reducing agent TCEP·HCl. The molar ratio of the reducing agent to the MBTMA units was set as 5/1. The signals between δ = 7.4- 8.2 ppm from the protons of MBT compared to the signals between δ = 2.6-4.5 ppm from VP before and after reduction were determined by ^{1}H NMR spectroscopy in $CDCl_3$ (**Figure 4.74**). For instance, it was found that the content of MBT in P2 after reduction decreased by ~ 25% compared to the content of MBT in the control sample dialyzed against distilled water, *i.e.* ~ 25% MBT was released during the reduction process. It should also be noted that on the contrary to the non-dialyzed copolymer P2, both reduced and control samples containing P2 showed a decrease of the MBT content. This was attributed to the diffusion of the low molecular weight polymer chains through the dialysis membrane.

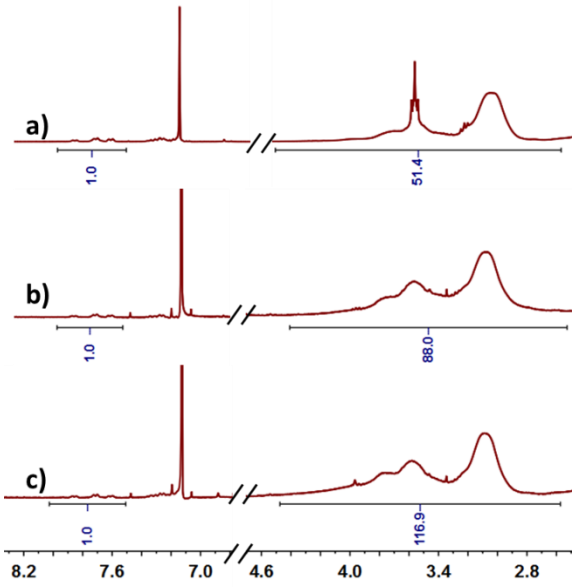

Figure 4.74 *^{1}H NMR spectra of **a**) the copolymer P2; **b**) the nanoparticles of P2 after dialysis against distilled water; **c**) the nanoparticles of P2 after dialysis against TCEP·HCl solution. All the samples were dried and then dissolved in $CDCl_3$.*

4.3.4 Encapsulation and release of hydrophobic payloads from the nanoparticles

To further investigate the assembly and disassembly behavior of the nanoparticles, the hydrophobic dye Nile Red was sequestered into the hydrophobic core of the nanoparticles. The encapsulation of Nile Red was achieved during the formation process of the copolymer assemblies. As a control sample, the same amount of Nile Red was mixed with water without nanoparticles. The emission spectra of Nile Red encapsulated in the nanoparticles and in water were detected as shown in **Figure 4.75**. The Nile Red dissolved in water did not show a significant emission intensity whereas the signal increased largely in the dispersions. Furthermore, it was found that the emission intensity of Nile Red increased as the molar ratio of hydrophobic segment in the copolymers increased (P3 > P2 > P1). Besides, the maximum of the emission wavelength of Nile Red exhibited a blue-shift from P1 to P3 as shown in **Figure 4.75**. These observations are explained by the enhanced hydrophobicity in the interiors of nanoparticles from P3 compared to P2 and P1 and that Nile Red shows an environment-dependent emission wavelength.[125]

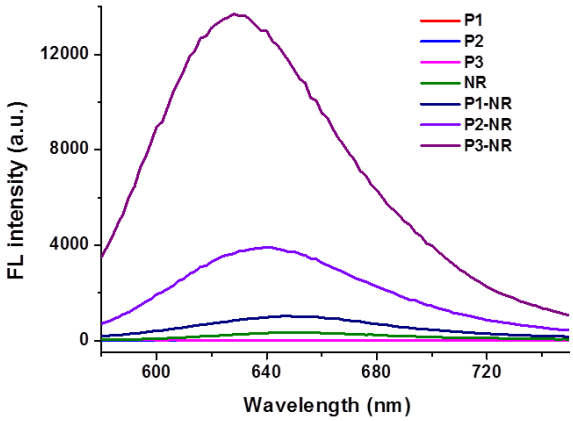

Figure 4.75 *Emission spectra of Nile Red in water (NR) or encapsulated in polymeric assemblies of P1 (P1-NR), P2 (P2-NR), or P3 (P3-NR).*

The nanoparticles encapsulating Nile Red were then reduced with TCEP·HCl, an efficient water-soluble reducing agent, with different concentrations. The release behavior of Nile Red from P2 and P3 nanoparticles was then detected by fluorescence spectroscopy after different time intervals (**Figure 4.76-4.77**). For example, the nanoparticles of P2 did not display any significant decrease in the emission intensity when no reducing agent (0 mM) or the reducing agent with a low concentration (0.25 mM, corresponding to a ratio TCEP/MBTMA of 1/1) was added. However, when the concentration of TCEP·HCl increased to 2.5 mM (TCEP/MBTMA = 10/1) or more, a significant decrease of the emission intensity was observed. A further increase of the concentration of the reducing agent resulted in a rapid decrease in the emission intensity of dye. The nanoparticles of P3 exhibited a similar release behavior as shown in **Figure 4.77**. These observations were attributed to the cleavage of the disulfide bonds in the copolymer chains and the subsequent release of Nile Red from the nanoparticles core. No large differences between the release profiles of Nile Red from P2 and P3 nanoparticles could be detected (**Figure 4.78**) except that P2 nanoparticles produced a burst release of the MBT during the first 20 min when 25 mM of the reducing agent (TCEP/MBTMA = 100/1) was used, *i.e.* ~60% was released. In comparison, the P3 nanoparticles showed a steadier release throughout the experimental time. This is due to the fact that the nanoparticles P2 contain less MBTMA and therefore the disruption of the hydrophobic domain is faster than for the P3 nanoparticles.

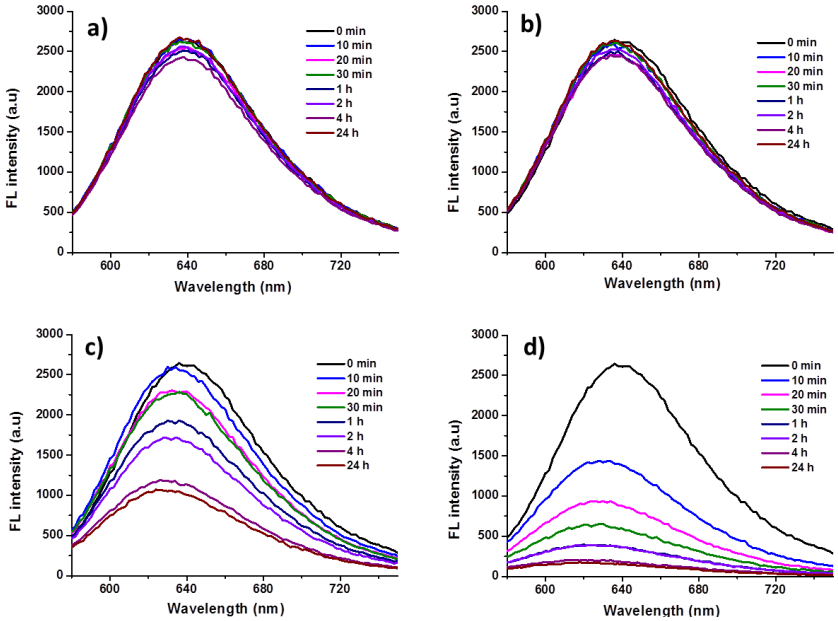

Figure 4.76 *Emission spectra of Nile Red in the dispersions of P2 after reduction by TCEP·HCl with different concentrations:* ***a****) 0 mM;* ***b****) 0.25 mM;* ***c****) 2.5 mM;* ***d****) 25 mM.*

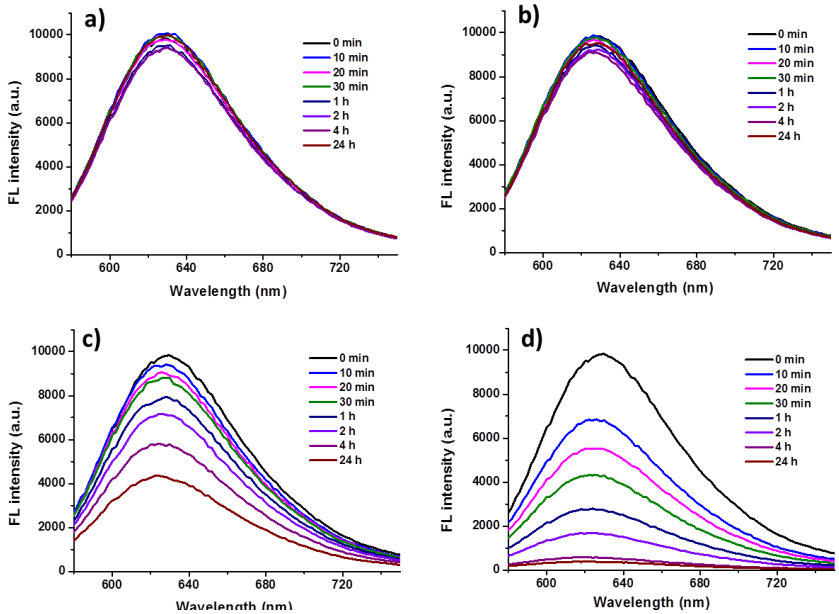

Figure 4.77 *Emission spectra of Nile Red in the dispersions of P3 after reduction by TCEP·HCl with different concentrations:* ***a****) 0 mM;* ***b****) 0.5 mM;* ***c****) 5 mM;* ***d****) 50 mM.*

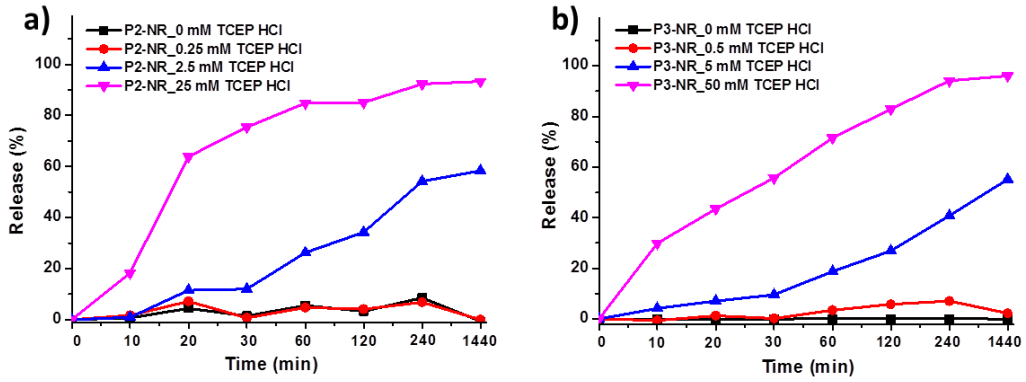

Figure 4.78 *Release curves of Nile Red from the nanoparticles of the polymers **a**) P2 and **b**) P3.*

Because the hydrochloric acid coming from the TCEP·HCl could have an influence on the fluorescence behavior of Nile Red due to a possible protonation of the dye,[126] the emission spectra of the P2 nanoparticles was also examined in the presence of hydrochloric acid in a solution having the same pH value as the TCEP·HCl solution. The difference between the emission intensity of Nile Red in the dispersion of P2 treated with HCl and TCEP·HCl is displayed in **Figure 4.79**. The signal of Nile Red decreased with time after being treated with TCEP·HCl whereas it remains relatively stable in the presence of HCl. This observation indicated that the decrease of the emission intensity of Nile Red in the dispersions of P2 and P3 can be mainly attributed to the reduction of the copolymers.

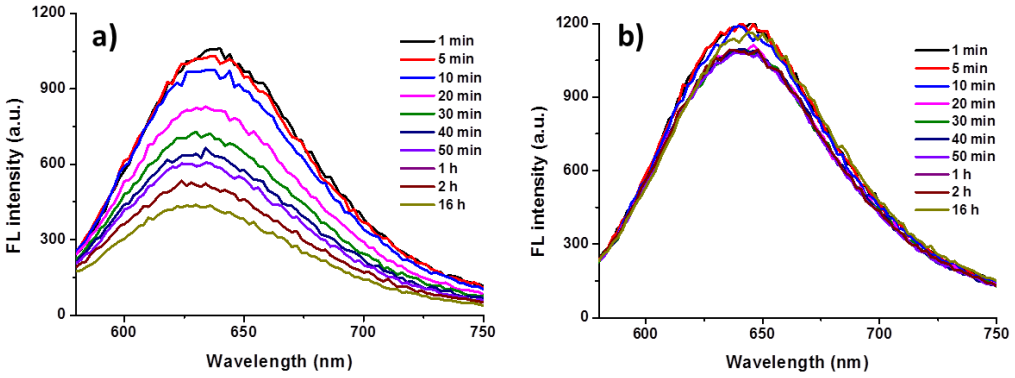

Figure 4.79 *Fluorescence emission spectra of Nile Red in polymer assemblies of P2 after addition of: **a**) TCEP·HCl with concentration of 5 mM and **b**) HCl aqueous solution with the same pH value to TCEP·HCl solution (pH ~ 2.3).*

4.3.5 Conclusion

In the present chapter, a series of amphiphilic copolymers with different amounts of functional and cleavable units (corrosion inhibitor) were prepared and self-assembled in

aqueous media. The formed nanoparticles are able to efficiently encapsulate hydrophobic payloads in their core so that a cleavage by chemical reduction leads to the release of the hydrophobic payload and to the release of the functional unit (corrosion inhibitor) present in the copolymer. Unlike other disulfide-based responsive delivery systems in which useless hydrophobic aggregates or non-functional byproducts are usually produced after reduction, the present system releases corrosion inhibitors which can be further used. This feature is of interest for optimizing the design of self-assembled nanostructured for dual-delivery of payloads for potential applications in drug-delivery or anti-corrosion.

4.4 Conducting fibers for self-healing application

4.4.1 Motivation

In the previous chapters, self-healing (SH) systems based mainly on capsules or particles were developed for anticorrosion applications. Fiber systems are also interesting for many applications due to their large surface area to volume ratio, the flexibility in surface functionalities, as well as their good mechanical performance.[127-129] In this chapter, attempts to produce conducting fibers for self-healing application are presented. The first two sections present the formation of inorganic conducting fibers of TiO_2. Different self-healing agents were incorporated into the core of formed fibers. Then fibers with the surface made of conducting polymers were further prepared via surface polymerization process. In the last section, multifunctional fibers prepared by colloid-electrospinning are prepared. Compared to the normal electrospinning technique, colloid-electrospinning enables it to form composite fibers with multifunctional properties by combinning the advantage of fibers and colloids, *e. g.* the functionality.

4.4.2 Preparation of TiO_2 fibers loaded with self-healing agents

Before the encapsulation of self-healing agents, hollow fibers with PVP/TiO_2 as shell and paraffin oil as core were formed with a previously reported method.[130] According to the reference, two immiscible liquid solutions were added into two syringes connected respectively to the outer metallic capillary and an inner silica capillary which were built in a coaxial manner as shown in **Figure 2.24**, **Chapter 2.5.2.** The shell material was a solution consisting of polyvinylpyrrolidone (PVP), titanium isopropoxide (Ti(O*i*Pr)$_4$), acetic acid, and ethanol. Heavy mineral oil was used as core material. After applying a high voltage to the outer metallic capillary, the Taylor cone was stretched by the electrostatic force to form a stable coaxial jet followed by the generation of nanofibers. Due to the hydrolysis reaction of Ti(O*i*Pr)$_4$ precursor during electrospinning process, PVP/TiO_2 was formed as the shell of the fibers. A hollow structure of nanofibers was then observed after extraction of the oil core as shown in **Figure 4.80**.

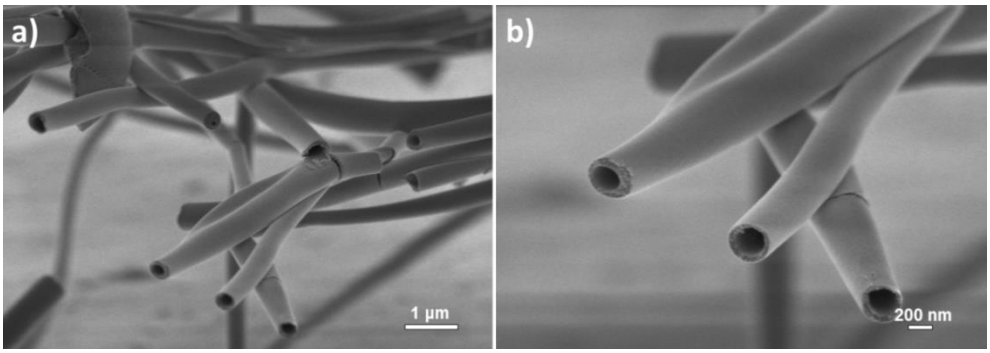

Figure 4.80 *SEM micrographs of PVP/TiO_2 fibers prepared by coaxial electrospinning with: low **a**) and high **b**) magnification. The flow rate of shell/core material was set as 1/0.1 mL h^{-1}. The paraffin oil in the core was extracted with octane.*

The same procedure was tried to generate TiO_2 core-shell fibers with self-healing agents as core material. Self-healing agents such as diglycidyl ether or dicarboxylic acid terminated polydimethylsiloxane (PDMS-DE or PDMS-DC) and dicyclopentadiene (DCPD) were used for the encapsulation. However, when the core material of paraffin oil was replaced by self-healing chemicals, no hollow fibers were found after trying different parameters for electrospinning according to the SEM micrographs as shown in **Figure 4.81**. Actually, due to the low viscosity of PDMS-DE (M_n ~ 800 g mol^{-1}, ~ 15 mPa·s) and PDMS-DC (M_w ~ 1000 g mol^{-1}, ~ 15-50 mPa·s) compared to paraffin oil (110-230 mPa·s), a stable Taylor cone was difficult to form during the electrospinning process. To increase the viscosity of the core material, the polymer PDMS (M_w ~ 153000 g mol^{-1}) without terminated functionality was mixed with the self-healing agents (PDMS/PDMS-DE, 1/5, wt/wt). The SEM micrographs of formed fibers are shown in **Figure 4.82.** No hollow structure was observed as stable Taylor cones were still not obtained.

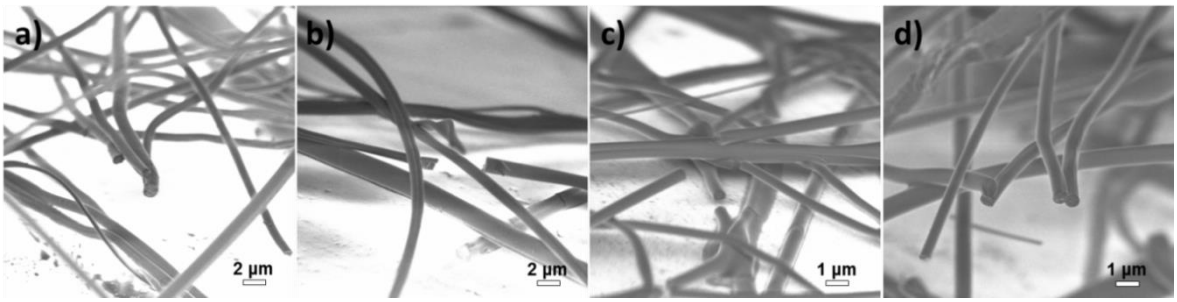

Figure 4.81 *SEM micrographs of PVP/TiO_2 fibers using **a**), **b**): PDMS-DE as core material and **c**), **d**): PDMS-DC as core material. The flow rate of shell/core material was set as 0.6/0.1 mL h^{-1} for **a**), **c**) and 1/0.1 mL h^{-1} for **b**), **d**). The core was extracted with octane for all the samples.*

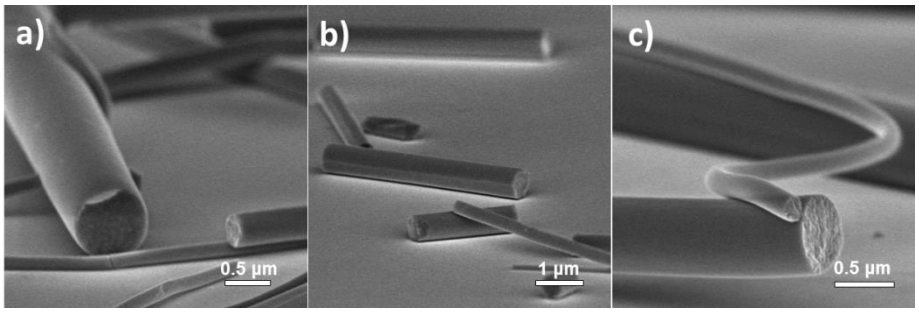

Figure 4.82 *SEM micrographs of PVP/TiO_2 fibers using PDMS/PDMS-DE as core material. The flow rate of shell/core material was set as:* ***a****) 3/0.1 mL h^{-1};* ***b****) 1/0.1 mL h^{-1}; and* ***c****) 0.6/0.1 mL h^{-1}.*

Then the mixture of paraffin with self-healing chemicals was tried. The preparation and characterization of the fiber samples were summarized in **Table 7**. When the mixture of paraffin oil and PDMS-DC was used as core material for electrospinning, hollow structures in the fibers were observed due to the removal of the core in both samples F1 and F2 as shown in **Figure 4.83**. The difference was that most of the fibers observed in sample F2 exhibited hollow structures while many fibers with solid core were obtain in sample F1 when less paraffin was used. This observation might be attributed to the unstable Taylor cone during electrospinning process of sample F1 when more PDMS-DC was present. Besides, core-shell nanofibers (**Figure 4.84**) were also easily formed by using DCPD/paraffin as core material indicating the successful encapsulation of DCPD.

Table 7 *Summary of TiO_2 fiber samples with paraffin/SH agent as core material.*

Sample	Shell material	Core material in weight ratio	Voltage (kV)	*WD*[a] (cm)	FL in shell/core[b] ($mL \cdot h^{-1}$)	Morphology
F1	PVP, $Ti(OiPr)_4$, EtOH, CH_3COOH	Paraffin/PDMS-DC 2/1	12	10.5	1/0.1	**Figure 4.83 a), b)**
F2		Paraffin/PDMS-DC 3/1				**Figure 4.83 c), d)**
F3		Paraffin/DCPD 1/1				**Figure 4.84**
F4		Paraffin/PDMS-DE/Lecithin 2/1/0.15	25	25	12/1	**Figure 4.85 a), b)**
F5		Paraffin/PDMS-DE/Lecithin 3/1/0.2			5/1	**Figure 4.85 c), d)**

[a] *WD = working distance;* [b] *Flow rate of shell/core material.*

However, the encapsulation of PDMS-DE into TiO_2 fibers was more difficult due to the unstable mixture of paraffin with PDMS-DE. Phase separation occurred after few minutes when the stirring of the mixed solution was stopped. To obtain a stable solution, lecithin was added as a surfactant to emulsify the mixed solution of paraffin/PDMS-DE. Core-shell structure of TiO_2 fibers was then observed by using paraffin/PDMS-DE with lecithin as core material. It should be noted that TiO_2 fibers with a solid core and smaller diameters compared to the hollow fibers were also formed as indicated in SEM micrographs (**Figure 4.85c, d**). This phenomenon was probably due to the interaction between acetic acid and PDMS-DE at the interface of the core and the shell during the electrospinning process, which resulted in an unstable Taylor cone.

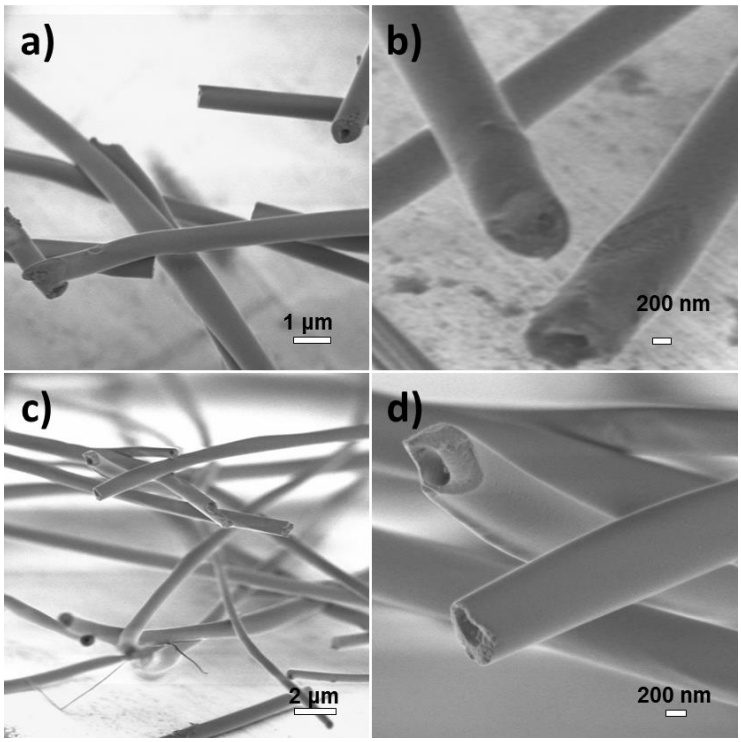

Figure 4.83 *SEM micrographs of PVP/TiO_2 fibers using paraffin/PDMS-DC as core material with different weight ratios of paraffin/PDMS-DC:* ***a****),* ***b****) 2/1 and* ***c****),* ***d****) 3/1.* ***b****) and* ***d****) are micrographs with higher magnification compared to* ***a****) and* ***c****). The core of fibers was extracted with octane for all the samples.*

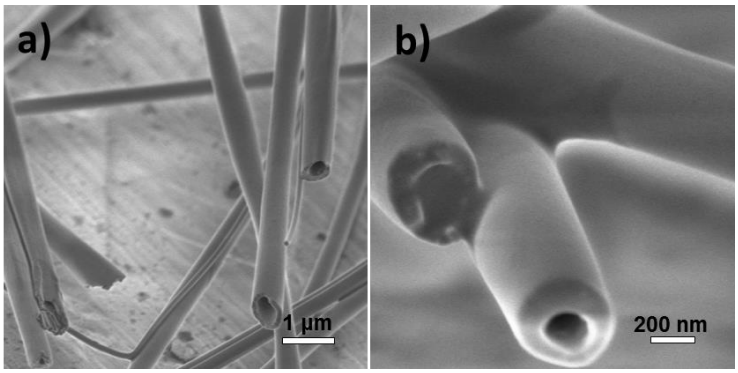

Figure 4.84 *SEM micrographs of PVP/TiO_2 fibers using paraffin/DCPD as core material.* ***b****) is a micrograph with a higher magnification compared to* ***a****). The core of the fibers was extracted with octane.*

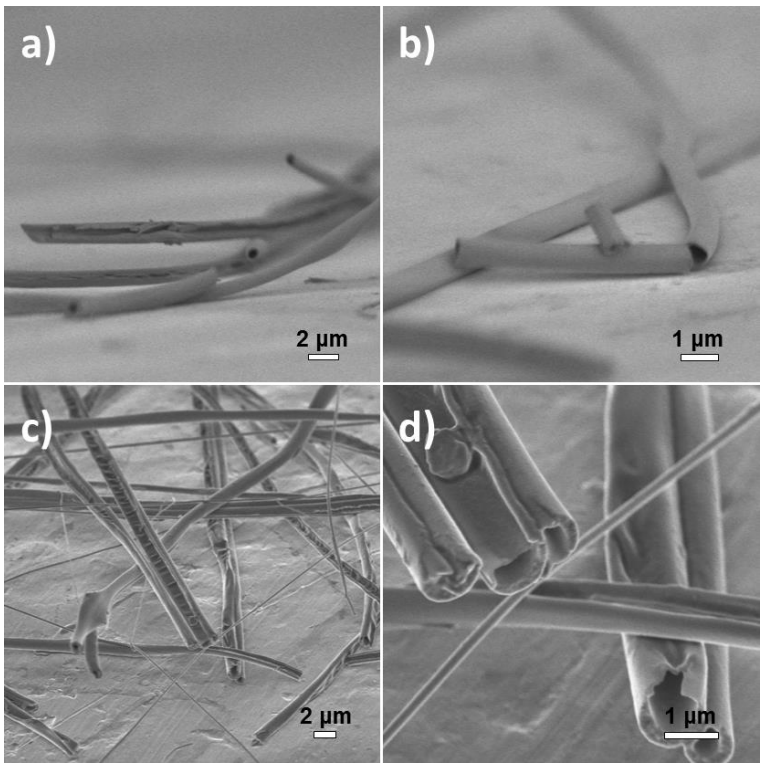

Figure 4.85 *SEM micrographs of PVP/TiO_2 fibers using paraffin/PDMS-DE/lecithin as core material with different weight ratios:* ***a****),* ***b****) 2/1/0.15 and* ***c****),* ***d****) 3/1/0.2.* ***b****) and* ***d****) are micrographs with higher magnification compared to* ***a****) and* ***c****). The core of fibers was extracted with octane for all the samples.*

4.4.3 Decoration of fibers with conducting polymers via surface polymerization

The formed TiO_2 fibers were then coated with conducting polymers by surface polymerization of monomers such as pyrrole. To achieve this goal, one piece of fiber mat was first immersed in an aqueous solution containing the oxidant APS for 3 h. Then the mat was taken out and placed in an aqueous solution of pyrrole for another 12 h. The color of the fiber mat changed from white to black after reaction. The morphology of the fibers before and after surface polymerization was observed by SEM as shown in **Figure 4.86**. It was found that the roughness of fibers increased after surface polymerization and small particles with diameter around 20-100 nm were generated on the surface of PPy@TiO2 fibers. These particles were assumed to be PPy nanoparticles. When the PVP/TiO_2 fibers were dispersed in APS solution, the PVP located close to the surface of fibers will be partly dissolved and meanwhile APS molecules entered into the small holes formed on the surface. After the fibers were immersed into solution of pyrrole, polymerization took place in these holes and generated PPy nanoparticles.

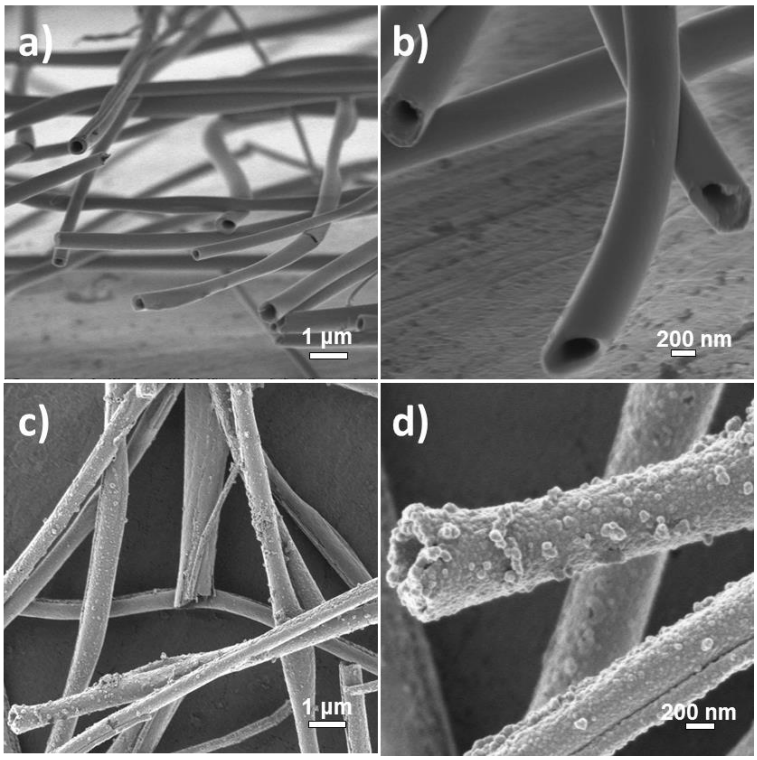

Figure 4.86 *SEM micrographs of **a**), **b**):TiO_2 and **c**), **d**): PPy@TiO_2 fibers. **b**) and **d**) represent micrographs with high magnification.*

4.4.4 Construction of multifunctional fibers based on colloid-electrospinning

By introducing one or more components in the initial solution for electrospinning, one could generate fiber materials with multifunctional properties.[131] Another possibility to provide the fibers more functionality is to combine electrospinning with another technique such as the emulsion technique.[132-135] This method provides the possibility to encapsulate functional materials into the emulsion droplets which are electrospun with the polymer solution afterwards. Besides, by mixing the miniemulsion dispersion containing nanoparticles with the electrospun polymer solution, fibers encapsulated with nanoparticles can also be formed.[136-138] The functionality of these nanoparticles can be then introduced in the formed fibers.

In the present section, we demonstrate a methodology to produce multifunctional fibers encapsulated with functional nanoparticles (NPs) and nanocapsules (NCs). **Figure 4.87** depicts the concept of the multifunctional fibers. Two different payloads are expected to be incorporated into the fiber matrix by previously encapsulating them into NPs or NCs. Stimuli-responsive release of these payloads are assumed to achieve by applying different triggers specific to the NPs or NCs.

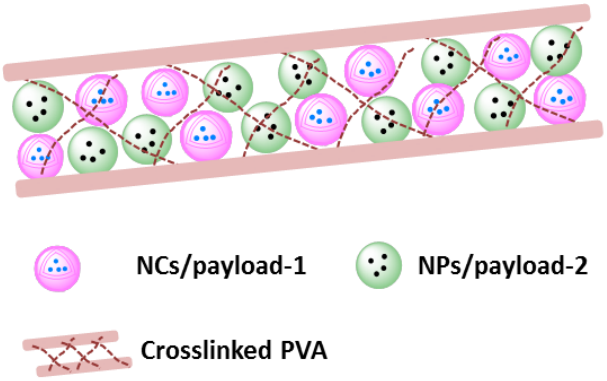

Figure 4.87 *Scheme representing crosslinked PVA fibers encapsulated with functional NPs and NCs.*

To prepare the multifunctional fibers, polyvinylferrocene (PVFc) nanoparticles loaded with diphenyl disulfide (DPS) and SiO_2 nanocapsules loaded with Irgasan were first synthesized. The preparation of PVFc nanoparticles was conducted by solvent evaporation process in miniemulsion. Dispersed chloroform phase containing PVFc and DPS was mixed with a continuous aqueous phase containing surfactant followed with miniemulsification. After the

evaporation of chloroform, PVFc/DPS nanoparticles were formed as shown in **Figure 4.88 (a, c)**.

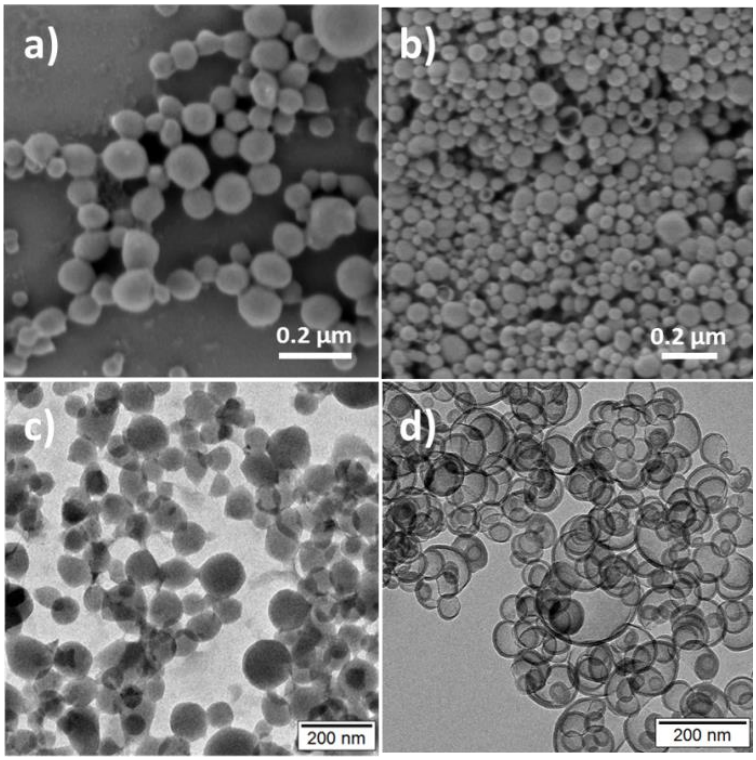

Figure 4.88 *SEM (**a**, **b**) and TEM (**c**, **d**) micrographs of: PVFc/DPS nanoparticles (**a**, **c**) and TiO_2/Irgasan (**b**, **d**) nanocapsules.*

To synthesize SiO_2 /Irgasan nanocapsules, a solution of TEOS, HD, Irgasan and xylene was first mixed and stirred with an aqueous solution of CTMA-Cl. The emulsification was then carried out by ultrasonicating the mixture. SiO_2 capsules loaded with Irgasan were obtained after the hydrolysis and condensation of TEOS **(Figure 4.88 b, d)**. The hydrodynamic diameters of the prepared NPs or NCs were found to be 124 ± 39 nm and 188 ± 22 nm, respectively, according to DLS measurements.

The prepared NPs or NCs are expected to be redox- or pH-responsive due to the stimuli-responsive property of the shell material, *i.e.* redox for PVFc and pH for SiO_2. DPS and Irgasan were chosen as the model compounds for the detection of release. The responsive release of Irgasan from SiO_2 NCs was investigated by using UV-Vis spectroscopy. **Figure 4.89** shows the release of Irgasan from SiO_2 NCs at pH ~ 12 or ~ 7. It was found that there was almost no release of Irgasan at pH ~ 7 but a fast release at pH ~ 12 indicating the pH triggered release behavior of the SiO_2 NCs. It is known that PVFc is a redox responsive

polymer and its hydrophilicity can be tuned upon oxidation reactions. Meanwhile, the hydrophobic sulfide in DPS can be converted to a hydrophilic sulfoxide or sulfone upon oxidation.[139] Thus, the release of DPS from PVFc/DPS nanoparticles upon oxidation potential is expected. The release of DPS can be then expected by detecting the signal change of DPS using ^{1}H NMR spectroscopy.

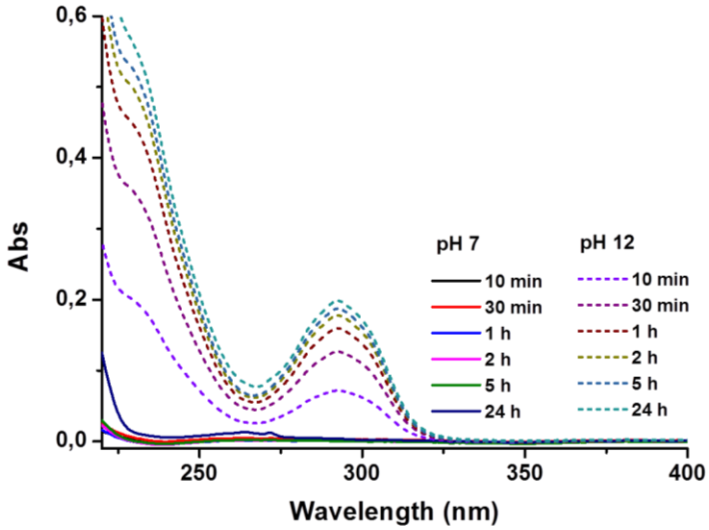

Figure 4.89 UV-Vis spectra of Irgasan released from SiO_2 NCs at different pH conditions: pH 7 (solid curves) and pH 12 (dashed curves).

PVA fibers loaded with PVFc/DPS NPs or SiO_2/Irgasan NCs were then prepared and their morphologies were evidenced by SEM and TEM micrographs as shown in **Figure 4.90**. These PVA fibers contained PVFc NPs with PVF/NPs ratio of 5/1 (wt/wt) or SiO_2 NCs with PVA/NCs ratio of 4/1 (wt/wt). It was found from SEM micrographs that well-defined PVA/NPs fibers with diameter ~ 150-350 nm and PVA/NCs fibers with diameter ~ 250-550 nm were observed. Moreover, PVFc NPs and SiO_2 NCs were clearly observed and found to be well distributed in PVA fibers according to the TEM micrographs. All these observations indicated the successful encapsulation of PVFc NPs and SiO_2 NCs into fibers.

Furthermore, the co-encapsulation of the PVFc NPs and SiO_2 NCs into PVA fibers was also achieved as shown in **Figure 4.91**. The weight ratio of PVA/NPs/NCs was set as 10/1/1.3 (wt/wt). Similarly, well-defined fibers with diameters of ~250-600 nm loaded with both NPs and NCs were formed.

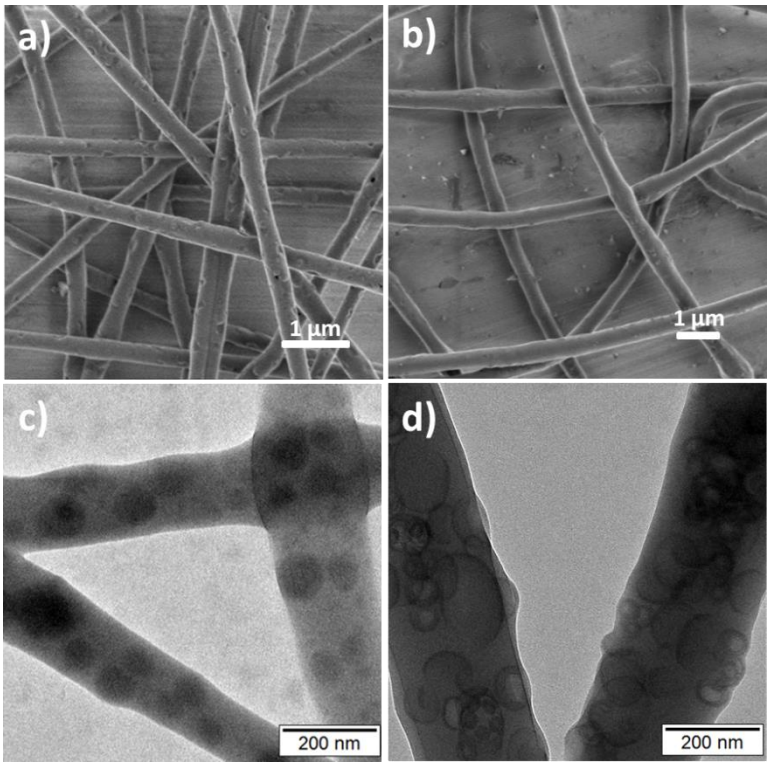

Figure 4.90 *SEM (**a**, **b**) and TEM (**c**, **d**) micrographs of: PVA fibers loaded with PVFc/DPS nanoparticles (**a**, **c**) and TiO_2/Irgasan nanocapsules (**b**, **d**).*

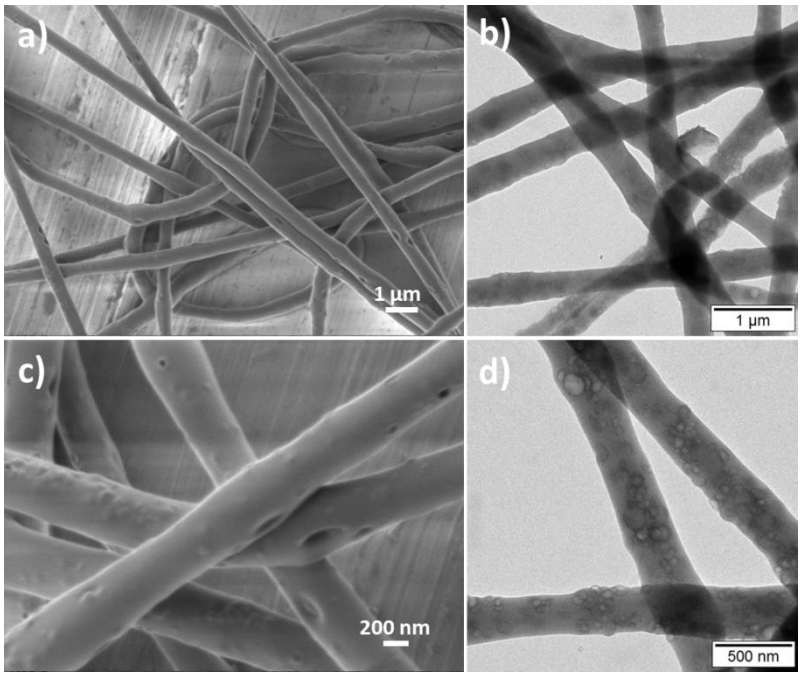

Figure 4.91 *SEM (**a**, **c**) and TEM (**b**, **d**) micrographs of: PVA fibers loaded with PVFc/DPS nanoparticles and TiO_2/Irgasan nanocapsules. **c** and **d** represent micrographs with higher magnification compared to **a** and **b**.*

It is known that non-crosslinked PVA nanofibers can be easily dissolved in an aqueous solution which hence limits their application. In the present system, multifunctional fibers encapsulated with two different components, *i.e.* PVFc/DPS NPs and SiO_2/Irgasan NCs were formed. This system is expected to exhibit dual responsive release of two payloads, *i.e.* Irgasan and DPS, due to the simultaneous incorporation of both redox-responsive PVFc NPs and pH-responsive SiO_2 NCs in the fibers. To make these fibers more available for potential application, it is necessary to improve their stability, *i.e.* crosslinking the fibers.

The crosslinking process was conducted according to a previously reported method.[140] By placing PVA fibers in glutaraldehyde/hydrochloric acid (GA/HCl) vapor for 1d, the crosslinking reaction took place between the hydroxyl group of PVA and the aldehyde group of GA in the presence of HCl. The SEM micrograph in **Figure 4.92** showed the morphology of corsslinked PVA/PVFc/SiO_2 fibers after immersed in water for 1d. The observation indicated that these crosslinked PVA/PVFc/SiO_2 fibers showed excellent stability against water which makes them promising in the application of delivery/carrier system.

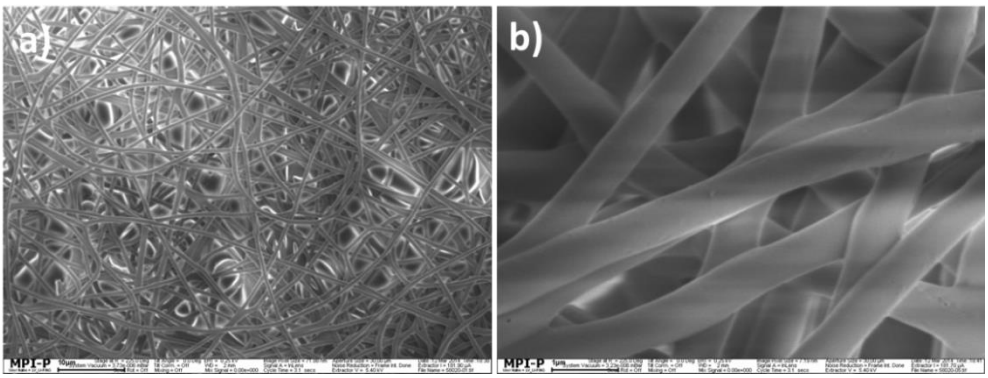

Figure 4.92 *SEM micrographs of crosslinked PVA/PVFc/SiO_2 fibers after being immersed in water for 1d with low (**a**) or high (**b**) magnification.*

4.4.5 Conclusion

In the first section of this chapter, conducting fibers with TiO_2 as shell and self-healing chemicals as core were prepared by using the coaxial electrospinning technique. All the self-healing chemicals (PDMS-DC, PDMS-DC, and DCPD) used in the system needed to be mixed with paraffin oil with a certain weight ratio to obtain a stable Taylor cone and form core-shell TiO_2 fibers. The second section was to modify the formed TiO_2 fibers with conducting polymers via surface polymerization.

In the last section, multifunctional fibers based on colloid-electrospinning were prepared. Redox-responsive PVFc nanoparticles loaded with DPS and pH-responsive SiO_2 nanocapsules loaded with Irgasan were synthesized by the miniemulsion technique. Then the NPs and NCs were encapsulated into PVA fibers by simple mixing them with PVA solution for electrospinning. The prepared multifunctional fibers could be crosslinked by GA/HCl vapor and were found to be stable against water. Future efforts will concentrate on the study of dual-responsive release of different compounds from the multifunctional fibers. These multifunctional fibers provide more possibilities for designing smart delivery/carrier systems.

4.5 References

[1] White, S. R.; Sottos, N. R.; Geubelle, P. H.; Moore, J. S.; Kessler, M. R.; Sriram, S. R.; Brown, E. N.; Viswanathan, S. *Nature* **2001**, *409*, 794.

[2] Chen, X.; Dam, M. A.; Ono, K.; Mal, A.; Shen, H.; Nutt, S. R.; Sheran, K.; Wudl, F. *Science* **2002**, *295*, 1698.

[3] Zheludkevich, M. L.; Shchukin, D. G.; Yasakau, K. A.; Möhwald, H.; Ferreira, M. G. S. *Chem. Mater.* **2007**, *19*, 402.

[4] Yuan, Y. C.; Yin, T.; Rong, M. Z.; Zhang, M. Q. *Express Polym. Lett.* **2008**, *2*, 238.

[5] Cordier, P.; Tournilhac, F.; Soulié-Ziakovic, C.; Leibler, L. *Nature* **2008**, *451*, 977.

[6] Cho, S. H.; White, S. R.; Braun, P. V. *Adv. Mater.* **2009**, *21*, 645.

[7] Hager, M. D.; Greil, P.; Leyens, C.; van der Zwaag, S.; Schubert, U. S. *Adv. Mater.* **2010**, *22*, 5424.

[8] Barisci, J. N.; Lewis, T. W.; Spinks, G. M.; Too, C. O.; Wallace, G. G. *J. Intell. Mater. Syst. Struct.* **1998**, *9*, 723.

[9] Rohwerder, M.; Michalik, A. *Electrochim. Acta* **2007**, *53*, 1300.

[10] Cecchetto, L.; Ambat, R.; Davenport, A. J.; Delabouglise, D.; Petit, J. P.; Neel, O. *Corros. Sci.* **2007**, *49*, 818.

[11] Rohwerder, M.; Duc, L. M.; Michalik, A. *Electrochim. Acta* **2009**, *54*, 607.

[12] Rohwerder, M.; Isik-Uppenkamp, S.; Amarnath, C. A. *Electrochim. Acta* **2011**, *56*, 1889.

[13] Fenelon, A. M.; Breslin, C. B. *Electrochim. Acta* **2002**, *47*, 4467.

[14] Marie, E.; Rothe, R.; Antonietti, M.; Landfester, K. *Macromolecules* **2003**, *36*, 3967.

[15] Zhao, Y.; Fickert, J.; Landfester, K.; Crespy, D. *Small* **2012**, *8*, 2954.

[16] Jamal, R.; Abdiryim, T.; Ding, Y.; Nurulla, I. *J. Polym. Res.* **2008**, *15*, 75.

[17] Wang, X.; Ray, S.; Gizdavic-Nikolaidis, M.; Easteal, A. J. *J. Polym. Sci., Polym. Chem.* **2012**, *50*, 353.

[18] Kim, Y. H.; Foster, J.; Chiang, J.; Heeger, A. J. *Synth. Met.* **1989**, *29*, 285.

[19] Fatuch, J. C.; Soto-Oviedo, M. A.; Avellaneda, C. O.; Franco, M. F.; Romao, W.; De Paoli, M. -A.; Nogueira, A. F. *Synth. Met.* **2009**, *159*, 2348.

[20] Albuquerque, J. E.; Mattoso, L. H. C.; Balogh, D. T.; Faria, R. M.; Masters, J. G.; MacDiarmid, A. G. *Synth. Met.* **2000**, *113*, 19.

[21] Yu, Y.; Zhang, Y.; Jiang, Z.; Zhang, X. *Langmuir* **2009**, *25*, 10002.

[22] Kim, H.; Jeong, S.-M.; Park, J.-W. *J. Am. Chem. Soc.* **2011**, *133*, 5206.

[23] Inzelt, G.; Pineri, M.; Schultze, J. W.; Vorotyntsev, M. A. *Electrochim. Acta* **2000**, *45*, 2403.

[24] Sherif, E.-S. M.; Es-Saheb, M.; El-Zatahry, A.; Kenawyand, E.-R.; Alkaraki, A. S. *Int. J. Electrochem. Sci.* **2012**, *7*, 6154.

[25] Souza, S. *Surf. Coat. Technol.* **2007**, *201*, 7574.

[26] Khelifa, F.; Druart, M.-E.; Habibi, Y.; Bénard, F.; Leclère, P.; Olivier, M.; Dubois, P. *Prog. Org. Coat.* **2013**, *76*, 900.

[27] Pereira da Silva, J. E.; Cordoba de Torresi, S. I. R.; Torresi, M. *Prog. Org. Coat.* **2007**, *58*, 33.

[28] Chougrani, K.; Boutevin, B.; David, G.; Seabrook, S.; Loubat, C. *J. Polym. Sci., Part A: Polym. Chem.* **2008**, *46*, 7972.

[29] Wang, L.-X.; Li, X.-G.; Yang, Y.-L. *React. Funct. Polym.* **2001**, *47*, 125.

[30] Mazur, M. *Langmuir* **2008**, *24*, 10414-10420.

[31] Blinova, N. V.; Stejskal, J.; Trchova, M.; Prokes, J.; Omastrova, M. *Eur. Polym. J.* **2007**, *43*, 2331.

[32] Chen, Z.; Wen, J.; Yan, C.; Rice, L.; Sohn, H.; Shen, M.; Cai, M.; Dunn, B.; Lu, Y. *Adv. Energy Mater.* **2011**, *1*, 551.

[33] Hotta,S.; Rughooputh, S. D. D. V.; Heeger, A. J. *Synth. Met.* **1987**, *22*, 79.

[34] Sato, M.-a.; Tanaka, S.; Kaeriyama, K. *J. Chem. Soc. Chem. Commun.* **1986**, 873.

[35] Elsenbaumer, R. L.; Jen, K. Y.; Oboodi, R. *Synth. Met.* **1986**, *15*, 169.

[36] Patil, A. O.; Ikenoue, Y.; Wudl, F.; Heeger, A. J. *J. Am. Chem. Soc.* **1987**, *109*, 1858.

[37] Wang, C.; Schindler, J. L.; Kannewurf, C. R. Kanatzidis, M. G. *Chem. Mater.* **1995**, *7*, 58.

[38] Jr, D. M.; Funt, B. L. *Synth. Met.* **1988**, *25*, 235.

[39] Aldissi, M. *Synth. Met.* **1986**, *13*, 87.

[40] Gustafsson, G.; Cao, Y.; Treacy, G. M.; Klavetter, F.; Colaner, N.; Heeger, A. J. *Nature* **1992***, 357*, 477.

[41] Kinlen, P. J.; Liu, J.; Ding, Y.; Graham, C. R.; Remsen, E. E. *Macromolecules* **1998**, *31*, 1735.

[42] Çirpan, A.; Alkan, S.; Toppare, L.; Hepuzer, Y.; Yağci, Y. *J. Polym. Sci.: Part A: Polym. Chem.* **2002**, *40*, 4131.

[43] Guner, Y.; Toppare, L.; Hepuzer, Y. Yagci, Y. *European Polymer Journal* **2004***, 40*, 1799.

[44] Mabey, W.; Mill, T. *J. Phys. Chem. Ref. Data* **1978**, *7*, 383.

[45] Perro, A.; Reculusa, S.; Ravaine, S.; Bourgeat-Lami, E.; Duguet, E. *Mater. Chem.* **2005**, *15*, 3745.

[46] Walther, A.; Müller, A. H. E. *Soft Matter* **2008**, *4*,663.

[47] Zhang, J.; Qiu, S.; Zhu, Y.; Huang, Z.; Yang, B.; Yang, W.; Wu, M.; Wu, Q.; Yang, J. *Polym. Chem.* **2013**, *4*, 459.

[48] Manoharan, V. N.; Elsesser, M. T.; Pine, D. J. *Science* **2003**, *301*, 483.

[49]Van Blaaderen, A. *Science* **2003**, *301*, 470.

[50] Srivastava, S.; Santos, A.; Critchley, K.; Kim, K. S.; Podsiadlo, P.; Sun, K.; Lee, J.; Xu, C.; Lilly, G. D.; Glotzer, S. C.; Kotov, N. A. *Science* **2010**, *327*, 1355.

[51] Wang, Y.; Wang, Y.; Breed, D. R.; Manoharan, V. N.; Feng, L.; Hollingsworth, A. D.; Weck, M.; Pine, D. J. *Nature* **2012**, *491*, 51.

[52] Li, F.; Josephson, D. P.; Stein, A. *Angew. Chem. Int. Ed.* **2011**, *50*, 360.

[53] Duguet, E.; Desert, A.; Perro, A.; Ravaine, S. *Chem. Soc. Rev.* **2011**, *40*, 941.

[54] Ling, X. Y.; Phang, I. Y.; Acikgoz, C.; Yilmaz, M.D.; Hempenius, M. A.; Vancso, G. J.; Huskens, J. *Angew. Chem. Int. Ed.* **2009**, *48*, 7677.

[55] Paleos, C. M.; Tsiourvas, D.; Sideratou, Z. *ChemBioChem* **2011**, *12*, 510.

[56] Chen, Q.; Bae, S. C.; Granick, S. *Nature* **2011**, *469*, 381.

[57] Gröschel, A. H.; Schacher, F.; Schmalz, H.; Borisov, O. V.; Zhulina, E. B.; Walther, A.; Müller, A. H. E. *Nat. Commun.* **2012**, *3*, 710.

[58] Gillespie, R. J.; Nyholm, R. S. *Rev. Chem. Soc.* **1957**, *11*, 339.

[59] Zerouki, D.; Baudry, J.; Pine, D.; Chaikin, P.; Bibette, J. *Nature* **2008**, *455*, 380.

[60] Kim, J. W.; Larsen, R. J.; Weitz, D. A. *Adv. Mater.* **2007**, *19*, 2005.

[61] Chaduc, I.; Parvole, J.; Duguet, E.; Ravaine, S.; Lansalot, M.; Bourgeat-Lami, E. *Polym. Chem.* **2012**, *3*, 3232.

[62] Wang, J. Y. ; Wang, Y.; Sheiko, S. S.; Betts, D. E.; DeSimone, J. M. *J. Am. Chem. Soc.* **2012**, *134*, 5801.

[63] Staff, R. H.; Rupper, P.; Lieberwirth, I.; Landfester, K.; Crespy, D. *Soft Matter* **2011**, *7*, 10219.

[64] Zhao, Y.; Landfester, K.; Crespy, D. *Soft Matter* **2012**, *8*, 11687.

[65] Schaeffel, D.; Staff, R. H.; Butt, H. J.; Landfester, K.; Crespy, D.; Koynov, K. *Nano Lett.* **2012**, *12*, 6012.

[66] Staff, R. H.; Schaeffel, D.; Turshatov, A.; Donadio, D.; Butt, H. J.; Landfester, K.; Koynov, K.; Crespy, D. *Small* **2013**, *9*, 3514.

[67] Qiu, P.; Jensen, C.; Charity, N.; Towner, R.; Mao, C. *J. Am. Chem. Soc.* **2010**, *132*, 17724.

[68] Hu, S. H.; Gao, X. *J. Am. Chem. Soc.* **2010**, *132*, 7234.

[69] Wang, Y.; Xu, H.; Ma, Y.; Guo, F.; Wang, F.; Shi, D. *Langmuir* **2011**, *27*, 7207.

[70] Zhang, J. N.; Qiu, S. L.; Zhu, Y. L.; Huang, Z. Q.; Yang, B. B.; Yang, W. L.; Wu, M. Y.; Wu, Q. Y.; Yang, J. J. *Polym. Chem.* **2013**, *4*, 1459.

[71] Siato, N.; Kagari, Y.; Okubo, M. *Langmuir* **2006**, *22*, 9397.

[72] Yabu, H.; Koike, K.; Motoyoshi, K.; Higuchi, T.; Shimomura, M. Macromol. *Rapid Commun.* **2010**, *31*, 1267.

[73] Crespy, D.; Landfester, K. *Beilstein J. Org. Chem.* **2010**, *6*, 1132.

[74] Zhao, Y.; Berger, R.; Landfester, K.; Crespy, D. *Polym. Chem.* **2014**, *5*, 365.

[75] Chen, Y. C.; Dimonie, V.; El-Aasser, M. S. *Macromolecules* **1991**, *24*, 3779.

[76] Torza, S.; Mason, S. G. *J. Colloid Interf. Sci.* **1970**, *33*, 67.

[77] Floudas, G.; Placke, P.; Stepanek, P.; Brown, W.; Fytas, G.; Ngai, K. L. *Macromolecules* **1995**, *28*, 6799.

[78] Khare, P. K.; Pandey, R. K.; Jain, P. L. *Bull. Mater. Sci.* **1999**, *22*, 1003.

[79] Akratopulu, K. C.; Kordulis, C.; Lycourghiotis, A. *J. Chem. Soc. Faraday Trans.* **1990**, *86*, 3437.

[80] Lee, D.; Omolade, D.; Cohen, R. E.; Rubner, M. F. *Chem. Mater.* **2007**, *19*, 1427.

[81] Jiang, J.; Oberdörster, G.; Biswas, P. *J. Nanopart. Res* **2009**, *11*, 77.

[82] Folli, A.; Pochard, I.; Nonat, A.; Jakobsen, U. H.; Shepherd, A. M.; Macphee, D. E. *J. Am. Ceram. Soc.* **2010**, *93*, 3360.

[83] Liu, R.; Zhao, X.; Wu, T.; Feng, P.Y. *J. Am. Chem. Soc.* **2008**, *130*, 14418.

[84] Klaikherd, A.; Nagami, C.; Thayumanayan, S. *J. Am. Chem. Soc*. **2009**, *131*, 4830.

[85] Bird, R.; Freemont, T.; Saunders, B. R. *Soft Matter* **2012**, *8*, 1047.

[86] Liang, K.; Such, G. K.; Zhu, Z.; Yan, Y.; Lomas, H.; Caruso, F. *Adv. Mater.* **2011**, *23*, H273.

[87] Huang, W. S.; MacDiarmid, A. G.; Epstein, A. J. *J. Chem. Soc. Chem. Commun*. **1987**, 1784.

[88] Lv, L.-P.; Zhao, Y.; Vilbrandt, N.; Gallei, M.; Vimalanandan, A.; Rohwerder, M.; Landfester, K.; Crespy, D. *J. Am. Chem. Soc*. **2013**, *135*, 14198.

[89] Vimalanandan, A.; Lv, L. - P.; Tran, T. H.; Landfester, K.; Crespy, D.; Rohwerder, M. *Adv. Mater*. **2013**, *25*, 6980.

[90] Love, J. C.; Estroff, L. A.; Kriebel, J. K.; Nuzzo, R. G.; Whitesides, G. M. *Chem. Rev.* **2005**, *105*, 1103.

[91] Wang, X.; Cai, X.; Hu, J.; Shao, N.; Wang, F.; Zhang, Q.; Xiao, J.; Cheng, Y. *J. Am. Chem. Soc*. **2013**, *135*, 9805.

[92] Kawaguchi, T.; Yasuda, H.; Shimazu, K. *Langmuir* **2000**, *16*, 9830.

[93] Han, S. W.; Joo, S. W.; Ha, T. H.; Kim, Y.; Kim, K. *J. Phys. Chem. B.* **2000**, *104*, 11987-11995.

[94] Bhatt, N.; Huang, P.-J. J.; Dave, N.; Liu, J. *Langmuir* **2011**, *27*, 6132.

[95] Han, J. C.; Han, G. Y. *Anal. Biochem*. **1994**, *220*, 5.

[96] Mahajanam, S. P. V.; Buchheit, R. G. *Corrosion* **2008**, *64*, 230.

[97] Shchukin, D. G.; Zheludkevich, M.; Yasakau, K.; Lamaka, S.; Ferreira, M. G. S.; Möhwald, H. *Adv. Mater.* **2006**, *18*, 1672.

[98] Shchukin, D. G.; Möhwald, H. *Adv. Funct. Mater*. **2007**, *17*, 1451.

[99] Abu, Y. M.; Aoki, K. *J. Electroanal. Chem.* **2005**, *583*, 133.

[100] Tallman, D.; Spinks, G.; Dominis, A.; Wallace, G. *J. Solid State Electrochem.* **2002**, *6*, 73.

[101] Paliwoda-Porebska,G.; Stratmann, M.; Rohwerder, M.; Potje-Kamloth, K.; Lu, Y.; Pich, A. Z.; Adler, H. J. *Corros. Sci.* **2005**, *47*, 3216.

[102] Kowalski, D.; Ueda, M.; Ohtsuka, T. *J. Mater. Chem.* **2010**, *20*, 7630.

[103] Paliwoda-Porebska, G.; Rohwerder, M.; Stratmann, M.; Rammelt, U.; Duc, L.; Plieth, W. *J. Solid State Electrochem.* **2006**, *10*, 730.

[104] Rohwerder, M.; Duc, L. M.; Michalik, A. *Electrochim. Acta* **2009**, *54*, 6075.

[105] Rohwerder, M. *Int. J. Mater. Res.* **2009**, *100*, 1331.

[106] Loto, R. T.; Loto, C. A.; Popoola, A. P. I. *J. Mater. Environ. Sci.* **2012**, *3*, 885.

[107] Saji, V. S. *Recent Patents on Corrosion Science* **2010**, *2*, 6.

[108] Kataoka, K.; Harada, A.; Nagasaki, Y. *Adv. Drug Del. Rev.* **2001**, *47*, 113.

[109] Rösler, A.; Vandermeulen, G. W. M.; Kolk, H.-A. *Adv. Drug Del. Rev.* **2001**, *53*, 95.

[110] Kabanov, A. V.; Batrakova, E. V.; Alakhov, V. Y. *J. Control. Release* **2002**, *82*, 189.

[111]Adams, M. L.; Lavasanifar, A.; Kwon, G. S. *J. Pharm. Sci.* **2003**, *92*, 1343.

[112] Roster, A.; Vandermeulen, G. W. M.; Klok, H. A. *Adv. Drug Del. Rev.* **2012**, *64*, 270.

[113] Rijcken, C. J. F.; Soga, O.; Hennink, W. E.; van Nostrum, C. F. *J. Control. Release* **2007**, *120*, 131.

[114] Rapoport, N. *Prog. Polym. Sci.* **2007**, *32*, 962.

[115] York, A. W.; Kirkland, S. E.; McCormick, C. L. *Adv. Drug Del. Rev.* **2008**, *60*, 1018.

[116] Wang, Y.; Xu, H.; Zhang, X. *Adv. Mater.* **2009**, *21*, 2849.

[117] Meng, F.; Zhong, Z.; Feijen, J. *Biomacromolecules* **2009**, *1*0, 197.

[118] Onaca, O.; Enea, R.; Hughes, D. W.; Meier, W. *Macromol. Biosci.* **2009**, *9*, 129.

[119]Stuart, M. A. C.; Huck, W. T. S.; Genzer, J.; Muller, M.; Ober, C.; Stamm, M.; Sukhorukov, G. B.; Szleifer, I.; Tsukruk, V. V.; Urban, M.; Winnik, F.; Zauscher, S.; Luzinov, I.; Minko, S. *Nat. Mater.* **2010**, *9*, 101.

[120] Ohsawa, M.; Suëtaka, W. *Corrosion Sci.* **1979**, *19*, 709.

[121] Zheludkevich, M. L.; Yasakau, K. A.; Poznyak, S. K.; Ferreira, M. G. S. *Corrosion Sci.* **2005**, *47*, 3368.

[122] Brzezinskal, E.; Ternay Jr., A. L. *J. Org. Chem.* **1994**, *59*, 8239.

[123] Tsarevsky, N. V.; Huang, J.; Matyjaszewski, K. J. *Polym. Sci.: Part A: Polym. Chem.* **2009**, *47*, 6839.

[124] Shervedani, R. K.; Hatefi-Mehrjardi, A.; Babadi, M. K. *Electrochimica Acta* **2007**, *52*, 7051.

[125] Stuart, M. C. A.; van de Pas, J. C.; Engberts, J. B. F. N. *J. Phys. Org. Chem.* **2005**, *18*, 929.

[126] Wagner, B. D.; Boland, P. G.; Lagona, J.; Isaacs, L. *J. Phys. Chem. B* **2005**, *109*, 7686.

[127] Huang, Z.-M.; Zhang, Y.-Z.; Kotaki, M.; Ramakrishna, S. *Compos. Sci. Technol*. **2003**, *63*, 2223.

[128] Yoo, H. S.; Kim, T. G.; Park, T. G. *Adv. Drug Del. Rev.* **2009**, *61*, 1033.

[129] Lu, X.; Wang, C.; Wei, Y. *small* **2009**, *5*, 2349.

[130] Li, D.; Xia, Y. *Nano Lett.* **2004**, *4*, 933.

[131] Wang, C.; Wang, M. *Front. Mater. Sci.* **2014**, *8*, 3.

[132] Lu, X.; Wang, C.; Wei, Y. *small* **2009**, *5*, 2349.

[133] Yarin, A. L. *Polym. Adv. Technol.* **2011**, *22*, 310.

[134] Qi, H.; Hu, P.; Xu, J.; Wang, A. *Biomacromolecules* **2006**, *7*, 2327.

[135] Su, Y.; Li, X.; Liu, X.; Mo, X.; Seeram, R. *Colloid. Surf. B: Biointerf*. **2009**, *73*, 376.

[136] Friedemann, K.; Turshatov, A.; Landfester, K.; Crespy, D. *Langmuir* **2011**, *27*, 7132.

[137] Friedemann, K.; Corrales, T.; Kappl, M.; Landfester, K.; Crespy, D. *small* **2012**, *8*, 144.

[138] Wohnhaas, C.; Friedemann, K.; Busko, D.; Landfester, K.; Baluschev, S.; Crespy, D.; Turshatov A. *ACS Macro Lett.* **2013**, *2*, 446.

[139] Napoli, A.; Valentini, M.; Tirelli, N.; Muller, M.; Hubbell, J. A. *Nature Mater.***2004***, 3*, 183.

[140] Destaye, A. G.; Lin, C.-K.; Lee, C.-K. *ACS Appy. Mater. Interfaces* **2013**, *5*, 4745.

5. Experimental Part

5.1 Experimental details for section 4.1

5.1.1 Materials

Aniline was purchased from Sigma Aldrich and distilled under vacuum before use. Sodium dodecyl sulfate (SDS, 99%), poly(dimethylsiloxane) diglycidyl ether terminated (PDMS-DE, M_n ~ 800 g mol^{-1}), pyrene (>99%), hydrazine aqueous solution (N_2H_4, 35 wt % in H_2O), potassium persulfate (KPS, ≥99%), hydrogen peroxide solution (H_2O_2, 34.5−36.5wt.%), 1, 4-dioxane (99.5%), dicyclohexylcarbodiimide (DCC, 99%), 4-dimethylaminopyridine (DMAP, ≥99%), methyl methacrylate (MMA, 99%), methacrylic acid (MAA, 99%), iron(III) chloride ($FeCl_3$, 97%), polyvinyl formal (PVF, M_w ~ 10,000 g mol^{-1}), titanium (IV) oxide (TiO_2, 45 ~ 47 wt.% in xylene, 99.9%), divinylbenzene (DVB, >99%), 2,2'-azobisisobutyronitrile (AIBN, 98%), poly(ethyleneglycol methacrylate) monomethyl ether (PEGMA, M_n ~360 and 950 g mol^{-1}), sodium 4-vinylbenzenesulfonate (VBS, >90%) and cetyltrimethylammonium bromide (CTAB, >99%) were supplied from Sigma Aldrich and used as received.

Pyrrole (Py, 99%), tetrahydrofuran (THF, ≥99.9%), ethylbenzene (EB, 99.8%), hexadecane (HD, 99%), methyl methacrylate (MMA, 99%), butyl acrylate (BA, >99%), ammonium persulfate (APS, 98%), dichloromethane (CH_2Cl_2, 99.8%), thiophene (99.5%), 3-thiophenemethanol (TM, 97%) chloroform (99%), hexadecane (HD, 99.8%) and 2-aminoethyl methacrylate hydrochloride (AEMA, 90%) were obtained from ACROS Organics and used without further purification.

Poly(vinyl alcohol) (PVA, 98−99% hydrolyzed, Alfa Aesar) with a molecular weight M_w of 27450 g mol^{-1} (measured by gel permeation chromatography, calibration with poly(ethylene oxide) (PEO) standards, 80% 0.1 M $NaNO_3$ in water/20% MeOH as eluent), polydimethylsiloxane carboxydecyldimethyl terminated (PDMS-DC, M_w ~ 1000 g mol^{-1}, ABCR), Lutensol AT50 (BASF), poly(vinyl alcohol) (PVA, M_w ~ 25000 g mol^{-1}, 88 mol% hydrolyzed, Polysciences Inc.), dodecyl methacrylate (DMA, >95%, Fluka), dimethyl vinylphosphonate (DVP, >85%, Fluka) were used as received. Octapyrrolylnaphthalene (OPN) was kindly donated by Dr. L. Chen (MPIP) who synthesized the monomer according to a previous report.[1] Distilled water was used throughout the work.

5.1.2 Redox responsive release of self-healing agents from PANI capsules

5.1.2.1 Synthesis of capsules loaded with self-healing agents

PANI capsules were prepared as follows: A mixture of aniline (0.49 mL, 5.38 mmol) and ethylbenzene (1.23 mL, 10.04 mmol) as hydrophobe was added to 6 mL of water containing 62.5 mg of SDS. After stirring under 1000 rpm for 1 h at room temperature, the emulsification was carried out by ultrasonicating the mixture for 240 s at 90% amplitude (Branson sonifier W450) under ice cooling. After emulsification, an aqueous solution of PVA (10 wt %) was mixed with the miniemulsion. Then, an aqueous solution of APS (1.23 g, 5.38 mmol in 1.67 mL of water) was added dropwise to the miniemulsion at room temperature. The color of the miniemulsion first turned brown then dark green as the polymerization proceeded. This sample was defined as PANI-1. The other PANI sample was obtained by increasing the concentration of monomer in the dispersed phase and was defined as PANI-2. The encapsulation process of self-healing agents was carried out during the formation of PANI capsules. PDMS-DE or PDMS-DC (60 wt % compared to monomer) was dissolved in the dispersed phase prior to the emulsification. The samples were defined as PANI/PDMS-DE and PANI/PDMS-DC, respectively.

To calculate the encapsulation efficiency, 102.5 mg of PANI/PDMS-DC or PANI/PDMS-DE capsules dispersions were first freeze-dried and then dissolved in a mixture of 1 mL of NMP and 1 mL of DMSO for 24 h. 0.4 mL of the solution was taken for ^{1}H NMR measurement in 0.7 mL of THF-d_8 with pyrene as internal standard. In parallel, same amounts of PANI/PDMS-DC or PANI/PDMS-DE capsules dispersions were purified by centrifugation in water. The collected capsules were then prepared by the aforementioned method for ^{1}H NMR spectroscopy measurement. The encapsulation efficiency of PDMS-DC in PANI capsules was obtained by comparing the signals of $-$Si-CH_3 from PDMS-DC around 0 ppm in ^{1}H NMR before and after purification. The encapsulation efficiencies for the PANI/PDMS-DE and PDMS DC systems were found to be ~ 94% and ~ 89%, respectively.

5.1.2.2 Redox responsive release of self-healing agents

Before the addition of oxidizing or reducing agents, the dispersions of PANI capsules were purified by centrifugation to remove PVA until a clear supernatant was observed. Certain amounts of PANI capsules dispersions were taken and added in hydrogen peroxide or

hydrazine solution with a molar ratio ANI unit to N_2H_4 or H_2O_2 equal to 1:43. After reaction and stirring for 12 h, an aliquot of the dispersion was taken for electron microscopy measurements. The rest of the sample was freeze-dried for further FT-IR, UV-vis measurements.

The redox release behavior of PANI capsules were detected as follows: the miniemulsion dispersion of PANI capsules after polymerization was first mixed with same weight of distilled water to lower the initial concentration. After that, several 5 mL glass vials were separately added in 102.5 mg of these diluted PANI capsules dispersion. Then 0.7 mL of deuterated tetrahydrofuran (THF-d_8) which dissolved certain amount of pyrene before use, together with 74 μL of N_2H_4 or H_2O_2 solution (molar ratio ANI unit to N_2H_4 or H_2O_2 1:43) were added. As a control, the same amount of distilled water was used instead of a N_2H_4 or H_2O_2 solution. After stirring for different times, the mixture was kept till phase separation occurred and the supernatant was taken for ^{1}H NMR measurements.

The release of PDMS-DE or PDMS-DC was detected by comparing the separated signal of –Si-CH_3 from PDMS-DE around $\delta \approx 0$ ppm with the signal of pyrene around $\delta \approx 8$–8.5 ppm after different times. To detect the total amount of self-healing agents inside of the release samples, same amount of diluted capsules dispersion was first freeze-dried and then dissolved in the mixture of 1 mL of DMSO and 1 mL of NMP under stirring for 12 h. Then 0.2 mL of the mixture was taken and added in 0.7 mL of THF-d_8/pyrene solution.

In the case of the sample that was first oxidized then reduced after 24 h of release, fresh hydrazine solution with the amount of twice as much as the initial amount of hydrogen peroxide solution was added into the oxidized sample after 24 h of release.

5.1.2.3 Incorporation of capsules into composite coatings

Incorporation of the capsules in PVA films:

Certain amounts of purified PANI/PDMS-DC capsule dispersions (4 wt.% of PANI + PDMS-DC) were first mixed with a 9 wt.% aqueous solution of PVA and then stirred for 3 min with a vortex. The ratio of PANI + PDMS-DC to PVA was 1 wt.%. Then the mixture was casted to form a 1.5 × 3 cm film on a microscope slide and dried at room temperature. To determine the stability of capsules in PVA matrix after the formation of film, the PVA matrix was removed by immersing the film in water for 12 h. Then the capsules were collected by

centrifugation and the morphology was studied by AFM. Some non-purified capsules were also freeze-dried and the amount of remaining PDMS-DC was determined by ^{1}H NMR in THF-d_8 (pyrene as internal standard) after dissolving the capsules in NMP/DMSO (1/1, vol/vol).

The amount of PDMS-DC in the recovered capsules was quantified by ^{1}H NMR spectroscopy and compared to the amount present in the capsules prior to embedding in PVA films. 88% of PDMS-DC could be recovered. Comparing this value with the encapsulation efficiency of 89% indicates that only a minor leakage (~ 1%) of the self-healing agents from the inner core of the capsules occurred.

Incorporation of the capsules in hydrophobic acrylate coatings:

Synthesis of the dispersion for the acrylate coating: A mixture of MMA (2.13 mL, 0.02 mol), BA (2.25 mL, 0.02 mol), and hexadecane (0.194 mL, 0.66 mmol) was added to 16 mL of water containing 100 mg of Lutensol AT 50 and 10 mg KPS. After stirring under 1000 rpm for 1 h at room temperature, the mixture was ultrasonicated for 120 s at 70% amplitude (Branson sonifier W450) under ice cooling. Before polymerization, the miniemulsion dispersion was degassed with Argon for 10 min. Then the reaction was carried in an oil bath at 72 °C for 20 h. After polymerization, a dispersion of poly(MMA-*co*-BA) nanoparticles with a solid content of 20 wt.% was obtained.

Preparation of the capsules/acrylate coatings: 50 μL of purified PANI/PDMS-DC dispersion (4 wt.% of PANI + PDMS-DC) was mixed with 50 μL of the acrylate dispersion (20 wt.%) and stirred for another 1 h. The ratio of PANI + PDMS-DC to poly(MMA-*co*-BA) was ~20 wt.%. Then 40 μL of the mixed dispersion was casted on a 2 × 2 cm silicon wafer and dried under room temperature. To observe the SEM cross section images of the film, the as-prepared silicon wafers with capsules-embedded poly(MMA-*co*-BA) film were first immersed into liquid nitrogen for 3 min and then quickly broken by tweezers. For the SEM-EDX measurements, the films were prepared on a thick carbon conductive tape instead of silicon wafer to eliminate all the signals of silicon from the substrate.

Deposition of the capsules/acrylate coating on a zinc plate:

Purified PANI/PDMS-DE (2.4 wt.% of PANI + PDMS-DE) or PANI/PDMS-DC (4 wt.% of PANI + PDMS-DC) capsules dispersion were first mixed with the poly(MMA-*co*-BA) dispersion (20 wt.% solid content). The weight ratios of capsule dispersion to polymer dispersion in the above

mixtures were around 50:50 and 70:30, respectively. Then 80 μL of each mixture was casted onto the surface of a zinc foil (1 × 2 cm, grinded with grinding paper, cleaned by ultrasonication in THF then ethanol for 5 min, rinsed with distilled water and dried under Argon). After drying at room temperature, a capsules/acrylate coating was formed on zinc. The zinc foil was then cut with a scissor and polished by using Hitachi cross-section polisher (ion milling machine). The EDX spectra were taken with an SEM (Zeiss LEO 1550 VP).

5.1.3 Colloidal system based on PPy and its derivatives

5.1.3.1 Formation of PPy nanostructures via miniemulsion polymerization

PPy nanoparticles and nanocapsules were prepared using a similar process that for PANI capsules. The difference is that, in some cases the feed ratio of monomer/solvents, dispersed/continuous phase, concentration of stabilizer, and reaction temperature were varied. The detailed preparation parameters were shown in **Table 2, Chapter 4**.

5.1.3.2 Porous nanoparticles based on PPy derivatives for supercapacitors

To prepare the porous nanoparticles, 100 mg of octapyrrolylnaphthalene (OPN) was dissolved in 2.1 mL of $CHCl_3$ followed by mixing with 20 mL of aqueous solution of SDS (200 mg) and stirred for 1 h at 1000 rpm at room temperature. The mixture was then sonicated with a sonifier (Branson W450D Digital, half inch tip) for 240 s (30 s plus, 15 s pause) at 90 % of amplitude in an ice-water bath. Then the miniemulsion was then left to evaporate for 30 min followed by adding dropwise an aqueous solution of APS (1.36 g in 1.5 mL of water). The reaction was carried out in an ice-water bath for 24 h. The color of the miniemulsion turned from yellow to dark brown as polymerization proceeded. After the polymerization, the product was centrifuged and washed several times with water until the supernatant became clear.

5.1.4 Other attempts

5.1.4.1 Synthesis of soluble conducting copolymers

To synthesize the monomer 3-methylthienyl methacrylate (MTM), 0.9 g of methacrylic acid (10.6 mol), 1 g of 3-thiophenemethanol (8.8 mol) and 20 mg of 4-dimethylaminopyridine (DMAP) were first dissolved in 15 mL of dichloromethane (CH_2Cl_2) at 0 °C. Then to the above solution, 2.18 g of dicyclohexylcarbodiimide (DCC) dissolved in 5 mL of CH_2Cl_2 was added

dropwise. The mixture was then stirred at room temperature for 24 h. After reaction, the solid salt generated was removed by filtration with paper filter. Then the products dissolved in CH_2Cl_2 was filtered through a silica gel column by using ethyl acetate/ petroleum ether (1:3, v:v) as eluent solvent. The final product was collected by evaporating all the solvent.

To synthesize copolymer poly(MMA-*co*-MTM), methyl methacrylate (MMA, 2.5 g), MTM (0.26 g) and V59 (27 mg) were dissolved in 30 mL of 1,4-dioxane and put in a round-bottomed flask with a stirring bar. After degassed with Argon for 10 min, the flask was sealed and kept stirring at 75 °C for 24 h. After polymerization, the product was purified for three times by precipitating in methanol and then dissolving in THF. The final product was then collected and dried at 45 °C under vacuum for 2 d.

The poly(MMA-*co*-MTM-*g*-PPy) or poly(MMA-*co*-MTM-*g*-PTP) copolymers were then prepared by adding pyrrole or thiophene monomers to the solution of poly(MMA-*co*-MTM) in THF followed with the addition of oxidant $FeCl_3$. In a typical procedure, 50 mg of poly(MMA-*co*-MTM) and 0.04 mL of pyrrole (0.57 mmol) was dissolved in 25 mL of THF. Then 0.15 g of $FeCl_3{\cdot}3H_2O$ was dissolved in 5 mL of THF and added into the above solution dropwise. After reaction for 24 h at room temperature, the products were filtered through a column filled with neutral aluminium oxide to remove the generated ferric salt. The final product was purified and collected by precipitating in methanol.

5.1.4.2 Decoration of colloid with TiO_2 nanoparticles

To prepare organic/inorganic hybrid particles, 250 mg of PVF and certain amounts of HD, and TiO_2/xylene were dissolved and stirred in 5 mL $CHCl_3$ for 30 min. Then 10 mL of SDS aqueous solution was added, followed by continuous stirring at 1000 rpm for 1 h. The emulsion was then sonicated with a sonifier (Branson W450D Digital, half inch tip) for 2 min (30 s plus, 15 s pause) in an ice-water bath. The miniemulsion was then kept stirring in an oil bath at 40 °C for 6 or 12 h to evaporate the chloroform. The composition of the dispersions was summarized in **Table 3, Chapter 4**.

To prepare the hybrid particles with two polymers, DMA and small amount of the crosslinker agent DVB were used to replace HD and 17 mg AIBN was added to the dispersed phase. Besides, 8.5 mg of a hydrophilic comonomer (3 wt.% compared to DMA/DVB) was dissolved in 10 mL of a 2 mg mL^{-1} aqueous solution of surfactant (SDS or CTAB). After the sonication

and solvent evaporation processes described previously (40 °C, 12 h), the miniemulsion dispersion was bubbled with Argon for 5 min and then put in an oil bath of 72 °C for 6 h to carry out the polymerization. All samples with varied preparation conditions are listed in **Table 4, Chapter 4.**

5.1.5 Characterization methods

The FTIR spectra of polymers were measured on KBr pellets using a Perkin-Elmer spectrum BX FT-IR spectrometer. All spectra were collected in the range of 400-4000 cm^{-1} with a resolution of 1 cm^{-1}. Freeze-dried PANI capsules were dissolved in *N*-methyl-2-pyrrolidone (NMP) for UV–vis measurements recorded with a Perkin-Elmer Lambda 25 UV–vis spectrometer. The morphology of the capsules were examined with a Gemini 1530 (Carl Zeiss AG, Oberkochem, Germany) scanning electron microscope (SEM) operating at 0.2 kV. Samples for SEM were prepared by dropping purified PANI capsule dispersions or diluted particle dispersions on silicon wafers and were dried at room temperature. The morphology of the capsules or particles was also studied using a transmission electron microscope (TEM) (Zeiss EM912) operating at an accelerating voltage of 120 kV. All samples were deposited on a 300 mesh carbon-coated copper grid. Atomic force microscope (AFM) measurements were carried on a commercial Bruker Dimension 3100 (NanoScope IIIa controller) setup in tapping mode. Hydrodynamic diameters (D_h) of the PANI capsules (dispersions diluted in 3 mg mL^{-1} of SDS aqueous solution) were determined with a dynamic light scattering (DLS) device (NICOMP 380, Santa Barbara) at a fixed angle of 90° and a laser diode running at 635 nm.

Energy-dispersive X-ray spectroscopy (EDX) measurement was carried on a scanning electron microscope (Hitachi SU8000) combined with a Bruker Axs XFlash 5010 under 5 kV. ^{1}H NMR spectra were measured at room temperature on a console Avance 300. The partition coefficient of the monomers aniline and pyrrole in the dispersed and continuous phases was estimated by mixing the two phases (same quantities as for the miniemulsions) but without surfactant and initiator. After stirring, the two phases were separated, isolated, and aliquots were taken to be dissolved in DMSO-d_6.

The partition coefficient f_M of the monomer was then calculated with the following equation:

$$f_M = \frac{c_{M(d\varphi)}}{c_{M(c\varphi)}}$$

with $c_{M(d\varphi)}$ and $c_{M(c\varphi)}$ being the concentrations of monomer in the dispersed and continuous phase, respectively. The apparent molecular weight of PANI were measured by gel permeation chromatography (GPC) using *N*-methyl-2-pyrrolidone (NMP)/LiBr as eluent.

Calorimetric measurements of aniline polymerization were performed in a μRC microreaction calorimeter (C3 Prozess- and Analysentechnik GmbH, Germany). After the preparation of aniline miniemulsions as described previously, 1 mL of the miniemulsions and a stir bar were added into a small vial without adding the initiator; 200 μL of molten octadecane was added above the miniemulsion heated at 40 °C and left to solidify at room temperature to form a thin film. After that, a drop of an APS aqueous solution (equimolar amount compared to the monomers) was added on the octadecane solid film. Then the vial was placed inside the sample cell of the calorimeter. The sample was left to equilibrate and the measurement was started by using a needle to break the film between the miniemulsion and the initiator solution. The heat flux generated during the polymerization of aniline was measured in function of the reaction time. Calorimetric measurements of the aniline polymerization in DMSO were conducted with the same method. Water was also used to replace APS aqueous solution to perform a control experiment.

CV measurements were carried out with a multipotentiostat VMP2 (Princeton Applied Research) with a custom-made cell. PANI capsules dispersed in water (10 mg mL^{-1}) were drop-casted on an ITO slide. The sample was dried overnight at room temperature and directly used for CV measurements. CV was measured under nitrogen in aqueous HCl (1 M) as electrolyte. Ag/AgCl reference electrode and Pt counter electrode were chosen and measurements were carried out with a scan rate of 50 mV s^{-1} in a range of −0.4 to 1.2 V. The PPy capsules dispersed in water (10 mg mL^{-1}) were deposited on a glassy carbon electrode. The electrode was dried overnight at room temperature and directly used for CV measurements. CV was measured under nitrogen atmosphere in 0.1 M aqueous phosphate buffered saline as electrolyte. Ag/AgCl reference electrode and Pt counter electrode were chosen with and measurements were carried out with a scan rate of 100 mV s^{-1} in a range of −0.2 to 1.0 V. All potentials refer to Ag/AgCl reference electrodes.

The pyrolysis process of POPN nanoparticles was performed in a furnace for 3 h at 800 °C or 600 °C in N_2. Thermal gravimetric analysis (TGA) was carried out on TGA 851 thermogravimetric analyzer at a heating rate of 5 °C min^{-1} in N_2. Electrochemical

measurements were carried out by a CHI760D electrochemical work station. CV measurements of POPN nanoparticles were performed in a three-electrode system. The working electrodes were prepared by mixing 80 wt.% of POPN nanoparticles (4 mg), 10 wt.% of acetylene black, and 10 wt.% of polytetrafluoroethylene (PTFE) binder dispersed in ethanol solvent, and then pressed on a platinum mesh network serving as a current collector. A platinum plate was used as counter electrode and a saturated calomel electrode (SCE) was used as reference electrode. 1 M H_2SO_4 was used as aqueous electrolyte.

5.2 Experimental details for section 4.2

5.2.1 Materials

Aniline was purchased from Sigma Aldrich and distilled under vacuum before use. Ethylbenzene (EB, 99.8%, ACROS Organics) and ammonium persulfate (APS, 98%, ACROS Organics) sodium dodecyl sulfate (SDS, 99%, Sigma Aldrich), 3-nitrosalicylic acid (3-NisA, ≥ 99.0%, Sigma Aldrich), 2-mercaptobenzothiazole (MBT, 97%, Sigma Aldrich) and tris(2-carboxyethyl)phosphine hydrochloride (TCEP·HCl, ≥98%, Sigma Aldrich), hydrogen tetrachloroaurate (III) trihydrate ($HAuCl_4 \cdot 3\ H_2O$, >99%, Alfa Aesar) and trisodium citrate (Alfa Aesar) were used as received. Poly(vinyl alcohol) (PVA, Alfa Aesar, 98-99% hydrolyzed) with a molecular weight M_w of 27,450 $g \cdot mol^{-1}$ (measured by gel permeation chromatography, calibration with poly(ethylene oxide) standards, 80% 0.1 M $NaNO_3$ in water/20% MeOH as eluent) was used as received. Distilled water was used through all the experiments if not specifically mentioned.

5.2.2 Synthesis of dual-responsive polyaniline capsules

5.2.2.1 Synthesis of PANI/3-NisA capsules

The preparation and purification process of PANI/3-NisA capsules were performed as follows: 0.27 mmol of 3-NisA, 5.38 mmol of aniline, and 10.04 mmol of ethylbenzene were first mixed and then added to 6 mL of an aqueous solution of SDS (62.5 mg). After pre-emulsification for 1 h under 1000 rpm at room temperature, the mixture was ultrasonicated for 4 min at 90% amplitude (Branson sonifier W450) with ice cooling. After emulsification, an aqueous solution of PVA (10 wt.%) was added into the miniemulsion followed by dropwise addition of an aqueous solution of APS (5.38 mmol in 1.67 mL water). After reaction under

room temperature for 12 h, the PANI/3-NisA capsules dispersion was purified by washing with water for several times until the supernatant was free of nanocapsules. Then all the capsules were collected by centrifugation under 8000 rpm for 5 min. PANI capsules without encapsulated 3-NisA were prepared similarly except that no 3-NisA was added into dispersed phase before the miniemulsion process. They were used as control sample. To determine the total amount of 3-NisA encapsulated into PANI capsules, UV-Vis spectra of 3-NisA released at pH 12.4 which is well above the pK_a of salicylic acid (~ 3.0) was recorded. It showed that after ~ 5 h the release of 3-NisA reached an equilibrium so the total amount of 3-NisA in PANI capsules could be estimated with the calibration curve of 3-NisA at pH 12.4 (**Figure 5.1**). After calculation, ~ 0.25 mg of 3-NisA was found to be encapsulated in the PANI capsules (~ 4.8 mg) which were measured for release. Therefore the weight ratio of 3-NisA to PANI capsules was estimated to be ~ 5%.

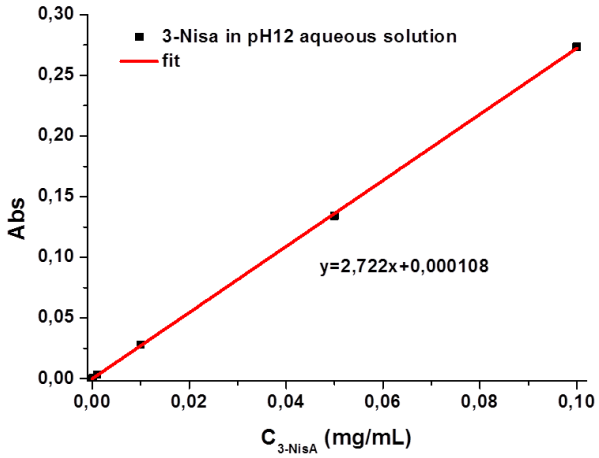

Figure 5.1 *Calibration curve for the 3-NisA in an aqueous solution of pH = 12.4.*

5.2.2.2 Synthesis of Au@PANI/3-NisA capsules

The synthesis of AuNPs with a diameter ~ 20 nm was carried out following a procedure reported previously.[2] 40 mg of $HAuCl_4 \cdot 3H_2O$ was first dissolved in 100 mL Milli-Q water and heated to boiling. Then, 0.11 g trisodium citrate dissolved in 10 mL of Milli-Q water was added rapidly to the afore-mentioned boiling solution. Boiling was continued until the color of solution turned ruby, indicating the formation of gold nanoparticles. Direct adsorption of AuNPs was carried out by slowly adding 0.4 mL of the prepared AuNPs (0.18 $mg \cdot mL^{-1}$) to 1 mL of a PANI aqueous dispersion (1 $mg \cdot mL^{-1}$). The weight ratio PANI capsule to AuNPs was 13:1. The mixture was stirred at 600 rpm at room temperature for 12 h.

5.2.2.3 Synthesis of MBT-s-Au@PANI/3-NisA capsules

To prepare MBT-AuNPs@PANI/3-NisA capsules, an aqueous solution of MBT (0.1 mg·mL^{-1}) was added dropwise in the dispersion of PANI/3-NisA capsules decorated with AuNPs. The feed ratio of MBT to PANI was set as 1:3.4 in weight. After stirring for 12 h, the dispersion was purified by centrifugation under 8000 rpm several times to remove free MBT until no signal of MBT could be detected by UV-Vis spectroscopy in the supernatant. Then, the collected capsules were redispersed in distilled water to get a capsule dispersion with a solid content of 0.48 wt.%. By using the calibration curve (**Figure 5.2**) of MBT dissolved in water, the amount of MBT incorporated on the capsules could also be estimated. The amount of bonded MBT was calculated to be 0.2 mg per 2.9 mg of measured PANI capsules, *i.e.* the weight ratio of MBT to PANI capsules was ~ 6.9 %.

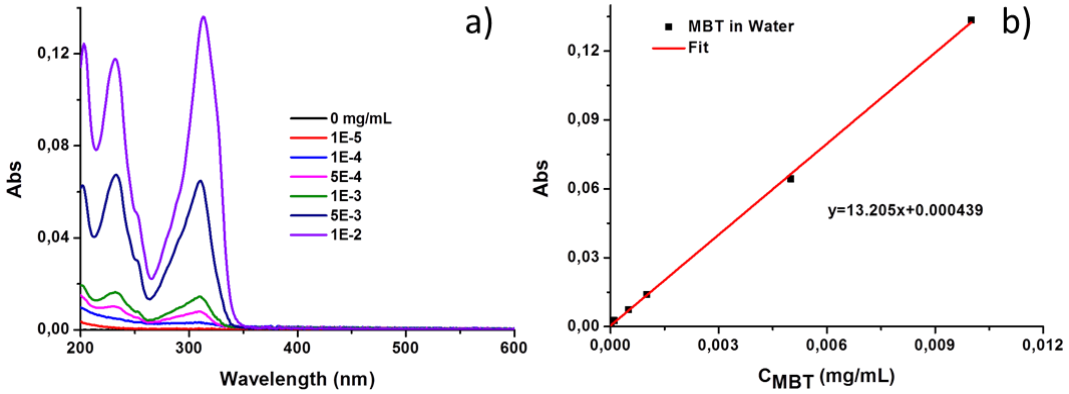

Figure 5.2 *a: UV-Vis spectra of MBT dissolved in water with different concentration; b: Calibration curve of MBT in water.*

5.2.3 pH responsive release of 3-NisA from MBT-Au@PANI/3-NisA capsules

The investigations on the release of 3-NisA from MBT-AuNPs@PANI/3-NisA capsules under different pH were carried out by dialysis. Three dispersions of capsules (1 g with a solid content of 0.48 wt.%) were placed inside a dialysis bag (MWCO 14000) and then immersed into 10 mL of an aqueous medium with pH values of 2.4, 8.6, or 12.4. After a given time, 0.5 mL of the solution outside the dialysis bag was taken out followed by the addition of an equal amount of fresh solution to keep the amount constant. The amount of released 3-NisA was determined by UV-Vis spectroscopy. A calibration curve was also drawn by measuring a series of 3-NisA solutions with known concentrations. As a control, the release behavior of 3-NisA from PANI/3-NisA capsules was also investigated following the same procedure. In the

case of pH 8.6, the pH value of the medium decreased to 6.4 during the release process. We used the beginning pH value of the medium to describe and discuss the release behavior.

5.2.4 Redox responsive release of MBT from MBT-Au@PANI/3-NisA capsules

The MBT-Au@ PANI/3-NisA capsule dispersions were first centrifuged several times until no MBT could be detected in the supernatant by UV-spectroscopy. To study the redox responsive release of MBT from the capsules, three dispersions of MBT-AuNPs@PANI/3-NisA capsules (0.6 g with a solid content of 0.48 wt.%) were placed inside a dialysis bag (MWCO 14000) and then immersed into 6 mL of an aqueous medium with 0, 0.25 or 2.5 $mg \cdot mL^{-1}$ TCEP·HCl, respectively. After a given time, 0.3 mL of the solution outside the dialysis bag was taken out followed by the addition of an equal amount of fresh solution to keep the amount constant. The solutions and capsules dispersions were degassed by Argon for 10 min before use. The amount of released MBT was determined by monitoring the peak $\lambda_{max} \sim 311$ nm by UV-Vis spectroscopy. A calibration curve was drawn by measuring a series of MBT solutions with known concentrations.

5.2.5 Release of 3-NisA and MBT under combined stimuli

To study the release of 3-NisA and MBT under combined stimuli (pH change and reduction), certain amounts of TCEP·HCl were dissolved in an aqueous solution of pH ~ 12.4 to obtain a solution with concentrations of TCEP·HCl of 0.25 mg mL^{-1} and 2.5 mg mL^{-1} that were named pH-R1 and pH-R2, respectively. The pH value of the two solutions after addition of TCEP·HCl did not change much. pH-R1 decreased to 12.3 and pH-R2 to 12.2. Afterwards, two dispersions of MBT-Au@PANI/3-NisA capsules (0.6 g with a solid content of 0.48%) were placed separately inside a dialysis bag (MWCO 14000) and then immersed into 6 mL of the above prepared solution pH-R1 and pH-R2, respectively. After different time intervals, 0.3 mL of the solution outside the dialysis bag was taken out followed by the addition of an equal amount of fresh solution. The amount of released 3-NisA and MBT were then determined by UV-Vis spectroscopy.

5.2.6 Electrochemically redox responsive capsules for corrosion protection

5.2.6.1 Synthesis of polyaniline capsules loaded with different corrosion inhibitors

The encapsulation process of corrosion inhibitor was carried out during the formation of PANI capsules. Corrosion inhibitor 3-NisA, MBT, BTA-COOH or DT (10 wt.% compared to monomer) was dissolved in the dispersed phase prior to the emulsification. The samples were defined as PANI/3-NisA, PANI/MBT, PANI/BTA-COOH or PANI/DT, respectively.

5.2.6.2 Incorporation of Au@PANI/3-NisA capsules to coatings on Zinc

Au@PANI/3-NisA capsules dispersions with a concentration of 57 μg μL^{-1} were directly drop-casted on zinc giving an average amount of 2.5 mg cm^{-2} with a thickness of 8 µm ± 2 µm and dried at 80 °C for 10 min. Then 10 wt.% of PVB solution in ethanol was used as binder and spin-coated on PANI capsules coating for three times at 3000 rpm and dried at 80 °C for 1 h.

5.2.6.3 Electrochemically redox responsive self-healing behavior

To investigate the self-healing performance and the corrosion driven cathodic delamination progress, a scratch was applied to the coating system with a scalpel. The defect was covered with 5 μL of 1 M KCl and subsequently introduced to the SKP chamber with a relative humidity of 92%. A commercial SKP system from KM Soft Control was used with a 100 µm NiCr tip. Calibration of the SKP tip was done on Cu/$CuSO_4$ (saturated) and all potentials are referred to standard hydrogen electrode (SHE). For monitoring the evolution of the corrosion potential in the defect the SKP tip was directly placed on the electrolyte drop. The delamination was measured according to the experimental procedures previously reported.[3]

5.2.7 Characterization methods

The morphology of the capsules was examined with a Gemini 1530 (Carl Zeiss AG, Oberkochem, Germany) scanning electron microscope (SEM) operating at 0.35 kV and a transmission electron microscope (TEM) (Jeol 1400) operating at an accelerating voltage of 120 kV. To prepare the SEM samples, the purified capsules dispersion was dropped on a silicon wafer and dried at room temperature. All the TEM samples were prepared by dropping the capsules dispersions on a copper grid (300 square mesh) coated with a carbon layer. The UV-Vis absorption spectra were recorded with a Perkin Elmer Lambda 25 UV/VIS

spectrometer. Cross-sections of the coating with PANI capsules were prepared by using Hitachi Ion Milling System E-3500.

5.3 Experimental details for section 4.3

5.3.1 Materials

2-Mercaptoethanol (Sigma Aldrich, ≥ 99%), triethylamine (Et_3N, ACROS, 99%), methacryloyl chloride (Sigma Aldrich, ≥97%), 1-vinyl-2-pyrrolidone (VP, Sigma Aldrich, ≥99%), 2,2'-azobisisobutyronitrile (AIBN, Sigma Aldrich, 98%), 1,4-dioxane (Sigma Aldrich, 99.5%), tris(2-carboxyethyl) phosphine hydrochloride (TCEP·HCl, Sigma Aldrich, ≥98%), Nile Red (Sigma Aldrich, ≥98%), tetrahydrofuran (THF, Sigma Aldrich, ≥99.9%), pyrene (Sigma Aldrich, >99%), and dithiothreitol (DTT, Alfa Aesar, 99%) were used without further purification. Distilled water was used throughout the work.

5.3.2 Synthesis of monomer containing unit of corrosion inhibitor

The synthesis and purification procedure of 2-benzothiazolyl-2'-methacryloyloxyethyl disulfide (MBTMA) was carried out following a previously reported method.[4,5] The ^1H NMR spectrum of the monomer ($CDCl_3$, δ, ppm) displayed the characteristic peaks of MBTMA: 1.95 (3H, CH_3-C=), 3.26 (2H, CH_2-S), 4.50 (2H, CH_2-O), 5.62 (1H, CH=), 6.15 (1H, CH=), 7.35 (1H, ArH), 7.45 (1H, ArH), 7.83 (1H, ArH) and 7.90 (1H, ArH).

5.3.3 Synthesis of amphiphilic copolymers via radical copolymerization

The amphiphilic copolymers (P1-P4) were synthesized by free radical copolymerization. In a typical procedure, 1 g of 1-vinyl-2-pyrrolidone, 54 mg of MBTMA, and 19 mg of AIBN were dissolved in 4 ml of 1,4-dioxane and placed in a round-bottom flask with a stirring bar. After degassing with Argon for 10 min, the bottle was sealed and the mixture was stirred at 72 °C for 24 h. After the reaction, the solvent in the flask was first evaporated to get a concentrated solution and then the product was purified and collected by precipitation in petroleum ether for three times. The obtained white powders were then dried in vacuum oven at 40 °C for 2 days. The product was named P1. The other copolymers were synthesized with the same procedure but with different feed ratios of monomers (P2, P3, and P4). The feed ratios, yields, and molecular weights can be found in **Table 6, Chapter 4.**

5.3.4 Self-assembly behavior of amphiphilic copolymers

10 mg of the copolymer P1, P2, P3 or P4 were separately dissolved in 10 mL of distilled water and placed in an ultrasonic water bath for 15 min. To determine the critical aggregation concentration (CAC), each assembly was prepared with a series of different concentrations. Then, 20 μL of stocked solution pyrene/chloroform with concentration of 0.1 mM were put in different vials followed with evaporation of chloroform. Then 2 mL of the dispersions with distinct concentration was added into the vials with pyrene. After 30 min of sonication, the solutions were kept still for another 3 h. The emission spectrum of pyrene was then detected by fluorescence spectroscopy. The excitation wavelength was set as 337 nm and the emission spectra were collected from 350 to 450 nm.

5.3.5 Encapsulation and redox-triggered release of Nile Red from assemblies

To encapsulate Nile Red into the copolymer nanoparticles, certain amount of Nile Red was first dissolved in THF to get a solution with a concentration of 10 mg mL^{-1}. Then 50 μL of the solution was taken and placed into a 10 mL vial. After removal of THF by evaporation, 5 mg of copolymer dissolved in 5 mL of distilled water was added. The vial with the above mixture was then placed in an ultrasonic water bath for 30 min. As a control, 5 mL of distilled water without copolymer was placed into a vial with Nile Red. All the obtained samples were filtrated by a hydrophilic PTFE filter with pore size of 0.45 μm to remove the aggregates of non-encapsulated or non-dissolved NR. The nanoparticles with NR were assigned as NP-NR. The control sample was named NR. To detect the release of Nile Red, fluorescence emission spectra of NP-NR samples reduced by TCEP·HCl with varied concentration were detected after different time intervals. The excitation wavelength was set as 550 nm. Emission spectra of Nile Red were examined from 580 nm to 750 nm.

5.3.6 Redox-triggered release of corrosion inhibitor from assemblies

The release of MBT molecules from the copolymer was conducted as follows: Certain amounts of polymers P1-P4 were separately dissolved in THF to get a solution with a concentration of 1 mg mL^{-1}. After degassing with Argon for 5 min, a certain amount of DTT was added to the solutions. The theoretical molar ratio of DTT to MBTMA unit was set to be 50/1. After 10 min, the characteristic peak of MBT in the solution was detected by UV-Vis spectroscopy.

The release of MBT molecules from polymer nanoparticles was determined by dialyzing the dispersions against an aqueous medium containing the reducing agent. In a typical procedure, 10 mL of the dispersion with a concentration of 1 mg mL^{-1} was first placed inside a dialysis bag (molecular weight cut-off of 14000 g mol^{-1}) and then immersed in 20 mL of water in which certain amount of TCEP·HCl was dissolved. The molar ratio of the reducing agent to MBTMA unit in the polymer was set as 5/1. For the control sample, an aqueous medium without reducing agent was used. The medium outside the dialysis bag was replaced by fresh medium once a day. After 3 days of dialysis, all the dispersions were dialyzed against distilled water to remove the reducing agent. The distilled water used throughout the procedure was degassed by Argon for 10 min before use. The dispersions in the dialysis bag were then collected and the water was evaporated under reduced pressure. The left solid was dissolved in $CDCl_3$ and analyzed by ^1H NMR spectroscopy. The released MBT was calculated by comparing the molar ratio of MBTMA unit to VP unit in the copolymer poly(VP-*co*-MBTMA) before and after reduction.

5.3.7 Characterization methods

The molecular weight (M_w) of the polymer samples were measured by gel permeation chromatography (GPC) (Agilent Technologies 1260 infinity) using dimethylformamide (DMF) as eluent. UV-Vis measurements were conducted with a Perkin-Elmer Lambda 25 UV-Vis spectrometer. The fluorescence emission spectra were examined with a Tecan Plater Reader Inifinte M1000. The morphology of the polymer nanoparticles was examined with a Gemini 1530 (Carl Zeiss AG, Oberkochem, Germany) scanning electron microscope (SEM) operating at 0.2 kV and a transmission electron microscope (TEM, Jeol 1400) operating at an accelerating voltage of 120 kV. The hydrodynamic diameters D_h of the nanoparticles in water were determined with a Nicomp™ 380 Submicron Particle Sizer (PSS-Nicomp) at an angle of 90°. ^1H NMR spectroscopy measurements were carried out on a Bruker AVANCE 300 MHz console at room temperature.

5.4 Experimental details for section 4.4

5.4.1 Materials

Polyvinylpyrrolidone (PVP, M_w ~ 1300000 g mol^{-1}), titanium isopropoxide (Ti(O*i*Pr)$_4$, 97%), acetic acid (≥99.7%), paraffin oil (110-230 mPa·s), lecithin (≥50%), octane (≥99%), dicyclopentadiene (DCPD, 97%), hexadecane (HD, 99%), glutaraldehyde (GA, 50wt.% in H_2O), hydrochloric acid (HCl, 36.5-38.0%), sodium dodecyl sulfate (SDS, 99%), poly(dimethylsiloxane) diglycidyl ether terminated (PDMS-DE, M_n ~ 800 g mol^{-1}, ~ 15 mPa·s), diphenyl disulfide (DPS, 99%) and Irgasan (≥97.0%) were purchased from Sigma Aldrich and used as received.

Polydimethylsiloxane carboxydecyldimethyl terminated (PDMS-DC, M_w ~ 1000 g mol^{-1}, ~ 15-50 mPa·s, ABCR), ammonium persulfate (APS, 98%, Acros Organics), pyrrole (Py, 99%, Acros Organics), tetraethoxysilane (TEOS, 98%, Alfa Aesar), cetyltrimethylammonium chloride (CTMA-Cl, 99%, Acros Organics), poly(vinyl alcohol) (PVA, M_w ~ 125 000 g mol^{-1}, 88 mol% hydrolyzed, Polysciences Inc.) and xylene (99%, Acros Organics,) were used without further purification. Poly(vinyl ferrocene) (PVFc, *M*w ~ 12,800 g mol^{-1}) was kindly donated by M. Gallei, Technical University of Darmstadt.

5.4.2 Preparation of TiO_2 fibers loaded with self-healing agents

The PVP/TiO_2 core-shell fibers with different core material were prepared as follows: To prepare shell material for the electrospining, 0.3 g of PVP, 2 mL of acetic acid and 5 mL of ethanol were first mixed and stirred at room temperature until PVP was completely dissolved. Then 3 mL of Ti(O*i*Pr)$_4$ was added to the PVP solution at 0 °C. The core material could be paraffin oil or mixture of paraffin oil with self-healing agent in different weight ratios as indicated in **Table 7, Chapter 4**.

The electrospinning process was performed by a commercial platform (ES1a, Electrospinz) equipped with a counter electrode covered with aluminum foil which was used as collector for fibers. The shell material and core material were added in to two syringes separately connected to the outer and inner part of the metallic coaxial needle. These two liquid were fed at a constant flow rate by using two syringe pumps (Bioblock, Kd Scientific). The flow rate, applied voltage and working distance (tip-to-collector distance) were varied during the

electrospinning process as shown in **Table 7, Chapter 4**. All the experiments were conducted at room temperature and the collected fibers were then left in air for another 1 h to allow $Ti(OiPr)_4$ a complete hydrolysis.

5.4.3 Decoration of fibers with conducting polymers via surface polymerization

To decorate the surface of as-prepared TiO_2 fibers with conducting polymers, one piece of TiO_2 fiber mat was first immersed in an aqueous solution containing oxidant APS for 3 h. Then the mat was taken out and placed in an aqueous solution of pyrrole for another 12 h.

5.4.4 Construction of multifunctional fibers based on colloid-electrospinning

To prepare multifunctional fibers, PVFc nanoparticles loaded with DPS (PVFc/DPS) and SiO_2 nanocapsules loaded with Irgasan (SiO_2/Irgasan) were first synthesized.

Preparation of PVFc/DPS nanoparticles: a mixture of PVFc (250 mg), HD (250 mg), DPS (10 mg) and chloroform (5 mL) was added to 10 mL of water containing 20 mg of SDS. After stirring under 1000 rpm for 1 h at room temperature, the emulsification was carried out by ultrasonicating the mixture for 120 s at 70% amplitude (Branson sonifier W450) in a pulse regime (30 s sonication, 10 s pause) under ice cooling. After emulsification, the miniemulsion was then kept stirring in an oil bath at 40 °C for 12 h to evaporate the chloroform.

Preparation of SiO_2/Irgasan nanocapsules: A solution of TEOS (1 g), HD (125 mg), Irgasan (30 mg) and xylene (0.5 g) was mixed and stirred with 30 mL of a 0.77 mg mL^{-1} aqueous solution of CTMA-Cl for 5 min. The emulsification was then carried out by ultrasonicating the mixture for 180 s at 70% amplitude (Branson sonifier W450) under ice cooling. After emulsification, the miniemulsion was kept stirring at room temperature for another 12 h to obtain the silica nanocapsules.

Preparation of multifunctional fibers loaded with PVFc/DPS nanoparticles and SiO_2/Irgasan nanocapsules: Certain amounts of PVA aqueous solution (15 wt.%), dispersions of as-prepared PVFc/DPS nanoparticles, and SiO_2/Irgasan nanocapsules were mixed and stirred for 3 min with a vortex. The final concentration of PVA in the mixture was 9.3 wt.% and the weight ratio of PVA/PVFc/SiO_2 was set as 10/1/1.3.

Then the mixture was electrospun by using a commercial platform (ES1a, Electrospinz) equipped with a counter electrode covered with aluminum foil. A syringe pump (Bioblock, Kd Scientific) was used to feed the mixture at a constant flow rate of 1 ml h^{-1} with the applied voltage of 15 kV and tip-to-collector distance of 10.5 cm. All the experiments were conducted at room temperature.

To crosslink the fibers, the PVA fiber mat was peeled off from the aluminum foil and placed in a sealed desiccator filled with glutaraldehyde/hydrochloric acid (GA/HCl) vapor for 1d.

5.4.5 Characterization methods

The morphology of the fibers, nanoparticles and nanocapsules were examined with a Gemini 1530 (Carl Zeiss AG, Oberkochem, Germany) scanning electron microscope (SEM) operating at 0.2 kV. Nanoparticle and nanocapsule samples for SEM measurements were prepared by dropping diluted dispersion on silica wafers and dried at room temperature. Fiber samples for SEM measurements were prepared by electrospinning fibers directly on silicon wafers or aluminum foil. To observe the cross-section morphology, the aluminum foil with TiO_2 fibers on the surface was cut with scissor. Morphologies of the fibers, nanoparticles and nanocapsules were also detected by a transmission electron microscope (TEM) (Jeol 1400) operating at an accelerating voltage of 120 kV. The nanoparticle and nanocapsule samples for TEM measurement were prepared by depositing their diluted dispersion on 300 mesh carbon-coated copper grids. The fiber samples for TEM measurement were prepared by directly electrospinning fibers on copper grid.

Hydrodynamic diameters (D_h) of PVFc nanoparticles and SiO_2 nanocapsules were determined with a dynamic light scattering (DLS) device (NICOMP 380, Santa Barbara) at a fixed angle of 90° and a laser diode running at 635 nm.

To detect the release of Irgasan from SiO_2/Irgasan nanocapsules at different pH, 0.6 mL of nanocapsule dispersion was placed in a dialysis bag (molecular weight cut-off of 14000 g mol^{-1}) and then immersed in 6 mL of water with different pH value. After different time intervals, 0.3 mL of the medium outside the dialysis bag was taken and replaced by equvilant amount of fresh medium. The solution taken out was then determined with a Perkin-Elmer Lambda 25 UV−vis spectrometer.

5.5 References

[1] Biemans, H. A. M.; Zhang, C.; Smith, P.; Kooijman, H.; Smeets, W. J. J.; Spek, A. L.; Meijer, E. W. *J. Org. Chem.* **1996**, *61*, 9012-9015.

[2] Gole, A.; Murphy, C. *J. Chem. Mater.* **2004**, *16*, 3633-3640.

[3] Frankel, G. S.; Stratmann, M.; Rohwerder, M.; Michalik, A.; Maier, B.; Dora, J.; Wicinski, M. *Corros. Sci.* **2007**, *49*, 2021-2036.

[4] Brzezinskal, E.; Ternay Jr., A. L. *J. Org. Chem.* **1994**, *59*, 8239-8244.

[5] Tsarevsky, N. V.; Huang, J.; Matyjaszewski, K. *J. Polym. Sci.: Part A: Polym. Chem.* **2009**, *47*, 6839-6851.

6. Conclusion

The main focus of this thesis is to develop new strategy for self-healing in corrosion protection based on stimuli-responsive capsules. Conducting polymers such as polyaniline were chosen for building the shell of capsules due to their important characteristics of being both pH- and redox responsive.

Firstly, polyaniline capsules were synthesized by oxidative polymerization using miniemulsion droplets as soft templates. The chemical structure and morphology of the PANI capsules was controlled by varying their oxidation states as shown by a combination of FT-IR and UV-vis spectroscopy, electron microscopy, and cyclic voltammetry measurements. Hydrophobic liquid self-healing agents were successfully encapsulated in the PANI capsules and their redox-responsive releases were monitored by ^{1}H NMR spectroscopy. The release could be stimulated upon reduction and delayed upon oxidation of the PANI shell. This is the first time that a release of hydrophobic chemicals was triggered by a redox stimulus from capsules formed with conducting polymers.

Secondly, polyaniline capsules with dual responsive properties were synthesized by miniemulsion polymerization followed by a post-modification of the PANI shell with gold nanoparticles. Two different corrosion inhibitors were successfully loaded in the hybrid nanocontainers. Unlike previous common systems where both payloads are released together, the two payloads could be released selectively and independently by activating the nanocontainers either by pH change or chemical reduction.

Thirdly, a series of amphiphilic copolymers bearing different amounts of functional and cleavable units, *i.e.* a corrosion inhibitor, as side groups were prepared. Polymer nanoparticles were obtained by self-assembly of the copolymers in water. The formed nanoparticles were able to efficiently encapsulate hydrophobic payloads in their core and their release was triggered by reductive cleavage of the copolymer. Unlike other disulfide-based delivery systems in which useless hydrophobic aggregates or non-functional byproducts are usually produced, this system had the priority to co-release a corrosion inhibitor.

Finally, conducting fibers with TiO_2 as shell and self-healing chemicals as core were prepared by the electrospinning process. After adjustment of the processing parameters, various self-

healing chemicals (PDMS-DC, PDMS-DC, and DCPD) could be encapsulated. In addition, the possibility to design multifunctional fibers loaded with stimuli-responsive nanoparticles and nanocapsules was also demonstrated by combining the electrospinning with the miniemulsion techniques. The fiber composites were then expected to exhibit dual-responsive property to release their payloads upon specific stimuli. Compared to the normal electrospinning process, the colloid-electrospinning method combines electrospinning with multifunctional colloid systems and provides possibility to develop smart fiber composites with multiple functionalities hence leads to more potential application.

Abbreviations and Characters

Abbreviations

1D, 2D, 3D	one-, two, three-dimensional
^{1}H NMR	proton nuclear magnetic resonance
3-NisA	3-nitrosalicylic acid
AEMA	2-aminoethyl methacrylate hydrochloride
AFM	atomic force microscopy
AIBN	2,2'-azobisisobutyronitrile
ANI	aniline
APS	ammonium persulfate
Au-S	gold-thiol
BA	butyl methacrylate
BTA-COOH	benzotriazolecarboxylic acid
CAC	critical aggregation concentration
CH_2Cl_2	dichloromethane
$CHCl_3$	chloroform
CIs	corrosion inhibitors
CTAB	cetyltrimethylammonium bromide
CTMA-Cl	cetyltrimethylammonium chloride
CV	cyclic voltammogram
D_2O	deuterium oxide
DA	Diels-Alder
DCC	dicyclohexylcarbodiimide
DCPD	dicyclopentadiene
DLS	dynamic light scattering
DLVO	Derjaguin and Landau, Verwey and Overbeek
DMA	dodeyl methacrylate
DMAP	4-dimethylaminopyridine
DMSO	dimethyl sulfoxide
DPS	diphenyl disulfide
DT	2,5-dimercapto-1,3,4-thiadiazole

DTT	dithiothreitol
DVB	divinylbenzene
DVP	dimethyl vinylphosphonate
EB	ethylbenzene
EDX	energy-dispersive X-ray spectroscopy
Et_3N	triethylamine
$FeCl_3$	iron(III) chloride
FR-IR	fourier transform infrared spectroscopy
GA	glutaraldehyde
e.g.	*exempli gratia;* for example
gold nanoparticles	AuNPs
GPC	gel permeation chromatography
H_2O_2	hydrogen peroxide
$HAuCl_4 \cdot 3\ H_2O$	hydrogen tetrachloroaurate (III) trihydrate
HCl	hydrochloric acid
HD	hexadecane
HOMO	highest occupied molecular orbital
HOPDMS	hydroxyl end-functionalized polydimethylsiloxane
ICPs	intrinsically conducting polymers
i.e.	*id est;* that is
KCl	potassium chloride
KPS	potassium persulfate
LUMO	lowest unoccupied molecular orbital
MAA	methacrylic acid
MBT	2-mercaptobenzothiazole
MBTMA	2-benzothiazolyl-2'-methacryloyloxyethyl disulfide
MMA	methyl methacrylate
MTM	3-methylthienyl methacrylate
N_2H_4	hydrazine
NCs	nanocapsules
NMP	N-methylpyrrolidinone

NPs	nanoparticles
NR	Nile Red
o/w	oil-in-water
OPN	octapyrrolylnaphthalene
PA	polyacetylene
PANI	polyaniline
PCL	poly(*ε*-caprolactone)
PDES	polydiethoxysiloxane
PDMS	polydimethylsiloxane
PDMS-DC	dicarboxylic acid-terminated polydimethylsiloxane
PDMS-DE	diepoxide-terminated polydimethylsiloxane
PEGMA	poly(ethyleneglycol methacrylate) monomethyl ether
PEO	poly(ethylene oxide)
PMMA	poly(methyl methacrylate)
PMT	photomultiplier detector
Poly(MMA-*co*-MTM-*g*-PPy)	poly(methyl methacrylate-*co*-3-methylthienyl methacrylate-*graft*-polypyrrole)
Poly(MMA-*co*-MTM-*g*-PTP)	poly(methyl methacrylate-*co*-3-methylthienyl methacrylate-*graft*-polythiophene)
poly(MMA-*co*-MTM)	poly(methyl methacrylate-*co*-3-methylthienyl methacrylate)
poly(VP-*co*-MBTMA)	poly(vinylpyrrolidone-*co*-2-benzothiazolyl-2'-methacryloyloxyethyl disulfide)
POPN	polyoctapyrrolylnaphthalene
PPy	polypyrrole
PT	polythiophene
PTFE	polytetrafluoroethylene
PVA	polyvinylalcohol
PVF	polyvinylformal
PVFc	polyvinylferrocene
PVP	polyvinylpyrrolidone
Py	pyrrole

rDA	retro-Diels-Alder
ROMP	ring-opening metathesis polymerization
R.T.	room temperature
St	styrene
SDS	sodium dodecyl sulfate
SEM	scanning electron microscope
SH	self-healing
SHE	standard hydrogen electrode
SKP	scanning kelvin probe
TCEP·HCl	tris(2-carboxyethyl) phosphine hydrochloride
TEM	transmission electron microscope
TGA	thermogravimetric analysis
THF	tetrahydrofuran
TiO_2	titanium (IV) oxide
$Ti(O\mathit{i}Pr)_4$	titanium isopropoxide
TM	3-thiophenemethanol
UV	ultraviolet
UV-vis	ultraviolet-visible
VBS	sodium 4-vinylbenzenesulfonate
w/o	water-in-oil

Characters and symbols

Greek

δ	thickness
ε	dielectric constant
η	shear viscosity
λ_D	Debye length
λ	wavelength
σ	interfacial tension
χ	Flory-Huggins parameter

ψ_0	stern potential

Latin

A	interfacial area
D	distance
D_h	hydrodynamic diameter
f	partition coefficient
ΔG	total free energy change
k_B	Boltzmann constant
M_n	number averaged molecular weight
M_w	weight averaged molecular weight
P_L	*Laplace* pressure
R	radius
S	spreading coefficient
T_g	glass transition temperature
x	degree of oxidation

Appendix

List of publications during PhD study

(1) **L. P. Lv**, Y. Zhao, N. Vilbrandt, M. Gallei, A. Vimalanandan, M. Rohwerder, K. Landfester, D. Crespy

Redox Responsive Release of Hydrophobic Self-Healing Agents from Polyaniline Capsules

J. Am. Chem. Soc. **2013,** *135*, 14198-14205

(2) **L. P. Lv**, K. Landfester, D. Crespy

Stimuli-Selective Delivery of two Payloads from Dual Responsive Nanocontainers

Chem. Mater. **2014**, 26, 3351-3353

(3) **L. P. Lv**, Y. Zhao, H.-X. Zhou, K. Landfester, D. Crespy

From Core-Shell and Janus Structures to Tricompartment Nanoparticles

Polymer **2014**, *55*, 715-720

(4) **L. P. Lv**, Y. Zhao, K. Landfester, D. Crespy

Chemical Encoding of Amphiphilic Copolymers for a Dual Controlled Release from their Assemblies

2014*, Submitted*

(5) A. Vimalanandan, **L. P. Lv**, T. H. Tran, K. Landfester, D. Crespy, M. Rohwerder

Redox-Responsive Self-Healing for Corrosion Protection

Adv. Mater. **2013**, *25*, 6980-6984

(6) Y. Zhao, D. Döhler, **L.-P. Lv**, W. H. Binder, K. Landfester, D. Crespy

Facile Phase-Separation Approach to Encapsulate Functionalized Polymers in Core–Shell Nanoparticles

Macromol. Chem. Phys. **2014**, *215*, 198-204

(7) **L. P. Lv**, K. Landfester, D. Crespy

Porous Nanoparticles for Supercapacitor. *In preparation*

List of publications before PhD study

(8) **L. P. Lv**, J. P. Xu, X. S. Liu, G. Y. Liu, X. Yang, J. Ji

Disulfide-Crosslinked Biomimetic Micelles: Formation, Thiol Reactivity and Cytotoxicity Behavior

Macromol. Chem. Phys. **2010**, *211*, 2292-2300

(9) Q. Jin, **L. P. Lv**, G. Y. Liu, J. P. Xu, J. Ji

Phenylboronic Acid as a Sugar- and pH-Responsive Trigger to Tune the Multiple Micellization of Thermo-Responsive Block Copolymer

Polymer **2010**, *51*, 3068-3074

(10) J.-P. Xu, X. Yang, **L. P. Lv**, Y. Wei, F. M. Xu, J. Ji

Gold Nanoparticles Stabilized Pluronic Micelles Exhibiting Glutathione Triggered Morphology Evolution Properties

Langmuir **2010**, *26*, 16841-16847

(11) G. Y. Liu, **L. P. Lv**, X. F. Hu, C. J. Chen, J. P. Xu, J. Ji

Biocompatible Poly (D, L-lactide)-block-Poly (2-methacryloyloxyethyl phosphorylcholine) Micelles for Drug Delivery

Macromol. Chem. Phys. **2011,** *212*, 643-651

(12) F.-M. Xu, J.-P. Xu, **L. P. Lv,** J. Ji

Bowl- and Porous Sphere-Shaped Supramolecular Assemblies and Their Application as Templates for Confined Assembly of Gold Nanoparticles

Soft Matter **2011,** *7*, 1114-1120

Oral and poster contributions

08/2012 **SPP-Workshop "Self-Healing Materials"**, Jenna, Germany

Oral presentation

"Heapocrates": Recent Advances

10/2012 **Bianual Meeting: Smart Polymers**, Mainz, Germany

Poster presentation

Nanocapsules of polyaniline and polypyrrole: preparation and redox-responsive properties

04/2013 **SPP-Workshop "Design and Generic Principles of Self-Healing Materials"**, Weimar, Germany

Oral presentation

Redox Responsive Release of Self-healing Agent for Anti-corrosion

06/2013 **4th International Conference on Self-Healing Materials**, Ghent, Belgium

Poster presentation (1st poster prize)

Redox-responsive release of self-healing agent for anticorrosion

09/2013 **Symposium on Self-Healing Materials**, Gouda, Netherlands

Poster presentation

Redox Responsive Capsules for Self-Healing in Corrosion Protection

06/2014 **4th International Colloids Conference**, Madrid, Spain

Oral presentation

Stimuli-Selective Release of Functional Payloads from Nanocontainers

07/2014 **5th International Conference on Advanced Nanomaterials**, Aveiro, Portugal

Oral presentation

Combining Nanofibers with Nanoparticles via Colloid-Electrospinning

Erklärung

Hiermit versichere ich gemäß § 10 Abs. 3d der Promotionsordnung vom 24.07.2007, dass ich die als Dissertation vorgelegte Arbeit selbst angefertigt und alle benutzten Hilfsmittel (Literatur, Apparaturen, Material) in der Arbeit angegeben habe.

Mainz, den _____

Li-Ping Lv